UNIVERSIDADE DE LISBOA
FACULDADE DE CIÊNCIAS
DEPARTAMENTO DE QUÍMICA E BIOQUÍMICA

Supported lipid bilayers with micro/nanodomains in the study of membrane lipid organization and interactions

Doutoramento em Bioquímica
Especialidade: Biofísica Molecular

Joaquim Trigo Marquês

Tese orientada pelo Doutor Rodrigo F. M. de Almeida e
pela Doutora Ana S. Viana

2015

Documento especialmente elaborado para a obtenção
do grau de Doutor

"Life, as science, is a journey in the pursuit of the unknown.
Make sure you make the most of it and share all the personal accomplishments with whom matters. But try not to do it through facebook."

Joaquim Marquês

Preface

Biomembranes are characterized by a great heterogeneity in their composition, in terms of both lipids and proteins, and by a unique lateral organization that leads to the generation of compartmentalized regions. These regions have been in focus in membrane biophysics and their formation, function and properties are currently hot topics in membrane studies. To answer these fundamental questions is crucial so that in a as short as possible time-window, we will be able to use and manipulate such regions to our benefit, finding feasible applications in disease therapy and diagnostic.

This dissertation aims to provide effective contributions for the following questions:

- How do lipid structure and composition determine membrane lateral organization?
- How can lipid composition and/or membrane lateral organization modulate membrane function, in particular its interaction with other molecules?
- How to take advantage of gold as a substrate for the application of supported lipid bilayers in the study of membrane-related phenomena using optical and electrochemical techniques?

To that end, the attainment of more specific goals is required.

- Can bulk techniques be conjugated with atomic force microscopy images in order to unravel complex phase diagrams for biologically relevant lipid mixtures?
- Is it atomic force microscopy a suitable technique to follow the effects promoted by small molecules in lipid membranes?
- Is it possible to observe nanoscale heterogeneities in gold-supported lipid bilayers?
- How to quantify changes in lipid nanodomains and their properties using high resolution label-free techniques?
- How to establish if a supported lipid bilayer has the required properties, such as planarity, continuity, compactness and stability?
- How sensitive can be the detection of electroactive molecules adsorbed onto SLB prepared on gold substrates?
- How to relate the information retrieved from cyclic voltammetry with the one from fluorescence spectroscopy for the characterization of the interaction of electroactive molecules with lipid membranes?

These are the goals that hopefully were achieved through the execution of the doctoral work that is the subject of this book.

The work presented in this thesis, which is included in the field of Biochemistry – Molecular Biophysics, was developed as a strict collaboration between the Molecular Biophysics and Interfacial Electrochemistry groups. The expertise from each group allowed to apply an unusual approach in the characterization of the lipid systems studied throughout this thesis by the use of a wide collection of techniques. All experimental results shown were obtained at Centro de Química e Bioquímica from Faculdade de Ciências da Universidade de Lisboa. Most of the data obtained during this thesis has already been published or is under consideration in peer view scientific journals, hence the main text of this thesis comprises the compilation of those published works.

In chapter I the general properties and lateral organization of lipid membranes (first subsection, which corresponds to a book chapter in the series *Advances in Planar Lipid Bilayers and Liposomes*, Vol. 22) as well as the formation of supported lipid bilayers in gold substrates (second subsection, review article in *Electrochimica Acta*) are discussed. In chapter II the working principles of the techniques used throughout this work along with their major applications in the context of lipid membrane domains is briefly described. Chapters III through VI describe the main results obtained during this thesis. In chapter III (under consideration in *Langmuir*) the phase behavior of the pseudo-binary lipid system *N*-stearoyl-phytoceramide and palmitoyloleoylphosphatidylcholine in its full hydration regime is thoroughly characterized and a phase diagram for this system proposed. Chapter IV (published in *BBA-Biomembranes*) describes the interplay between the effects of ethanol on lipid bilayers with their composition (from single-component to three-component) and phase behavior. Chapter V (published in *Soft Matter*) discusses the formation of multicomponent phase-coexistence lipid bilayers directly on bare gold, whereas chapter VI (published in *Langmuir*) describes the formation of supported lipid bilayers on modified gold surfaces and also the interaction of a biological relevant compound, epinephrine, with lipid membranes, whether liposomes or supported, in this case using the newly developed platform.

In the final section of this thesis the overall conclusions of this work are presented. There, it is intended to highlight the common threads along the work presented throughout this thesis, and to establish more general relationship between this work and selected reports from literature

considered as important marks within the topics of the thesis t. Finally, to conclude this manuscript future directions are suggested.

At this point I feel it is necessary to acknowledge all the people or institution that, directly or not, have contributed for the success of this thesis. During the course of my PhD I had the privilege of being surrounded by many generous, friendly and kind people who had made my days, or at least the great majority of them, a pleasure for the last years.

My first acknowledgement goes, inevitably, to my supervisors, Doctor Ana Viana and Doctor Rodrigo de Almeida, (the order is just to respect the etiquette that says ladies first because I like them both equally) that over the last years have given me their guidance, support, teaching and mostly their fully commitment and friendship.

To Professor Jorge Correia and Doctor Pedro Lima whom, despite of their senior age, are playful I would like to thank for their good advices and entertaining moments.

My friends and colleagues from the Molecular Biophysics (André Bastos, André Cordeiro, Francisto Branco, Ana Margarida, António Soure, Alena Khmelinskaia, Natércia Rodrigues, Eva Zupancic, Catarina Antunes, Telma Santos, Andreia Santos, Filipa Santos, Ana Carreira, Andreia Sousa, Telmo Paiva) and Interfacial Electrochemistry (Inês Almeida, Ana Matos, Isabel Ornelas, Joana Cabrita, Ana Melato, Ana Mourato, Virgínia Ferreira, Yu Niu, Wei Liu, Kang) groups that contributed to a fantastic work environment, I am grateful for their friendship, companionship and, even sometimes, fruitful scientific discussions.

I would also like to express my gratitude to the people that, one way or another, had contributed to this thesis:
Enzymology group who let me use their power sonicator for the preparation of lipid vesicles throughout the thesis;
Professor Luísa Serralheiro who has made available the flavonoid compounds from her lab.

I thank Centro de Química e Bioquímica for receiving me and put at my disposal everything I needed, whether reagents or equipment, for carrying out the experimental work that has culminate in this thesis.

I thank the Fundação para a Ciência e Tecnologia for my PhD fellowship SFRH/BD/64442/2009 and the Byophysical Society for sponsoring my participation in two congresses.
I would also like to present my gratitude to Professor Gang Jin who have kindly receive me in China, under the 6th Sino-Portugal Scientific and Technological Cooperation of 2013-2015, for about a month, giving me the opportunity to broaden my horizons and work with a very power optical technique – total internal reflection imaging ellipsometry.

To my good friends Bastos and Catarina (my little apprentice) I want make a special acknowledgment cause with them hard working hours seemed more like hard laughing hours without compromising working efficiency.
I would also like to present my gratitude to my good friends Cordel and my two walking liposomes – Inna and Pinie, for the lovely moments we have enjoyed since we know each other.

Lastly but not the least… Margarida I thank you! For your love, constant motivation, support, patience (a lot, I believe) and especially for making every day much more shining. Finally, I thank my family, my parents and brother (who have bugged me with many questions about what I do), who have gave me their love and their unequivocal support, who have settled the example and encouraged me to pursuit my objectives, and to whom a simple expression of thanks does not suffice.

Contents

My contribution to the articles included in the thesis:

1.1. Marquês, J.T., Antunes, C.A.C., Santos, F. C., de Almeida, R. F. M. (2015) Biomembrane Organization and Function: The Decisive Role of Ordered Lipid Domains, Advances in Planar Lipid Bilayers and Liposomes, Elsevier Inc. 2015, Vol 22.

Took an active part in the planning of the paper and the writing.

1.2. Marquês, J.T., de Almeida, R.F.M., Viana, A.S. (2014) Lipid bilayers supported on bare and modified gold - formation, characterization and relevance of lipid rafts. Electrochim. Acta 126, 139-150. DOI: 10.1016/j.electacta.2013.07.117.

Writing of the paper

3. **Marquês, J.T.; Cordeiro, A.M.; Viana, A.S.; Herrmann, A.; Marinho, H.S.; de Almeida, R.F.M. (2015) Formation and properties of membrane-ordered domains by phytoceramide: role of sphingoid base hydroxylation, Langmuir, 31, 9410-9421. DOI: 10.1021/acs.langmuir.5b02550.**

   Atomic force microscopy experiments, fluorescence spectroscopy and X-ray scattering data analysis and interpretation. Contribution to the definition of the phase diagram and to the writing of the paper.

4. **Marquês, J.T., Viana, A.S., and de Almeida, R.F.M. (2011) Ethanol effects on binary and ternary supported lipid bilayers with gel/fluid domains and lipid rafts. Biochim. Biophys. Acta - Biomembr. 1808: 405-414. doi:10.1016/j.bbamem.2010.10.006.**

   Took an active part in the planning of and performed all the experiments. Took an active part in the writing of the paper.

5. **Marquês, J.T., de Almeida, R.F.M., Viana, A.S. (2012) Biomimetic membrane rafts stably supported on unmodified gold. Soft Matter 8:2007-2016. DOI: 10.1039/C2SM06738B.**

   Took an active part in the planning of and performed all the experiments. Took an active part in the writing of the paper.

6. **Marquês, J.T., Viana, A.S., de Almeida, R.F.M. (2014) A Biomimetic Platform to Study the Interactions of Bioelectroactive Molecules with Lipid Nanodomains. Langmuir, 30, 12627-12637. DOI: 10.1021/la503086a.**

   Took an active part in the planning of and performed all the experiments. Took an active part in the writing of the paper.

Papers to which I have contributed that are not included in the thesis:

- Almeida, I., Marquês, J., Liu, W., Yu, N., de Almeida, R.F.M., Jin, G., Viana, A.S., Lipid/decanethiol mixtures for simple assembly of efficient immunosensing interfaces. *Accepted* in Colloids and Surfaces B: Biointerfaces.

- R.F.M. de Almeida, J.T. Marquês, L.C. Silva (2014) Chapter 2. Biophysics of Lipid Rafts and their Interplay with Ceramide: Studies in Model Systems and Biological Insights In: Lipid Rafts: Properties, Controversies and Roles in Signal Transduction Ed. Dan Sillence, Nova Publishers, NY, pp 21-52.

- Marquês, J.T. and de Almeida, R.F.M. (2013) Application of Ratiometric Measurements and Microplate Fluorimetry to Protein Denaturation: An Experiment for Analytical and Biochemistry Students. J. Chem Educ. 90, 1522-1527. http://dx.doi.org/10.1021/ed300599d.

List of abbreviations and symbols

Abbreviations

2H-NMR Deuterium Nuclear Magnetic Resonance

2OHOA 2-hydroxyoleic acid

AFM Atomic Force Microscopy

Chol Cholesterol

Cer Ceramide

CV Cyclic Voltammetry

Cys L-Cysteine

di-8-ANEPPS 4-(2-[6-(Dioctylamino)-2-naphthalenyl]ethenyl)-1-(3-sulfopropyl)pyridinium inner salt

DMPC 1,2-dimyristoyl-*sn*-glycero-3-phosphocholine

DOPC 1,2-dioleoyl-*sn*-glycero-3-phosphocholine

DPH Diphenylhexatriene

DPPC 1,2-dipalmitoyl-*sn*-glycero-3-phosphocholine

DPTL 2,3-di-O-phytanoyl-*sn*-glycerin-1-tetraethyleneglycol-lipoic acid ester

DSC Differential Scanning Calorimetry

EIS Electrochemical Impedance Spectroscopy

EPR Electron Paramagnetic Resonance

FCS Fluorescence Correlation Spectroscopy

FRAP Fluorescence Recovery After Photobleaching

FRET Förster's Resonance Energy Transfer

GM1 Monosialotetrahexosylganglioside (Ganglioside G_{M1})

GPI Glycosylphosphatidylinositol

GPMV Giant Plasma Membrane Vesicles

GUV Giant Unilamellar Vesicles

IR	Infrared
LB	Langmuir-Blodgett
LS	Langmuir-Schaffer
LUV	Large Unilamellar Vesicles
MLV	Multilamellar Vesicles
MUA	11-Mercaptoundecanoic acid
NMR	Nuclear Magnetic Resonance
PC	Phosphatidylcholine
PCer	N-palmitoyl-D-*erythro*-sphingosine
PE	Phosphatidylethanolamine
PLAP	Placental Alkaline Phosphatase
PM-IRRAS	Polarization Modulation-Infrared Reflection-Absorption Spectroscopy
POPC	1-palmitoyl-2-oleoyl-*sn*-glicero-3-phosphocholine
PSM	N-palmitoyl-D-*erythro*-sphingosylphosphorylcholine
QCM	Quatz-Crystal Microbalance
SAM	Self-assembled Monolayer
SL	Sphingolipid
SLB	Supported Lipid Bilayer
SM	Sphingomyelin
SMase	Sphingomyelinase
SPR	Surface Plasmon Resonance
STED	Stimulated Emission Depletion
STM	Scanning Tunneling Microscopy
SUV	Small Unilamellar Vesicles
tBLM	tethered Bilayer Lipid Membranes
TIRF	Total Internal Reflectance Fluorescence
***t*-PnA**	*trans*-parinaric acid
TX-100	Octylphenol ethylene oxide condensate

UQ10 Ubiquinone-10

UV Ultraviolet

X Molar Fraction

Symbols

α Absorption coefficient

d Tthickness

Δ Ellipsometric phase parameter

ΔE_p Redox peak separation, V

E Potential of an electro versus a reference, V

$E_{1/2}$ Measured half-wave potential, V

F Faraday constant, $9.648523415(39) \times 10^4$ C mol^{-1}

f_0 Resonant frequency, Hz

h Plank constant. $6.62606876(52) \times 10^{-34}$ J s

k Extinction coefficient

l_d Liquid disorded

l_o Liquid ordered

ν Potential rate, V s^{-1}

n Refractive index or number of electrons

$\tilde{N}$ Complex refractive index

Φ Angle of incidence or propagation

Ψ Ellipsometric amplitude parameter

Q Charge, C

s_o Solid ordered

t Time, s

R_q Root mean square roughness

<*r*> Fluorescence anisotropy

$\frac{R^p}{R^s}$	Fresnel coefficients in p and s directions
T	Absolute temperature, K
T_m	Main gel-to-fluid phase transition temperature
$\bar{\tau}$	Lifetime weighted quantum yield or amplitude averaged lifetime
Γ	Surface coverage, mol cm^{-2}

Resumo

As membranas biológicas apresentam na sua composição, além de proteínas, um vasto número de espécies lipídicas e, por conseguinte, são estruturas bastante complexas. Atualmente, o estudo da sua organização lateral em domínios assim como as suas propriedades e funções a elas associadas são um dos campos de investigação mais ativos em biofísica. A forma como a composição ou organização lateral da membrana podem influenciar a interação de pequenas moléculas com esta é, igualmente, outro dos focos da investigação em biomembranas. O trabalho descrito ao longo desta dissertação teve como principais objetivos a caracterização, por diversas técnicas, de diversos sistemas modelo de membranas biológicas, ora lipossomas ora bicamadas lipídicas suportadas (SLB) de variadas composições e, consequentemente, com comportamento de fases distinto; o desenvolvimento de uma plataforma de deteção de espécies electroativas adsorvidas ou incorporadas em SLB usando ouro como substrato sólido para a deposição da bicamada; o estudo da interação de pequenas moléculas, como o caso do etanol e da epinefrina, uma molécula electroativa, com bicamadas lipídicas exibindo um comportamento de fases bastante variado – fluido, gel, coexistência gel/fluido e coexistência líquido ordenado (l_o) / líquido desordenado (l_d), que mimetiza os domínios lipídicos conhecidos como jangadas lipídicas.

Neste trabalho estudou-se o comportamento de fases da mistura binária 1-palmitoil-2-oleoil-*sn*-glicero-3-fosfocolina (POPC) / *N*-octadecanoil(2*S*,3*S*,4*R*)-2-amino-1,3,4-octadecanetriol (Fitoceramida (PhyCer)). O POPC é um dos fosfolípidos mais abundante nas membranas celulares de organismos eucariotas enquanto a PhyCer é a principal ceramida, esqueleto dos esfingolípidos complexos, em importantes grupos taxonómicos como plantas e fungos. Através da informação recolhida a partir de diversas técnicas propõe-se o diagrama de fases para esta mistura. Neste estudo recorreu-se tanto a bicamadas lipídicas em suspensão (lipossomas) como a SLB. Usou-se a espectroscopia de fluorescência com recurso a sondas fluorescentes de membrana como o ácido *trans*-parinárico (*t*PnA) e o 1,6-difenil-1,3,5-hexatrieno (DPH), as quais são extremamente sensíveis ao ambiente em seu redor e através de cujas propriedades biofísicas é possível inferir acerca da composição da membrana em termos de domínios. Enquanto o *t*PnA se distribui preferencialmente nas fases mais rígidas, em particular o gel, o DPH é uma sonda que se distribui equitativamente ao longo de toda a membrana e, portanto, reporta a ordem global desta. Recorreu-se, igualmente, à análise por microscopia de força atómica (AFM), a qual devido à sua extrema

resolução lateral (na ordem dos nm) e vertical (na ordem dos Å) permite distinguir detalhes, como diferenças de alturas entre diferentes domínios de membrana, na topografia de SLB. A espectroscopia de difração de raio-X também foi usada na medida em fornece informação relacionada com o empacotamento lateral dos lípidos numa bicamada. Os resultados obtidos mostram que o comportamento de fases desta mistura difere daquele já publicado para outras ceramidas quando também misturadas com POPC. O diagrama de fases proposto prevê a existência de diferentes regiões de coexistência de fases, e, principalmente, antecipa a existência de complexos POPC:PhyCer para determinadas proporções destes lípidos. As estequiometrias são conforme se segue: POPC 3 : 1 PhyCer e POPC 1 : 2 PhyCer. Estes complexos são vistos como entidades moleculares com características próprias e apresentam propriedades biofísicas muito semelhantes àquelas já descritas para os domínios gel identificados *in vivo* em levedura *Saccharomyces cerevisiae*.

No decurso desta tese investigou-se a forma como a organização lateral da membrana pode modular a interação de pequenas moléculas com esta. Estudaram-se os casos do etanol, da quercetina e da epinefrina. Os efeitos do etanol foram analisados para SLB formadas em silício e mica, que é um substrato atomicamente liso e carregado negativamente a pH neutro e, portanto, adequado à deposição de lípidos. Neste estudo usaram-se os lípidos 1,2-dipalmitoil-*sn*-glicero-3-fosfocolina (DPPC), 1,2-dioleoil-*sn*-glicero-3- fosfocolina (DOPC), *N*-palmitoil-D-eritro-esfingosilfosforilcolina (PSM) e colesterol (Chol). Foram, igualmente, estudadas bicamadas exibindo diferentes comportamentos de fase: apenas fluido (DOPC), apenas gel (DPPC e DPPC:Chol 98:2), coexistência gel/fluido (DPPC:DOPC 1:1 e 92:8) e, finalmente, coexistência l_o/l_d (DPPC:DOPC:Chol 2:2:1 e PSM:DOPC:Chol 2:2:1). Os efeitos do etanol sobre as diferentes bicamadas foram seguidos em tempo real por AFM. Para todos os sistemas estudados observou-se o adelgaçamento da bicamada seguido de expansão em consequência da interação com o etanol. Relativamente aos sistemas com separação de fases, enquanto para o sistema gel/fluido, a baixas concentrações de etanol, o adelgaçamento verifica-se apenas para a fase fluida, para os sistemas l_o/l_d o adelgaçamento ocorre em simultâneo nas duas fases. Contudo, em ambas as situações apenas se observa a expansão da fase mais fluida, o que leva a um aumento da fração de domínios desordenados cujas principais causas serão uma variação na tensão superficial na interface água/lípido e diminuição do ponto de fusão que, em conjunto, levarão a um aumento da desordem das cadeias acilo, aumento do ângulo de inclinação das cadeias acilo e, ainda, interdigitação. De

referir ainda que o uso de duas misturas ternárias permitiu perceber se os efeitos induzidos pelo etanol seriam dependentes da composição lipídicas ou, por outro lado, do tipo de domínios presentes. Tendo em conta que as alterações observadas foram idênticas para ambos os sistemas ternários DPPC:DOPC:Chol 2:2:1 e PSM:DOPC:Chol 2:2:1 concluiu-se que o tipo de fase influencia mais os efeitos provocados pelo etanol que o tipo de lípido presente na composição das bicamadas.

Um dos trabalhos fulcrais no decorrer desta tese foi o desenvolvimento de SLB em superfícies de ouro. Como até à data da realização dos estudos descritos nesta tese eram escassos os trabalhos encontrados na literatura a descrever a formação de bicamadas em ouro com separação de fases ou mais do que um componente, pretendeu-se investigar quais as condições experimentais que favorecem a formação de SLB compostas por 3 lípidos distintos e com separação de fases l_o/l_d. O ouro é um substrato metálico condutor e com propriedades que permitem a aplicação de inúmeras técnicas de superfície de elevada sensibilidade. No entanto, tem sido descrito que a hidrofobicidade deste metal é representa um grande constrangimento à formação de SLB nesta superfície. Bicamadas planas e contínuas com jangadas lipídicas, diferindo em espessura da membrana circundante em cerca de 1,5 nm, conforme comprovado por AFM, foram depositadas diretamente em ouro nu através da fusão de vesículas unilamelares pequenas ou grandes e na ausência total de qualquer sal. De facto, observou-se que a presença de NaCl promove a formação de túbulos ao invés de uma bicamada plana, conforme revelado pelas imagens obtidas AFM e as espessuras dos filmes lipídicos estimadas por elipsometria. As SLB preparadas diretamente em ouro são estáveis numa larga gama de potenciais o que torna o seu uso adequado ao estudo da interação da epinefrina com membranas lipídicas. No entanto, ficou também provada a influência do substrato metálico nas características da bicamada uma vez que foi obtida uma proporção domínios ordenados/domínios desordenados diferente da prevista pelo diagrama de fases para essa mistura obtido em suspensões de lipossomas e, por outro lado, observam-se corrugações na fase mais desordenada que são consequência do ambiente assimétrico dos dois lados da bicamada. Enquanto as cabeças dos fosfolípidos do folheto virado para a superfície de ouro encontram-se num ambiente praticamente desprovido de água, o mesmo não se verifica relativamente ao folheto do topo da bicamada. Adicionalmente, os domínios identificados por AFM apresentavam formas muito angulares e, portanto, diferentes das já descritas para lipossomas em suspensão. Este aspeto deve-se ao facto de o filme lipídico seguir a topologia do ouro que é caracterizada por terraços

monoatómicos. Para ultrapassar estas limitações, inclusivamente o elevado grau de hidrofobicidade do ouro que dificulta a formação de SLB contínuas, modificou-se a superfície previamente à formação da SLB. Esta modificação foi feita com uma monocamada automontada de L-cisteína, a qual apresenta um grupo tiol que estabelece uma ligação muito forte ao ouro e por outro lado torna a superfície deste metal mais hidrofíla e, portanto, mais propícia à adsorção de lípidos. Adicionalmente, pelo facto da monocamada de cisteína ser curta e pouco compacta não impede trocas eletrónicas entre o substrato metálico e espécies electroativas, tornando-se, desta forma, uma modificação adequada aos objetivos pretendidos. Dados de AFM, elipsometria e voltametria cíclica mostram que as SLB formadas sobre ouro modificado com cisteína são contínuas, compactas e estáveis.

Outra molécula cuja interação com a membrana foi também avaliada é a epinefrina. A epinefrina apresenta duas propriedades, fluorescência e eletroatividade, que permitem o uso de um leque de técnicas mais vasto na caracterização da sua interação com a membrana, incluindo a espectroscopia de fluorescência e técnicas eletroquímicas. A avaliação da interação da epinefrina foi, então, concretizada tanto por intermédio de espectroscopia de fluorescência usando lipossomas, como através do uso da plataforma acima descrita com recurso a voltametria cíclica. De referir ainda que uma grande variedade de sistemas lipídicos foram empregues conforme se descreve: fluido (DOPC), gel (DPPC), gel/fluido (DPPC:DOPC 1:1), l_o/l_d (DPPC:DOPC:Chol 2:2:1 e DPPC:DOPC:Chol 2:2:1 com 10 % de ganglióside G_{M1}) e l_o (DPPC:DOPC:Chol 11:1:8). Fazendo uso da fluorescência intrínseca da epinefrina concluiu-se que esta interage fracamente com membranas lipídicas. No entanto, apesar desta interação ser fraca, a epinefrina foi claramente detetada por voltametria cíclica quando adsorvida em SLB formadas sobre ouro modificado com cisteína. Foi, ainda, possível aferir que na bicamada fluida ficou adsorvida uma maior quantidade de epinefrina. É de realçar que os dados provenientes de voltametria cíclica permitiram estimar um coeficiente de partição membrana/água (de cerca de 1.13×10^4 para a membrana em fase fluida) para a epinefrina. Finalmente, uma das principais observações deste estudo é a capacidade das diferentes bicamadas preparadas, independentemente da sua composição ou comportamento de fases, estabilizarem a epinefrina do ponto de vista estrutural, impedindo a sua oxidação, a qual ocorre espontaneamente a pH neutro em soluções aquosas.

Este trabalho mostra como a combinação de várias técnicas experimentais pode ser importante e como permite chegar a conclusões que de outra forma não seria possível. Ao longo

desta tese são descritas múltiplas evidências que demonstram, não só como a composição da membrana influencia as suas propriedades biofísicas, mas também a capacidade que a organização lateral da membrana tem de influenciar os mecanismos de interação de pequenas moléculas com esta.

A plataforma desenvolvida no decurso desta tese abre perspetivas não só na condução de estudos que visam investigar as propriedades gerais das membranas mas também como também no potencial desenvolvimento de interfaces para biossensores com transdução de sinal ótico ou eletroquímico.

Palavras-chave

- Microscopia de força atómica;
- Modificação da superfície de ouro;
- Diagramas de fase de lípidos;
- Técnicas óticas e eletroquímicas;
- Domínios de esfingolípidos e jangadas.

Abstract

The lateral organization of lipid bilayers into domains, such as lipid rafts or gel domains, and how they influence the properties and function of membranes is a current topic in biophysics. In this work, the properties of single and multicomponent lipid bilayers (whether supported on a solid substrate or free in solution as liposomes) exhibiting different phase behavior were studied by a wide range of characterization techniques – atomic force microscopy, ellipsometry, cyclic voltammetry, quartz crystal microbalance, surface plasmon resonance and fluorescence spectroscopy.

The phase diagram for the binary mixture 1-palmitoyl-2-oleoyl-*sn*-glycero-3-phosphocholine (POPC) / *N*-octadecanoyl(2*S*,3*S*,4*R*)-2-amino-1,3,4-octadecanetriol (Phytoceramide (PhyCer)) is proposed by combining data from different techniques. The formation of complexes between POPC and PhyCer with properties similar to those found for gel domains *in vivo* is anticipated. These POPC/PhyCer complexes occur at two distinct stoichiometries, 3:1 and 1:2.

The influence of membrane lateral organization was investigated in the context of the interaction of small molecules with lipid bilayers, namely ethanol and epinephrine. The effects of ethanol were studied in supported lipid bilayers (SLB) formed on mica spanning a phase behavior from single fluid to liquid ordered (l_o) / liquid disordered (l_d) phase coexistence. It was concluded that the lateral organization of lipids into domains, but not the specific lipid composition, plays a determinant role on the effects induced by ethanol.

Another purpose of this work was to study the properties of supported lipid bilayers (SLB) formed on gold surfaces. For the first time raft-containing SLB were formed directly on bare gold and the substrate seems to influence the properties of the lipid bilayer since an unexpected proportion of lipid domains was obtained and corrugations were observed in the liquid disordered phase. A lipid-based biosensing interface consisting on a SLB formed on top of a L-cysteine-modified gold was also developed for the detection of membrane-interacting electroactive molecules.The interaction of epinephrine, an electroactive molecule, was evaluated using both liposomes and SLB formed on Lcysteine-modified gold. Despite the weak interaction between epinephrine and liposomes as determined by fluorescence spectroscopy, its redox signal could be clearly detected by cyclic voltammetry when adsorbed on SLB of various compositions. Moreover, voltammetric data allowed to estimate a membrane/water partition coefficient for epinephrine. The

results presented show how lateral membrane organization and composition may influence its function and properties.

Keywords

- Atomic force microscopy;
- Gold surface modification
- Lipid phase diagrams
- Optical and electrochemical techniques
- Sphingolipid domains and rafts

Chapter I

Introduction

1.1. Biomembrane organization and function: the decisive role of ordered lipid domains

Biomembrane Organization and Function: The Decisive Role of Ordered Lipid Domains

Joaquim T. Marquês, Catarina A.C. Antunes, Filipa C. Santos, Rodrigo F.M. de Almeida[1]

Centro de Química e Bioquímica, Faculdade de Ciências, Universidade de Lisboa, 1749-016 Lisboa, Portugal
[1]Corresponding author: e-mail address: rfalmeida@fc.ul.pt

Contents

Abstract

There has been a great effort to study lipid lateral organization in biomembranes in the past decades, in order to unravel the structural basis and functional significance of membrane lipid domains. However, in both respects fundamental doubts still persist, and recent results have widened this topic well beyond lipid rafts. In particular, the detection of sphingolipid-enriched gel domains in the yeast *Saccharomyces cerevisiae* plasma membrane, which are not the prototypical liquid ordered, sterol-enriched lipid rafts, will be described.

The critical role of ordered lipid domains will be demonstrated with biophysical studies of membrane lipid organization in living cells and in model systems, concerning mammalian and fungal membranes. Membrane interactions with different types of bioactive molecules will be briefly presented, including endogenous molecules such as the

Advances in Planar Lipid Bilayers and Liposomes
ISSN 1554-4516
http://dx.doi.org/10.1016/bs.adplan.2015.06.002

hormone epinephrine or membrane proteins, as well as drugs, including anticancer and antitubercular compounds. Strategies to tackle the complexity of living cell membranes will be discussed, in an attempt to reach a compromise between lipid lamellar phases in artificial or reconstituted systems and observations in living cells.

The development of new and improved biomimetic systems might provide answers to some of the open questions in the lipid domains field. Therefore, new lipid bilayer membrane models containing lipid domains stably formed on a conducting support (gold), where powerful surface and electrochemical techniques can be employed, will also be presented. The redox behavior of the catecholamine hormone epinephrine studied in such system showed that the lipid bilayer has a crucial role for the hormone chemical stability.

1. WHY ARE MEMBRANE ORDERED DOMAINS A CURRENT RESEARCH TOPIC?

Biological membranes are presently described as a mosaic of domains with different lipid and protein compositions, properties, and functions. Biomembranes from different sources will exhibit both distinct protein/lipid ratios and lipid compositions. In fact, the interplay between lipid–lipid interactions, unique for each lipid composition, and lipid association with proteins gives rise to microdomains, allowing for the compartmentalization of the vast biological functions performed by biomembranes [1–3]. Lipids are characterized by a great structural diversity, both in terms of their polar head group and the length and unsaturation degree of their hydrocarbon chains [4–6] (a few examples are given in Fig. 1). Such multiplicity of structures may induce the lateral segregation of lipids into domains with distinctive properties in terms of size [1,7,8], rigidity[9,10], and thickness [11,12], just to name a few.

Moreover, several pathologies, including cancer and neurodegenerative conditions, are characterized by specific alterations in lipid composition and hence membrane biophysical properties [13,14]. The molecular mechanism of action of many drugs involves at some point their effect on membrane lipid organization (the membrane lipid therapy principle) [15]. However, this therapeutic target has been subexploited.

Despite the accumulated evidence for the physiological role of membrane domains, their involvement in disease and potential as targets for innovative therapies, many questions regarding this subject are still under debate [1,2,16]. Thus, there is an unprecedented interest in studying the biophysical behavior of both lipids and proteins in order to understand better

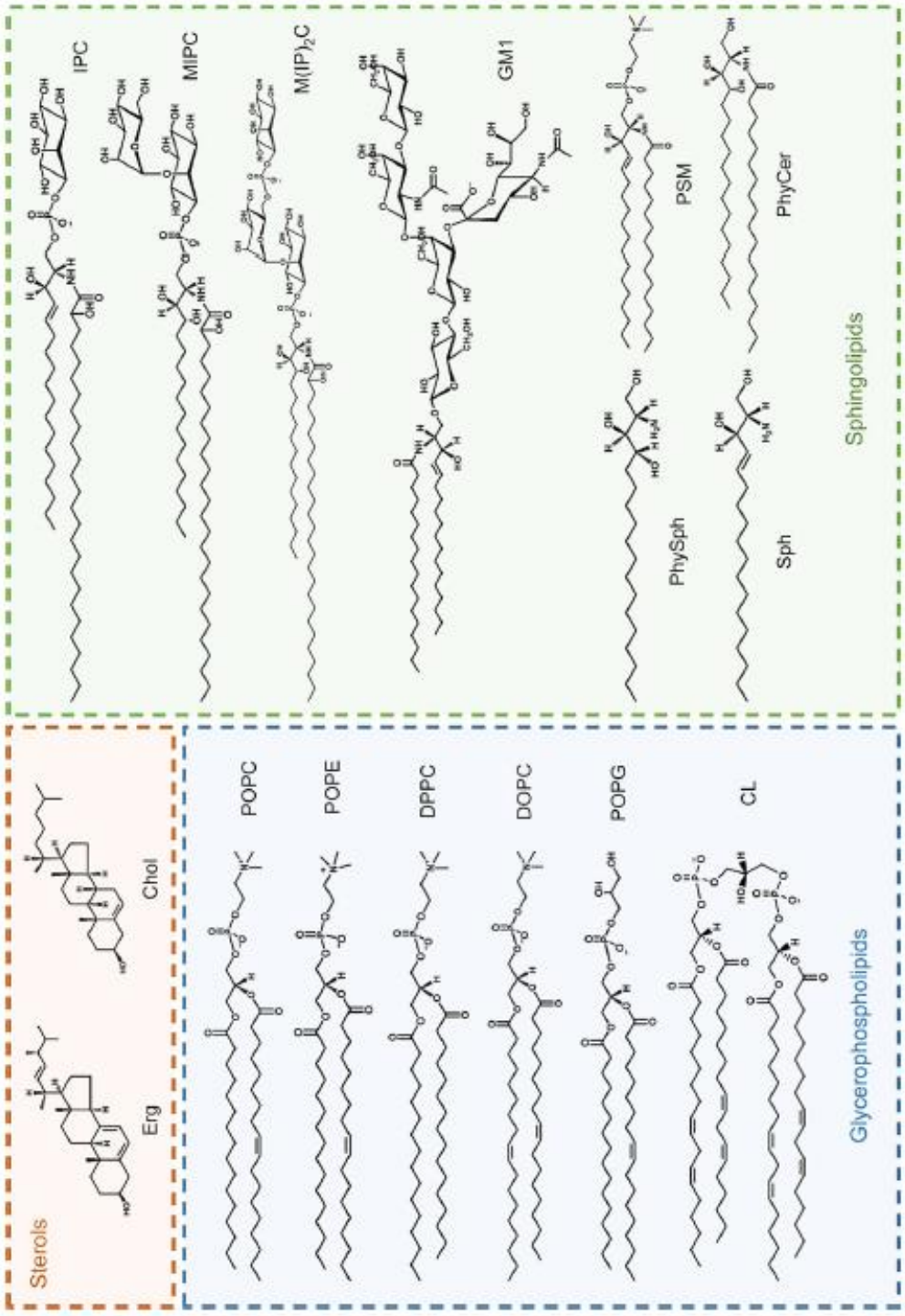

Figure 1 See legend on next page.

biomembranes, and how they affect the modes of action of drugs that have the plasma membrane (PM) as their target, and associated resistance mechanisms, as is the case of many antifungal agents in clinical use, and new compounds directed toward other pathologies such as cancer and Alzheimer's disease [13,17–20].

In an attempt to clarify which properties best describe the functional domains/microdomains often formed in biological membranes, and how they respond upon exposure to certain stimulus, model systems that mimic some of the features of biomembranes such as liposomes and supported lipid bilayers (SLBs) have been widely employed (e.g., Refs. [7,11,21–26]) (Fig. 2). These model systems have proved to be valuable tools in membrane research, whether basic or applied [27]. Although the exact nature of these functional domains is currently known to be diverse, the fact that all should be formed and stabilized by favorable interactions between its components strongly suggests that they are in general ordered domains, whether gel (or solid ordered, So), liquid ordered (Lo), or even crystalline, since expectedly the acyl chains are more tightly packed and/or headgroups establish more interactions giving rise to a network of molecules with a more defined spatial arrangement [16,28]. In addition, there should be restrictions to lateral diffusion of both lipids and proteins so that these domains have the necessary life span to perform their function.

Membrane ordered domains will thus be the main focus of this chapter. Their molecular origin, how to study them *in vivo* and mimic them *in vitro*, and how they influence the interaction of the membrane with relevant molecules will be discussed, with an emphasis on reaching the compromise between *in vivo* and *in vitro* approaches.

Figure 1 Structures of lipids commonly found in the membranes of different organisms and used in model systems to mimic the biophysical properties of biological membranes. Examples of studies involving most of these lipids are given along the text. Erg, ergosterol; Chol, cholesterol; POPC, 1-palmitoyl-2-oleoyl-*sn*-glycero-3-phosphocholine; POPE, 1-palmitoyl-2-oleoyl-*sn*-glycero-3-phosphoethanolamine; DPPC, 1,2-dipalmitoyl-*sn*-glycero-3-phosphocholine; DOPC, 1,2-dioleoyl-*sn*-glycero-3-phosphocholine; POPG, 1-palmitoyl-2-oleoyl-*sn*-glycero-3-phospho-(1′-rac-glycerol); CL, cardiolipin (in the example with four linoleoyl chains); IPC, inositolphosphorylceramide; MIPC, mannosylinositolphosphorylceramide; M(IP)2C,mannosyldiinositolphosphorylceramide; GM1, ganglioside G_{M1}; PhySph, phytosphingosine (4-hydroxysphinganine); PSM, *N*-palmitoyl-D-erythro-sphingosylphosphorylcholine; Sph, sphingosine; PhyCer, phytoceramide (in the example, *N*-stearoyl-phytosphingosine).

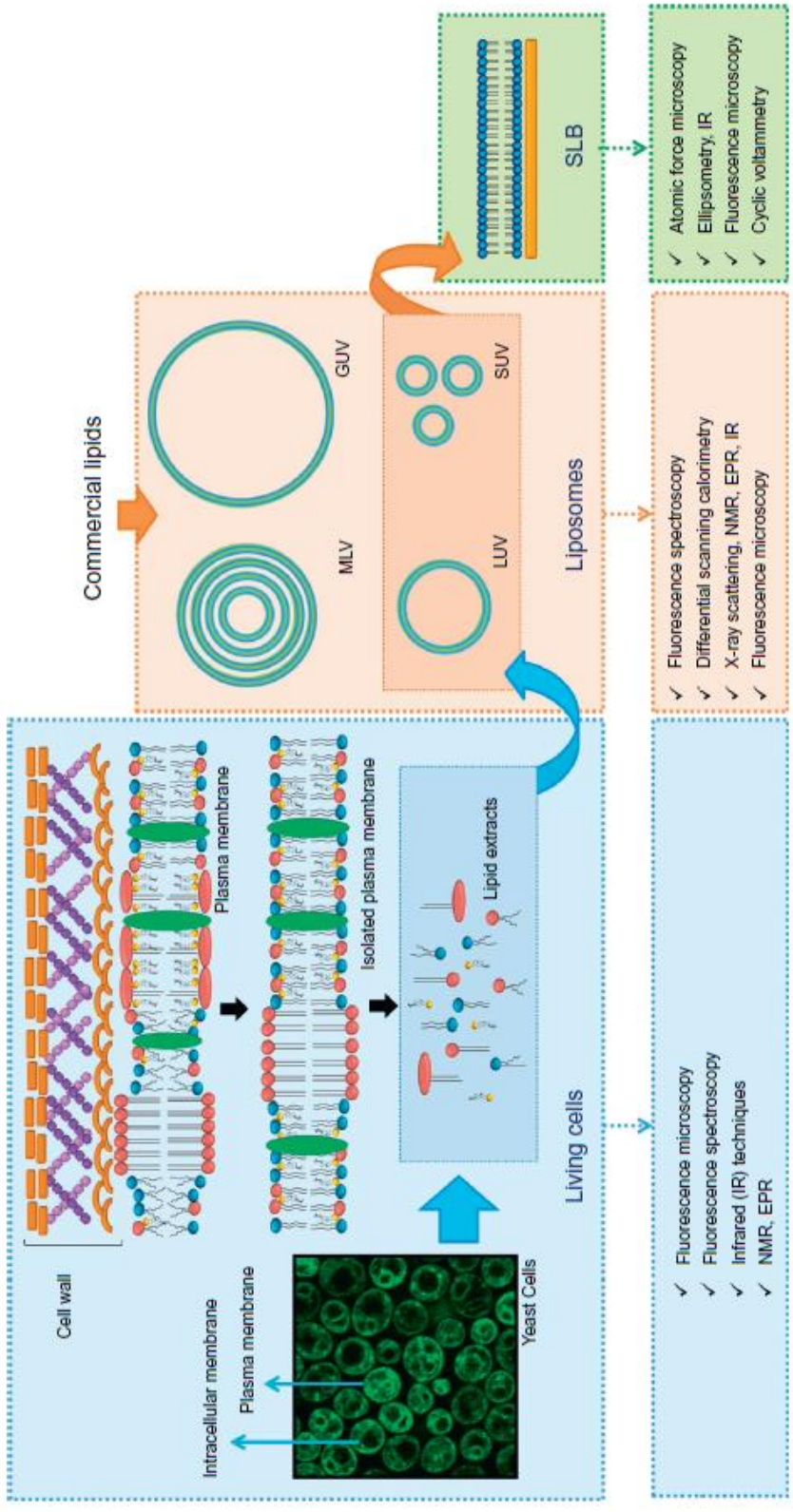

Figure 2 See legend on next page.

2. WHY DO LIPIDS FORM ORDERED DOMAINS?

Sphingolipids (SL) (Fig. 1) are major lipid components of the PM of eukaryotes and their organization in the PM is crucial for many cellular vital functions [29]. Changing SL composition can profoundly impact membrane biophysical properties and the organization of the PM (e.g., Refs. [9,10,30]).

SLs are usually the cell membrane components with the highest main phase transition temperature (T_m), i.e., the temperature at which the lipids undergo a transition from a gel phase with the acyl chains highly ordered and packed to a fluid phase, with low order and packing (also known as Ld phase) [31]. Therefore, SLs hold large responsibility for the lateral segregation of lipids and are important components of membrane ordered domains (Fig. 3). The fact that they have high T_m values means that at room temperature, at inner human body temperature (37 °C), or at the optimal growth temperature of many microorganisms (e.g., 30 °C), if isolated, they could exist in a gel or So phase, rather than in the fluid state usually attributed to biological membranes.

Typically, it has been considered that lipid domains require both SLs and a sterol (cholesterol (Chol) in mammalian cells, ergosterol (Erg) in fungi and

Figure 2 Study of membrane ordered domains spanning different degrees of complexity from living cells to membrane model systems (liposomes and supported lipid bilayers, SLB). Exemplifying with *S. cerevisiae* cells, the intact cells contain a cell wall, as well as plasma and intracellular membranes. The cell wall can be removed by enzymatic digestion or other methods, which can *per se* alter the PM organization. The PM can be isolated by ultra-centrifugation and analyzed in this form. Lipid extracts can be obtained from whole membrane preparations or from isolated PM. In turn, these extracts can be reconstituted into different types of liposomes (MLV, multilamellar vesicles; GUV, giant unilamellar vesicles; LUV, large unilamellar vesicles; SUV, small unilamellar vesicles) according to the intended application. The liposomes can further be used to form SLB on a solid support. Commercial lipids with high degree of purity can also be used to prepare membrane model systems with the desired composition, usually from simple one-component up to more complex three- or four-component mixtures, both liposomes and SLB, and can be characterized by the same techniques as the reconstituted systems. On the other hand, ordered domains in living cells can only be studied with a narrower range of techniques. The examples correspond to some of the most widely used approaches in the context of membrane ordered domain studies and do not intend to be an exhaustive list of the techniques available or a review of the literature. Further details and specific examples are given in the text. The image on the left was obtained by laser scanning confocal fluorescence microscopy of *S. cerevisiae* erg6Δ cells (BY4741; MATa, his3Δ1, leu2Δ0, met15Δ0, ura3Δ0, YML008c::kanMX4) harvested in mid-exponential phase and labeled with 2 μM 4-(2-(6-(dibutylamino)-2-naphthalenyl)ethenyl)-1-(3-sulfopropyl)-pyridinium (di-4-ANEPPS) at 24 °C.

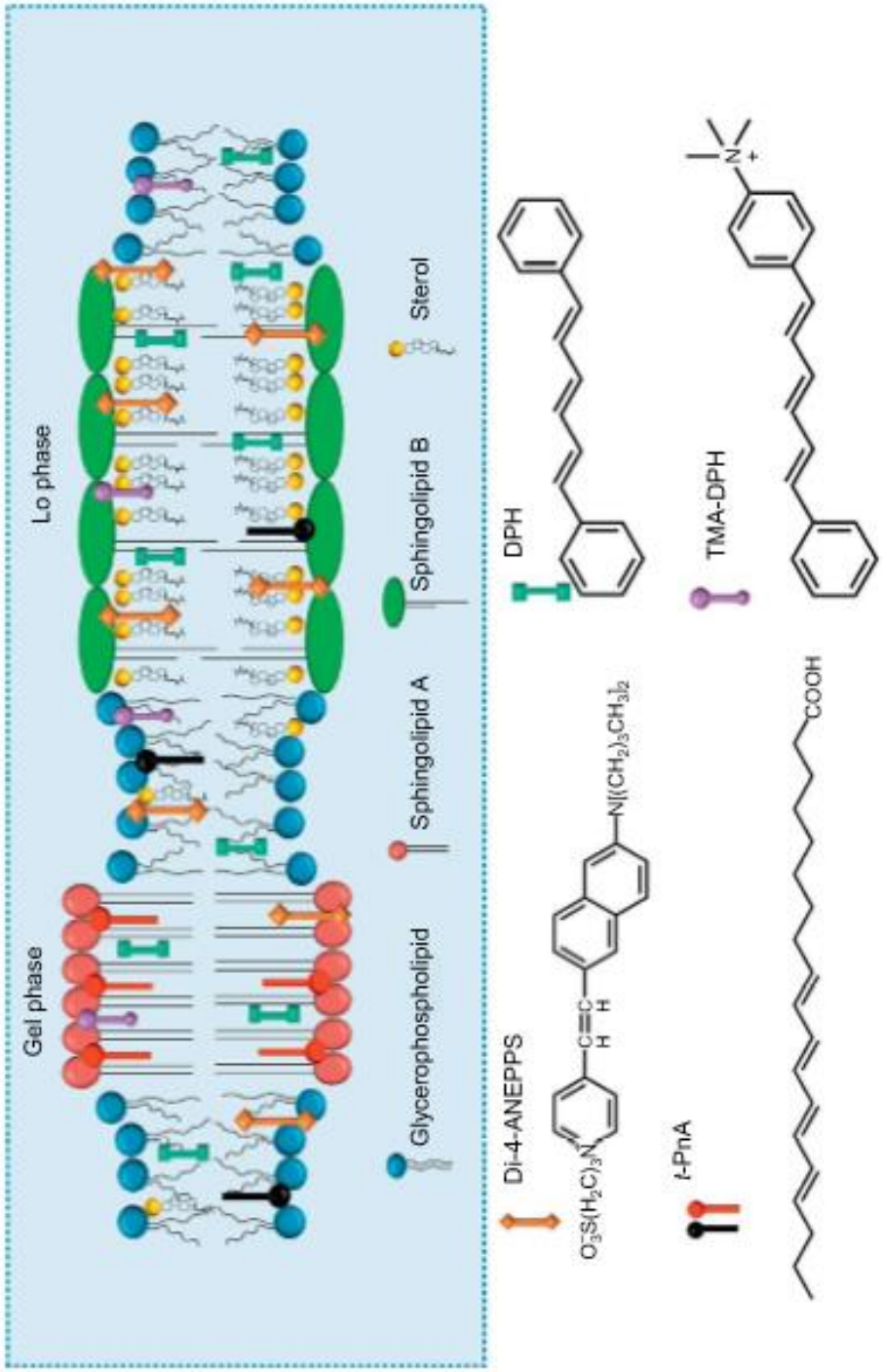

Figure 3 See legend on next page.

other lower eukaryotic cells), phytosterols in plants (Fig. 1), and are in the Lo phase [2,32], the so-called lipid rafts (Fig. 3). Major sterols of the PM of the different eukaryotic kingdoms are able to induce this Lo phase, when mixed with certain lipids, but this feature is not common to all sterols, placing the Lo-forming ability of sterols as a chief feature in the molecular evolution of eukaryotes [16]. Regarding ordered domains, sterols can be described from two antagonistic perspectives: the Lo state has properties between those of the gel and the Ld, and a high sterol content is able to abolish gel/fluid phase separation situations, by forming a single Lo phase. For intermediate proportions, sterols can induce Ld/Lo or Lo/gel phase separation in an otherwise single-phase bilayer (see Section 4.2) [22,23]. In mammalian cells, lipid rafts are transient in time and have, in general, dimensions below optical resolution, but in *Saccharomyces cerevisiae*, the PM contains temporally stable microdomains that can be seen by optical microscopy with well-defined localization [2]. Of these distinct membrane compartments, the best studied are MCC for membrane compartment occupied by Can1p and MCP for membrane compartment occupied by Pma1p [2]. MCC colocalizes with the Erg-labeling agent filipin, unlike MCP which has been associated to SLs. However, the relation of these compartments with lipid rafts is still unclear [16]. The recent finding of yet unknown pathways for complex SLs biosynthesis in *S. cerevisiae* suggests that the biological roles of these lipids may be underestimated [33].

Lipid domains have been considered to some extent synonyms of lipid rafts in a state resembling the Lo phase found in membrane model systems

Figure 3 Schematic depiction of a lipid bilayer exhibiting different lipid phases—Ld, Lo, and gel. The predicted location of fluorescent probes, such as di-4-ANEPPS, 1,6-diphenyl-1,3,5-hexatriene (DPH), *trans*-parinaric acid (*t*-PNA), and 1-(4-trimethylammoniumphenyl)-6-phenyl-1,3,5-hexatriene (TMA-DPH), in the different lamellar lipid phases is also depicted. The polar headgroups of sphingolipids are represented in red (gray in the print version) and green (gray in the print version) (types A and B), and that of phospholipids in blue (dark gray in the print version). Sterols (Lo-forming) are represented by a ring system. Di-4-ANEPPS presents sensitivity to polarity and hydration patterns in the headgroup region, and membrane dipole potential; partition and fluorescence quantum yield favorable to sterol-rich domains; DPH reports the global order of the membrane in the hydrophobic core; *t*-PnA reports acyl chain packing, has preferential partition for gel phases (red (gray in the print version) *t*-PnA), but can be found also in Lo and Ld phases where it presents lower quantum yield (black *t*-PnA); TMA-DPH, similar to DPH, reports the global order of the membrane, but is anchored at the membrane surface by the TMA group and is more sensitive to hydration.

in a sea of Ld fluid [2]. However, the current view of biomembranes has been changing [16], in light of recent observations such as our finding of gel domains in yeast [9], and of a significant fraction of slowly diffusing or even immobile proteins in plants and fungi [2,34]. In both Ld and Lo phases, molecular diffusion in the plane of the membrane is quite fast, though slightly slower in the Lo. The much smaller lateral diffusion coefficients of gel or crystalline lipid phases are more consistent with the low lateral mobility of some proteins. While such low mobility could be attributed at least in part to interactions with the cell wall, proteins or protein clusters stable for at least a few minutes were also found in the PM of mammalian cells using super-resolution optical techniques [35].

The highly rigid gel domains found by us in the PM of *S. cerevisiae* [9] are sterol-free and thus quite different from the typical Lo-like rafts (Fig. 3). Thus, their discovery highlights fundamental differences between yeast and mammalian membranes [2]. Glycosylphosphatidylinositol (GPI)-anchored proteins, which are important for pathogenicity, virulence, and resistance in pathogens such as *Candida albicans* [36], are also present in *S. cerevisiae* SL domains [9]. Other authors found that membrane depolarization reduces significantly the amount of gel-like microdomains in yeast PM [37]. An important biological role for these domains has been suggested also in the endoplasmic reticulum of budding yeast where they seem to be involved in the confinement of misfolded proteins into the mother compartment of budding cells [38].

To fully understand the organization of membrane lipids and the biological roles of lipid domains/rafts, it is necessary to invest in innovative methods for the preparation and analysis of membrane model systems. In this respect, our group has recently achieved the formation of SLB with either Lo/Ld or gel/fluid phase coexistence on a bare metallic gold surface [24]. The coexistence of nano/microdomains was demonstrated by atomic force microscopy (AFM) imaging (Fig. 4A), ideally suited to detect thickness differences on the order of ~1 nm, which corresponds to the range of height gap between ordered and disordered lipid domains. Since, up to date, most studies concerning lipid membranes on metallic surfaces rarely employed other than single-lipid or single-phase systems [39–45], not only did our study show the possibility of forming multicomponent lipid bilayers (1,2-dioleoyl-*sn*-glycero-3-phosphocholine (DOPC)/1,2-dipalmitoyl-*sn*-glycero-3-phosphocholine (DPPC)/Chol 2:2:1 without or with 10 mol% ganglioside G_{M1} (Fig. 1) and DOPC/DPPC 1:1) on metallic substrates [24,25] but also brought to discussion the relevance of using in this kind

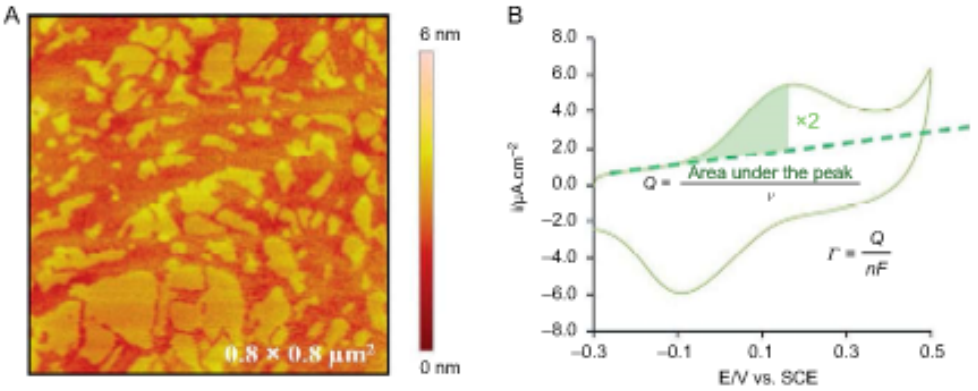

Figure 4 Planar lipid bilayers supported on a conducting substrate (Au(111)). (A) AFM image of a three-component SLB, DPPC/DOPC/Chol (2:2:1), deposited directly on a bare gold surface. (B) Cyclic voltammogram of epinephrine adsorbed in a fluid bilayer of DOPC prepared on a cysteine-modified gold electrode to improve bilayer stability, illustrating how to determine the surface coverage (Γ) of the electroactive species adsorbed on the surface. Q, charge, ν, sweep rate, n, number of electrons transferred (two in the case of epinephrine), F, Faraday's constant. For further details, see Ref. [25]. *Adapted from Ref. [24].*

of studies lipid mixtures that more closely resemble the organization of biomembranes [46]. The fact that lipid bilayers exhibiting lipid rafts can be prepared on a metallic surface opens new prospects in the study of membranes' biophysical properties, since both the optical and conductive properties of this kind of substrates can be advantageously used in their characterization, in addition to high-resolution surface techniques such as AFM.

3. WHAT IS THE RELEVANCE OF PLANAR LIPID BILAYERS AND LIPOSOMES FOR THE STUDY OF ORDERED DOMAINS?

The use of model systems allows the direct assessment of the biophysical properties of lipid bilayers with a defined composition and also the direct inspection of the action of external molecules on membrane properties. While in a biological system there will be multiple interactions at play within the membrane and also with other structures, such as the cytoskeleton or the cell wall [9,34,47], a model system is a simplified version of biological membranes, where a controlled environment is established and any measured property is more easily assigned. In addition, many times the existence or formation of certain specific domains in biological membranes can only

be acknowledged because their properties have already been described in model systems and attributed to a given lipid phase and/or the presence of specific lipids (e.g., Refs. [9,48]). Nonetheless, biological systems remain as the final source of proof for the occurrence of microdomains with specific properties, or the formation of special lipid structures such as in the polarized growth of PM in plants [49] and fungi [50–52] or protrusions in epithelial cells [53].

Sometimes the properties measured in model systems may not find total correspondence *in vivo*. For example, using liposome suspensions, it was determined that the presence of phytosphingomyelin, which has an extra hydroxylation in position C-4 of the sphingoid base (phytosphingosine, Fig. 1), instead of SM renders the gel phase more stable [54]. However, it has been reported that the absence of C-4 hydroxyl group in SLs leads to a decrease in the fluidity of the membrane of *S. cerevisiae* [55]. Bias of the results obtained *in vivo* and with model systems are many times attributed to the role of proteins or to lipid components that were not present in the model system. This discrepancy can be used to improve the model system in order to better mimic the *in vivo* situation (see Section 4).

Results obtained in living cells are also affected by their dynamic nature, which precludes employing certain techniques and methodological approaches. While in stationary systems, such as liposomes or SLB (Fig. 2), the lipid composition is a controlled variable, highly dynamic systems, such as any living cell, exhibit variations in lipid composition over time, in addition to the biological variability between cells and populations. When trying to change the amount of a certain lipid in a biomembrane, processes such as membrane traffic and cellular metabolism that contribute for the time-dependent membrane lipid composition may override the intended compositional change. AFM is an excellent tool to detect nanoscale properties of the lipid domains such as their height gap from the surrounding bilayer, size, and shape [8,11], and even viscoelastic properties [56]. However, it would not be possible to gather information with the same level of detail from an intact cell membrane due to its crowded surface.

Thus, model systems, by establishing a controlled environment, are a credited approach for the study of lipid domains. However, not every observation made for model systems can be directly translated to *in vivo* situations. Establishing firm relations between the different membrane microdomains, their biophysical counterparts and biological role requires an integrated approach in which all levels of complexity are studied in parallel, in order to gather information on both domain organization and membrane biophysical properties.

Among membrane model systems, liposomes and SLB are, by far, the most employed. Liposomes are more suitable for characterizing bulk properties of the system, i.e., information averaged over a large number of molecules and/or lipid vesicles. On the other hand, SLB might be more appropriate when trying to locally inspect the surface properties of the lipid bilayers. Thus, liposomes and SLB can be viewed as complementary (Fig. 2) when studying membrane organization and biophysical properties (e.g., Ref. [25]).

Fluorescence spectroscopy is, perhaps, one of the most employed techniques in the study of liposomes in suspension, and together with fluorescence microscopy are among the few that can be used with similar approaches to *in vitro* and *in vivo* situations [57]. Using multilamellar vesicles (MLVs) or large unilamellar vesicles (LUVs) and suitable fluorescent probes, a quantitative description can be made of the lipid phases present and of the effect of, for example, adding an extra lipid to the system [7,22,58]. Lipid systems with varying lipid compositions shall exhibit different phases and domains (Fig. 5), hence distinct biophysical properties. Different probes will also report on different membrane properties, such as acyl chain packing, membrane surface or dipole potentials, and water penetration (Fig. 3). One important experimental approach is time-resolved fluorescence spectroscopy. In particular, using *t*-PnA, a unique membrane probe with strong preference for and increased fluorescence quantum yield in gel phases, it is possible to detect gel domains even when these constitute less than 5% of the membrane [58,59]. Moreover, it is possible to distinguish Lo domains from gel domains from the characteristic fluorescence lifetime of the probe in each phase [60]. These results combined to those obtained with other probes (Fig. 3) give a thorough description of the biophysical properties and domain organization of the membrane under study, either cellular [9] or model [9,59,60].

4. HOW TO BETTER UNDERSTAND ORDERED DOMAINS AND THEIR FUNCTION IN CELL MEMBRANES?

4.1 Can the Diversity of Lipid Domains Be Determined?

Currently, it is recognized that some cellular compartments and membrane microdomains exhibit a characteristic lipid composition both in terms of the polar head group moiety and acyl chain length and unsaturation degree [3,61–64]. Lipidomic approaches have revealed that membranes comprise a great variety of lipid species [4,5,65]. In *S. cerevisiae*, a total of 250 molecular

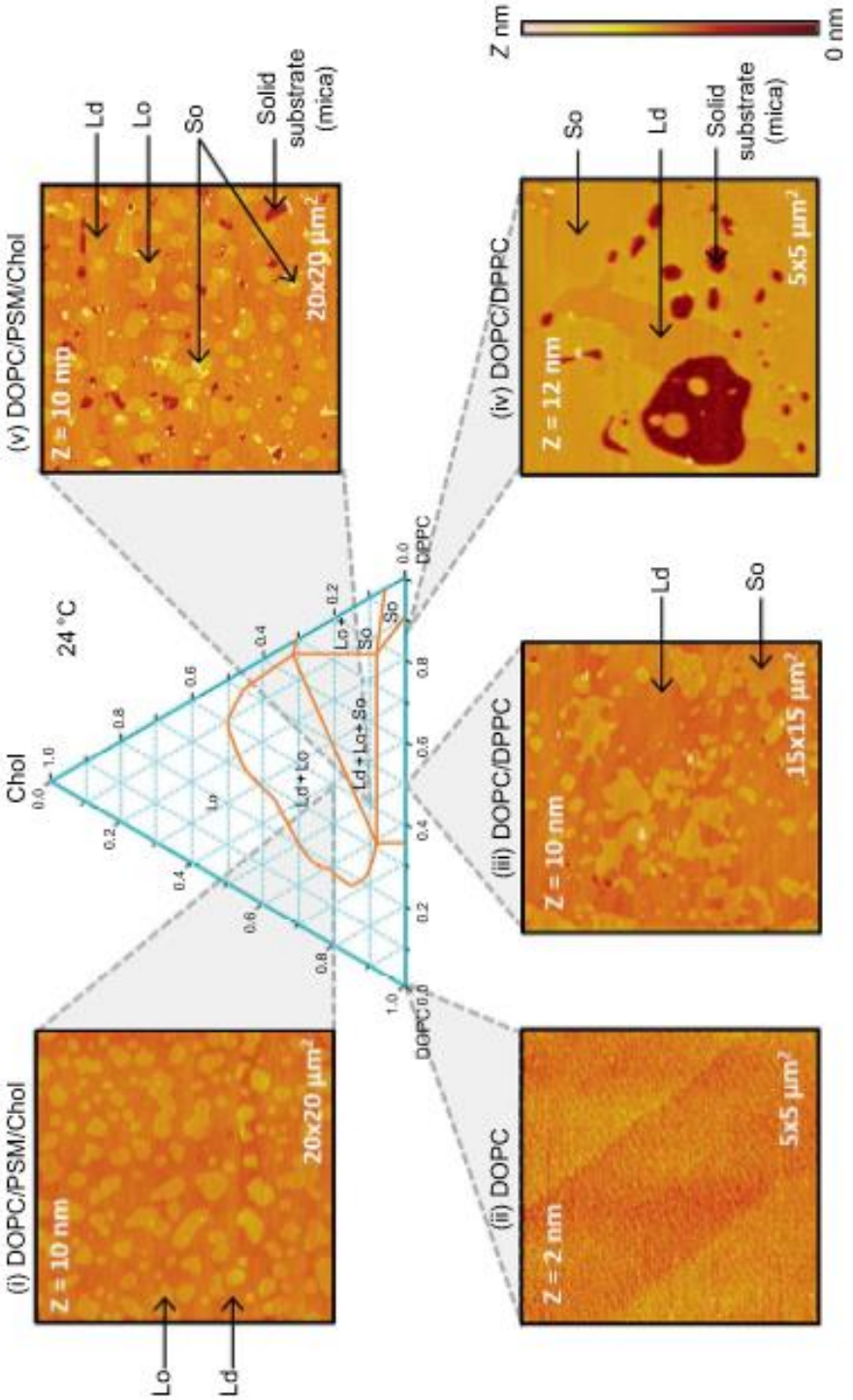

Figure 5 See legend on next page.

lipid species and 21 major lipid classes were identified [4]. In mouse macrophages, the number of lipid species may rise over 400 [6]. Potentially, the diversity of lipid domains can match the number of lipid species. This number is however reduced because many lipids will have quite similar structures and T_m and will not tend to phase-separate, others are not present in sufficient amounts to be segregated from the remainder lipids, and sterols can have a homogenizing effect as mentioned above and possibly other molecules can too. Moreover, the biophysical variety of these domains shall be identical to the array of lipid lamellar phases that can be identified in model systems—fluid or Ld, Lo, gel or So, crystalline. Occasionally, the lipid phases will not totally explain how lipids organize the variety of membrane domains.

In this context, *S. cerevisiae* is a particularly relevant organism to address important questions regarding membrane microdomain organization and function. As mentioned in the previous paragraph, its lipidome has been recently analyzed by mass spectrometry approaches [66]. It presents a major Lo-forming sterol in its PM (Erg) and only three classes of complex SLs, which are mostly acylated with a C26:0-2-OH acyl chain, inositolphosphorylceramide (IPC), mannosylinositolphosphorylceramide (MIPC), and mannosyldiinositolphosphorylceramide ($M(IP)_2C$) [67] (Fig. 1). Thus, it is expected that the diversity of domains is quite restricted as compared, e.g., to a human cell. *S. cerevisiae* has other features that render its lipidome much simpler, such as the absence of polyunsaturated fatty acids [62]. Using deletion mutants of *S. cerevisiae*, or other model organisms such as *Neurospora crassa*, that are unable to synthesize a certain SL or sterol is quite useful. However, inhibiting the synthesis of one lipid will eventually lead to changes in the levels of many others. In particular, when studying the

Figure 5 Phase diagram for the ternary mixture DOPC/DPPC/Chol obtained at 24 °C, where the different regions of phase coexistence can be distinguished. Surrounding the diagram are AFM images corresponding to SLB of different lipid compositions (indicated in the phase diagram) and spanning a wide range of membrane phase behavior: (i) a three-component SLB exhibiting Lo/Ld phase separation; (ii) a pure DOPC SLB in the Ld phase (note the expanded *z*-scale: the bilayer is completely flat); (iii) a binary SLB displaying gel (So)/Ld phase coexistence, with predominance of the Ld; (iv) a binary SLB with a gel (So)/Ld coexistence with a larger fraction of gel phase; (v) a ternary-component SLB showing a Ld/Lo/So three-phase coexistence. As the lipid composition varies so does the phase behavior, with lipid domains displaying different sizes and shapes according to their physical nature, and area fractions of the lipid phases quantitatively related to the molar proportions of the phases predicted by the phase diagram. *Adapted from Ref. [2].*

role of certain SL ordered membrane domains, it is important to ensure that the sterol profile remains fairly unchanged when compared to the wild type. There are not that many situations where this is verified because there are genetic interactions between sterol and SL biosynthetic pathways [68]. Therefore, whenever possible, the analysis of lipid profiles should precede or accompany the biophysical studies carried out *in vivo* or with isolated cellular membranes (e.g., Ref. [69]). Our group has focused on yeast mutants that maintain a sterol profile quite similar to the wt in order to understand the role of small structural alterations of SLs in membrane properties. One such mutant is scs7Δ which lacks the 2-hydroxylation on the fatty acyl chain of SLs [68,70] and one other is ipt1Δ [20,71].

The main antifungal therapies currently in clinical use act at the level of the PM of fungi, taking advantage of the known differences between the membrane of such organisms and human cells. One of the most striking examples is the already mentioned absence of Chol whose role is played in fungi by Erg (Fig. 1). Despite the subtlety of the structural differences between these two molecules, its presence in the membranes gives them markedly distinct biophysical properties [72–75]. Other examples show that minute structural differences in lipids can induce marked changes in biophysical behavior with important biological implications (e.g., Refs. [10,30,69]). Thus, the models used should reflect such differences.

In the case of bacteria cell membranes, other lipids come into play. In a recent study, through a biophysical approach, it was assessed which membrane model would better mimic the PM of Gram-positive bacteria. By measuring the minimal inhibitory concentration of aurein peptides against intact bacteria and correlating it with the behavior of these peptides in model membrane systems, it was determined that POPC/POPG (1:1) and cardiolipin (CL)/POPG (1:1) (Fig. 1) are suitable models to gain insight on the mode of action of aurein peptides on *Staphylococcus aureus*, whereas POPE/POPG (1:1) (Fig. 1) lipid system is more indicated to mimic *Bacillus cereus* [76].

4.2 How Many Different Lipids Are Required to Mimic a Biological Membrane?

The advantage of biomimetic model systems is their simplicity; therefore, they should incorporate a limited number of components, and their complexity increased only if absolutely required. Sometimes it is better to use simpler models sharing the property of interest with the biological counterpart, for example, acyl chain order, as measured through the fluorescence

anisotropy of a given probe, than to prepare a very complicated mixture that ultimately will never match the biological system, and presents more challenges regarding results interpretation. However, since the PM is highly heterogeneous and compartmentalized, the development of membrane models that mimic this heterogeneity is essential [2] and at some point the use of lipid mixtures will be mandatory.

To avoid misinterpretations and obtain an accurate and quantitative description (e.g., a phase diagram), the complexity of the system should be increased stepwise. As the complexity of the lipid mixtures increases, a complete description of the lipid domains requires the use of more techniques or more probes when using fluorescence spectroscopy/microscopy approaches [58].

As described above, the presence of SL-enriched gel domains in the PM of *S. cerevisiae* was established [9]. Therefore, it is important to characterize the biophysical properties (e.g., thermotropic behavior) of these gel domains and evaluate their function. One-component model systems are useful as they allow the biophysical characterization of pure lipids and even evaluate other biomolecules' interactions with this specific lipid. For instance, the T_m of pure IPC, one of the major yeast SLs, determined by DPH fluorescence anisotropy (measure of a probe rotational dynamics) was 53.4 °C. Comparing with the T_m of pure 18-carbon acyl chain variant of sphingomyelin (C18-SM, Fig. 1), determined to be 44.0 °C, the higher T_m of IPC indicates a tighter packing of IPC molecules in the gel phase as compared to sphingomyelin (SM) [32]. In particular, the T_m of IPC is quite close to the one determined for gel domains in reconstituted PM lipid extracts, suggesting that IPC is an important component of these domains [9]. In this way, membrane model systems that mimic biological gel domains can be mainly formed by saturated long-chain SLs with a high T_m [9,72] or more artificially by saturated glycerophospholipids with a similar T_m. However, because many membrane properties arise due to the presence of lateral heterogeneities, one-component systems are only a starting point.

Phase diagrams became essential tools in the study of lipid domains [77,78]. They can be obtained through multiple procedures and express the phase behavior for a plethora of lipid systems, whether single or multicomponent. An example is given in Fig. 5. Phase diagrams translate in a graphical representation the interactions between lipids in a mixture and how these dictate the phase behavior, according to lipid proportions or other parameters, such as temperature or pressure. The analysis of phase diagrams allows for the preparation of lipid mixtures exhibiting the desired phase

behavior, e.g., single Lo, gel/fluid, or Ld/Lo bilayers, and with the desired proportions of lipid phases. Therefore, the most biologically relevant lipid compositions can be easily identified. Another important aspect is that by knowing the phase behavior for the chosen lipid system, all the subsequent studies, such as disclosing the interaction of drugs with the membrane, shall be more conveniently interpreted and quantitative information can be retrieved, such as the partition coefficient of a drug or protein between two different lipid phases (e.g., Refs. [79,80]).

Two types of binary mixtures are important to understand ordered lipid domain formation and properties. Membrane models with one sterol and one phospholipid are essential to characterize the lipid–sterol interactions, particularly the Lo-forming ability of the sterol. For example, the phase behavior of the binary mixtures DOPC/Chol and DPPC/Chol at room temperature showed no formation of Lo phase in mixtures of DOPC and Chol, whereas there was gel/Lo phase coexistence for DPPC/Chol at this temperature (Fig. 5). None of these could be used to mimic putative raft-like Lo/Ld membrane domains. Mixtures of two phospholipids are mostly used to study gel/fluid phase separation, as illustrated in Fig. 5 for the binary mixtures of DPPC and DOPC, 1:1 and 88:12 (Fig. 5) [23]. For example, the biophysical study of the binary mixture POPC/PhyCer (see Fig. 1 for structures) revealed that the compactness of PhyCer-rich gel domains in a fluid POPC matrix is quite similar to the one observed for the SL-rich gel domains detected in living *S. cerevisiae* cells [9] (in both cases long fluorescence lifetime of *t*-PnA is ~40 ns at 24 °C).

Many of the tools used to investigate mammalian cell membranes were not applied to the PM of yeast, but it is the application of those same techniques that will highlight the differences between them [72]. Therefore, we characterized photophysical properties of fluorescent membrane probes in yeast cell membranes and liposomes that mimic the membranes of these organisms and to date have been used almost exclusively in mammalian cells. In particular, since DPH and *t*-PnA cannot be used in fluorescence microscopy due to absorption and emission mostly in the UV region and photobleaching [57], we have used other membrane probes which absorb and emit in the visible range [72]. The full range of Ld/Lo phase coexistence of POPC/Erg [81] and gel/Lo for DPPC/Erg [82], which contain the physiological levels of Erg in yeast PM [69,71], were used to conclude that Rhodamine-DOPE labels specifically disordered domains, as in models of animal cells, but *N*-7-Nitrobenz-2-oxa-1,3-diazol-4-yl-1,2-dipalmitoyl-sn-glycero-3-phosphoethanolamine (NBD-DPPE) is not useful for yeast domains whereas

it is a good probe for Lo domains in mammalian membranes. 4-(2-(6-(dibutylamino)-2-naphthalenyl)ethenyl)-1-(3-sulfopropyl)-pyridinium (di-4-ANEPPS) (and analogues) are good probes for yeast Erg-rich Lo domains [72], as previously reported for Chol-containing membranes (Fig. 3).

Regarding their role in the intracellular distribution of proteins and lipids, signal transduction and many other cellular functions, the small (20–100 nm), heterogeneous, highly dynamic, sterol and SL-enriched domains [83], known as lipid rafts, are the type of domains more actively studied. Several studies have shown that ternary lipid mixtures are the membrane models that better mimic these types of domains, which should contain one sterol and two other lipids, both glycerophospholipids or one SL, differing significantly in their T_m (low T_m and high T_m lipid) [22,23,77]. In ternary mixtures containing an SL as the high T_m lipid, the coexistence of two fluid phases as a result of preferential interaction between SLs and sterols has been detected. For instance, an equimolar mixture of *N*-palmitoylsphingomyelin (PSM), phosphatidylcholine (PC), and cholesterol shows domains in the Lo state, rich in SM and Chol that mimic lipid rafts, coexisting with an Ld phase [7,23], enriched in PC representing the surrounding fluid membrane in PM. The more artificial system DOPC:DPPC:Chol (Fig. 5) has similar behavior (note AFM image for the 2:2:1 composition). In both mixtures, the phase diagram shows not only Ld/Lo, Ld/So, and Lo/So but also a three-phase coexistence situation, Ld/Lo/So (Fig. 5). This situation should be more relevant than the typical Ld/Lo, at least in the case of yeast PM, since both Lo and gel (So) domains have been identified. From these ternary phase diagrams, it can be anticipated that in PM with a high Chol concentrations, Lo-like phase should predominate [16]. This notion is supported by the photophysical parameters of a series of laurdan dyes, such as general polarization, anisotropy, and fluorescence lifetime for a set of model liposomes exhibiting Ld, Lo, or gel phases compared to the ones obtained for probes incorporated in the PM of living fibroblasts [48].

The ternary system DOPC/DPPC/Chol was used to study the role of lipid phases and domains on the interactions of the membrane with ethanol [11]. The phase diagram in Fig. 5 was used to prepare SLB with compositions corresponding to the different single- and two-phase situations and confirmed by AFM as shown by the images around the phase diagram. For comparison, the system DOPC/PSM/Chol was also employed. In this study, we have concluded that the interaction of ethanol with lipid bilayers depends not so much on the type of high T_m lipid, but rather that it is

strongly affected by the type and number of lipid phase(s) present, and moreover on the phase domain organization and proportion [11].

Ternary model systems allow for a better understanding of the influence of the lateral heterogeneities of lipids in membrane protein distribution and functionality [84,85]. Through the evaluation of the sequestration and oligomerization of membrane proteins in the presence of coexisting Lo and Ld domains, an affinity of urokinase receptor (uPAR), a GPI-anchored protein, for Lo lipid regions and a sequestration behavior of uPAR were reported in a planar model membrane platform with raft-mimicking lipid mixtures (ternary system DOPC/DPPC/Chol in equimolar DOPC–DPPC proportion and different Chol contents) [84].

Quaternary systems can also be used to understand the effect that changes in lipid composition of the PM caused by bioactive molecules, growth condition or other challenges, have on its structure and biophysical properties. For instance, to better understand the mechanism of action of 2-hydroxyoleic acid (2OHOA) as an anticancer agent, mixtures of POPC, POPE, and PSM were used because these three phospholipid classes were the ones that suffered the major alterations in U118 glioma cells, before and after treatment with this antitumor compound. In addition, Chol was included due to its abundance in the PM and strong influence in its biophysical properties [13,86]. Through this work, it was concluded that the alterations observed in the levels of phospholipid classes increase the lateral packing of SM/Chol-enriched Lo. The comparison with lipid extracts allowed to conclude on the role of the changes in acyl chain composition (note that the same acyl chains were present in the different phospholipids used in the model systems), and it could be concluded that the remodeling of the phospholipid acyl chains with 2OHOA leads to a global membrane order decrease [34]. Such drastic changes on membrane organization are undoubtedly important for the anticancer effects of 2OHOA [13,15].

4.3 In What Situations Other Biomembrane Features Should Be Comprised?

With the mixtures described above and others with similar compositions, the intention is usually to mimic the outer leaflet of the PM, where most of the SLs reside and form domains, and in this respect, the absence of lipid transversal asymmetry should be a minor issue. In fact, the gel domains found in yeast PM seem to be similar whether they are detected directly in living cells, isolated PM, or PM lipid extracts reconstituted in liposomes, where lipid asymmetry is lost [9]. In these latter, the compactness of the gel domains

was slightly higher, but this is more probably due to the absence of proteins than due to the loss of asymmetry. Nonetheless, probe analogues with charged groups that label exclusively the outer leaflet of the PM (e.g., TMA-DPH) [87] can be used to establish a more direct comparison with living cell labeling and assess the importance of transmembrane lipid asymmetry.

To examine the importance of an asymmetric lipid environment in protein–membrane interactions, polymer-tethered lipid bilayers were prepared layer by layer through the Langmuir–Blodgett (LB)/Langmuir–Schaefer (LS) technique. To provide homogeneous Ld-forming and Lo–Ld phase-separating lipid mixtures, LB composition was DOPC/Chol (2:1) with 5 mol% diC18M50 (1,2-dioctadecyl-*sn*-glycero-3-*n*-poly(2-methyl-2-oxazoline)), and LS (top leaflet) was DOPC/DPPC/Chol (1:1:1). The results in this asymmetric system were confronted with those obtained in symmetric lipid bilayers in this same work, and an influence of bilayer asymmetry on the sequestering of integrins in ternary raft-mimicking lipid mixtures was demonstrated [85].

To understand the formation of ordered domains, or the interaction of bioactive molecules and proteins/peptides with the inner leaflet of the PM, very different compositions from the examples given above should be used (e.g., Refs. [88,89]). In fact, although recent advances have been achieved both experimentally and theoretically, there is still a large *gap* in the number of studies and our understanding of lipid organization in the inner leaflet as compared to the outer leaflet of eukaryotic PM [90].

In the context of ordered domain formation, it is important to note that while the PM of eukaryotes is rich in Lo-forming sterol, the inner membranes have much lower levels of Chol, or Erg in the case of yeast [62,91]. Moreover, the composition of each organelle membrane is unique, as very well exemplified by the presence of CL almost exclusively in the inner mitochondrial membrane [3], and little is known about ordered domains in these membranes, but their biophysical properties will certainly be very different from those in the PM [59].

Another relevant feature is the pH characteristic of different membrane compartments. In particular, whereas the environment in the cytosolic side of the PM is close to neutrality in terms of pH, this is not the case for other organelles. To predict the biophysical consequences of sphingosine (Sph) accumulation in lysosomes occurring in Niemann–Pick type C (NPC) patients and compare to the possible effects on the PM, studies using POPC (fluid) and POPC/PSM/Chol lipid bilayers (Ld/Lo) at two different pH values were carried out [92]. The study with POPC allowed concluding that

the major consequence of Sph accumulation is the formation of an Sph-rich gel-like phase. The study with the ternary mixture pointed to the fact that the stability of this gel decreases as the fraction of Lo raft-like domains increases. Moreover, in both cases, the alterations induced by Sph were markedly different whether the PM neutral pH or the lysosomal pH of 5.0 was being used.

In the context of antitubercular drug research, both membrane interactions and the effect of pH are crucial [93,94]. During its distribution in the body, antitubercular agents, such as the first-line drug isoniazid (Inh), face different pH environments from the near neutral physiological pH found in the blood and in the cytoplasm of target cells to the acidic pH of the macrophage compartments, in which the infectious agent *Mycobacterium tuberculosis* (MTb) resides. The latter ranges from pH 6.2 to 5.0, depending on the activation state of the macrophage [95]. Concomitantly, it was found that Inh interaction with simple model membranes is pH dependent [96].

Cells in different stages, or stimulated under different physiological and pathological situations, present different membrane lipid composition and properties. In yeast, different cell growth conditions often lead to strong enrichment of certain SL subclass [66]. Cellular adaptation to hydrogen peroxide in *S. cerevisiae* leads to changes of the PM physical properties concomitant with a reduction by 80% of 2-hydroxy-very-long-chain fatty acids [69]. Therefore, there is no unique model that faithfully reproduces the biophysical properties of a given organism cell membrane. The stepwise approach here described (Fig. 2), ranging from a single-component model system, through more complex models systems, membrane lipid extracts, isolated PM, and finally living cells, combined with detailed quantitative information retrieved from complementary biophysical approaches, will allow the understanding at a molecular level of the lipid-dependent organization of the PM. Spanning a large range of molar proportions of the lipid mixtures and using the appropriate phase diagrams to establish quantitative relations between biophysical properties and lipid composition will solve most of the problems related to variations in lipid proportions with growth condition, stimuli, etc., because these differences are contained in the several compositions studied in the model systems and the trend in biophysical properties quantitatively related with these compositions. With this knowledge, it is possible to improve the design of suitable PM model systems to pursue further studies and answer other pressing questions regarding, on the one hand, PM structure and dynamics, and on the other hand, drug membrane interactions.

5. WHAT ABOUT BIOELECTROACTIVE MOLECULES AND THEIR REDOX BEHAVIOR?

Besides the influence that distinct lipid domains can exert in the interaction of foreign molecules with the membrane, they can also modulate the redox behavior of electrochemically active molecules. Biological electroactive molecules have been studied in a more biomimetic context in recent years, in lipid systems with diversified phase behavior.

Epinephrine interaction with lipid bilayers has only very recently been disclosed, using complementary biophysical approaches, for a wide range of lipid compositions—fluid (DOPC), gel (DPPC), fluid/gel (DOPC/DPPC 1:1), and Lo/Ld (DOPC/DPPC/Chol 2:2:1) [25]. It was determined, by fluorescence spectroscopy, using epinephrine intrinsic fluorescence, that epinephrine interacts, although weakly, with all lipid bilayers investigated. In terms of its redox properties, epinephrine did not display a distinct behavior regarding the lipid bilayer to which it was associated. This means that the oxidation peak occurs at the same potential and oxidation–reduction peak separation is also identical in all cases. However, cyclic voltammetry showed that about the triple of epinephrine molecules adsorbed to the fluid bilayer when compared to the remaining lipid systems (Fig. 4B explains how these values are obtained). The most striking observation was, however, that all the lipid membranes studied, independently of their lipid composition or phase behavior, stabilized epinephrine from the chemical point of view. While free in solution at pH 7.4, epinephrine degrades through irreversible oxidation over time (forming polymers or cyclizing); when bound to a membrane it maintains its chemical structure and becomes protected against structural alterations, as shown by cyclic voltammetry, since the same oxidation and reduction peaks were continuously registered over time for epinephrine when bound to the membranes [25]. Thus, the lipid bilayer environment of cell membranes may act as a reservoir of stabilized hormone molecules, contributing to their biological activity.

Ubiquinone-10 (UQ10) cyclic voltammetry on lipid monolayers supported on a mercury electrode has shown a positive shift and a broadening of the oxidation peak when incorporated into an Lo/Ld (DOPC/PSM/Chol) membrane in opposition to a gel/fluid (DOPC/PSM) membrane [97]. Regarding the distribution of UQ10, the authors report that it tends to segregate in UQ10-rich pools in a pure gel membrane, while

it preferentially localizes in the fluid phase when incorporated into a gel/fluid system. Moreover, in an Lo/Ld matrix, UQ10 is mainly located along the boundaries of Ld and Lo phases [97].

6. WHY STUDY BIOMEMBRANE ORDERED DOMAINS? AN INTRIGUING COINCIDENCE BETWEEN *IN VITRO* AND *IN VIVO* STUDIES

When the cell membrane is envisioned as a therapeutic target, it is not enough to consider each individual molecular interactions, since molecules diffuse laterally at high speed (lateral diffusion coefficients which may be on the order of 10^{-8} cm^2 s^{-1}) and provide numerous interactions in a very short time range [1]. Unlike most "classical" drugs that in principle act specifically on a target molecule, usually a protein, those directed to biomembranes can have as mechanism of action the changes caused in lipid organization and biophysical properties, so it is not possible to identify a single molecular target.

The biological actions of 2-hydroxylated fatty acids (2OHFAs) have been intensely studied in the past few years regarding, among other aspects, the alterations they promote in the membrane biophysical properties. Recent studies have shown that mono- and polyunsaturated hydroxylated fatty acids are promising agents for the treatment of tumors [13,17], 2-hydroxyoleic acid (2OHOA), Alzheimer's disease [18], 2-hydroxydocosahexaenoic acid (2OHDHA), and to display high antiinflammatory effects [98], 2-hydroxyarachidonic acid (2OHARA). We established that these 2OHFA can spontaneously insert into membranes, and that generally, they induce both a decrease in the global membrane order and in the packing of acyl chains as probed by DPH and *t*-PnA [26]. These observations were transversal to all types of lipid phases analyzed individually—gel, Ld, Lo. Nonetheless, Lo seemed to exhibit the highest resistance to the disordering effect induced by the 2OHFA [26] (Fig. 6A). This phase was, however, the one that underwent the most significant changes at the lipid–water interface as detected by di-4-ANEPPS (Fig. 6B) [26]. Those changes include the hydration state, solvent relaxation dynamics, and especially the dipole potential. In the case of Chol-containing Lo membranes, the large dipole potential which is due to the interactions between Chol and SM is reduced almost to the levels of Ld and gel which are (practically) devoid of Chol. Such dramatic effect was attributed to a

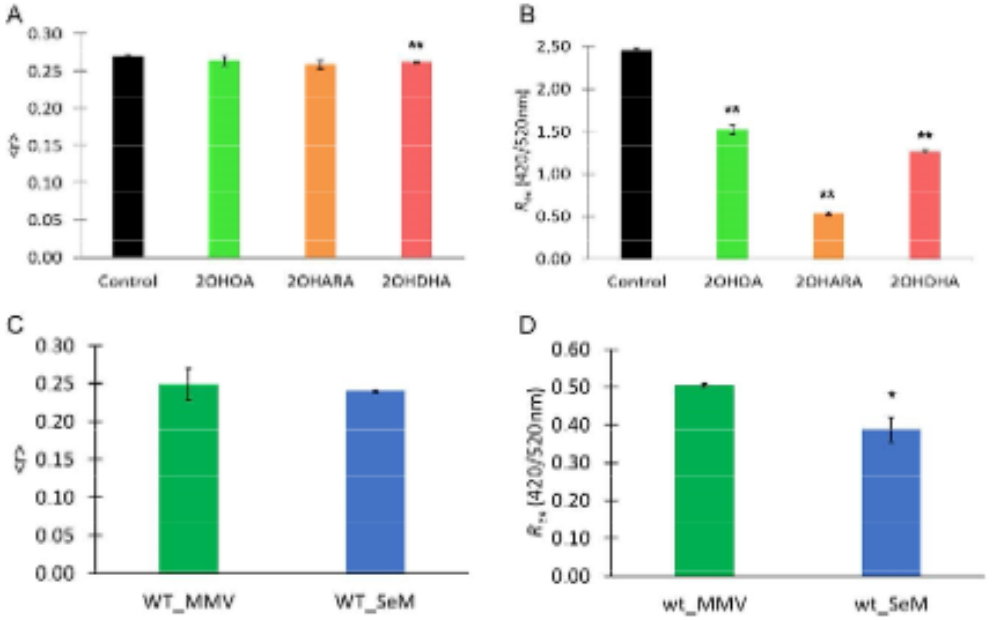

Figure 6 Fluorescence spectroscopy analysis of POPC/PSM/Chol (25.2:35.5:39.3 mol ratio) vesicles with a single Lo phase in the absence and presence of 2-hydroxylated fatty acids (A, B) and of living *Neurospora crassa* conidia grown in different culture media (MMV, Vogel's minimal medium; SeM, supplemented Vogel's medium) at 30 °C (C, D). (A, C) DPH steady-state fluorescence anisotropy. (B, D) membrane dipole potential expressed as the ratio of di-4-ANEPPS fluorescence intensity produced by excitation at 420 nm to that produced by excitation at 520 nm, R_{ex} (420 nm/520 nm). The values are the mean ± SD of at least three independent experiments. $^{*}p < 0.01$, $^{**}p < 0.001$ vs. control (A, B); SeM vs. MMV (C, D). 2OHOA, 2-hydroxyoleic acid (C18:1); 2OHARA, 2-hydroxyarachidonic acid (C20:4); and 2OHDHA, 2-hydroxydocosahexaenoic acid (C22:6).

competition of the hydroxyl group from 2-OHFA with the one from Chol for hydrogen bonding with the SL headgroup [26].

While it is established that the abundance of PM SL classes depends on growth conditions in *S. cerevisiae*, we were interested to know if similar observations are valid for a more complex, multicellular organism, the filamentous fungus *N. crassa*. Therefore, we studied the dependence of membrane biophysical properties on growth media in *N. crassa* conidia (Fig. 6C and D). We observed that the steady-state anisotropy of DPH, reflecting the global order of the membrane, for wt cells in supplemented Vogel's medium (SeM) when compared to wt in Vogel's minimal medium (MMV) is identical (Fig. 6C). However, as can be seen in Fig. 6D, comparing the ratio of the di-4-ANEPPS fluorescence intensity that is known to be proportional to the membrane dipole potential [99], wt grown in SeM showed a clearly

smaller ratio relatively to wt grown in MMV, by ~23%. This is an example of an *in vivo* experiment that illustrates how membrane biophysical properties and organization can be significantly affected without noticeable changes of global membrane order/fluidity, with an intriguing parallel to the example of the previous paragraph describing the effect of 2OHOA in Lo model membranes.

7. CONCLUDING REMARKS

Membrane ordered domains, their formation, properties, organization, and biological functions are a pressing matter in the study and comprehension of biological membranes [100]. Throughout this chapter, it was sought to highlight the preponderance that ordered phases exhibit not only as abundant constituents of the PM but also as key modulators of membrane function and organization. Novel strategies and complementary approaches to investigate ordered domains were presented. These tools will allow to further explore their properties and biological roles. Further developments are, however, undoubtedly necessary.

From the examples presented in this work, and many more, it can be safely affirmed that ordered lipid domains are decisive for membrane organization and they should always be considered when trying to understand lipid–protein interactions as well as membrane interactions with other bioactive molecules. This is true whether dealing with endogenous compounds, such as epinephrine and UQ10, or even bioactive lipids such as Sph or drugs, and examples were given related to, e.g., cancer and microbial infections.

In that regard, the topic of how to design and improve membrane model systems mimicking chief properties of biomembranes, in particular those related to ordered domains, was given special emphasis. The importance of studying different lipid systems with distinct complexity degrees, both in terms of lipid composition and phase behavior, spanning a large range of proportions of their components and framed within the quantitative tools provided by phase diagrams was established. The use of complementary biophysical approaches, namely employing multiple fluorescent dyes that report different membrane domains and biophysical properties, is required to fully understand membrane organization and membrane–drug interactions. The awareness of how each technique can be applied to only a few or to most types of membrane systems, such as SLB or liposomes, isolated PM or membranes of living cells, will help to tackle the membrane ordered domains challenge.

ACKNOWLEDGMENTS

This work was financed by Portuguese national funds through Fundação para a Ciência e a Tecnologia (F.C.T., I.P.): Ph.D. fellowship SFRH/BD/64442/2009; research grant PEst 2015–2020 (UID/Multi/00612/2013), and IF2012 initiative (POPH, Fundo Social Europeu).

REFERENCES

[1] E.L. Elson, E. Fried, J.E. Dolbow, G.M. Genin, Phase separation in biological membranes: integration of theory and experiment, Annu. Rev. Biophys. 39 (2010) 207–226.
[2] J. Malinsky, M. Opekarova, G. Grossmann, W. Tanner, Membrane microdomains, rafts, and detergent-resistant membranes in plants and fungi, Annu. Rev. Plant Biol. 64 (2013) 501–529.
[3] W. Stillwell, An Introduction to Biological Membranes, first ed., Elsevier, San Diego, CA, 2013.
[4] C.S. Ejsing, J.L. Sampaio, V. Surendranath, E. Duchoslav, K. Ekroos, R.W. Klemm, K. Simons, A. Shevchenko, Global analysis of the yeast lipidome by quantitative shotgun mass spectrometry, Proc. Natl. Acad. Sci. U.S.A. 106 (2009) 2136–2141.
[5] J.L. Sampaio, M.J. Gerl, C. Klose, C.S. Ejsing, H. Beug, K. Simons, A. Shevchenko, Membrane lipidome of an epithelial cell line, Proc. Natl. Acad. Sci. U.S.A. 108 (2011) 1903–1907.
[6] E.A. Dennis, R.A. Deems, R. Harkewicz, O. Quehenberger, H.A. Brown, S.B. Milne, D.S. Myers, C.K. Glass, G. Hardiman, D. Reichart, A.H. Merrill Jr., M.C. Sullards, E. Wang, R.C. Murphy, C.R.H. Raetz, T.A. Garrett, Z. Guan, A.C. Ryan, D.W. Russell, J.G. McDonald, B.M. Thompson, W.A. Shaw, M. Sud, Y. Zhao, S. Gupta, M.R. Maurya, E. Fahy, S. Subramaniam, A mouse macrophage lipidome, J. Biol. Chem. 285 (2010) 39976–39985.
[7] R.F.M. De Almeida, L.M.S. Loura, A. Fedorov, M. Prieto, Lipid rafts have different sizes depending on membrane composition: a time-resolved fluorescence resonance energy transfer study, J. Mol. Biol. 346 (2005) 1109–1120.
[8] C.B. Yuan, J. Furlong, P. Burgos, L.J. Johnston, The size of lipid rafts: an atomic force microscopy study of ganglioside GM1 domains in sphingomyelin/DOPC/cholesterol membranes, Biophys. J. 82 (2002) 2526–2535.
[9] F. Aresta-Branco, A.M. Cordeiro, H.S. Marinho, L. Cyrne, F. Antunes, R.F.M. De Almeida, Gel domains in the plasma membrane of saccharomyces cerevisiae highly ordered, ergosterol-free, and sphingolipid-enriched lipid rafts, J. Biol. Chem. 286 (2011) 5043–5054.
[10] C.R. Vieira, J.M. Munoz-Olaya, J. Sot, S. Jimenez-Baranda, N. Izquierdo-Useros, J.L. Abad, B. Apellaniz, R. Delgado, J. Martinez-Picado, A. Alonso, J. Casas, J.L. Nieva, G. Fabrias, S. Manes, F.M. Goni, Dihydrosphingomyelin impairs HIV-1 infection by rigidifying liquid-ordered membrane domains, Chem. Biol. 17 (2010) 766–775.
[11] J.T. Marquês, A.S. Viana, R.F.M. De Almeida, Ethanol effects on binary and ternary supported lipid bilayers with gel/fluid domains and lipid rafts, Biochim. Biophys. Acta 1808 (2011) 405–414.
[12] P.J. Quinn, C. Wolf, An X-ray diffraction study of model membrane raft structures, FEBS J. 277 (2010) 4685–4698.
[13] G. Barcelo-Coblijn, M. Laura Martin, R.F.M. de Almeida, M. Antonia Noguera-Salva, A. Marcilla-Etxenike, F. Guardiola-Serrano, A. Lueth, B. Kleuser, J.E. Halver, P.V. Escriba, Sphingomyelin and sphingomyelin synthase (SMS) in the

malignant transformation of glioma cells and in 2-hydroxyoleic acid therapy, Proc. Natl. Acad. Sci. U.S.A. 108 (2011) 19569–19574.
[14] L. Ginsberg, J.R. Atack, S.I. Rapoport, N.L. Gershfeld, Evidence for a membrane lipid defect in Alzheimer disease, Mol. Chem. Neuropathol. 19 (1993) 37–46.
[15] P.V. Escriba, J.M. Gonzalez-Ros, F.M. Goni, P.K. Kinnunen, L. Vigh, L. Sanchez-Magraner, A.M. Fernandez, X. Busquets, I. Horvath, G. Barcelo-Coblijn, Membranes: a meeting point for lipids, proteins and therapies, J. Cell. Mol. Med. 12 (2008) 829–875.
[16] R.F.M. de Almeida, E. Joly, Crystallization around solid-like nanosized docks can explain the specificity, diversity, and stability of membrane microdomains, Front. Plant Sci. 5 (2014) 14.
[17] V. Llado, A. Gutierrez, J. Martinez, J. Casas, S. Teres, M. Higuera, A. Galmes, C. Saus, J. Besalduch, X. Busquets, P.V. Escriba, Minerval induces apoptosis in Jurkat and other cancer cells, J. Cell. Mol. Med. 14 (2010) 659–670.
[18] M.A. Fiol-deRoque, R. Gutierrez-Lanza, S. Teres, M. Torres, P. Barcelo, R.V. Rial, A. Verkhratsky, P.V. Escriba, X. Busquets, J.J. Rodriguez, Cognitive recovery and restoration of cell proliferation in the dentate gyrus in the 5XFAD transgenic mice model of Alzheimer's disease following 2-hydroxy-DHA treatment, Biogerontology 14 (2013) 763–775.
[19] F.C. Santos, A.S. Fernandes, A. Videira, R.F.M. de Almeida, Biophysical characterization of Neurospora crassa membrane and its sensitivity to Staurosporine, Eur. Biophys. J. 42 (2013) S52.
[20] C.A.C. Antunes, J.T. Marquês, A.S. Viana, H.S. Marinho, R.F.M. De Almeida, Sphingolipid domains of Saccharomyces cerevisiae strain resistant to nystatin and miconazole: towards a relation between membrane biophysical properties and resistance to antifungal drugs, Biomed. Biopharm. Res. 11 (2014) 266.
[21] R.F.M. De Almeida, L.M.S. Loura, A. Fedorov, M. Prieto, Nonequilibrium phenomena in the phase separation of a two-component lipid bilayer, Biophys. J. 82 (2002) 823–834.
[22] R.F.M. de Almeida, A. Fedorov, M. Prieto, Sphingomyelin/phosphatidylcholine/cholesterol phase diagram: boundaries and composition of lipid rafts, Biophys. J. 85 (2003) 2406–2416.
[23] R.F. de Almeida, J. Borst, A. Fedorov, M. Prieto, A.J. Visser, Complexity of lipid domains and rafts in giant unilamellar vesicles revealed by combining imaging and microscopic and macroscopic time-resolved fluorescence, Biophys. J. 93 (2007) 539–553.
[24] J.T. Marquês, R.F.M. De Almeida, A.S. Viana, Biomimetic membrane rafts stably supported on unmodified gold, Soft Matter 8 (2012) 2007–2016.
[25] J.T. Marquês, A.S. Viana, R.F.M. de Almeida, A biomimetic platform to study the interactions of bioelectroactive molecules with lipid nanodomains, Langmuir 30 (2014) 12627–12637.
[26] A. Khmelinskaia, M. Ibarguren, R.F.M. de Almeida, D.J. Lopez, V.A. Paixao, H. Ahyayauch, F.M. Goni, P.V. Escriba, Changes in membrane organization upon spontaneous insertion of 2-hydroxylated unsaturated fatty acids in the lipid bilayer, Langmuir 30 (2014) 2117–2128.
[27] O.G. Mouritsen, Life—As a Matter of Fat: The Emerging Science of Lipidomics, first ed., Springer-Verlag, Berlin, Heidelberg, 2005.
[28] P.J. Quinn, A lipid matrix model of membrane raft structure, Prog. Lipid Res. 49 (2010) 390–406.
[29] J.C. Holthuis, T. Pomorski, R.J. Raggers, H. Sprong, G. Van Meer, The organizing potential of sphingolipids in intracellular membrane transport, Physiol. Rev. 81 (2001) 1689–1723.

[30] L. Guo, D. Zhou, K.M. Pryse, A.L. Okunade, X. Su, Fatty acid 2-hydroxylase mediates diffusional mobility of raft-associated lipids, GLUT4 level, and lipogenesis in 3T3-L1 adipocytes, J. Biol. Chem. 285 (2010) 25438–25447.
[31] D. Marsh, Handbook of Lipid Bilayers, second ed., CRC Press, Taylor & Francis Group, Boca Raton, FL, 2013.
[32] C. Klose, C.S. Ejsing, A.J. Garcia-Saez, H.J. Kaiser, J.L. Sampaio, M.A. Surma, A. Shevchenko, P. Schwille, K. Simons, Yeast lipids can phase-separate into micrometer-scale membrane domains, J. Biol. Chem. 285 (2010) 30224–30232.
[33] C. Vionnet, C. Roubaty, C.S. Ejsing, J. Knudsen, A. Conzelmann, Yeast cells lacking all known ceramide synthases continue to make complex sphingolipids and to incorporate ceramides into glycosylphosphatidylinositol (GPI) anchors, J. Biol. Chem. 286 (2011) 6769–6779.
[34] A. Martiniere, J. Runions, Protein diffusion in plant cell plasma membranes: the cell-wall corral, Front. Plant Sci. 4 (2013) 515.
[35] S.K. Saka, A. Honigmann, C. Eggeling, S.W. Hell, T. Lang, S.O. Rizzoli, Multi-protein assemblies underlie the mesoscale organization of the plasma membrane, 2nd ed., Nat. Commun. 5 (2014), article number 4509.
[36] G.S. Victoria, B. Yadav, L. Hauhnar, P. Jain, S. Bhatnagar, S.S. Komath, Mutual co-regulation between GPI-N-acetylglucosaminyltransferase and ergosterol biosynthesis in Candida albicans, Biochem. J. 443 (2012) 619–625.
[37] P. Herman, J. Vecer, M. Opekarova, P. Vesela, I. Jancikova, J. Zahumensky, J. Malinsky, Depolarization affects the lateral microdomain structure of yeast plasma membrane, FEBS J. 282 (2015) 419–434.
[38] L. Clay, F. Caudron, A. Denoth-Lippuner, B. Boettcher, S.B. Frei, E.L. Snapp, Y. Barral, A sphingolipid-dependent diffusion barrier confines ER stress to the yeast mother cell, eLife 3 (2014) e01883.
[39] L. Zheng, L. Xiong, D. Zheng, Y. Li, Q. Liu, K. Han, W. Liu, K. Tao, S. Yang, J. Xia, Bilayer lipid membrane biosensor with enhanced stability for amperometric determination of hydrogen peroxide, Talanta 85 (2011) 43–48.
[40] A.I. Michaloliakos, G.P. Nikoleli, C.G. Siontorou, D.P. Nikolelis, Rapid flow injection electrochemical detection of arochlor 1242 using stabilized lipid membranes with incorporated sheep anti-PCB antibody, Electroanalysis 24 (2012) 495–501.
[41] M.B. Fritzen-Garcia, V.C. Zoldan, I.R.W.Z. Oliveira, V. Soldi, A.A. Pasa, T.B. Creczynski-Pasa, Peroxidase immobilized on phospholipid bilayers supported on au (111) by DTT self-assembled monolayers: application to dopamine determination, Biotechnol. Bioeng. 110 (2013) 374–382.
[42] M. Li, M. Chen, E. Sheepwash, C.L. Brosseau, H. Li, B. Pettinger, H. Gruler, J. Lipkowski, AFM studies of solid-supported lipid bilayers formed at a Au(111) electrode surface using vesicle fusion and a combination of Langmuir-Blodgett and Langmuir-Schaefer techniques, Langmuir 24 (2008) 10313–10323.
[43] J. Ekeroth, P. Konradsson, F. Hook, Bivalent-ion-mediated vesicle adsorption and controlled supported phospholipid bilayer formation on molecular phosphate and sulfate layers on gold, Langmuir 18 (2002) 7923–7929.
[44] X. Wang, M.M. Shindel, S.W. Wang, R. Ragan, A facile approach for assembling lipid bilayer membranes on template-stripped gold, Langmuir 26 (2010) 18239–18245.
[45] B.P. Oberts, G.J. Blanchard, Formation of air-stable supported lipid monolayers and bilayers, Langmuir 25 (2009) 2962–2970.
[46] J.T. Marquês, R.F.M. de Almeida, A.S. Viana, Lipid bilayers supported on bare and modified gold—formation, characterization and relevance of lipid rafts, Electrochim. Acta 126 (2014) 139–150.
[47] A. Kusumi, T.K. Fujiwara, R. Chadda, M. Xie, T.A. Tsunoyama, Z. Kalay, R.S. Kasai, K.G.N. Suzuki, Dynamic organizing principles of the plasma membrane

that regulate signal transduction: commemorating the fortieth anniversary of singer and Nicolson's fluid-mosaic model, Annu. Rev. Cell Dev. Biol. 28 (2012) 215–250.
[48] S. Mazeres, E. Joly, A. Lopez, C. Tardin, Characterization of M-laurdan, a versatile probe to explore order in lipid, membranes, F1000Research 3 (2014) 172.
[49] P. Liu, R.-L. Li, L. Zhang, Q.-L. Wang, K. Niehaus, F. Baluska, J. Samaj, J.-X. Lin, Lipid microdomain polarization is required for NADPH oxidase-dependent ROS signaling in Picea meyeri pollen tube tip growth, Plant J. 60 (2009) 303–313.
[50] N. Takeshita, Y. Higashitsuji, S. Konzack, R. Fischer, Apical sterol-rich membranes are essential for localizing cell end markers that determine growth directionality in the filamentous fungus Aspergillus nidulans, Mol. Biol. Cell 19 (2008) 339–351.
[51] S.W. Martin, J.B. Konopka, Lipid raft polarization contributes to hyphal growth in Candida albicans, Eukaryot. Cell 3 (2004) 675–684.
[52] V. Wachtler, S. Rajagopalan, M.K. Balasubramanian, Sterol-rich plasma membrane domains in the fission yeast Schizosaccharomyces pombe, J. Cell Sci. 116 (2003) 867–874.
[53] D.M. Owen, P.M. Lanigan, C. Dunsby, I. Munro, D. Grant, M.A. Neil, P.M. French, A.I. Magee, Fluorescence lifetime imaging provides enhanced contrast when imaging the phase-sensitive dye di-4-ANEPPDHQ in model membranes and live cells, Biophys. J. 90 (2006) L80–L82.
[54] S. Jaikishan, J.P. Slotte, Stabilization of sphingomyelin interactions by interfacial hydroxyls—a study of phytosphingomyelin properties, Biochim. Biophys. Acta 1828 (2013) 391–397.
[55] S. Uemura, F. Shishido, M. Tani, T. Mochizuki, F. Abe, J.-I. Inokuchi, Loss of hydroxyl groups from the ceramide moiety can modify the lateral diffusion of membrane proteins in S. cerevisiae, J. Lipid Res. 55 (2014) 1343–1356.
[56] S. Garcia-Manyes, G. Oncins, F. Sanz, Effect of ion-binding and chemical phospholipid structure on the nanomechanics of lipid bilayers studied by force spectroscopy, Biophys. J. 89 (2005) 1812–1826.
[57] A.E. Bastos, S. Scolari, M. Stockl, R.F. Almeida, Applications of fluorescence lifetime spectroscopy and imaging to lipid domains in vivo, Methods Enzymol. 504 (2012) 57–81.
[58] B.M. Castro, R.F. de Almeida, L.C. Silva, A. Fedorov, M. Prieto, Formation of ceramide/sphingomyelin gel domains in the presence of an unsaturated phospholipid: a quantitative multiprobe approach, Biophys. J. 93 (2007) 1639–1650.
[59] B.M. Castro, L.C. Silva, A. Fedorov, R.F.M. de Almeida, M. Prieto, Cholesterol-rich fluid membranes solubilize ceramide domains: implications for the structure and dynamics of mammalian intracellular and plasma membranes, J. Biol. Chem. 284 (2009) 22978–22987.
[60] R.F. de Almeida, L.M. Loura, M. Prieto, Membrane lipid domains and rafts: current applications of fluorescence lifetime spectroscopy and imaging, Chem. Phys. Lipids 157 (2009) 61–77.
[61] U. Igbavboa, J. Hamilton, H.Y. Kim, G.Y. Sun, W.G. Wood, A new role for apolipoprotein E: modulating transport of polyunsaturated phospholipid molecular species in synaptic plasma membranes, J. Neurochem. 80 (2002) 255–261.
[62] R. Schneiter, B. Brugger, R. Sandhoff, G. Zellnig, A. Leber, M. Lampl, K. Athenstaedt, C. Hrastnik, S. Eder, G. Daum, F. Paltauf, F.T. Wieland, S.D. Kohlwein, Electrospray ionization tandem mass spectrometry (ESI-MS/MS) analysis of the lipid molecular species composition of yeast subcellular membranes reveals acyl chain-based sorting/remodeling of distinct molecular species en route to the plasma membrane, J. Cell Biol. 146 (1999) 741–754.
[63] B. Brugger, B. Glass, P. Haberkant, I. Leibrecht, F.T. Wieland, H.G. Krausslich, The HIV lipidome: a raft with an unusual composition, Proc. Natl. Acad. Sci. U.S.A. 103 (2006) 2641–2646.

[64] S. Ramanadham, F.F. Hsu, S. Zhang, A. Bohrer, Z.M. Ma, J. Turk, Electrospray ionization mass spectrometric analyses of phospholipids from INS-1 insulinoma cells: comparison to pancreatic islets and effects of fatty acid supplementation on phospholipid composition and insulin secretion, Biochim. Biophys. Acta 1484 (2000) 251–266.
[65] K. Ekroos, C.S. Ejsing, U. Bahr, M. Karas, K. Simons, A. Shevchenko, Charting molecular composition of phosphatidylcholines by fatty acid scanning and ion trap MS3 fragmentation, J. Lipid Res. 44 (2003) 2181–2192.
[66] C. Klose, M.A. Surma, M.J. Gerl, F. Meyenhofer, A. Shevchenko, K. Simons, Flexibility of a eukaryotic lipidome—insights from yeast lipidomics, PLoS One 7 (2012) e35063.
[67] R.L. Lester, R.C. Dickson, Sphingolipids with inositolphosphate-containing head groups, Adv. Lipid Res. 26 (1993) 253–274.
[68] X.L. Guan, C.M. Souza, H. Pichler, G. Dewhurst, O. Schaad, K. Kajiwara, H. Wakabayashi, T. Ivanova, G.A. Castillon, M. Piccolis, F. Abe, R. Loewith, K. Funato, M.R. Wenk, H. Riezman, Functional interactions between sphingolipids and sterols in biological membranes regulating cell physiology, Mol. Biol. Cell 20 (2009) 2083–2095.
[69] N. Pedroso, A.C. Matias, L. Cyrne, F. Antunes, C. Borges, R. Malhó, R.F. de Almeida, E. Herrero, H.S. Marinho, Modulation of plasma membrane lipid profile and microdomains by H2O2 in Saccharomyces cerevisiae, Free Radic. Biol. Med. 46 (2009) 289–298.
[70] X.L. Guan, M.R. Wenk, Mass spectrometry-based profiling of phospholipids and sphingolipids in extracts from Saccharomyces cerevisiae, Yeast 23 (2006) 465–477.
[71] A. Leber, P. Fischer, R. Schneiter, S.D. Kohlwein, G. Daum, The yeast mic2 mutant is defective in the formation of mannosyl-diinositolphosphorylceramide, FEBS Lett. 411 (1997) 211–214.
[72] A.E.P. Bastos, H.S. Marinho, A.M. Cordeiro, A.M. de Soure, R.F.M. de Almeida, Biophysical properties of ergosterol-enriched lipid rafts in yeast and tools for their study: characterization of ergosterol/phosphatidylcholine membranes with three fluorescent membrane probes, Chem. Phys. Lipids 165 (2012) 577–588.
[73] D.A. Mannock, R. Lewis, R.N. McElhaney, A calorimetric and spectroscopic comparison of the effects of ergosterol and cholesterol on the thermotropic phase behavior and organization of dipalmitoylphosphatidylcholine bilayer membranes, Biochim. Biophys. Acta 1798 (2010) 376–388.
[74] A. Arora, H. Raghuraman, A. Chattopadhyay, Influence of cholesterol and ergosterol on membrane dynamics: a fluorescence approach, Biochem. Biophys. Res. Commun. 318 (2004) 920–926.
[75] S. Shrivastava, A. Chattopadhyay, Influence of cholesterol and ergosterol on membrane dynamics using different fluorescent reporter probes, Biochem. Biophys. Res. Commun. 356 (2007) 705–710.
[76] J.T.J. Cheng, J.D. Hale, M. Elliott, R.E.W. Hancock, S.K. Straus, The importance of bacterial membrane composition in the structure and function of aurein 2.2 and selected variants, Biochim. Biophys. Acta 1808 (2011) 622–633.
[77] D. Marsh, Cholesterol-induced fluid membrane domains: a compendium of lipid-raft ternary phase diagrams, Biochim. Biophys. Acta 1788 (2009) 2114–2123.
[78] D. Marsh, Liquid-ordered phases induced by cholesterol: a compendium of binary phase diagrams, Biochim. Biophys. Acta 1798 (2010) 688–699.
[79] R.F. de Almeida, L.M. Loura, M. Prieto, A. Watts, A. Fedorov, F.J. Barrantes, Cholesterol modulates the organization of the gammaM4 transmembrane domain of the muscle nicotinic acetylcholine receptor, Biophys. J. 86 (2004) 2261–2272.

[80] B.M. Castro, R.F. de Almeida, E. Goormaghtigh, A. Fedorov, M. Prieto, Organization and dynamics of Fas transmembrane domain in raft membranes and modulation by ceramide, Biophys. J. 101 (2011) 1632–1641.
[81] L. Silva, A. Coutinho, A. Fedorov, M. Prieto, Competitive binding of cholesterol and ergosterol to the polyene antibiotic nystatin. A fluorescence study, Biophys. J. 90 (2006) 3625–3631.
[82] Y.W. Hsueh, K. Gilbert, C. Trandum, M. Zuckermann, J. Thewalt, The effect of ergosterol on dipalmitoylphosphatidylcholine bilayers: a deuterium NMR and calorimetric study, Biophys. J. 88 (2005) 1799–1808.
[83] D. Lingwood, K. Simons, Lipid rafts as a membrane-organizing principle, Science 327 (2010) 46–50.
[84] Y. Ge, A.P. Siegel, R. Jordan, C.A. Naumann, Ligand binding alters dimerization and sequestering of urokinase receptors in raft-mimicking lipid mixtures, Biophys. J. 107 (2014) 2101–2111.
[85] N.F. Hussain, A.P. Siegel, Y. Ge, R. Jordan, C.A. Naumann, Bilayer asymmetry influences integrin sequestering in raft-mimicking lipid mixtures, Biophys. J. 104 (2013) 2212–2221.
[86] M.L. Martin, G. Barceló-Coblijn, R.F.M. de Almeida, M.A. Noguera-Salvà, S. Terés, M. Higuera, G. Liebisch, G. Schmitz, X. Busquets, P.V. Escribá, The role of membrane fatty acid remodeling in the antitumor mechanism of action of 2-hydroxyoleic acid, Biochim. Biophys. Acta 1828 (2013) 1405–1413.
[87] F. Abe, T. Hiraki, Mechanistic role of ergosterol in membrane rigidity and cycloheximide resistance in Saccharomyces cerevisiae, Biochim. Biophys. Acta 1788 (2009) 743–752.
[88] C. Wan, V. Kiessling, D.S. Cafiso, L.K. Tamm, Partitioning of synaptotagmin I C2 domains between liquid-ordered and liquid-disordered inner leaflet lipid phases, Biochemistry 50 (2011) 2478–2485.
[89] T.-Y. Wang, J.R. Silvius, Cholesterol does not induce segregation of liquid-ordered domains in bilayers modeling the inner leaflet of the plasma membrane, Biophys. J. 81 (2001) 2762–2773.
[90] R. Shlomovitz, M. Schick, Model of a raft in both leaves of an asymmetric lipid bilayer, Biophys. J. 105 (2013) 1406–1413.
[91] G. van Meer, D.R. Voelker, G.W. Feigenson, Membrane lipids: where they are and how they behave, Nat. Rev. Mol. Cell Biol. 9 (2008) 112–124.
[92] E. Zupancic, A.C. Carreira, R.F. de Almeida, L.C. Silva, Biophysical implications of sphingosine accumulation in membrane properties at neutral and acidic pH, J. Phys. Chem. B 118 (2014) 4858–4866.
[93] V. Dartois, The path of anti-tuberculosis drugs: from blood to lesions to mycobacterial cells, Nat. Rev. Microbiol. 12 (2014) 159–167.
[94] M. Pinheiro, M. Arede, C. Nunes, J.M. Caio, C. Moiteiro, M. Lucio, S. Reis, Differential interactions of rifabutin with human and bacterial membranes: implication for its therapeutic and toxic effects, J. Med. Chem. 56 (2013) 417–426.
[95] M. Gengenbacher, S.H. Kaufmann, Mycobacterium tuberculosis: success through dormancy, FEMS Microbiol. Rev. 36 (2012) 514–532.
[96] M. Pinheiro, A.S. Silva, S. Pisco, S. Reis, Interactions of isoniazid with membrane models: implications for drug mechanism of action, Chem. Phys. Lipids 183 (2014) 184–190.
[97] L. Becucci, F. Scaletti, R. Guidelli, Gel-phase microdomains and lipid rafts in monolayers affect the redox properties of Ubiquinone-10, Biophys. J. 101 (2011) 134–143.
[98] D.H. Lopez, M.A. Fiol-deRoque, M.A. Noguera-Salva, S. Teres, F. Campana, S. Piotto, J.A. Castro, R.J. Mohaibes, P.V. Escriba, X. Busquets, 2-Hydroxy

arachidonic acid: a new non-steroidal anti-inflammatory drug, PLoS One 8 (2013) e72052.

[99] M.F. Vitha, R.J. Clarke, Comparison of excitation and emission ratiometric fluorescence methods for quantifying the membrane dipole potential, Biochim. Biophys. Acta 1768 (2007) 107–114.

[100] V.D. Gordon, P.A. Beales, G.C. Shearman, Z. Zhao, J.M. Seddon, W.C.K. Poon, S.U. Egelhaaf, Solid-like domains in mixed lipid bilayers: effect of membrane lamellarity and transition pathway, in: I. Aleš, V.K. Chandrashekhar (Eds.), In: Advances in Planar Lipid Bilayers and Liposomes, vol. 20, Elsevier Inc., Oxford, UK, 2014, pp. 137–154.

1.2. Lipid bilayers supported on bare and modified gold – Formation, characterization and relevance of lipid rafts

Electrochimica Acta 126 (2014) 139–150

Contents lists available at ScienceDirect

Electrochimica Acta

journal homepage: www.elsevier.com/locate/electacta

Review article

Lipid bilayers supported on bare and modified gold – Formation, characterization and relevance of lipid rafts

J.T. Marquês, R.F.M. de Almeida **, A.S. Viana *,[1]

Centro de Química e Bioquímica, Departamento de Química e Bioquímica, Faculdade de Ciências da Universidade de Lisboa, Ed. C8, Campo Grande, 1749-016 Lisboa, Portugal

ARTICLE INFO

Article history:
Received 28 May 2013
Received in revised form 18 July 2013
Accepted 19 July 2013
Available online 27 July 2013

Keywords:
Planar lipid bilayers
Membrane phase-separation
Lipid domains
Chemically modified gold
Atomic force microscopy

ABSTRACT

Supported lipid bilayers (SLB) comprise a very important set of model systems of biomembranes. In particular, they can be prepared on metallic surfaces such as gold electrodes, which allow a number of electrochemical studies and applications that could not be undertaken with other types of model systems, such as liposome suspensions. Also of special relevance is lipid bilayer composition, especially those combinations of lipids which permit the formation of biologically relevant membrane domains such as lipid rafts. Indeed, membrane domain organization is a crucial feature concerning not only the biophysical properties of the bilayer itself, but also the behavior and bioactivity of membrane-interacting biomolecules. In spite of its relevance, the presence of bilayer domains has not been central in many investigations involving lipid bilayers supported on conductive surfaces. Moreover, air exposed gold surface is hydrophobic, which is not ideally suitable to establish a proper interaction with the lipids polar head group. To overcome such limitation different strategies may be adopted, encompassing the fine tuning of the buffer conditions and previous surface modification by hydrophilic self-assembled monolayer (SAM) or thiolipids. This review will be focused on the formation and characterization of SLB and lipid rafts on gold substrates, illustrating the range of applications of such platforms, with examples of the study of electroactive molecules and the development of new biosensing interfaces.

1. Introduction

Biological membranes are complex structures comprising a great variety of proteins and lipids organized in several time and length scales. According to their functions biomembranes exhibit different protein/lipid ratios and also distinct lipid compositions. In many biophysical studies the use of simplified models composed by a few lipid species, many times incorporating a protein of interest, is required. These membrane model systems have emerged as excellent tools for both basic membrane research and applications, such as drug–membrane interaction and biosensing [1–7]. Lipids can be classified in different groups including phospholipids, sphingolipids, and sterols (Fig. 1a), presenting structures that can differ between organisms, cells and even sub-cellular compartments. The structural and functional diversity of lipids is such that two recent lipidomics initiatives have emerged, and a new classification system for lipid molecules was proposed [8,9]. Also, depending on the polar head groups and the length and unsaturation degree of the hydrocarbon chains, lipids confer distinct properties to the biomembranes. For instance, a single phospholipid bilayer can undergo several thermotropic phase transitions, such as the gel to fluid that occurs at the main transition temperature, T_m. Upon this transition, the bilayer changes from a highly ordered, compact and slow lateral diffusion arrangement (gel) to a disordered one (fluid). These properties are important to be considered when choosing the appropriate model to study a given physical–chemical membrane process. In many steps of the preparation of membrane model systems, including SLBs, a temperature higher than the highest T_m of the lipid mixture used is required. We have observed that under the same conditions that are appropriate for the formation of a planar SLB on gold for a low T_m lipid, tubular structures are formed when using a high T_m lipid [10]. Long-chain, saturated phospholipids are usually in the gel phase at room temperature (Fig. 1a – DPPC, PSM, GM1 and ceramide), whereas unsaturated ones are in the fluid phase (Fig. 1a – DOPC, POPC). An extensive collection of lipid phase transition temperatures can be found elsewhere [11]. By using a binary mixture of lipids from these groups, a bilayer presenting gel/fluid phase coexistence is obtained. These phases are organized into domains sharing some properties with the heterogeneities found in biological membranes [12].

* Corresponding author. Tel.: +351 21750000; fax: +351 217500088.
** Corresponding author. Tel.: +351 217500924; fax: +351 217500088.
E-mail addresses: rfalmeida@fc.ul.pt (R.F.M. de Almeida), anaviana@fc.ul.pt (A.S. Viana).
[1] ISE Member.

0013-4686/$ – see front matter © 2013 Elsevier Ltd. All rights reserved.
http://dx.doi.org/10.1016/j.electacta.2013.07.117

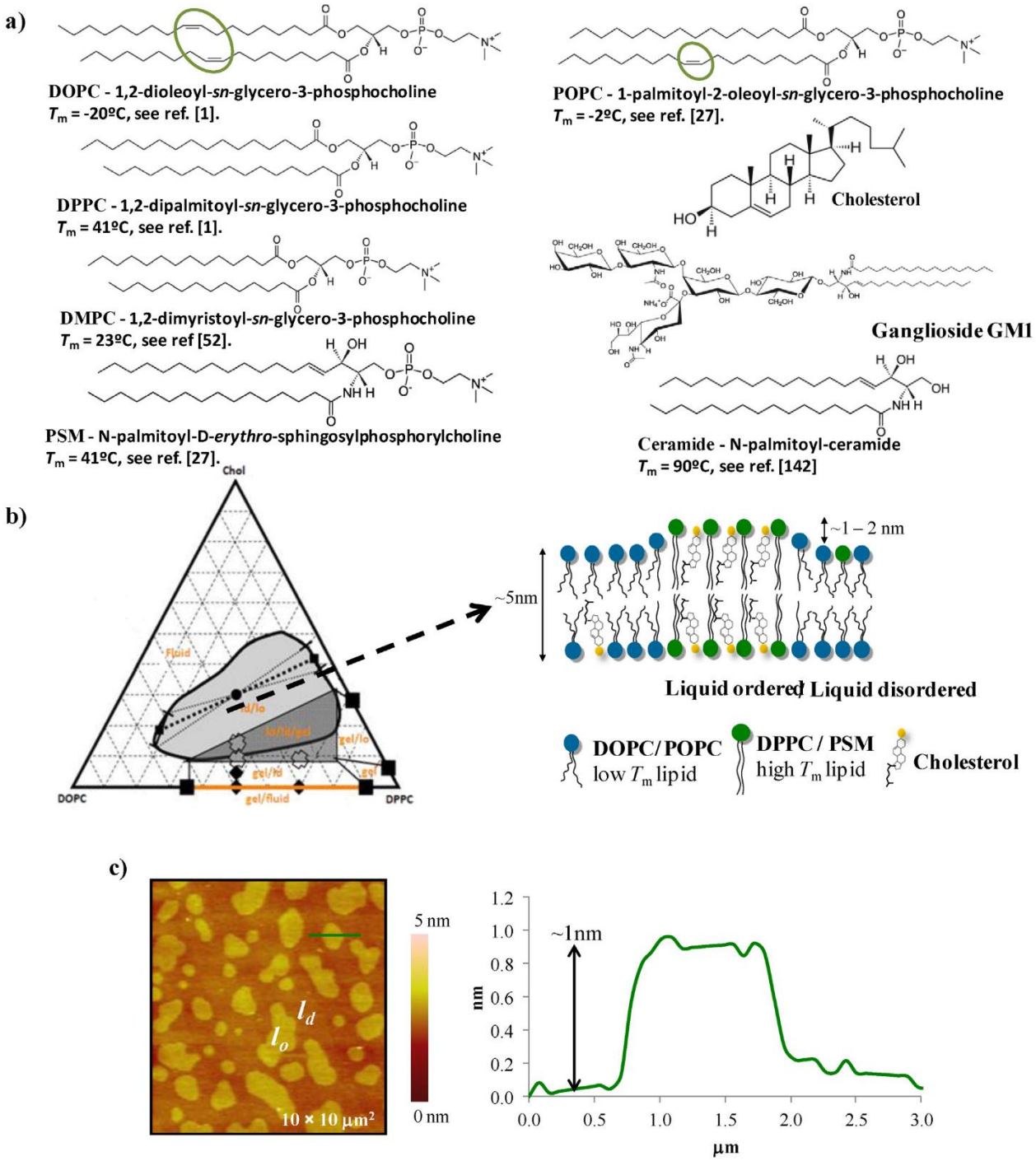

Fig. 1. (a) Structure lipids commonly employed in model systems of biomembranes. (b) Ternary phase diagram at 23 °C of a simple lipid mixture, DOPC/DPPC/cholesterol, that leads to phase coexistence between l_d and l_o (lipid rafts) and the schematic representation of those domains with typical thickness values. The phase diagram was obtained for free-standing bilayers [30]. (c) Tapping mode AFM topographic image in buffer solution of a DOPC/PSM/cholesterol (2:2:1 molar ratio) lipid bilayer formed on mica, where it is possible to distinguish two different lipid phases – thicker l_o domains and the surrounding l_d phase. The topographic profile on the right corresponds to the green line in the image. (For interpretation of the references to color in this figure legend, the reader is referred to the web version of this article.)

1.1. Lipid rafts: their relevance and how to mimic them

Of particular importance are the lipid domains found in eukaryotic organisms designated as lipid rafts, due to their involvement in many cellular functions, such as intracellular distribution of proteins, signal transduction, and by modulating the activity of membrane proteins [13–16]. These highly specialized structures have been defined as being small (sub-micrometer range), heterogeneous and dynamic domains enriched in cholesterol and sphingolipids [17]. The acyl chains of the lipids enriched in these domains exhibit a higher degree of saturation than the ones in the surrounding membrane and pack tightly with certain sterol molecules [18–20]. In the case of mammalian cells, the presence of cholesterol (Fig. 1a) in these microdomains drives the formation

of a liquid ordered (l_o) phase (Fig. 1b) whose fluidity is closer to that of the gel, but the lateral mobility is much higher [21–23]. Because these structures are transient in time its direct observation in vivo is still a challenge. However, by making use of model systems containing domains that mimic the presence of cellular lipid rafts it was possible to visualize them and determine their size which may vary from a few nanometers (less than 100 nm) to almost 1 μm depending on various factors such as lipid composition, temperature and presence of multivalent lipid-binding proteins [1,22,24]. They are thicker than the surrounding membrane in a range that may go from ca. 1 nm to 2 nm (Fig. 1b and c) [1,23,24]. A layer thickness difference of raft-like domains can be generated incorporating complex glycolipids, such as ganglioside GM1 [10]. To generate a model system mimicking the properties of lipid rafts it is necessary to use a ternary mixture of lipids composed by cholesterol and two other lipids, phospholipids or sphingolipids (Fig. 1b) differing significantly in their T_m [25–27]. Under certain lipid proportions these ternary lipid mixtures lead to the coexistence of l_o domains, which mimic lipid rafts, and liquid disordered (l_d) phase, which simulates the fluid surrounding membrane. When intending to prepare a lipid bilayer with a certain fraction of l_o domains, a phase diagram (Fig. 1b) is used to select the adequate molar proportion of each lipid. Lipid phase diagrams are very useful when working with multicomponent mixtures, particularly those containing cholesterol, as they give the phase boundaries for the phase coexistence and a collection of lipid phase diagrams is available [11,28,29]. For example the PSM/DOPC/Cholesterol and DPPC/DOPC/Cholesterol ternary mixtures at the 2:2:1 molar proportions exhibit l_o/l_d phase coexistence (Fig. 1b and c) which makes them suitable to simulate the lipid and domain environment of biomembranes [30,31]. In addition to creating a biomimetic environment that can be used to characterize membrane–biomolecule interactions in a more biologically relevant manner, the preparation of novel membrane model systems displaying this type of phase coexistence may also prove useful to better understand in vivo formation and properties of lipid raft themselves, since this is a research field where many open questions persist [13,20].

1.2. Supported lipid bilayers

Among model systems that mimic important properties of cellular membranes planar lipid bilayers formed onto solid supports, commonly designated as SLB, will be the main focus of this review. Other membrane model systems such as liposome suspensions of LUV (large unilamellar vesicles) or MLV (multilamellar vesicles) are quite suitable for obtaining bulk information on the system, i.e., to obtain information averaged over a very large number of molecules and vesicles. It is undoubtedly the best system to characterize the general biophysical properties of membranes with a given composition, whether equilibrium or dynamic and membrane–biomolecule interactions. However, these suspensions do not allow for spatial resolution, and therefore complementary imaging techniques are required [32]. For example, confocal fluorescence microscopy allows to depict micron scale domains and major morphological changes (e.g., vesiculation, tabulation) in giant free standing bilayers [30,31]. Supported lipid bilayers, apart from the possible influence of the solid support on membrane properties, due to their essentially flat geometry allow the use of sensitive surface techniques with sub-nanometer axial and lateral resolution such as AFM [10], and sub-nanometer vertical resolution over a large scanned area, in the case of ellipsomery [33], crucial when studying nanodomains such as lipid rafts. Force spectroscopy can be also used to obtain local thickness and spatially resolved information on viscoelastic properties on SLB [34], which can also be studied in giant vesicles by micropipette aspiration technique [35], but without spatial resolution. These free standing bilayers do not allow for electrochemical measurements that SLB provide on a conducting surface. These platforms can be tailored at different levels, all possible of being optimized according to the target application. Importantly, the ability to form SLB on conductive substrates allows studying the effect of an applied external potential during or after SLB formation, to characterize membrane organization and molecular interactions by electrochemical methods, as well as their use in electrochemical biosensors. As discussed below, chemical modification of the substrate can be easily performed to confer adequate properties (e.g., charge and polarity) to the surface for lipid deposition. Moreover, when preparing SLB the use of a raft-forming lipid mixture is advantageous because it provides a more biomimetic environment. In addition, the expected presence of domains differing in ca. 1.5 nm thickness from the surrounding membrane can be used to confirm that the formation of a planar and uniform bilayer was achieved.

A wide range of high resolution and sensitivity surface techniques can be employed to study SLB, with several examples given along the text, such as Atomic Force Microscopy (AFM), Scanning Tunneling Microscopy (STM), Quartz-Crystal Microbalance (QCM), Ellipsometry, Surface Plasmon Resonance (SPR), Reflectance Infrared Spectroscopy, or Total Internal Reflectance Fluorescence (TIRF). SLB can be prepared essentially by two widely reported methods – Langmuir–Blodgett (LB) and/or Langmuir–Schaffer (LS) transfer [36–40] and through the fusion of vesicles [1,41–43]. Briefly, using the LB/LS approach, monolayers of lipids, spread on the air–water interface are successively transferred to a solid support. In this method by moving the teflon barriers of a Langmuir trough it is possible to accurately control the surface pressure at which the monolayers are transferred. By plotting surface pressure as a function of the interfacial area, compression/decompression isotherms are generated providing information on the mean molecular area, physical state, and organization of the lipid molecules. To form a lipid bilayer on a solid support the first leaflet is transferred by pulling the support through the monolayer (LB technique) and the transfer of the second monolayer is achieved by LB or LS transfer, vertical or horizontal dipping, respectively, being the horizontal dipping the mainly used method. The great advantages of this method are the possibility to control the compactness of the layers as well as to form asymmetric lipid bilayers, i.e., having each of the two leaflets with different lipid composition. This asymmetry is an important property of cellular membranes [36–40,44].

The method of vesicle fusion involves the preparation of a suspension of small unilamellar vesicles (SUV), usually prepared by sonication and with a diameter ranging from 25 to 80 nm, or LUV, frequently prepared by extrusion and with a more defined diameter dependent on the chosen pore size of the filter. The suspension is dropped over the solid support and incubated to allow the adsorption of the vesicles on the surface, their deformation, fusion and rupture with the top bilayer rolling/sliding over the bottom bilayer [1,41–43,45,46]. According to the type of solid substrate several experimental details should be optimized, such as the buffer ionic strength, presence of bivalent ions (e.g., Ca^{2+} or Mg^{2+}), vesicles size distribution and lipid concentration required to trigger the initial formation of bilayer patches, essential to generate an uniform lipid film. The method of fusion of vesicles is simple and enables the preparation of lipid bilayers with pre-incorporated membrane proteins.

Most lipid phase diagrams are determined using free-standing bilayers, i.e., liposome suspensions. In this way, it is easy to predict the presence of l_o/l_d phase coexistence in the outcoming SLB, and/or to assess the effects of SLB formation and lipid–substrate interactions on the phase behavior of the mixture if the departure situation was a liposome suspension with an established phase diagram. In case of LB/LS bilayers, the presence of domains, as well as their fraction and shape are highly dependent on the surface

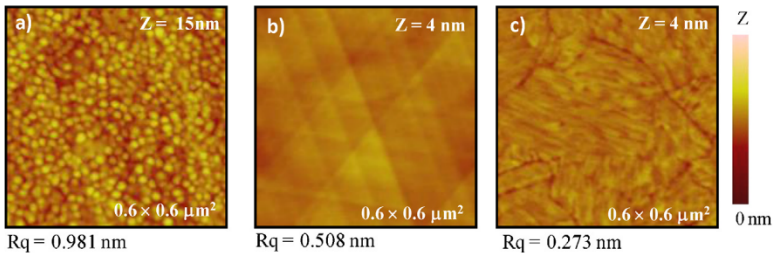

Fig. 2. AFM images of different types of gold electrodes used to prepare supported lipid bilayers: (a) evaporated gold (50 nm) on glass with ca. 2 nm chromium undercoat, (b) thin layer gold (200 nm) evaporated on glass with a 2–4 nm chromium undercoat after flame-annealing, and (c) template stripped gold from silicon surface.

pressure applied, which may render more difficult the assessment of the changes that were induced by the deposition process [38].

Mica is the most commonly employed solid support due to its atomic flatness, hydrophilicity and negative charge at neutral pH, which are proper characteristics to drive the interaction between the solid surface and the lipids polar head group. The experimental conditions to form SLB on this substrate are well established [41,42,47]. The SLB formed on mica have proved to be valuable model systems allowing the study of lipid bilayers properties (e.g., viscoelastic, thickness, phase coexistence), effect of salts and ionic strength on membrane mechanic resistance and of a high number of small molecules, such as drugs, anesthetics, and peptides, on membrane organization [1–3,34,48–50]. Silicon and glass have also been extensively employed [1,51]. Among the conductive surfaces used, gold presents electrical, biocompatible and optical properties allowing for a broad range of applications [10,52–56]. However, the formation of SLB on gold (whether bare or modified) is not as easily accomplished as in mica as explored below in this review.

2. Supported lipid bilayers on gold

In this section, strategies to obtain planar lipid bilayers on gold substrates with different lipid domain organization will be discussed. Special attention will be given to the properties of the gold surface, bare or chemically modified, and experimental details to take into account when using the method of vesicle fusion.

2.1. Gold substrates

Several types of gold substrates have been used to prepare SLB, differing on their crystallography, morphology, and roughness (Fig. 2). The most widely used gold substrate consists on a thin film of gold evaporated or sputtered on silicon or glass with a chromium undercoat (Fig. 2a) constituted by small grains with a diameter of ca. 15–20 nm and a root-mean-square (rms) roughness (R_q) of ca. 1 nm (0.6 μm × 0.6 μm) (Fig. 2a). Single-crystal gold (1 1 1) was used mainly for high-resolution electrochemical STM and surface IR studies [57,58]. Extensively employed are also the thin layer gold on mica or borosilicate glass (with a chromium undercoat as well), which can be flame-annealed to produce large crystallites with a preferred crystallographic (1 1 1) orientation; the surface of these crystallites is atomically flat, exhibiting the typical triangularly shaped monoatomic terraces, with a R_q close to 0.5 nm (0.6 μm × 0.6 μm; Fig. 2b). However, these large crystallites are surrounded by deep valleys which create undesired discontinuities on the surface and these features arise as one disadvantage of this type of gold electrode. Considering that the substrate roughness may influence the formation of planar and continuous SLB, the granulated gold has limited use, because it hinders the process of bilayer formation in most cases, promoting intact vesicle adsorption [45]. Additionally, it would be difficult to identify small topographical details, for example raft-like domains (ca. 1.5 nm), in the lipid film. They are commonly employed in QCM and SPR assays, essentially because the electrodes specially developed to perform these techniques cannot undergo an aggressive process such as flame annealing. Another type of gold substrate frequently used to form pinhole free SLB, as confirmed by electrochemical impedance spectroscopy (EIS), is the template stripped gold [59]. This can be prepared on mica or silicon (Fig. 2c, R_q ca. 0.3 nm), providing a very flat gold surface in a range of a few square micrometer. Since it is a virtually uncontaminated surface, template stripped gold is a promising substrate for a clear observation of lipid domains and protein distribution in SLBs.

2.2. Lipid vesicles interaction with bare gold surfaces

The hydrophobic nature of gold surfaces when exposed to air raises many difficulties when trying to build a SLB directly on bare gold. Indeed, a number of studies on a bare gold substrate report the absence of a planar bilayer arrangement, essentially driven by absence of vesicles rupture [10,60,61]. QCM studies have shown that depending on the type of substrate, namely evaporated gold or silicon dioxide, different structural arrangements can be formed, including adsorbed intact vesicles and planar bilayers [45,60,62], respectively (Fig. 3a and b). On evaporated gold the deposition of egg-phosphatidylcholine (egg-PC), fluid at room temperature mostly POPC (Fig. 1a), SUV leads to a fast and pronounced decrease in frequency, indicating a great increase of mass on the surface, and also to a significant increment in dissipation, consistent with the adsorption of intact vesicles, which undergo deformation due to quartz crystal shear stress [60] (Fig. 3a). On silicon, a more hydrophilic substrate, a fast reduction of frequency is observed upon the addition of SUV with the same composition until a critical surface density is achieved, after which a slight frequency increase occurs (Fig. 3b). In parallel, the dissipation, which augments during the initial process of vesicles adsorption, returns to its starting value revealing the rupture of the lipid vesicles driving the formation of a lipid bilayer, with the concomitant release of water [60] (Fig. 3b). An important aspect related with QCM measurements is that the frequency shift accounts also for the water contained inside the vesicles. Thus the value of the equilibrium frequency is intimately associated with the size distribution and quantity of liposomes adsorbed on the surface and consequently it may differ in each experiment.

The incomplete and unidirectional fusion of lipid vesicles leading to the formation of lipid tubular structures was observed by AFM on bare flame-annealed gold for both binary DOPC/DPPC (1:1) (Fig. 4a) and ternary DOPC:DPPC:chol (1:1:1) mixtures, [10] when employing the conditions that drive the assembly of a SLB on mica-buffer containing 150 mM NaCl and 5 mM $CaCl_2$ (Fig. 1c). These lipid tubules, which follow the triangular shape of gold monoatomic terraces, have a thickness close to 9 nm as retrieved by ellipsometry [10]. In another study conducted on pristine template stripped gold, a similar thickness (8.9 nm) was obtained by force spectroscopy

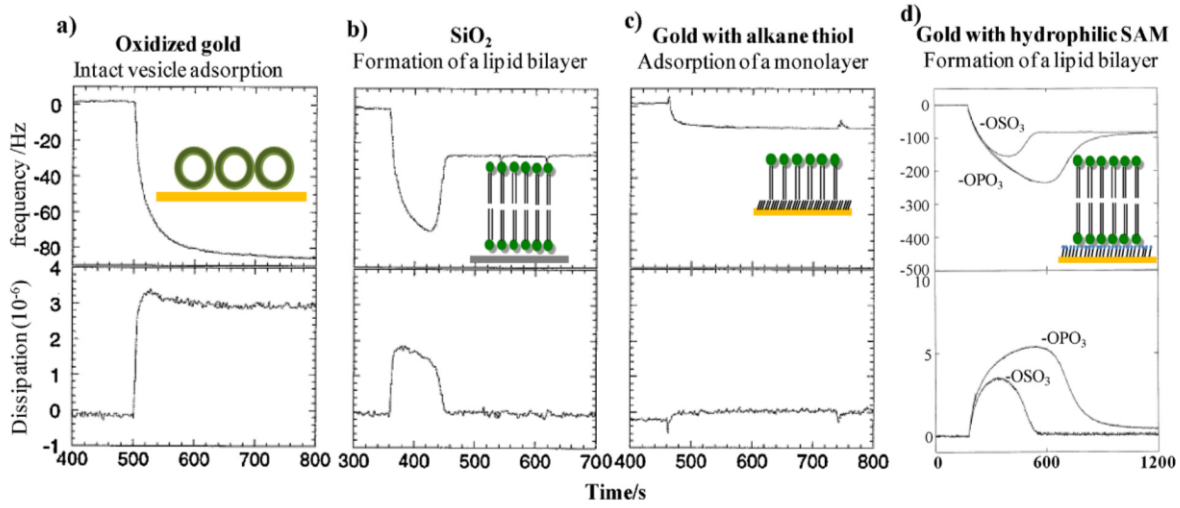

Fig. 3. QCM detection through the change in QCM resonant frequency (top row) and dissipation versus time (bottom row) of (a) adsorption of intact egg-PC vesicles on oxidized gold, (b) formation of an egg-PC bilayer on silicon dioxide, (c) formation of an egg-PC monolayer on top of a methyl-terminated SAM (octadecylmercaptan) modified gold surface and (d) formation of an egg-PC bilayer onto a modified gold surface with a hydrophilic SAM (OPO_3^{2-} and OSO_3^- terminated). Insets: pictorial representation of the lipid arrangements obtained in each situation.

Adapted from Refs. [60] and [83] with permission requested to Elsevier and the American Chemical Society, respectively.

for intact POPC vesicles adsorbed on the surface, which yielded two rupture events corresponding to the two times that the probe encounters a bilayer of an intact vesicle when approaching the substrate [61].

Several reasons can been pointed out to explain the inability to form planar SLB on gold, such as crystallographic orientation [52] and cleaning procedures, which may yield surfaces with different degrees of hydrophilicity. However, as described in Fig. 3a, intact 12.5 nm radius vesicles adsorbed on the surface without planar SLB formation even on an oxidized gold surface with a water contact angle of 5° [63]. The importance of vesicle size has also been acknowledged, because liposomes with higher diameter deform and fuse more easily [46], although it has been reported that the presence of a minor population of smaller vesicles amongst the larger ones could promote SLB formation [52]. Finally, the vesicle suspension medium used to drive the deposition of lipids is also a crucial factor.

2.2.1. *Preparing SLB on bare gold*

Independently of the substrate used, buffer composition is one of the most important aspects when working with SLB. The reported studies where the outcome was the adsorption of vesicles onto an oxidized bare gold surface employed a buffer with 100–150 mM of NaCl [45,60–62], salt concentrations usually used to meet biological requirements. However, chloride ions may chemisorb to the gold surface [64], hindering lipid–substrate interactions which play a pivotal role in the process of vesicle deformation and rupture with concomitant formation of a SLB [42,43,45,46,62]. Moreover, chloride anions tend to bind to the trimethylammonium group of choline present in the polar head region of phosphatidylcholine and sphingomyelin (see Fig. 1a) rendering them with a global negative charge [65] and thus weakening the affinity between lipid polar head group and neutral gold surface. NaCl also stabilizes vesicles in suspension inhibiting vesicle–vesicle interaction [66] making their rupture and fusion more difficult to occur especially if the vesicle–substrate interaction is not as strong as the one found for hydrophilic substrates. The first reports of a planar single-phase lipid bilayer (DMPC and DMPC/cholesterol mixture) supported on bare gold, confirmed by high resolution AFM, were from Lipkowski's group, using a buffer containing NaF instead of NaCl [52,57,67–69]. Although also an halogen, fluoride anions should not interact so effectively with the lipids polar head group since it has been shown that the binding ability to the trimethylammonium group increases along the lyotropic series, i.e., as the halogen radius becomes larger [65]. SLB prepared by the LB/LS transfer and the method of fusion of vesicles were topographically similar with estimated bilayer thickness of 5.1 nm for the LB/LS method [67] and close to 4 nm for the method of vesicles fusion [52]. In fact, both methods of preparation produce smooth and uniform SLB, however lipid films prepared by the method of fusion of vesicles are generally more defective, less ordered and their acyl chains are more tilted [70–72], as shown by polarization modulation-infrared reflection-absorption spectroscopy (PM-IRRAS). This technique has been employed to study the conformation and orientation of the lipid molecules directly adsorbed on the gold surface, through the analysis of the CH stretching bands. By PM-IRRAS it was possible to assess the physical state of DOPC and DMPC pure lipid bilayers at ~20 °C, fluid and gel-like, respectively [57]. Moreover, DMPC film exhibits a tilt in the acyl chains relative to the surface normal close to 29° at potentials below −0.5 V, with a solvation layer between the metal surface and the lipid polar head group [57]. Above −0.2 V the lipid molecules are in direct contact with the surface, leading to an increment in the tilt of the acyl chains to ~42° and a significant increase in the hydration of the lipids polar headgroup [57,69]. This effect is shown in Fig. 5 through the PM-IRRAS spectra of DMPC in the CH stretching region, recorded as a function of electrode potential. The result of spectra analysis is evidenced in Fig. 5b, where a clear increase of the tilt angle is observed for higher potentials. It is also possible to infer that the introduction of 30% cholesterol into a DMPC bilayer has a pronounced influence in the orientation, hydration and conformation properties of DMPC molecules in the bilayer, as reflected by a decrease in CH bands intensity and frequency shift (Fig. 5) [73]. In this binary system the effect of the potential is less evident. A similar result was observed for the addition of 10% of GM1 where a decrease of about 10° in the tilt of acyl chains in a DMPC film prepared by LB/LS deposition was obtained [74].

Our group has also been able to prepare flat and uniform lipid bilayers on bare gold in the absence of any salt in the deposition buffer (Fig. 4b) [10]. These bilayers (ca. 4 nm obtained by ellipsometry) were prepared from a ternary DOPC:DPPC:cholesterol mixture that expectedly leads to raft formation. Indeed, l_o/l_d phase

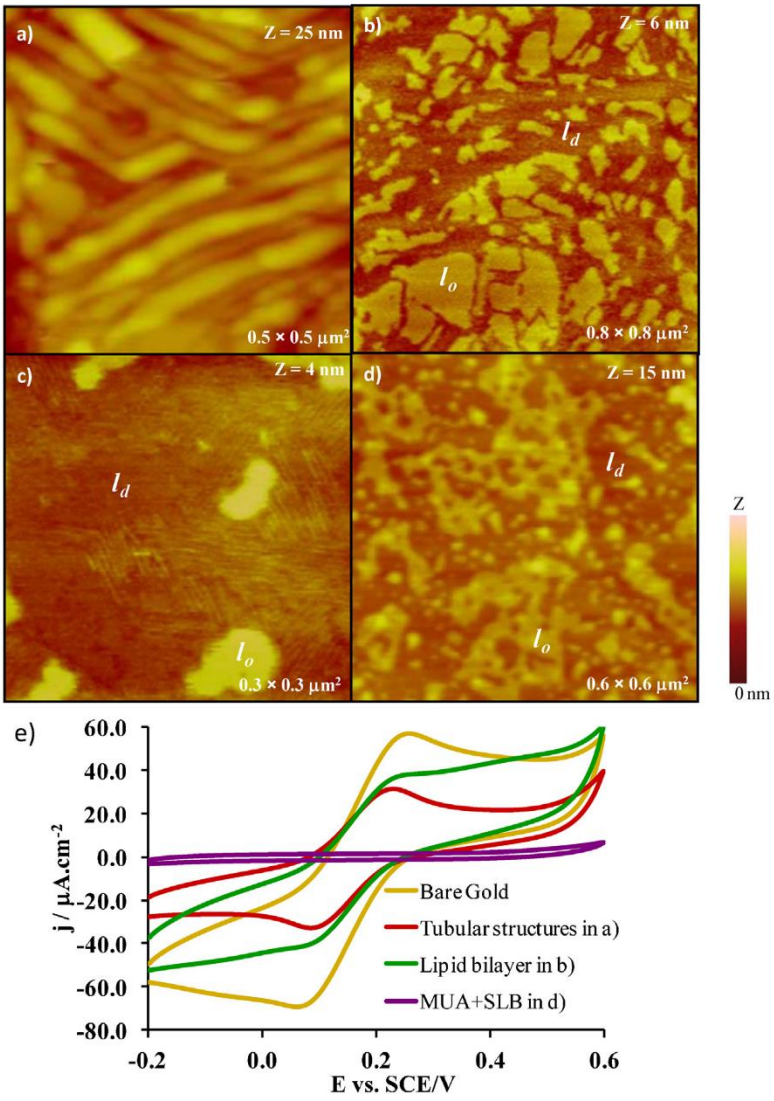

Fig. 4. AFM topographic images acquired in the tapping mode with a liquid cell of (a) DOPC/DPPC (1:1 mol:mol) tubular structures obtained using the conditions optimal for the formation of a planar lipid bilayer on mica; (b) DOPC/DPPC/cholesterol (2:2:1 mol ratio) film prepared in the absence of salt, where the raft-like l_o domains are evident; (c) detail showing corrugations in a planar lipid bilayer with the same ternary composition; (d) planar lipid bilayer with the same composition supported on a MUA modified gold surface; (e) blocking effect of the lipid bilayer assemblies shown in (a), (b), (d) evaluated by cyclic voltammetry of the ferricyanide redox process. The total blocking effect obtained for the MUA+SLB arrangement is due to the very compact nature of the underlying SAM.

Adapted from Ref. [10] with permission requested to the Royal Society of Chemistry.

separation, where ordered domains differing in height ~1.8 nm from the surrounding fluid phase, were clearly observed by AFM. This difference is higher than the one typically observed in mica (Fig. 1c), which could be explained by a thicker water cushion under l_o as compared to l_d domains, in the case of gold. Another interesting feature is the difference in shape of the domains, which is round for free-standing bilayers [30,31] and SLB on mica [1,24], whereas on Au (1 1 1) follows its characteristic monoatomic terraces. A topographical particularity of lipid bilayers supported directly on gold is the presence of corrugations (Fig. 4d) [10,52] that arise as a consequence of the asymmetric environment at which the two leaflets of the bilayer are exposed. A periodicity around 5.5 nm was obtained for a DMPC bilayer [52] and close to 10 nm for a DOPC/DPPC/Chol bilayer (Fig. 4d) [10]. The relatively hydrophobic gold surface on the inner side and the aqueous solution on the top leading to those undulations are a proof of the formation of a bilayer arrangement.

Concerning the proportion of lipid domains, for the DOPC/DPPC/Chol or DOPC/PSM/Chol ternary mixtures at the molar proportions 2:2:1, it has been found that the ~43% fraction of ordered domains predicted by the phase-diagram [30,31], obtained for free-standing vesicles, is also found for SLB on mica [1]. However, on gold, raft-like domains display an area fraction close to 23% [10], which after correcting for the difference in molecular mean area between the two phases, yields a slightly lower value. It was observed that the T_m of a pure DMPC bilayer on gold decreases by 2 °C [52], with respect to free standing liposomes, pointing to a higher disordering of acyl chains, consistent with a reduced fraction of lipid rafts in the ternary mixture.

The proven ability to form a bilayer with l_o domains in a fluid matrix on bare gold provides an attractive model to study protein and other raft-interacting biomolecules using electrochemical approaches. Cyclic voltammetry has been thoroughly used to evaluate the integrity and compactness of lipid bilayers deposited

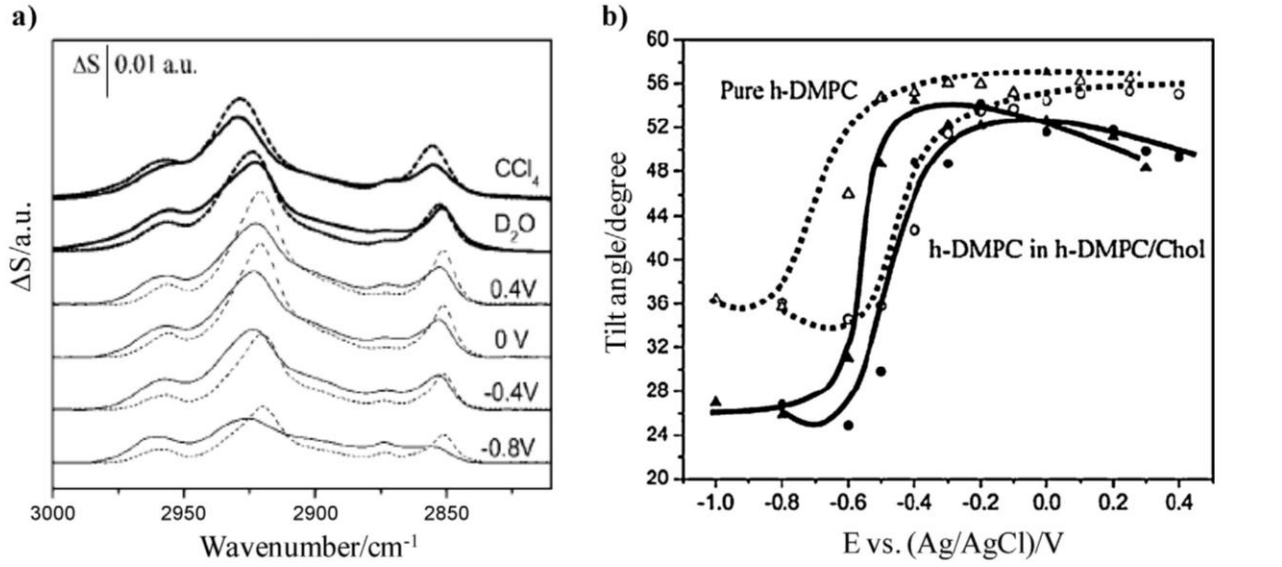

Fig. 5. (a) PM-IRRAS spectra in the CH stretching region of a pure DMPC bilayer (dashed line) and a binary 7:3 DMPC/cholesterol bilayer (solid line) on a gold (1 1 1) electrode surface in 0.1 M NaF/D_2O solution at different potential values as indicated. The top two pairs of spectra (thick lines) were calculated for a 5.5 nm-thick film of randomly oriented molecules, using the optical constants for DMPC or DMPC/cholesterol (7:3) mixtures for solutions in CCl_4 (top line) and vesicle dispersions in D_2O (second line). (b) Acyl chains tilt angle versus electric potential of a pure DMPC bilayer (dashed lines) and binary DMPC/cholesterol bilayer (solid lines).
Reproduced from Ref. [73] with permission requested to the American Chemical Society.

on several modified gold electrodes, by measuring their blocking effect to the redox processes of electroactive molecules, such as potassium ferricyanide ($K_3Fe(CN)_6$) or hexamine ruthenium (III) chloride ($Ru(NH_3)_6Cl_3$) [10,75–80]. The blocking properties of the lipid structures described above, for binary and ternary mixtures, leading to tubules or to planar membranes with domains, were also investigated by cyclic voltammetry in 1 mM $K_3Fe(CN)_6$ 50 mM Hepes solution, and the voltammograms are shown in Fig. 4e [10]. The current intensity values were constant under repetitive potential cycling, showing that the lipid assemblies on gold are stable. The voltammograms obtained for both lipid bilayers have distinct shapes, as a reflex of a more permeable assemble (tubules) or a more compact molecular arrangement with small pores (Fig. 4e) [10]. The redox signals of ferricyanide are not totally suppressed after bilayers deposition, which might be advantageous and encourages the use of unmodified gold as solid support for bilayers, once the detection of other electrochemical processes is still possible to follow in such arrangements, for instance in enzymatic biosensors.

2.3. SLB on chemically modified gold

2.3.1. Self-assembled monolayers

A common strategy employed to confer gold surfaces the suitable physical and chemical properties for a given application is their modification by the spontaneous adsorption of alkanethiol monolayers [81,82], which can be easily tailored (e.g., using different terminal groups and chain lengths). Concurrently, to generate a lipid bilayer on gold, the substrate is frequently modified with hydrophilic and charged thiolated SAM (Fig. 6a). This surface modification will facilitate the interaction with lipids polar head group and subsequently the formation of a lipid bilayer arrangement. In contrast, when using a hydrophobic octadecylmercaptan SAM, a monolayer of egg-PC is obtained (Fig. 3c) [60], due to the favored interaction between the hydrophobic acyl chains with the modified substrate. A similar profile with a lower frequency change than the one obtained for intact vesicle adsorption was observed, consistent with the deposition of a monomolecular lipid layer. Numerous SAM have been employed effectively in what concerns the generation of a SLB. In a QCM study addressing the effect of bivalent cations concentration on the process of bilayer formation, thiolated SAM with terminal $-OSO_3^-$ and $-OPO_3^{2-}$ groups, that are negatively charged at pH 8.0, were successfully used (Fig. 3d) [83]. The oscillation frequency versus time profile after the addition of egg-PC vesicle suspension corroborates vesicle adsorption and fusion to originate a planar lipid bilayer. It was observed that vesicle adsorption is suppressed in the absence of Mg^{2+}, occurring at 1 mM but without spontaneous SLB formation, and is more efficient at 5 mM leading, in these conditions to spontaneous planar SLB formation [83]. In contrast, the use of a –OH terminated SAM in the same study lead to the adsorption of intact vesicles without rupture [83].

The modification with 11-mercaptoundecanoic acid (MUA) confers negative charge to the surfaces at neutral pH and thus it is also a suitable and common approach to drive the formation of SLB [10,84]. A bivalent cation is also required to mediate the interaction between the phosphate group of the lipids and the negative charge of the SAM carboxylate group. On this modified gold surface the formation of lipid domains mimicking the presence of lipid rafts was obtained (Fig. 4d) [10,84] and, as expected, l_o domains were more rigid than l_d, evaluated through force curve spectroscopy [84]. Ellipsometric thickness together with contact angle measurements confirmed the formation of a DMPC SLB (ca. 5 nm) on 6-mercapto-1-hexanol and zirconated 6-mercapto-1-hexylphosphate SAM [76]. However, in the latter the bilayer is not stable over time, eventually turning into a monolayer arrangement (ca. 2.5 nm).

Monolayers of more complex design have also been used. A hydrophilic 1-thio-β-D-glucose (Fig. 5a) monolayer was employed in LB/LS transfers in order to improve the transfer and stability of the inner leaflet composed of GM1 (Fig. 1a), DMPC and cholesterol through the interaction between GM1 and SAM glycidic moieties [85]. Another successful strategy is the use of mixed self-assembled monolayers in which one of the components is frequently an alkanethiol and a thiolipid which will be described in the next sub-section.

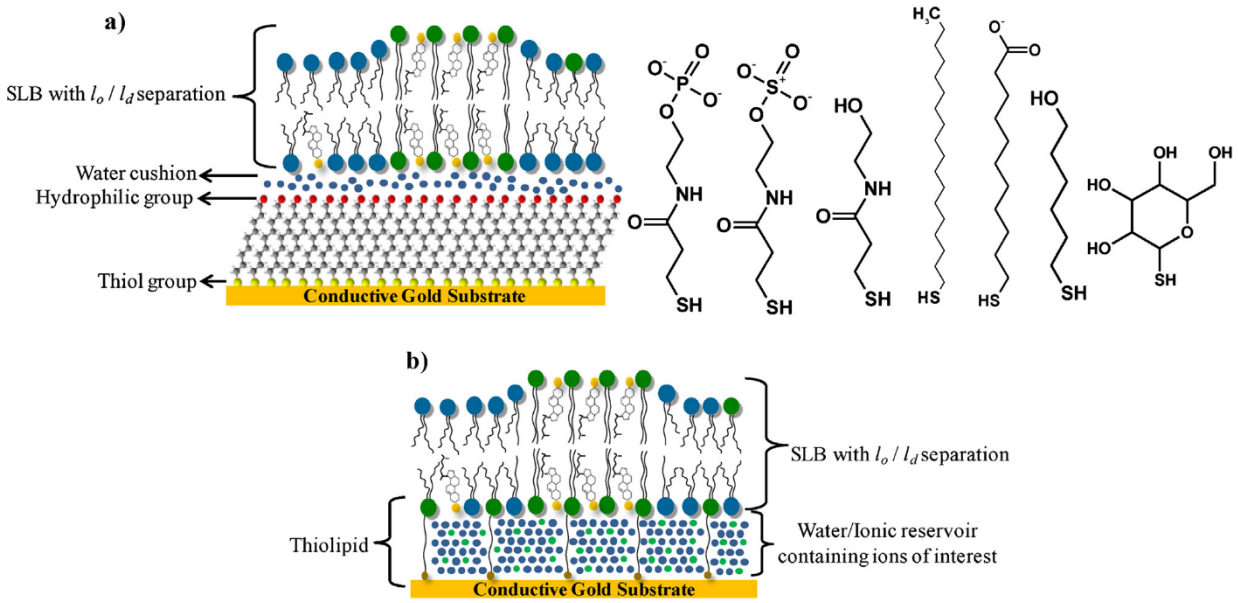

Fig. 6. (a) Schematic representation of a ternary SLB with l_d/l_o phase separation onto a conductive gold surface modified with a hydrophilic SAM and structure of molecules used for SAM preparation, corresponding to the examples given along the text. (b) Schematic representation of a tethered lipid bilayer membrane with a preformed sparse thiolipid SAM.

2.3.2. *Tethered lipid bilayer membranes*

Thiolipids are an alternative approach to build biomimetic lipid bilayers on gold surfaces (Fig. 6b). These thiolipids consist on a lipid moiety linked to a thiol-modified tether that anchors to the gold surface and acts as a spacer between the gold and the lipid promoting the decoupling between the membrane and the metallic surface (Fig. 6b). The bilayer so formed is commonly designated tethered bilayer lipid membranes (tBLM). Usually, the thiolated molecules are tailored synthesized, although there are already a few commercially available ones. To conduct the formation of a tBLM, frequently a monolayer of the chosen thiolipid is prepared and the formation of the lipid bilayer can be carried out by LB/LS transfer or vesicle fusion [59,86–89].

The 2,3-di-O-phytanoyl-sn-glycerin-1-tetraethyleneglycol-lipoic acid ester (DPTL) system, which is one of the most popular, was developed about ten years ago by Knoll and co-workers [86]. A pure monolayer of the thiolipid only allows little water incorporation in the spacer region which may hamper the functional incorporation of proteins [90–92]. The resulting bilayers have high membrane resistance and low capacitance, e.g., 3–55 MΩ cm^2 and 0.6–1.1 μF cm^{-2}, respectively [90]. A model system mimicking biological membranes should exhibit capacitances in the range between 0.8 and 1.0 μF cm^{-2} [93–95]. Other groups also reported the inability of pure systems of thiolipid monolayers to incorporate large proteins in a functional manner [56,87]. Another drawback of a high concentration of the thiolipid is the limited lateral motion of the lipids. Recent SPR studies show how lipid mobility can be differentially affected by two different thiolated-lipid like SAMs through monitoring the binding event of cholera toxin to enriched domains of GM1, used as a simple model of lipid rafts [96].

For these reasons, increasing importance has been given to mixed monolayer systems made of a thiolipid and another thiolated molecule with the purpose of diluting the amount of thiolipid on the surface [56,59,88,97–99]. On these mixed assemblies the formation of a lipid bilayer by the method of fusion of vesicles is still possible and the tBLM exhibit resistance and capacitance values compatible with the study of membrane proteins [56,97]. This bilayer arrangement creates a water reservoir (Fig. 6b) reducing the hydrophobic influence of the electrode surface allowing the accommodation of functional membrane proteins [5,100,101].

The tBLM are frequently used for the incorporation of ion channels and to study their activity [5,56,92], which is possible due to the high membrane resistance of these systems. The capacitance and resistance of the lipid films can be estimated by EIS, which allows inferring about the compactness, integrity and sealing properties of the bilayer [55,59,86,88,90,102]. A process of vesicles fusion on a surface can also be monitored by EIS through a decrease in capacitance and an increase in resistance due to the formation of an insulating bilayer [103,104]. This electrochemical technique has also been successfully exploited to study membrane pore-forming cyclic peptides such as valinomycin and gramicidin [56,59,77,104], where in many cases the external leaflet of the tBLM is prepared from natural lipid extracts of bacteria or yeasts. In general, the EIS data retrieved from the application of an equivalent circuit that better represents the bilayer assemble, indicates a substantial drop in membrane resistance due to flow of ions across the bilayers. A combined CV and EIS approach was used to study a tethered lipid membrane on template stripped gold, prepared from *Escherichia coli* extracts, containing ubiquinol oxidase (cytochrome bo_3). Cyclic voltammetric data revealed catalytic activity of the protein toward ubiquinol species, and EIS enabled to derive diffusion coefficients of ubiquinone (10^{-13}–10^{-12} cm^2/s) [102].

3. Current and potential applications of raft-containing SLB on gold

The diverse assemblies that have been described throughout this review, Au/SLB, Au/SAM/SLB or Au/tBLM, have countless potentialities both in the development of more fundamental studies concerning membrane-related phenomenon and in applied research. Although not all the studies addressed in this section were performed on gold surfaces, they are good examples of the potential application of these SLB on conductive surfaces. One of the most exploited applications of these assemblies is the study of redox processes involving membrane-associated proteins, such as cytochromes c and P450 [105–108] and myoglobin [107,109] as well as other electroactive molecules. A relevant case is that of

ubiquinol molecules [102,110–112], which are proton and electron carriers associated to the respiratory chain in both mitochondrial and bacterial membranes. In their reduced form they act as antioxidants inhibiting lipid peroxidation in biomembranes [113–116]. Thus, their study in membrane-like environments is of crucial importance in order to mimic their natural media, particularly in bilayers displaying phase coexistence. Indeed, Guidelli and co-workers have recently shown how different lipid compositions and thus different lipid domains (fluid/gel coexistence –DOPC/PSM, l_o/l_d – DOPC/PSM/Chol) have a profound influence both in the redox properties of ubiquinone-10 (UQ10) and in its distribution throughout the membrane [112]. Cyclic voltammetric results obtained for lipid monolayers on a mercury electrode reveal a positive shift and also a broadening in the oxidation peak when UQ10 is incorporated into a DOPC/PSM/Chol membrane relatively to a DOPC/PSM one [112]. Moreover, they found that in a pure gel membrane UQ10 tends to segregate into UQ-rich pools, whereas in a gel/fluid matrix it tends to localize in the fluid phase, while when associated to a l_o/l_d membrane is chiefly distributed along the boundaries of the lipid rafts [112]. This subject will certainly be further explored in the near future, and raft-containing SLB on gold constitutes an excellent model to conduct some of those studies. The advantage of using conductive solid supports is the ability of using electrochemical techniques to characterize this phenomenon.

SLB on gold have also been used to address the alterations induced in the membrane morphology, structure, viscoelasticity or permeability by incorporation of proteins and peptides [47,117,118].

Lipid-ion channels are a case in which membrane composition and phase behavior are especially important [119,120]. These channels can be formed when a certain lipid aggregates and, as a consequence, the membrane structure is highly rearranged. For aggregation to occur it is hypothesized that domains enriched in the channel forming lipid are required. Frequently, these domains are lipid rafts. The use of a specifically conceived device to measure conductance on SLB enabled to follow the dynamics of pore formation by ceramide [120]. Ceramide-based lipid ion channels are involved in at least one apoptotic programmed cell death route. In the initial phase of apoptosis ceramide tends to segregate in the mitochondrial outer membrane driving the formation of pores which lead to the release of intermembrane space proteins including pro-apoptotic factors [121–124]. On another hand, it is established that ceramide domain formation is highly dependent on the overall lipid composition, particularly on cholesterol levels [125]. Lipid composition may also play a pivotal role in the performance of protein ion channels, as illustrated by several studies showing the modulation of membrane-associated proteins activity by the presence or absence of cholesterol [126,127] and by the type of bilayer-constituent lipids [128–130]. Other application of these SLB assemblies on a gold substrate is their use as a biosensor platform which undoubtedly benefits from the formation of stable SLB able to incorporate proteins or other molecules that may provide a transducing bio-activity [6,131–141]. In this regard, SLB based platforms were built for the detection of glucose [135], glutamate [141], uric acid [136], dopamine [133], hydrogen peroxide [132] or antigen/antibody recognition events [140].

4. Conclusions

Despite the difficulties associated with the formation of SLB on a gold surface, planar bilayers can be assembled onto this substrate essentially by two methods – LB/LS transfer and vesicle fusion. In order to overcome the hydrophobicity of gold, chemical modifications are required – using hydrophilic self-assembled monolayers, thiolipids or a mixture of both – otherwise special attention has to be given to buffer conditions, as for example chloride anions prevent the formation of a planar lipid bilayer directly on gold. The lipid bilayer arrangements can be characterized by electrochemical methods and most surface techniques, providing detailed information about the kinetics of bilayer formation, the thickness, morphology and degree of hydration of the lipid film and the orientation and conformation of the lipid molecules.

As described above, a more biomimetic membrane should display lateral heterogeneities, namely, gel/fluid and l_d/l_o lipid domains. However, this is usually not the case in SLB studies on conductive substrates. Presently, these features can be formed on gold and have been observed by high resolution imaging. Current investigation is undergoing to build platforms with controlled domain organization in order to explore their role on small electrochemically active compounds – membrane interactions, and membrane protein activity, eventually improving biosensor performance.

Acknowledgements

The authors acknowledge funding from Fundação para a Ciência e a Tecnologia, Portugal, received through PEst-OE/QUI/QUI0612/2011 and Ciência 2007. J.T.M. acknowledges PhD scholarship SFRH/BD/64442/2009.

References

[1] J.T. Marques, A.S. Viana, R.F.M. De Almeida, Ethanol effects on binary and ternary supported lipid bilayers with gel/fluid domains and lipid rafts, Biochimica et Biophysica Acta: Biomembranes 1808 (2011) 405–414.
[2] K. El Kirat, Y.F. Dufrene, L. Lins, R. Brasseur, The SIV tilted peptide induces cylindrical reverse micelles in supported lipid bilayers, Biochemistry 45 (2006) 9336–9341.
[3] A. Berquand, M.P. Mingeot-Leclercq, Y.F. Dufrene, Real-time imaging of drug–membrane interactions by atomic force microscopy, Biochimica et Biophysica Acta: Biomembranes 1664 (2004) 198–205.
[4] Z.V. Leonenko, D.T. Cramb, Revisiting lipid – general anesthetic interactions (I): thinned domain formation in supported planar bilayers induced by halothane and ethanol, Revue Canadienne de Chimie 82 (2004) 1128–1138.
[5] I. Koper, Insulating tethered bilayer lipid membranes to study membrane proteins, Molecular Biosystems 3 (2007) 651–657.
[6] E. Reimhult, K. Kumar, Membrane biosensor platforms using nano- and microporous supports, Trends in Biotechnology 26 (2008) 82–89.
[7] X.B. Lin, C.L. Wang, M. Wang, K. Fang, N. Gu, Computer simulation of the effects of nanoparticles' adsorption on the properties of supported lipid bilayer, Journal of Physical Chemistry C 116 (2012) 17960–17968.
[8] E. Fahy, S. Subramaniam, H.A. Brown, C.K. Glass, A.H. Merrill, R.C. Murphy, C.R.H. Raetz, D.W. Russell, Y. Seyama, W. Shaw, T. Shimizu, F. Spener, G. van Meer, M.S. VanNieuwenhze, S.H. White, J.L. Witztum, E.A. Dennis, A comprehensive classification system for lipids, Journal of Lipid Research 46 (2005) 839–861.
[9] E. Fahy, S. Subramaniam, R.C. Murphy, M. Nishijima, C.R.H. Raetz, T. Shimizu, F. Spener, G. van Meer, M.J.O. Wakelam, E.A. Dennis, Update of the LIPID MAPS comprehensive classification system for lipids, Journal of Lipid Research 50 (2009) S9–S14.
[10] J.T. Marques, R.F.M. De Almeida, A.S. Viana, Biomimetic membrane rafts stably supported on unmodified gold, Soft Matter 8 (2012) 2007–2016.
[11] D. Marsh, Handbook of Lipid Bilayers, CRC Press, Taylor & Francis Group, 2013.
[12] F. Aresta-Branco, A.M. Cordeiro, H.S. Marinho, L. Cyrne, F. Antunes, R.F.M. De Almeida, Gel domains in the plasma membrane of *Saccharomyces cerevisiae* highly ordered, ergosterol-free and sphingolipid-enriched lipid rafts, Journal of Biological Chemistry 286 (2011) 5043–5054.
[13] D. Lingwood, K. Simons, Lipid rafts as a membrane-organizing principle, Science 327 (2010) 46–50.
[14] M. Edidin, The state of lipid rafts: from model membranes to cells, Annual Review of Biophysics and Biomolecular Structure 32 (2003) 257–283.
[15] K. Jacobson, O.G. Mouritsen, R.G. Anderson, Lipid rafts: at a crossroad between cell biology and physics, Nature Cell Biology 9 (2007) 7–14.
[16] J. Malinsky, M. Opekarova, G. Grossmann, W. Tanner, Membrane microdomains, rafts, and detergent-resistant membranes in plants and fungi, Annual review of plant biology 64 (2013) 501–529.
[17] L.J. Pike, Rafts defined: a report on the keystone symposium on lipid rafts and cell function, Journal of Lipid Research 47 (2006) 1597–1598.
[18] H.J. Risselada, S.J. Marrink, The molecular face of lipid rafts in model membranes, Proceedings of the National Academy of Sciences of the United States of America 105 (2008) 17367–17372.
[19] A.E.P. Bastos, S. Scolari, M. Stöckl, R.F.M. de Almeida, Applications of fluorescence lifetime spectroscopy and imaging to lipid domains in vivo, in: P.M. Conn (Ed.), Methods in Enzymology, Imaging and Spectroscopic Analysis of

Living Cells Optical and Spectroscopic Techniques, Academic Press, 2012, pp. 57–81 (Chapter 3).
[20] E.L. Elson, E. Fried, J.E. Dolbow, G.M. Genin, Phase separation in biological membranes: integration of theory and experiment, Annual Reviews of Biophysics 39 (2010) 207–226.
[21] P. Sengupta, B. Baird, D. Holowka, Lipid rafts, fluid/fluid phase separation, and their relevance to plasma membrane structure and function, Seminars in Cell & Developmental Biology 18 (2007) 583–590.
[22] R.F.M. De Almeida, L.M.S. Loura, A. Fedorov, M. Prieto, Lipid rafts have different sizes depending on membrane composition: a time-resolved fluorescence resonance energy transfer study, Journal of Molecular Biology 346 (2005) 1109–1120.
[23] S. Chiantia, N. Kahya, J. Ries, P. Schwille, Effects of ceramide on liquid-ordered domains investigated by simultaneous AFM and FCS, Biophysical Journal 90 (2006) 4500–4508.
[24] C.B. Yuan, J. Furlong, P. Burgos, L.J. Johnston, The size of lipid rafts: an atomic force microscopy study of ganglioside GM1 domains in sphingomyelin/DOPC/cholesterol membranes, Biophysical Journal 82 (2002) 2526–2535.
[25] M.C. Giocondi, P.E. Milhiet, P. Dosset, C. Le Grimellec, Use of cyclodextrin for AFM monitoring of model raft formation, Biophysical Journal 86 (2004) 861–869.
[26] A. Bunge, P. Muller, M. Stockl, A. Herrmann, D. Huster, Characterization of the ternary mixture of sphingomyelin, POPC, and cholesterol: support for an inhomogeneous lipid distribution at high temperatures, Biophysical Journal 94 (2008) 2680–2690.
[27] R.F.M. de Almeida, A. Fedorov, M. Prieto, Sphingomyelin/phosphatidylcholine/cholesterol phase diagram: boundaries and composition of lipid rafts, Biophysical Journal 85 (2003) 2406–2416.
[28] D. Marsh, Cholesterol-induced fluid membrane domains: a compendium of lipid-raft ternary phase diagrams, Biochimica et Biophysica Acta: Biomembranes 1788 (2009) 2114–2123.
[29] D. Marsh, Liquid-ordered phases induced by cholesterol: a compendium of binary phase diagrams, Biochimica et Biophysica Acta: Biomembranes 1798 (2010) 688–699.
[30] R.F.M. De Almeida, J. Borst, A. Fedorov, M. Prieto, A.J.W.G. Visser, Complexity of lipid domains and rafts in giant unilamellar vesicles revealed by combining imaging and microscopic and macroscopic time-resolved fluorescence, Biophysical Journal 93 (2007) 539–553.
[31] S.L. Veatch, S.L. Keller, Miscibility phase diagrams of giant vesicles containing sphingomyelin, Physical Review Letters 94 (2005).
[32] R.F.M. de Almeida, L.M.S. Loura, M. Prieto, Membrane lipid domains and rafts: current applications of fluorescence lifetime spectroscopy and imaging, Chemistry and Physics of Lipids 157 (2009) 61–77.
[33] M.C. Howland, A.W. Szmodis, B. Sanii, A.N. Parikh, Characterization of physical properties of supported phospholipid membranes using imaging ellipsometry at optical wavelengths, Biophysical Journal 92 (2007) 1306–1317.
[34] S. Garcia-Manyes, G. Oncins, F. Sanz, Effect of ion-binding and chemical phospholipid structure on the nanomechanics of lipid bilayers studied by force spectroscopy, Biophysical Journal 89 (2005) 1812–1826.
[35] H.V. Ly, M.L. Longo, The influence of short-chain alcohols on interfacial tension, mechanical properties, area/molecule, and permeability of fluid lipid bilayers, Biophysical Journal 87 (2004) 1013–1033.
[36] L.K. Tamm, H.M. Mcconnell, Supported phospholipid-bilayers, Biophysical Journal 47 (1985) 105–113.
[37] B. Seantier, M.C. Giocondi, C. Le Grimellec, P.E. Milhiet, Probing supported model and native membranes using AFM, Current Opinion in Colloid & Interface Science 13 (2008) 326–337.
[38] B.L. Stottrup, S.L. Veatch, S.L. Keller, Nonequilibrium behavior in supported lipid membranes containing cholesterol, Biophysical Journal 86 (2004) 2942–2950.
[39] K. El Kirat, S. Morandat, Y.F. Dufrene, Nanoscale analysis of supported lipid bilayers using atomic force microscopy, Biochimica et Biophysica Acta: Biomembranes 1798 (2010) 750–765.
[40] J.M. Crane, L.K. Tamm, Role of cholesterol in the formation and nature of lipid rafts in planar and spherical model membranes, Biophysical Journal 86 (2004) 2965–2979.
[41] M.P. Mingeot-Leclercq, M. Deleu, R. Brasseur, Y.F. Dufrene, Atomic force microscopy of supported lipid bilayers, Nature Protocols 3 (2008) 1654–1659.
[42] R.P. Richter, R. Berat, A.R. Brisson, Formation of solid-supported lipid bilayers: an integrated view, Langmuir 22 (2006) 3497–3505.
[43] I. Reviakine, A. Brisson, Formation of supported phospholipid bilayers from unilamellar vesicles investigated by atomic force microscopy, Langmuir 16 (2000) 1806–1815.
[44] I. Czolkos, A. Jesorka, O. Orwar, Molecular phospholipid films on solid supports, Soft Matter 7 (2011) 4562–4576.
[45] E. Reimhult, F. Hook, B. Kasemo, Intact vesicle adsorption and supported biomembrane formation from vesicles in solution: influence of surface chemistry, vesicle size, temperature, and osmotic pressure, Langmuir 19 (2003) 1681–1691.
[46] V.P. Zhdanov, B. Kasemo, Comments on rupture of absorbed vesicles, Langmuir 17 (2001) 3518–3521.
[47] Z.V. Leonenko, A. Carnini, D.T. Cramb, Supported planar bilayer formation by vesicle fusion: the interaction of phospholipid vesicles with surfaces and the effect of gramicidin on bilayer properties using atomic force microscopy, Biochimica et Biophysica Acta: Biomembranes 1509 (2000) 131–147.
[48] S. Morandat, K. El Kirat, Membrane resistance to Triton X-100 explored by real-time atomic force microscopy, Langmuir 22 (2006) 5786–5791.
[49] Z. Leonenko, E. Finot, D. Cramb, AFM study of interaction forces in supported planar DPPC bilayers in the presence of general anesthetic halothane, Biochimica et Biophysica Acta: Biomembranes 1758 (2006) 487–492.
[50] S. Garcia-Manyes, G. Oncins, F. Sanz, Effect of temperature on the nanomechanics of lipid bilayers studied by force spectroscopy, Biophysical Journal 89 (2005) 4261–4274.
[51] M. Halter, Y. Liao, R.M. Plocinik, D.C. Coffey, S. Bhattacharjee, U. Mazur, G.J. Simpson, B.H. Robinson, S.L. Keller, Molecular self-assembly of mixed high-beta zwitterionic and neutral ground-state NLO chromophores, Chemistry of Materials 20 (2008) 1778–1787.
[52] M. Li, M. Chen, E. Sheepwash, C.L. Brosseau, H. Li, B. Pettinger, H. Gruler, J. Lipkowski, AFM studies of solid-supported lipid bilayers formed at a Au(1 1 1) electrode surface using vesicle fusion and a combination of Langmuir–Blodgett and Langmuir–Schaefer techniques, Langmuir 24 (2008) 10313–10323.
[53] I. Almeida, V.C. Ferreira, M.F. Montemor, L.M. Abrantes, A.S. Viana, One-pot approach to modify nanostructured gold surfaces through in situ dithiocarbamate linkages, Electrochimica Acta 83 (2012) 311–320.
[54] Y. Niu, A.I. Matos, L.M. Abrantes, A.S. Viana, G. Jin, Antibody oriented immobilization on gold using the reaction between carbon disulfide and amine groups and its application in immunosensing, Langmuir 28 (2012) 17718–17725.
[55] R. Naumann, S.M. Schiller, F. Giess, B. Grohe, K.B. Hartman, I. Karcher, I. Koper, J. Lubben, K. Vasilev, W. Knoll, Tethered lipid bilayers on ultraflat gold surfaces, Langmuir 19 (2003) 5435–5443.
[56] J.K.R. Kendall, B.R.G. Johnson, P.H. Symonds, G. Imperato, R.J. Bushby, J.D. Gwyer, C. van Berkel, S.D. Evans, L.J.C. Jeuken, Effect of the structure of cholesterol-based tethered bilayer lipid membranes on ionophore activity, ChemPhysChem 11 (2010) 2191–2198.
[57] I. Zawisza, X.M. Bin, J. Lipkowski, Spectroelectrochemical studies of bilayers of phospholipids in gel and liquid state on Au(1 1 1) electrode surface, Bioelectrochemistry 63 (2004) 137–147.
[58] S. Sek, S. Xu, M. Chen, G. Szymanski, J. Lipkowski, STM studies of fusion of cholesterol suspensions and mixed 1,2-dimyristoyl-sn-glycero-3-phosphocholine (DMPC)/cholesterol vesicles onto a Au(1 1 1) electrode surface, Journal of the American Chemical Society 130 (2008) 5736–5743.
[59] L.J.C. Jeuken, N.N. Daskalakis, X.J. Han, K. Sheikh, A. Erbe, R.J. Bushby, S.D. Evans, Phase separation in mixed self-assembled monolayers and its effect on biomimetic membranes, Sensors and Actuators B: Chemical 124 (2007) 501–509.
[60] C.A. Keller, B. Kasemo, Surface specific kinetics of lipid vesicle adsorption measured with a quartz crystal microbalance, Biophysical Journal 75 (1998) 1397–1402.
[61] X. Wang, M.M. Shindel, S.W. Wang, R. Ragan, A facile approach for assembling lipid bilayer membranes on template-stripped gold, Langmuir 26 (2010) 18239–18245.
[62] I. Pfeiffer, S. Petronis, I. Koper, B. Kasemo, M. Zach, Vesicle adsorption and phospholipid bilayer formation on topographically and chemically nanostructured surfaces, Journal of Physical Chemistry B 114 (2010) 4623–4631.
[63] A. Krozer, M. Rodahl, X-ray photoemission spectroscopy study of UV/ozone oxidation of Au under ultrahigh vacuum conditions, Journal of Vacuum Science & Technology A: Vacuum, Surfaces, and Films 15 (1997) 1704–1709.
[64] Z.C. Shi, J. Lipkowski, Chloride adsorption at the Au(1 1 1) electrode surface, Journal of Electroanalytical Chemistry 403 (1996) 225–239.
[65] S.A. Tatulian, Effect of lipid phase-transition on the binding of anions to dimyristoylphosphatidylcholine liposomes, Biochimica et Biophysica Acta 736 (1983) 189–195.
[66] M.M.A.E. Claessens, B.F. van Oort, F.A.M. Leermakers, F.A. Hoekstra, M.A.C. Stuart, Charged lipid vesicles: effects of salts on bending rigidity, stability, and size, Biophysical Journal 87 (2004) 3882–3893.
[67] M.H. Chen, M. Li, C.L. Brosseau, J. Lipkowski, AFM studies of the effect of temperature and electric field on the structure of a DMPC-cholesterol bilayer supported on a Au(1 1 1) electrode surface, Langmuir 25 (2009) 1028–1037.
[68] I. Burgess, M. Li, S.L. Horswell, G. Szymanski, J. Lipkowski, J. Majewski, S. Satija, Electric field-driven transformations of a supported model biological membrane—an electrochemical and neutron reflectivity study, Biophysical Journal 86 (2004) 1763–1776.
[69] X. Bin, I. Zawisza, J.D. Goddard, J. Lipkowski, Electrochemical and PM-IRRAS studies of the effect of the static electric field on the structure of the DMPC bilayer supported at a Au(1 1 1) electrode surface, Langmuir 21 (2004) 330–347.
[70] J. Lipkowski, Building biomimetic membrane at a gold electrode surface, Physical Chemistry Chemical Physics 12 (2010) 13874–13887.
[71] I. Zawisza, X.M. Bin, J. Lipkowski, Potential-driven structural changes in Langmuir–Blodgett DMPC bilayers determined by in situ spectroelectrochemical PM IRRAS, Langmuir 23 (2007) 5180–5194.
[72] C.L. Brosseau, X. Bin, S.G. Roscoe, J. Lipkowski, Electrochemical and PM-IRRAS characterization of DMPC plus cholesterol bilayers prepared using Langmuir–Blodgett/Langmuir–Schaefer deposition, Journal of Electroanalytical Chemistry 621 (2008) 222–228.
[73] X.M. Bin, S.L. Horswell, J. Lipkowski, Electrochemical and PM-IRRAS studies of the effect of cholesterol on the structure of a DMPC bilayer supported at an

Au(1 1 1) electrode surface, part 1: properties of the acyl chains, Biophysical Journal 89 (2005) 592–604.
[74] C.L. Brosseau, J. Leitch, X. Bin, M. Chen, S.G. Roscoe, J. Lipkowski, Electrochemical and PM-IRRAS a glycolipid-containing biomimetic membrane prepared using Langmuir–Blodgett/Langmuir–Schaefer deposition, Langmuir 24 (2008) 13058–13067.
[75] D. Matyszewska, E. Wypijewska, R. Bilewicz, Influence of membrane organization on the interactions between persistent pollutants and model membranes, Bioelectrochemistry 87 (2012) 192–198.
[76] B.P. Oberts, G.J. Blanchard, Formation of air-stable supported lipid monolayers and bilayers, Langmuir 25 (2009) 2962–2970.
[77] S.R. Jadhav, D.X. Sui, R.M. Garavito, R.M. Worden, Fabrication of highly insulating tethered bilayer lipid membrane using yeast cell membrane fractions for measuring ion channel activity, Journal of Colloid and Interface Science 322 (2008) 465–472.
[78] R. Campos, R. Kataky, Electron transport in supported and tethered lipid bilayers modified with bioelectroactive molecules, Journal of Physical Chemistry B 116 (2012) 3909–3917.
[79] A. Zebrowska, P. Krysinski, Z. Lotowski, Electrochemical studies of blocking properties of solid supported tethered lipid membranes on gold, Bioelectrochemistry 56 (2002) 179–184.
[80] B.P. Oberts, G.J. Blanchard, Headgroup-dependent lipid self-assembly on zirconium phosphate-terminated interfaces, Langmuir 25 (2009) 13918–13925.
[81] A.S. Viana, M. Kalaji, L.M. Abrantes, Self-assembled monolayers of Vitamin B-12 disulphide derivatives on gold, Electrochimica Acta 47 (2002) 1587–1594.
[82] Z.H. Wang, A.S. Viana, G. Jin, L.M. Abrantes, Immunosensor interface based on physical and chemical immunoglobulin G adsorption onto mixed self-assembled monolayers, Bioelectrochemistry 69 (2006) 180–186.
[83] J. Ekeroth, P. Konradsson, F. Hook, Bivalent-ion-mediated vesicle adsorption and controlled supported phospholipid bilayer formation on molecular phosphate and sulfate layers on gold, Langmuir 18 (2002) 7923–7929.
[84] S. Ip, J.K. Li, G.C. Walker, Phase segregation of untethered zwitterionic model lipid bilayers observed on mercaptoundecanoic-acid-modified gold by AFM imaging, Langmuir 26 (2010) 11060–11070.
[85] A.H. Kycia, J.P. Wang, A.R. Merrill, J. Lipkowski, Atomic force microscopy studies of a floating-bilayer lipid membrane on a Au(1 1 1) surface modified with a hydrophilic monolayer, Langmuir 27 (2011) 10867–10877.
[86] S.M. Schiller, R. Naumann, K. Lovejoy, H. Kunz, W. Knoll, Archaea analogue thiolipids for tethered bilayer lipid membranes on ultrasmooth gold surfaces, Angewandte Chemie-International Edition 42 (2003) 208–211.
[87] L.H. He, J.W.F. Robertson, J. Li, I. Karcher, S.M. Schiller, W. Knoll, R. Naumann, Tethered bilayer lipid membranes based on monolayers of thiolipids mixed with a complementary dilution molecule. 1. Incorporation of channel peptides, Langmuir 21 (2005) 11666–11672.
[88] A. Erbe, R.J. Bushby, S.D. Evans, L.J.C. Jeuken, Tethered bilayer lipid membranes studied by simultaneous attenuated total reflectance infrared spectroscopy and electrochemical impedance spectroscopy, Journal of Physical Chemistry B 111 (2007) 3515–3524.
[89] B.R. Dorvel, H.M. Keizer, D. Fine, J. Vuorinen, A. Dodabalapur, R.S. Duran, Formation of tethered bilayer lipid membranes on gold surfaces: QCM-Z and AFM study, Langmuir 23 (2007) 7344–7355.
[90] A. Junghans, I. Koper, Structural analysis of tethered bilayer lipid membranes, Langmuir 26 (2010) 11035–11040.
[91] J. Kunze, J. Leitch, A.L. Schwan, R.J. Faragher, R. Naumann, S. Schiller, W. Knoll, J.R. Dutcher, J. Lipkowski, New method to measure packing densities of self-assembled thiolipid monolayers, Langmuir 22 (2006) 5509–5519.
[92] I.K. Vockenroth, P.P. Atanasova, A.T.A. Jenkins, I. Koper, Incorporation of alpha-hemolysin in different tethered bilayer lipid membrane architectures, Langmuir 24 (2008) 496–502.
[93] V.L. Sukhorukov, W.M. Arnold, U. Zimmermann, Hypotonically induced changes in the plasma-membrane of cultured-mammalian-cells, Journal of Membrane Biology 132 (1993) 27–40.
[94] C. Solsona, B. Innocenti, J.M. Fernandez, Regulation of exocytotic fusion by cell inflation, Biophysical Journal 74 (1998) 1061–1073.
[95] L.J. Gentet, G.J. Stuart, J.D. Clements, Direct measurement of specific membrane capacitance in neurons, Biophysical Journal 79 (2000) 314–320.
[96] G. Margheri, R. D'Agostino, L. Becucci, R. Guidelli, B. Tiribilli, M. Del Rosso, Surface plasmon resonance as detection tool for lipids lateral mobility in biomimetic membranes, Biomedical Optics Express 3 (2012).
[97] H. Basit, A. Van der Heyden, C. Gondran, B. Nysten, P. Dumy, P. Labbe, Tethered bilayer lipid membranes on mixed self-assembled monolayers of a novel anchoring thiol: impact of the anchoring thiol density on bilayer formation, Langmuir 27 (2011) 14317–14328.
[98] F. Heinrich, T. Ng, D.J. Vanderah, P. Shekhar, M. Mihailescu, H. Nanda, M. Losche, A new lipid anchor for sparsely tethered bilayer lipid membranes, Langmuir 25 (2009) 4219–4229.
[99] D.J. McGillivray, G. Valincius, D.J. Vanderah, W. Febo-Ayala, J.T. Woodward, F. Heinrich, J.J. Kasianowicz, M. Losche, Molecular-scale structural and functional characterization of sparsely tethered bilayer lipid membranes, Biointerphases 2 (2007) 21–33.
[100] W. Knoll, I. Koper, R. Naumann, E.K. Sinner, Tethered bimolecular lipid membranes – a novel model membrane platform, Electrochimica Acta 53 (2008) 6680–6689.
[101] E.K. Sinner, S. Ritz, R. Naumann, S. Schiller, W. Knoll, Self-Assembled Tethered Bimolecular Lipid Membranes, Elsevier Academic Press Inc., San Diego, 2009.
[102] L.J.C. Jeuken, S.A. Weiss, P.J.F. Henderson, S.D. Evans, R.J. Bushby, Impedance spectroscopy of bacterial membranes: coenzyme-Q diffusion in a finite diffusion layer, Analytical Chemistry 80 (2008) 9084–9090.
[103] I.K. Vockenroth, P.P. Atanasova, J.R. Long, A.T.A. Jenkins, W. Knoll, I. Koper, Functional incorporation of the pore forming segment of AChR M2 into tethered bilayer lipid membranes, Biochimica et Biophysica Acta: Biomembranes 1768 (2007) 1114–1120.
[104] L. Rose, A.T.A. Jenkins, The effect of the ionophore valinomycin on biomimetic solid supported lipid DPPTE/EPC membranes, Bioelectrochemistry 70 (2007) 387–393.
[105] Z. Salamon, G. Tollin, Interfacial electrochemistry of cytochrome-C at a lipid bilayer modified electrode – effect of incorporation of negative charges into the bilayer on cyclic voltammetric parameters, Bioelectrochemistry and Bioenergetics 26 (1991) 321–334.
[106] Z. Zhang, A.E.F. Nassar, Z.Q. Lu, J.B. Schenkman, J.F. Rusling, Direct electron injection from electrodes to cytochrome P450(cam) in biomembrane-like films, Journal of the Chemical Society: Faraday Transactions 93 (1997) 1769–1774.
[107] J.F. Rusling, Enzyme bioelectrochemistry in cast biomembrane-like films, Accounts of Chemical Research 31 (1998) 363–369.
[108] Y.X. Liu, W.Z. Wei, Detection of cytochrome c at biocompatible nanostructured au-lipid bilayer-modified electrode, Analytical Sciences 24 (2008) 1431–1436.
[109] A.E.F. Nassar, Z. Zhang, N.F. Hu, J.F. Rusling, T.F. Kumosinski, Proton-coupled electron transfer from electrodes to myoglobin in ordered biomembrane-like films, Journal of Physical Chemistry B 101 (1997) 2224–2231.
[110] M.R. Moncelli, L. Becucci, A. Nelson, R. Guidelli, Electrochemical modeling of electron and proton transfer to ubiquinone-10 in a self-assembled phospholipid monolayer, Biophysical Journal 70 (6) (1996) 2716–2726.
[111] D. Marchal, W. Boireau, J.M. Laval, J. Moiroux, C. Bourdillon, Electrochemical measurement of lateral diffusion coefficients of ubiquinones and plastoquinones of various isoprenoid chain lengths incorporated in model bilayers, Biophysical Journal 74 (4) (1998) 1937–1948.
[112] L. Becucci, F. Scaletti, R. Guidelli, Gel-phase microdomains and lipid rafts in monolayers affect the redox properties of ubiquinone-10, Biophysical Journal 101 (1) (2011) 134–143.
[113] C.A. Yu, L. Yu, Mitochondrial ubiquinol-cytochrome-c reductase complex – crystallization and protein:ubiquinone interaction, Journal of Bioenergetics and Biomembranes 25 (1993) 259–273.
[114] A.Y. Mulkidjanian, Ubiquinol oxidation in the cytochrome bc(1) complex: reaction mechanism and prevention of short-circuiting, Biochimica et Biophysica Acta: Bioenergetics 1709 (2005) 5–34.
[115] L. Ernster, P. Forsmark, K. Nordenbrand, The mode of action of lipid-soluble antioxidants in biological membranes. Relationship between the effects of ubiquinol and vitamin E as inhibitors of lipid peroxidation in submitochondrial particles, Journal of nutritional science and vitaminology (1992) 548–551.
[116] L. Ernster, P. Forsmarkandree, Ubiquinol – an endogenous antioxidant in aerobic organisms, Clinical Investigator 71 (1993) S60–S65.
[117] E. Briand, M. Zach, S. Svedhem, B. Kasemo, S. Petronis, Combined QCM-D and EIS study of supported lipid bilayer formation and interaction with pore-forming peptides, Analyst 135 (2010) 343–350.
[118] T. Wilkop, D.K. Xu, Q. Cheng, Characterization of pore formation by streptolysin o on supported lipid membranes by impedance spectroscopy and surface plasmon resonance spectroscopy, Langmuir 23 (2007) 1403–1409.
[119] T. Heimburg, Lipid ion channels, Biophysical Chemistry 150 (2010) 2–22.
[120] C. Shao, B. Sun, M. Colombini, D.L. DeVoe, Rapid microfluidic perfusion enabling kinetic studies of lipid ion channels in a bilayer lipid membrane chip, Annals of Biomedical Engineering 39 (2011) 2242–2251.
[121] G. Kroemer, B. Dallaporta, M. Resche-Rigon, The mitochondrial death/life regulator in apoptosis and necrosis, Annual Review of Physiology 60 (1998) 619–642.
[122] M. Crompton, The mitochondrial permeability transition pore and its role in cell death, Biochemical Journal 341 (1999) 233–249.
[123] P. Bernardi, L. Scorrano, R. Colonna, V. Petronilli, F. Di Lisa, Mitochondria and cell death – mechanistic aspects and methodological issues, European Journal of Biochemistry 264 (1999) 687–701.
[124] J. Narula, P. Pandey, E. Arbustini, N. Haider, N. Narula, F.D. Kolodgie, B. Dal Bello, M.J. Semigran, A. Bielsa-Masdeu, G.W. Dec, S. Israels, M. Ballester, R. Virmani, S. Saxena, S. Kharbanda, Apoptosis in heart failure: release of cytochrome c from mitochondria and activation of caspase-3 in human cardiomyopathy, Proceedings of the National Academy of Sciences of the United States of America 96 (1999) 8144–8149.
[125] B.M. Castro, L.C. Silva, A. Fedorov, R.F.M. de Almeida, M. Prieto, Cholesterol-rich fluid membranes solubilize ceramide domains: implications for the structure and dynamics of mammalian intracellular and plasma membranes, Journal of Biological Chemistry 284 (2009) 22978–22987.
[126] H.M. Chang, R. Reitstetter, R.P. Mason, R. Gruener, Attenuation of channel kinetics and conductance by cholesterol – an interpretation using structural stress as a unifying concept, Journal of Membrane Biology 143 (1995) 51–63.
[127] C. Baier, C. Gallegos, V. Levi, F. Barrantes, Cholesterol modulation of nicotinic acetylcholine receptor surface mobility, European Biophysics Journal 39 (2010) 213–227.

[128] H.M. Chang, R. Reitstetter, R. Gruener, Lipid-ion channel interactions – increasing phospholipid headgroup size but not ordering acyl chains alters reconstituted channel behavior, Journal of Membrane Biology 145 (1995) 13–19.
[129] S.S. Antollini, F.J. Barrantes, Unique effects of different fatty acid species on the physical properties of the torpedo acetylcholine receptor membrane, Journal of Biological Chemistry 277 (2002) 1249–1254.
[130] V.L. Perillo, G.A. Fernández-Nievas, A.S. Vallés, F.J. Barrantes, S.S. Antollini, The position of the double bond in monounsaturated free fatty acids is essential for the inhibition of the nicotinic acetylcholine receptor, Biochimica et Biophysica Acta: Biomembranes 1818 (2012) 2511–2520.
[131] M.Z. Yue, X. Zhu, Y.Q. Zheng, T. Hu, L.M. Yang, X.P. Wu, Amphotericin B ion channel mimetic sensor: a new type of potassium-selective sensor based on electrode-supported hybrid bilayer membranes, Electrochimica Acta 73 (2012) 78–85.
[132] L. Zheng, L. Xiong, D. Zheng, Y. Li, Q. Liu, K. Han, W. Liu, K. Tao, S. Yang, J. Xia, Bilayer lipid membrane biosensor with enhanced stability for amperometric determination of hydrogen peroxide, Talanta 85 (2011) 43–48.
[133] M.B. Fritzen-Garcia, V.C. Zoldan, I.R.W.Z. Oliveira, V. Soldi, A.A. Pasa, T.B. Creczynski-Pasa, Peroxidase immobilized on phospholipid bilayers supported on Au(1 1 1) by DTT self-assembled monolayers: application to dopamine determination, Biotechnology and Bioengineering 110 (2013) 374–382.
[134] B.A. Cornell, V.L.B. BraachMaksvytis, L.G. King, P.D.J. Osman, B. Raguse, L. Wieczorek, R.J. Pace, A biosensor that uses ion-channel switches, Nature 387 (1997) 580–583.
[135] M. Trojanowicz, A. Miernik, Bilayer lipid membrane glucose biosensors with improved stability and sensitivity, Electrochimica Acta 46 (2001) 1053–1061.
[136] T. Nakaminami, S.i. Ito, S. Kuwabata, H. Yoneyama, A biomimetic phospholipid/alkanethiolate bilayer immobilizing uricase and an electron mediator on an au electrode for amperometric determination of uric acid, Analytical Chemistry 71 (1999) 4278–4283.
[137] L. Steller, M. Kreir, R. Salzer, Natural and artificial ion channels for biosensing platforms, Analytical and Bioanalytical Chemistry 402 (2012) 209–230.
[138] S. Kissler, S. Pierrat, T. Zimmermann, H. Vogt, H.K. Trieu, I. Koper, CMOS based capacitive biosensor with integrated tethered bilayer lipid membrane for real-time measurements, Biomedizinische Technik 57 (2012).
[139] M. Andersson, H.M. Keizer, C. Zhu, D. Fine, A. Dodabalapur, R.S. Duran, Detection of single ion channel activity on a chip using tethered bilayer membranes, Langmuir 23 (2007) 2924–2927.
[140] A.I. Michaloliakos, G.P. Nikoleli, C.G. Siontorou, D.P. Nikolelis, Rapid flow injection electrochemical detection of arochlor 1242 using stabilized lipid membranes with incorporated sheep anti-PCB antibody, Electroanalysis 24 (2012) 495–501.
[141] G. Favero, L. Campanella, S. Cavallo, A. D'Annibale, M. Perrella, E. Mattei, T. Ferri, Glutamate receptor incorporated in a mixed hybrid bilayer lipid membrane array, as a sensing element of a biosensor working under flowing conditions, Journal of the American Chemical Society 127 (2005) 8103–8111.
[142] J. Shah, J.M. Atienza, R.I. Duclos, A.V. Rawlings, Z. Dong, G.G. Shipley, Structural and thermotropic properties of synthetic C16:0 (palmitoyl) ceramide: effect of hydration, Journal of Lipid Research 36 (1995) 1936–1944.

Chapter II

Characterization techniques

In this chapter, the principles of the main characterization techniques used throughout this work will be briefly described. The surface characterization (AFM, ellipsometry, QCM and SPR) and electrochemical (cyclic voltammetry) techniques will be mentioned first, followed by a general overview of fluorescence spectroscopy, as a tool to assess the biophysical properties of free standing lipid bilayers (liposomes) and interaction of bioactive molecules with those liposomes. Both surface and electrochemical techniques were employed in the characterization of SLB, the solid substrates (mica, silicon and bare and modified gold) used for the preparation of those SLB and in the study of the interaction of small molecules with lipid membranes. Since there is a great complementarity regarding the techniques employed throughout this thesis, their combined use allows for a comprehensive characterization of the systems under investigation. For example, for SLB prepared on gold, electrochemical, optical and scanning probe techniques can be employed in their characterization and, thus, it is possible to conclude about the thickness, compactness, stability and continuity of SLB as well as assess the presence of lipid domains.

2.1. Atomic Force Microscopy

AFM is an exceptional technique for obtaining morphological information on any type of surface, providing it is sufficiently rigid, and also structural details for very flat materials, with lateral resolution in the nanometer scale and a vertical resolution in the Ånsgström range. The sample can be probed whether exposed to air or immersed into a liquid and under different conditions, such as at different temperatures. In this work AFM was used, at a first instance, to gather information concerning the organization and morphological arrangement of SLB and lipid films formed on different solid substrates, namely mica, silicon and gold. During this thesis, AFM was also employed to follow the effects that small molecules promote in the organization of lipid bilayers displaying a wide range of compositions and consequently exhibiting distinct phase behavior. AFM can have indeed a broad spectrum of biological applications, spanning from the study of DNA and lipid bilayers to cells, as it will be discussed ahead under section 2.1.3.

This scanning probe microscopy can analyze areas that may go from less than 1 nm^2 up to 10000 μm^2 or higher. Additionally, samples with distinct degrees of roughness can be analyzed since the vertical scale may range up to 8 to 10 μm. This technique is also suitable to investigate attractive and repulsive, short- and long-range atomic and molecular forces in the order of 10^{-12}

Newton. Since its operational principle is the variation of forces established between the surface and an interacting probe, it is not required that analyzed samples are electrically conductive, and therefore there is no need for metallic coating or even the use of dyes or other contrast agent in opposition to other microscopic techniques. In addition, AFM is non-destructive allowing the same sample to be imaged over time, before and after different treatments, and enables the sample to be reused e.g., for characterization with other techniques.[1-3] In fact, during this thesis, the same sample prepared on gold substrate was, frequently, analyzed by AFM, ellipsometry and cyclic voltammetry.

Figure 1 shows a schematic representation of one of the main components of an atomic force microscope. Its operation is based on scanning and probing a sample by an extremely sharp tip that is mounted at the end of a cantilever. As the tip interacts with the surface, the cantilever undergoes a vertical deflection (up or down) acting as a spring sensitive to slight variations in force. The most common approach to measure these variations is the use of a laser beam focused on the cantilever end, which is reflected into a position sensitive photodetector. Consequently, topographic variations in the sample will induce alterations in the cantilever angle, which, in turn, generates different voltages in the detector. These voltages are recorded and sent to a computer for processing and formation of the topographic image.

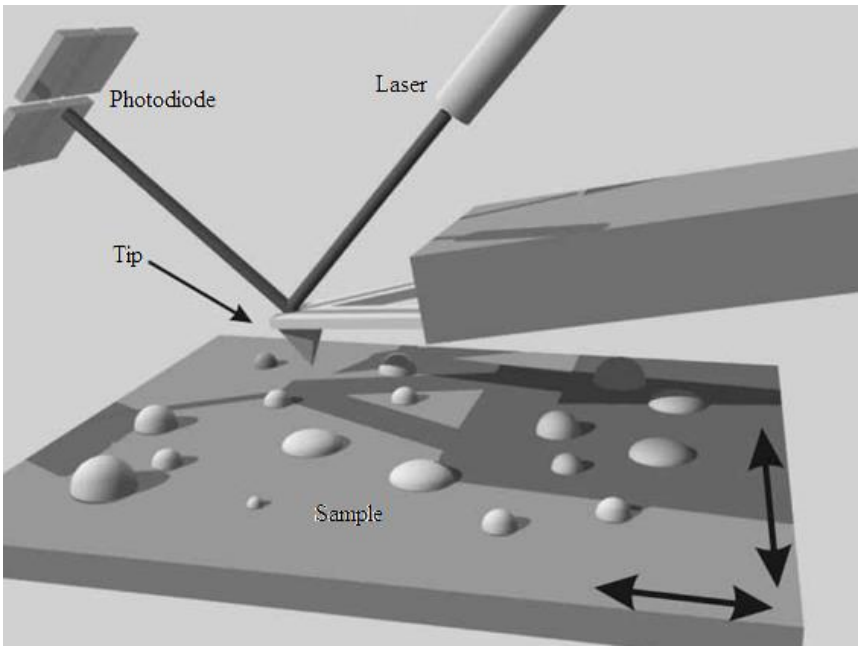

Figure 1 – Schematic representation of operation of an atomic force microscope. The sample is moved by a piezoelectric scanner. As the sample is scanned, the movement of the tip is detected by the photodiode through a laser beam reflected from the back of the cantilever. Adapted from ref.[1]

2.1.1. Modes of operation

This section will focus on the modes of operation related to the acquisition of topographic images. According to the purpose of an experiment and considering the general properties of a sample three main modes of operation can be employed. In Figure 2 the relation between the forces (attractive or repulsive) generated upon tip-sample interaction and the different modes of operation is illustrated.

Contact Mode

In this mode of operation, which can be also designated by constant force mode, the forces ruling the tip-sample interaction are the interatomic repulsive ones. The tip is kept in contact with the surface of the sample and the cantilever deflection is held constant during the scanning through a feedback loop. The feedback acts in order to maintain the tip-sample separation constant along the scan independently on the topographic features of the sample. In this sense, a topographic image is formed and image contrast depends on the applied force, which in turn, depends on the spring force of the cantilever. The major advantage of this mode is its high resolution even for samples with large variations in height. However, because the tip is kept in close contact with the sample large lateral forces are generated, which can damage soft biological samples or polymer networks. In order to minimize the influence of the tip on the sample surface, this mode can be performed in liquids allowing for a significant reduction of the capillary forces generated between the tip and the sample during the scanning.[1-3]

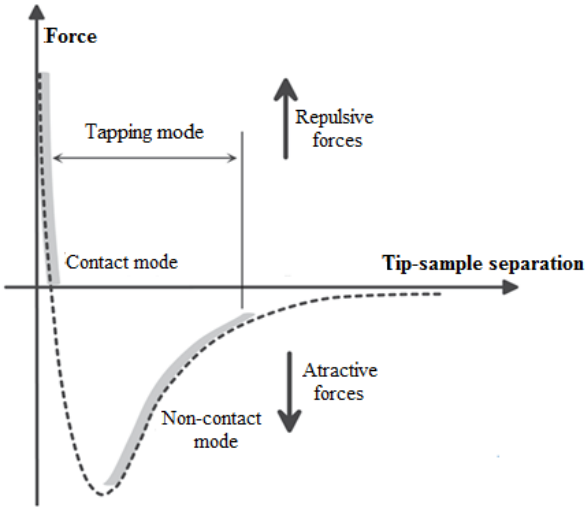

Figure 2 – Expected behavior of the idealized forces between tip and sample according to their separation. The separation range at which each mode of operation works is also highlighted. Adapted from ref[2].

Non-Contact Mode

In this mode of operation the forces governing the tip-sample interaction are the attractive van der Walls or long-range forces. Concretely, a cantilever oscillating at a frequency close to its resonance frequency is brought into proximity of the sample surface without touching it. As a consequence of the interaction a frequency shift in the oscillation of the cantilever is induced. Through a feedback loop this oscillation is kept at a fixed frequency or amplitude and a topographic map of the sample surface is generated. Though a good vertical resolution can be obtained, its lateral resolution is not as good as the one attained with other scanning modes since the tip-sample interaction is not very strong in this mode. Consequently, the sample suffers no damage by virtue of the complete absence of any contact between the tip and the samples. The fact that this mode cannot be performed in liquids constitutes its main drawback. The presence of a single layer of water might be sufficient to trap the tip onto the surface of (supposedly) dried samples since the low oscillating amplitude does not drive the required energy to promote the detachment of the tip.[1-3]

Tapping Mode

This is perhaps the most employed mode, especially for the analysis of soft surfaces as in the case of biological samples. In this mode, also designated as intermittent contact mode, the forces in play are both attractive and repulsive depending on the tip-sample separation (Figure 2). An oscillating cantilever is brought into close contact with the sample which causes a dampening of the oscillation amplitude. Similarly to other modes, a feedback loop is used. It maintains the oscillation amplitude at a fixed value by either lifting or lowering the sample (or the tip, depending on the equipment used). In contact mode, the axial and lateral resolutions are better than for the non-contact, and relatively to the contact mode, the tapping involves minimal tip-sample interaction, which leads to a great reduction of the lateral forces that may damage soft samples.[1-3]

In the oscillating modes besides topography further information can be retrieved. In the case of *tapping* mode by comparing the applied oscillation and the actual one, a phase signal is generated, which is intimately related to the local mechanical and chemical properties of the sample. In that sense, regions of the sample with the same height, although displaying distinct chemical properties will interact differently with the tip and thus generate unique phase signals allowing for their differentiation.[1-3]

This mode of operation in solution was the one used throughout this work. Although it is common to find in the literature concerning the analysis of SLB results obtained in the contact mode, in the present thesis, tapping mode was used. This was done to ensure that the information contained in the topographic image had minimal influence of the tip in the sample. In this way, lateral forces were greatly reduce and thus any damage promoted by imaging in contact could be avoided, which enabled a clear observation of membrane domains, e.g. lipid rafts, which could not be detected in this work with a similar resolution using contact mode. This can be especially relevant in the case of studying the effect of small molecules on lipid bilayers where a change in the shape and thickness of lipid domains occurs over time. Also, for the characterization of lipid tubular structures which can be highly deformable when compared to a planar lipid bilayer, tapping mode can be advantageous over contact mode.

2.1.2. Instrumentation

The atomic force microscope is comprised by innumerous components. The key components of an atomic force microscopic are described next.

Tip and Cantilever

As mentioned above the tip is mounted at the end of a cantilever and is one of the crucial components of the microscope since it is the element that interacts with the sample generating the topographical images. Usually, the assembly tip/cantilever is fabricated in silicon, silicon nitride or diamond. The most important parameters that define a good tip are the sharpness of its apex, measured by the radius of curvature, and the ratio between the height of the tip and the width of its base. Generally, the sharper the tip the most detailed (highest resolution) will be the final AFM image.[1-3]

Cantilevers are constructed with two distinct geometries, rectangular and triangular, which, essentially, respond differently to torsional/lateral forces that can affect the resolution of topographic images. The most important characteristic of a cantilever are its dimension, resonance frequency and spring constant, which is a measure of the cantilever flexibility. Shorter cantilevers allow for a greater resolution. The resonance frequency should be high in order to avoid interferences from the inherent vibrations of the building and the acoustical noise. Soft cantilevers

(with low spring constant) and of low resonance frequency are suitable for the analysis of samples immersed in a liquid both in contact and resonance mode, whereas stiff cantilevers (higher spring constant) with high resonance frequency are indicated for the study of samples in resonance mode in air.[1-3] In the present work soft triangular cantilevers (Figure 3a) were employed since lipid bilayers are a soft and compressible biological sample. Moreover, in order to confer a more biomimetic environment the samples were imaged in buffer solutions at physiological pH.

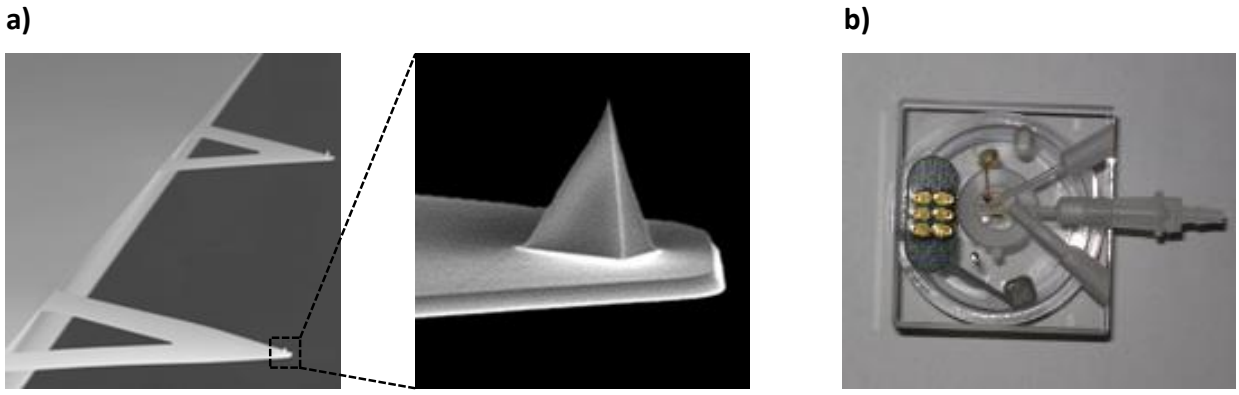

Figure 3 – Triangular cantilevers used throughout this thesis for imaging in liquids with a detail of the tip (a) and the liquid cell used for experiments carried out with the sample immerse in buffer (b). In (a) tip height may go from 2.5 μm to 8.0 μm, whereas its radius is close to 2 nm.

Piezoelectric Scanner

The AFM scanner is made of piezoelectric materials which are characterized by a singular property. They undergo an alteration of their dimensions upon the application of an electric field. Considering that the applied voltages are strictly controlled, extremely exact movements in x, y and z directions can be made. Instruments may display one of two configurations; either the sample is mounted directly on top of the scanner or the assembly tip-cantilever is mounted on the scanner, above the sample that, in this case, is fixed. The first condition allows for a higher scanning rate and the visualization of larger areas, whereas the latter permits the use of samples with larger dimensions.[1-3] The first configuration is the one used thourghout this thesis. Although this design imposes a restriction in sample size it was not a limiting factor for the AFM analysis carried out. However, this configuration demands extra caution when working in liquids in order to avoid the contact of the liquid with the scanner.

Photodetector

As mentioned above the method of detection is based on the reflection of a laser beam from the top of the cantilever into a position sensitive photodetector. This photodetector consists of two (or four) photodiodes side by side. With this configuration any minimal deflection of the cantilever will promote a variation in the angle of the reflected laser and consequently the spot at which the laser hits the detector. Thus, the difference between the signals coming from the two (or four) photodiodes will indicate the position of the laser on the detector and therefore the angular deflection of the cantilever. Since the distance between the cantilever and the detector is three orders of magnitude higher than the length of the cantilever, this method of detection enables to significantly magnify the movements of the tip with great sensitivity. The configuration of the atomic force microscope allows detecting with high accuracy the movements of the cantilever and thus providing a detailed topographic image of the surface.[1-3]

All AFM experiments described and presented throughout this work were performed with the sample immersed in liquid and at room temperature using a liquid cell (Figure 3b). A Multimode Nanoscope IIIa (Digital Instruments, Veeco) was used. Topographic images were obtained in tapping mode and keeping the force exerted on the sample as low as possible by continuously adjusting the "set point" parameter. Scan rate was close to 1.9 Hz. Before each experiment the glass support where the cantilever is mounted was washed several times with water and ethanol. The cantilevers used were fabricated in silicon nitride with a resonance frequency close to 9 kHz in liquid.

2.1.3. Biological Applications

AFM imaging can be used to study a great diversity of biologically-related mechanisms. One of the biological applications of AFM is in the study of nucleic acids, where it can be used to evaluate the structural damage in chromosomes upon exposure to radiation[4,5], to study the conformation of the double helix[6], to measure the mechanical properties of DNA and its modulation by additions of small molecules[7-8]. The study of protein-protein or protein-membrane interactions at the molecular level has also benefited from the use of AFM[9-11]. For example it has been possible to study the dependence of amyloid fibril formation with lipid composition, charge and phase as well as the aggregation of amyloid-beta peptide in various lipid systems[12,13] or even

the inibhition of islet amyloid polypeptide fibril formation by compounds with therapeutic potential[14]. Recently, with the introduction of high-speed AFM a new field of applications emerges and it has been possible, for example, to follow the motion of membrane protein assemblies in SLB[15]. The imaging of living cells has also been reported[16,17] with real time visualization of supramolecular assemblies of proteins in the surface of cell membrane of living cells[18-21] (Figure 4). AFM can also find application in following cellular processes such as endocytosis[22]. A consequent derivation of using AFM in the inspection of living cells is the use of functionalized tips in order to chemically map the surface of the membrane and in this way determine the precise location of target proteins[23].

The first reports concerning the study of SLB by AFM date from more than 20 years ago[24]. Due to its unique vertical resolution, the heterogeneity of supported lipid bilayers can be probed with extremely high spatial resolution and because of that it has been widely used in the characterization of membrane domains, namely lipid rafts. Concretely, the presence of such lipid domains differing in height, from the surrounding bilayer, by ~1 nm can be clearly depicted with this technique[25,26] (as showns in chapters III, IV and V). The remarkable resolution of AFM has also helped in the characterization of corrugated lipid bilayers formed on gold substrates[27] (see also chapter V). Furthermore, it is possible to follow, in real time, the changes induced by small molecules, such as anesthetics, in the structure of the lipid bilayer[28,29] (discussed in chapter IV).

Figure 4 – Example of supramolecular structures observed by AFM. Here, the structure of photosynthetic complexes of *Rhodospirillum photometricum* is illustrated. Adapted from reference [19]

Recently, super-resolution optical techniques have witnessed an unprecedented growth[30]. Still, AFM emerges as one of the main techniques regarding the characterization of lipid bilayers. Due to its versatility it can gather a considerable amount of information concerning different properties of the lipid bilayers. It is possible to assess the topography of the lipid films and thus not

only quantitatively evaluate the phase behavior of the lipid system under study but also to determine the thickness of each lipid phase. Furthermore, AFM enables to study the mechanical properties of lipid bilayers. As mentioned above, in this work, AFM was employed to assess the topography (nano/mirco-domains, thickness changes) and evaluate the quality and organization (phase area fractions, domains size, shape) of multicomponent biomimetic lipid films formed on diverse solid substrates (mica, silicon, gold), whether modified or not in the case of gold electrodes. Moreover, AFM phase data has also been used to more easily assign gel and fluid phases as a consequence of their distinct mechanical properties, as shown in chapter IV.

2.2. Ellipsometry

2.2.1. Principles

As shall be detailed in chapters V and VI, ellipsometry is an optical technique that can be used for estimating the thickness of a thin film, by determining the change in the optical properties of the surface before and after film formation. Its combination with AFM allows to effectively evaluate the quality of the lipid bilayers prepared. Ellipsometric measurements rely on the incidence of a polarized light beam on a surface and on its re-polarization after reflection.

When light is traveling in one environment (air or solution) and encounters a new one (substrate) part will be reflected and part will be refracted[31-33] (Figure 5a). The interaction of light with this new medium can be described by the complex index of refraction $\tilde{N}$, as follows:

$$\tilde{N} = n - ik \qquad \text{eq.1}$$

where n is the index of refraction and k is the extinction coefficient and i denotes the imaginary number. The extinction coefficient is related to the absorption coefficient (α) through the following expression:

$$k = \frac{\lambda}{4\pi}\alpha \qquad \text{eq.2}$$

where λ is the wavelength of the incident light beam. If the new medium is transparent to the incident beam wavelength no light is absorbed and $k = 0$. Hence, $\tilde{N} = n$.

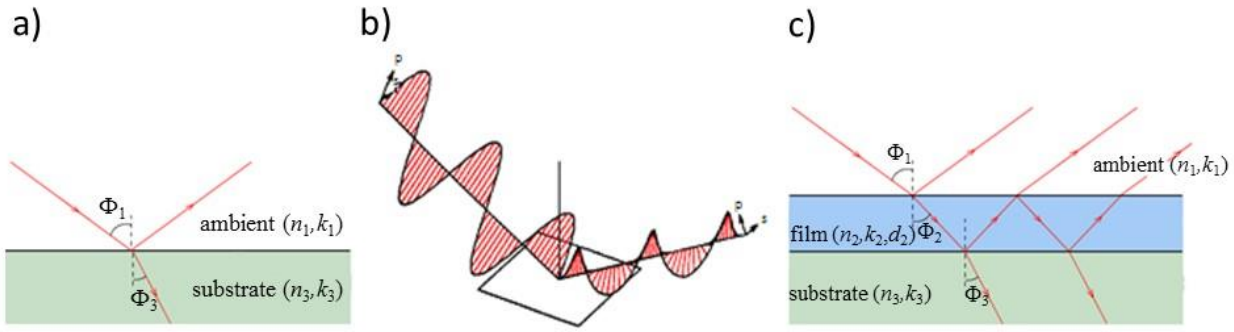

Figure 5 – Schematic representation of (a) specular reflection for a two phase model (air (or solution)-substrate), (b) modification of the amplitude and phase parameters in the parallel and perpendicular directions of an incident linearly polarized beam upon reflection from a surface, and (c) propagation of an incident beam through a three-component system (air (or solution)-film-substrate).

The portion of light that enters the new medium at an angle Φ_1 does not propagate in the same direction. Instead, it is refracted to a different angle, Φ_3. Φ_1 and Φ_3 are related by the "Snell's law" as follows:

$$\widetilde{N}_1 \sin \phi_1 = \widetilde{N}_3 \sin \phi_3 \qquad \text{eq.3}$$

For dielectric materials eq.3 becomes:

$$n_1 \sin \phi_1 = n_3 \sin \phi_3 \qquad \text{eq.4}$$

As mentioned above, in ellipsometry a linearly (or elliptically) polarized light beam hits a surface and its re-polarization state after reflection is analysed. Upon reflection a change of both phase and amplitude of the polarization components of light in directions *p* (parallel) and *s* (perpendicular) to the plane of incidence occurs (Figure 5b). The ellipsometric amplitude and phase parameters designated by Ψ and Δ, respectively, are defined in the fundamental equation of ellipsometry:

$$tan\Psi e^{i\Delta} = \frac{R^p}{R^s} \qquad \text{eq.5}$$

where R^p and R^s correspond to the ratio of the Fresnel reflection coefficients for parallel and perpendicular polarizations, respectively. The parallel and perpendicular Fresnel reflection coefficients are given by:

$$R_{12}^{p} = \frac{\tilde{N}_3 \cos\phi_1 - \tilde{N}_1 \cos\phi_3}{\tilde{N}_3 \cos\phi_1 + \tilde{N}_1 \cos\phi_3} \qquad R_{12}^{s} = \frac{\tilde{N}_1 \cos\phi_1 - \tilde{N}_3 \cos\phi_3}{\tilde{N}_1 \cos\phi_1 + \tilde{N}_3 \cos\phi_3} \qquad \text{eq.6}$$

In a situation of multiple interfaces, for example for a film-covered substrate (Figure 5c) the Fresnel coefficients will also depend on the thickness of the film. In this condition they are obtained by adding the total reflected rays. To describe the total reflection on a three-phase model, Drude's equation is used as follows:

$$R_{123}^{p} = \frac{R_{12}^{p} + R_{23}^{p} \exp(-i2\beta)}{1 + R_{12}^{p} R_{23}^{p} \exp(-i2\beta)} \qquad R_{123}^{s} = \frac{R_{12}^{s} + R_{23}^{s} \exp(-i2\beta)}{1 + R_{12}^{s} R_{23}^{s} \exp(-i2\beta)} \qquad \text{eq.7}$$

where R_{12} and R_{23} stand for the Fresnel reflection coefficients for the air/film and film/substrate interface, respectively. β represents the phase delay due to film thickness and is given by:

$$\beta = 2\pi \left(\frac{d}{\lambda}\right) \tilde{N}_2 \cos\phi_2 \qquad \text{eq.8}$$

where *d* stands for the thickness of the film.

When studying a film-covered surface as exemplified in Figure 5c, the Fresnel coefficients will depend not only on the refraction index of the surface and the film but also on the thickness of the film. Thus, employing a three-phase model – substrate/film/ambient – Ψ and Δ will be a function of the optical parameters of the system as follows

$$\Psi,\Delta = \Psi,\Delta[n_1, n_2, n_3, k_2, k_3, \Phi_1, \lambda, d] \qquad \text{eq.9}$$

The above description concerning light interaction with matter was based on refs.[31-33]

2.2.2. Instrumentation and Biological Applications

In this section, the optical elements of an ellipsometer (Figure 6) as well as their function will be mentioned briefly. First, a monochromatic source of light is necessary. Nowadays, this is

achieved by using a laser. Still, the use of a polychromatic source with monochromators can also be employed, especially if more than one wavelength is necessary. The beam generated by the light source will pass through a polarizer, which will linearly polarize the incident beam. After this the beam reaches another optical element designated as compensator, retarder or quarter-wave plate. Typically, this compensator (birefringent material) is an anisotropic optical element, i.e., with a refractive index that can be decomposed in two components. The compensator will transform the linearly polarized light into elliptically polarized light and it has two axes perpendicular to each other, a fast one and a slow one. The component of the electromagnetic wave aligned with the fast axis will pass the compensator faster than the component aligned with the slow axis, which will introduce a phase shift and linearly polarized light is converted into elliptically polarized light. In the instrument used in this work the compensator is not active and thus the light reaching the surface is linearly polarized. After reflection on a surface a phase shift from 0 to 360° can be introduced as well as an attenuation of the components of the electromagnetic wave may occur. The reflected beam then reaches another linear polarizer, the analyser, and finally the photodetector.[32-34]

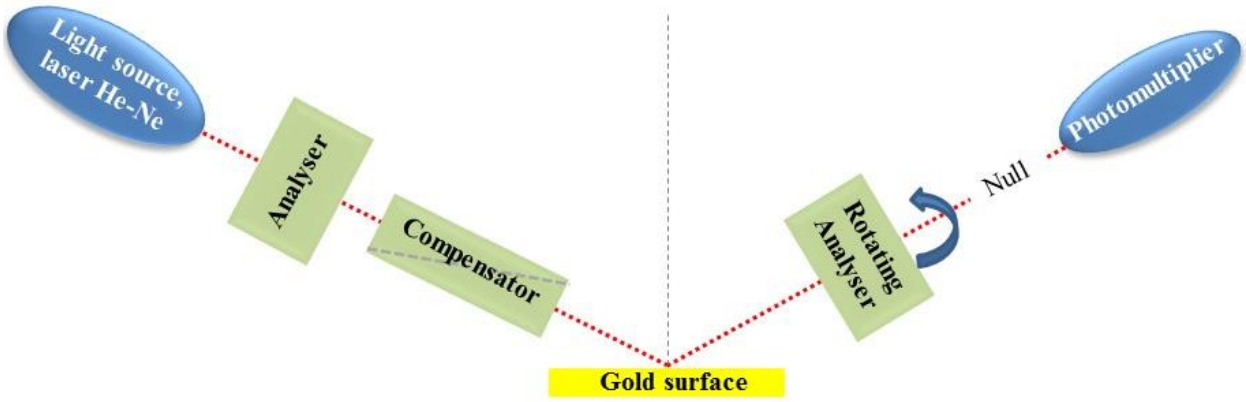

Figure 6 – Schematic representation of a rotating analyser ellipsometer. See text for details.

The orientation of the optical axes of the optical elements referred above is adjusted so that the ellipticity of the incident beam is exactly cancelled by reflection, i.e. the reflected beam is linearly polarised. In this way the null condition is achieved on the detector. In the instrument used a constant compensator azimuth of 45º is used. Then, the measurement consists on finding the angular readings of the polariser, P_{null}, and analyser, A_{null}, for which the intensity of the light reaching the photodetector is extinguished ("null point"). In this case, the relationship of Ψ and Δ

to P_{null} and A_{null}, is translated in terms of the following expressions, $\Delta = 270^{o} - 2P_{null}$ and $\Psi = A_{null}$.[32,33]

In this work, ellipsometry was used to evaluate the thickness of lipid films formed on both bare and modified gold surfaces. Ellipsometric measurements were performed with the sample exposed to air and at 70^{0} using a SE 400 Ellipsometer produced by SENTECH INSTRUMENTS equipped with a He-Ne laser (632.8 nm). Prior to each experiment the ellipsometric parameters (Ψ and Δ) of the bare gold substrate were measured. This procedure is important because not only is essential in order to estimate the thickness of the lipid films that will be formed on the surface but also it allows to attest that the gold surface is properly cleaned since this metal surface exhibits characteristic Ψ and Δ values. The thickness of the lipid layers was estimated from the variation of the ellipsometric parameters before and after vesicles deposition, using a three-phase model. As discussed above (eq. 9) for each λ the optical properties of a thin film depend on three parameters, n_2 and k_2, and the thickness of the film, d. However, these variables cannot be directly estimated from ellipsometric measurements at a single wavelength and incident angle, which yield only two measurable parameters, Ψ and Δ. In the case of transparent films, where $k = 0$, the solution is straightforward. If absorbing films are being considered, different strategies have been employed in order to solve this problem, which include reflectometric measurements, multiangle and multisample analysis[35-36]. Thin hydrocarbon layers are expected to be nearly transparent, and therefore their extinction coefficient, k, should be close to zero; however it was found that for these modified surfaces k, although very small, is not zero at the working wavelength, and therefore the real part of the refractive index, had to be fixed at 1.5, a value frequently employed for hydrocarbon layers[37] and determined to be the refractive index of gel lipids[38], in order to estimate the film thickness.

The use of ellipsometry to study lipid films formed on solid substrates is not very popular, though some examples can be found in literature. Ellipsometry has been used to follow the preparation of a cholesterol-based tether SAM for the generation of photopatterned lipid membrane arrays[39]; it has also been employed to monitor both the interaction of poly(amido amine) dendrimers and DNA aggregates with POPC lipid bilayers[40] and the influence of antimicrobial peptide melittin in the structure of diverse lipid binary systems[41]. This surface technique has been successfully employed in the study of the kinetics and dynamics of the process of SLB formation[42,43]. Moreover, the application of imaging ellipsometry has been shown to be suitable in

the quantitative characterization of SLB regarding their bilayer thicknesses, phase separation, and even the ligand-receptor binding interaction[44]. Regarding the work developed during this thesis, ellipsometry was an essential approach, in combination with AFM, in order to evaluate if the lipid films prepared on gold were spread throughout the substrate and, equally important, if a bilayer arrangement and not a multibilayer (or unfused vesicles) was being formed, as shall be elucidated in chapters V and VI. Moreover, the powerful axial resolution of ellipsometry allows to discriminate between lipids bilayer varying in composition and phase behaviour, as it is demonstrated also in chapters V and VI.

2.3. Cyclic Voltammetry

Cyclic voltammetry was the electrochemical technique employed in this work and it was used to study electroactive species in solution and adsorbed on or close to the electrode surface. In cyclic voltammetry a current intensity (*i*) is measured, as a result of oxidation or reduction of electroactive species in solution (faradaic reactions), upon the application of a potential sweep at a variable rate to a working electrode. The potential scan is performed in a defined direction, stopping at a selected value, at which the scan direction is inverted until it reaches another chosen value (Figure 7a) [45-49]. A cyclic voltammogram (Figure 7b) is obtained when a potential cycle, identical to the one described, is executed. In this work, a reversible electroactive system, $K_3Fe(CN)_6$ was used to evaluate the blocking properties of the SLB formed on bare or modified gold surfaces towards its redox process. Reversible systems are characterized by a fast electronic transfer where the concentration ratio between oxidized and reduced species is described by the Nernst equation. Also, the potential at which the current peak is verified for both oxidation and reduction is not changing with scan rate, and the ratio between anodic and cathodic peak currents is equal to one. For species in solution the current intensity is proportional to the square root of the scan rate according to the Randles-Sevcik equation [45-49]:

$$i_p = 0.4463nF\sqrt{\frac{nFD}{RT}}AC\sqrt{\nu} \qquad \text{eq.10}$$

where i_p is the peak current (A), *n* stands for the number of electrons transferred during the process, *F* is the Faraday constant (C/mol), *D* the diffusion coefficient (cm^2/s), *R* the gas constant ($JK^{-1}mol^{-1}$), *T* the absolute temperature (K), *A* the area of the electrode (cm^2), *C* the concentration (mol/cm^3) and ν is the scan rate (V/s).

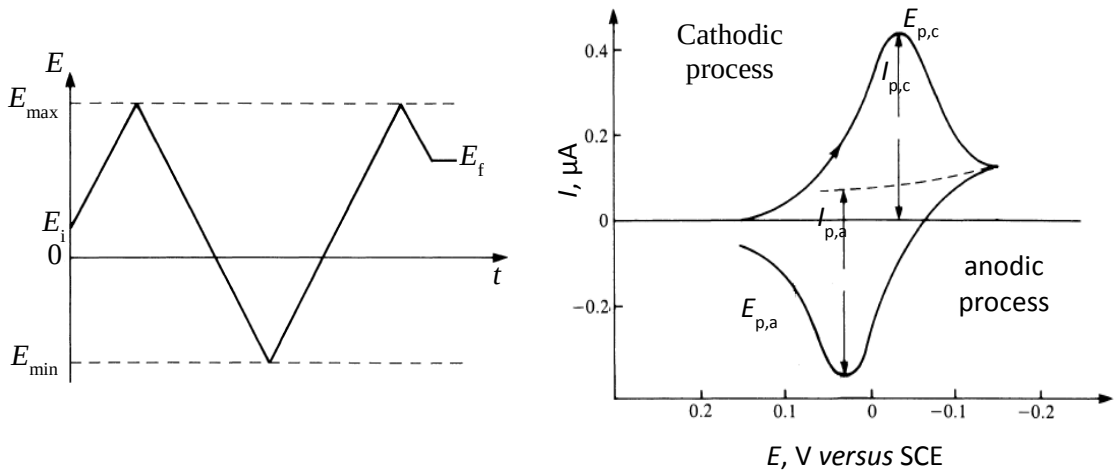

Figure 7 – The applied potential as a function of time in cyclic voltammetry is illustrated in a) showing the initial, E_i, final, E_f, maximum, E_{max}, and minimum, E_{min}, potentials. In b) an example of a cyclic voltammogram for a reversible system is shown with $E_{p,c}$ and $E_{p,a}$ corresponding to the potential of cathodic and anodic peak, respectively and $I_{p,c}$ and $I_{p,a}$ corresponding to the current of cathodic and anodic peak, respectively. Adapted from ref[46].

The electrochemical behavior of electroactive species adsorbed on the electrode surface or immobilized in its vicinity was also studied. In this particular work, the redox behavior of epinephrine and quercetin adsorbed onto SLB of various compositions was investigated. For adsorbed species the peak current is no longer dependent on their diffusion, rather it depends on the surface coverage (Γ) according to the following expression[45,46]:

$$i_p = \frac{n^2 F^2 A \Gamma \nu}{4RT} \qquad \text{eq.11}$$

Surface coverage (mol/cm^2) can also be retrieved by integrating the area under the oxidation or reduction peak after extrapolating and subtracting the charging current baseline, as exemplified in Figure 8. This procedure ensures that the contribution of the capacitive current, generated by the formation of the double layer, is eliminated and only the faradaic current, which arises from the electronic exchange between the electrode and the electroactive species, is counted. In the voltammetric experiments carried out in the course of this thesis involving lipid bilayers the electrical double layer has been significantly reduced after surface modification with lipids, which is coherent with previous reports that show a substantial reduction of the double layer capacitance after layer deposition[50], as a consequence of a lower amount of solvent and electrolyte ions in the immediate vicinity of the gold electrode. By performing the procedure referred above surface

coverage can be more accurately determined. Surface coverage is related to charge (Q), in Coulomb, by the following relationship:

$$\Gamma = \frac{Q}{nFA} \qquad \text{eq.12}$$

One important consideration withdrawn from eq. 11 is that the peak current intensity for adsorbed molecules depends linearly on the sweep rate, instead of the square root of the scan rate as verified for free species in solution.

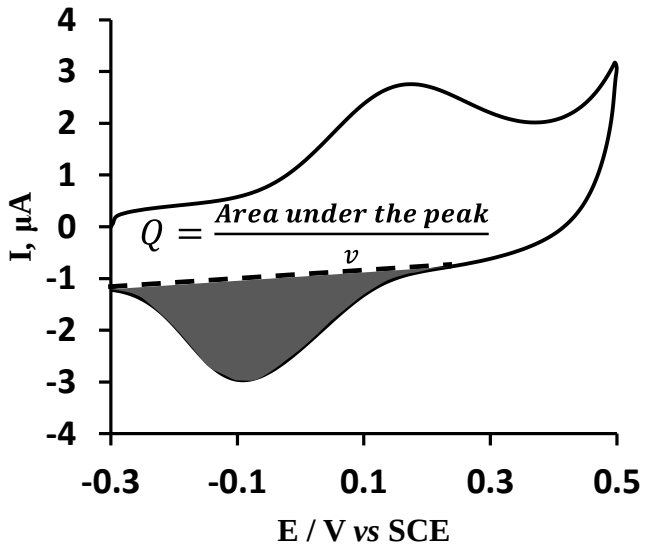

Figure 8 – – Exemplificative voltammogram to illustrate the area under the reduction peak after subtracting the charging current baseline (dashed line) which corresponds to the integration of the current involved in the process, therefore yielding the value of total charge that is related to the surface coverage. See text for details.

Cyclic voltammetry was conducted using a PARSTAT 2263 electrochemical station produced by AMETEK (Princeton Applied Research). A three electrode Teflon cell was used to carry out electrochemical measurements using a gold slide as working electrode, a saturated calomel electrode (SCE) as reference electrode and, finally, a platinum foil served as counter-electrode (Figure 9). The geometric area of the working electrode was defined by an O´ring and determined to be 0.5 cm^2. The electrolyte solution was degassed with ultrapure nitrogen before each experiment.

Electrochemical methods have been employed not only in the assessment of the compactness and integrity of SLB formed on diverse gold surfaces, but also in the analysis of membrane-related redox processes. These include the study of the redox process of membrane-associated proteins, such as cytochromes c and P450[51-53] or ion channels[54], and other biologically important electroactive molecules, as in the case of ubiquinol molecules[55-57], as well as the investigation of the changes in permeability promoted by the insertion of proteins or peptides into the lipid membrane[58,59]. In this work cyclic voltammetry has allowed to evaluate the blocking properties of the lipid films formed on gold surfaces and, therefore, to conclude about their extension and compactness. During this thesis, SLB that completely block the redox signal of $K_3Fe(CN)_6$ have been prepared, which enables to study electroactive molecules adsorbed on that SLB, as discussed ahead in chapter VI. Moreover, the use of cyclic voltammetry allowed to estimate surface coverages in the range of 10^{-11} mol.cm^{-2}, which shows the great sensitivity of this technique. By cyclic voltammetry it was also possible to observe that epinephrine, whose redox process in solution has irreversible characteristics (no reduction peak is detected in the potential range applied), presents a quasi-reversible behavior when adsorbed onto a lipid membrane, as illustrated under chapter VI.

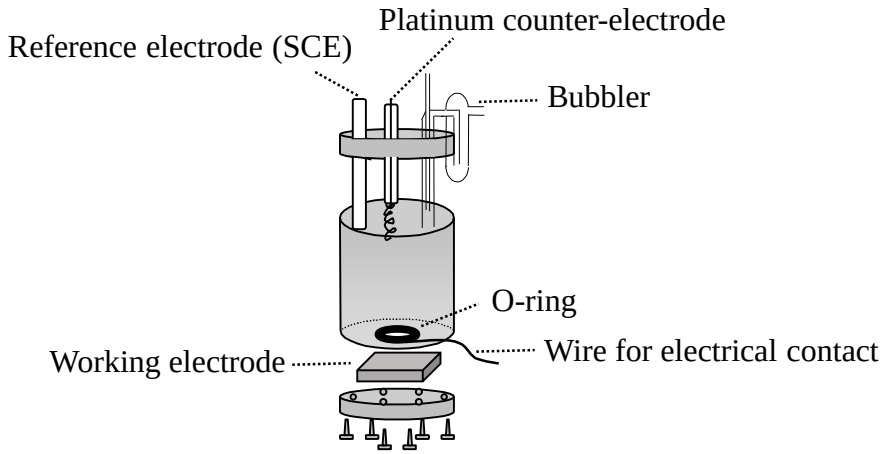

Figure 9 - Schematic representation of the electrochemical cell used in cyclic voltammetric experiments

2.4. Quartz Crystal Microbalance

Quartz crystal microbalance (QCM) can measure with high sensitivity mass variations, which can go down to 1 – 0.1 ng/cm^2 under favourable conditions[60]. Since QCM follows reactions over time the resulting data includes both kinetic and equilibrium information. The sensitive detection of QCM is achieved by using an oscillating quartz wafer[60-63]. This quartz wafer is a piezoelectric material (deforms in the presence of an electric field, as mentioned previously) and is cut from a single crystal of quartz at a defined angle[60, 62,63]. Typically, AT-cut crystals are used, which are cut at an angle of +35°10'[60].

In QCM two electrodes are deposited on opposite sides of the quartz wafer. They are used to generate an oscillating electric field perpendicular to the crystal surface, which induces a mechanical oscillation in the crystal. The direction of the oscillation is dependent on the orientation of the crystal lattice and for AT-cut crystals the mechanical shear oscillation is efficiently generated, in which the displacements, induced by the electric field, are parallel to the surface. The resonant frequency of this oscillation is intimately related to the thickness of the quartz crystal. The thicker the quartz wafer the lower the resonant frequency.[61-63]

There are multiple factors that can influence the frequency at which the crystal oscillates. They include the physical properties of the crystal (thickness, density and shear modulus), and other physical quantities such as the density and viscosity of the phases contacting each side of the crystal, pressure differences across the crystal or temperature, which are, usually, kept constant during the course of the experiment. The mass attached to the crystal is the physical quantity that changes during QCM experiments. These variations are effectively measured by QCM and the relationship between changes in mass and crystal oscillating frequency are expressed in terms of the Sauerbrey equation, which is derived assuming that the assembly of the crystal and adsorbed material is rigid[61-63]:

$$\Delta f = -\frac{2f_0^2}{A\sqrt{\rho_q \mu_q}}\Delta m \qquad \text{eq.13}$$

In this equation Δf is the frequency variation in Hz, f_0 stands for the resonant frequency, which for the instrument used in this work was determined by the manufacturer to be 8 MHz, A is the

piezoelectroative area of the crystal, ρ_q corresponds to the density of quartz which is 2.648 g/cm^3, $\mu_q$is the shear modulus of quartz for an AT-cut crystal which has a value of 2.947x10^{11} g/cm/s^{2}and Δm expresses the change in mass (in g). Considering all the parameters stated above, our QCM exhibits a sensitivity of 6.9 x 10^{-9} g/Hz. A straightforward outcome of the above expression is that a dampening in frequency is a consequence of an increase in mass and the extent of the variation of frequency is directly proportional to mass change.

Besides monitoring the change in frequency, Δf, it is also possible to follow variation in dissipation, ΔD. While the change in frequency is sensitive to mass variation, dissipation is sensitive to the viscoelastic properties of the film deposited on the crystal. A QCM instrument equipped with the possibility of performing dissipation measurements (QCM-D) will allow to gain insight into changes occurring in the film at the level of its hydration degree and viscoelastic or structural properties. It also allows to validate the application of Sauerbrey equation since the variation in frequency may be affected by the viscoelastic properties of the film. QCM has been employed to assess the deposition of lipid vesicles and consequent bilayer formation on diverse substrates, such as silicon dioxide or bare and modified gold electrodes[64-67]. In this experiments QCM-D is very useful due to its ability to distinguish between intact vesicles adsorbed on the surface or the presence of a lipid bilayer[64,65, 67], or even monolayer, as a consequence of the different viscoelastic properties of each type of lipid film. Thus, dissipation allows to easily ascribe the moment of vesicle rupture since there is a transition from a high dissipation regime (intact vesicles) to a low or zero dissipation regime (planar lipid bilayer)[65, 68]. This process can be also detected by monitoring oscillation frequency changes since the transition from intact vesicles to a planar lipid bilayer involves the release of the water molecules contained inside the vesicles[65, 68].

In this work, QCM was used to evaluate the interaction of lipid vesicles with both bare and modified gold surfaces in order to establish the preference of lipids towards different surfaces, whether bare gold or gold modified with MUA or L-cysteine. The gravimetric experiments were conducted in a 420 model CH Instruments electrochemical QCM. The adsorption was carried out at 23 ± 1 °C onto a 8 MHz AT-cut quartz crystal coated with 100 nm of gold fitted in a one-compartment Teflon cell (CH Instruments). After a stable baseline was reached, lipid vesicles were added to the system and their adsorption was followed over time until a new stabilization of the frequency signal was achieved.

2.5. Surface Plasmon Resonance

Surface plasmon resonance (SPR) is an optical phenomenon that allows to follow interactions (usually binding events) in real-time in a non-invasive and label-free way. Upon the binding event, a change in mass takes place with a concomitant increase in the refractive index, which in turn leads to a shift in the resonance angle. This sequence of events makes SPR very sensitive to reactions occurring near the surface. Similarly to QCM, SPR follows reactions over time, thus the resulting data includes both kinetic and equilibrium information.[69,70]

In SPR the energy carried by the photons of incident light excites the oscillating valence electrons of the metallic surface. The resonance state occurs only if the frequency of the photons of light equals the natural frequency of the metal electrons, i.e. under conditions of attenuated total reflection. SPR transducers usually employ a prism on top of which a metallic substrate is placed (Figure 10). At a particular incident angle, the total internal reflection condition is met and light penetrates into the optical substrate. This condition persists until the incident angle decreases to a critical angle at which some of the light is refracted across the surface. When the total internal reflection state is attained, the conditions for the generation of surface plasmons are reached and then the energy from photons is transferred to the metal electrons. As a consequence, a plasmon resonant wave will be generated at the interface between metal and a dielectric material. The evanescent electric field connected to this plasmon resonant wave has a limited penetration depth into the dielectric medium, in the order of ¼ of the incident light wavelength.[69-71]

The angle required to maintain the surface plasmon is very sensitive to variations of the refractive index near the metal surface. It is this principle that allows to follow in real time reactions taking place close to the surface.

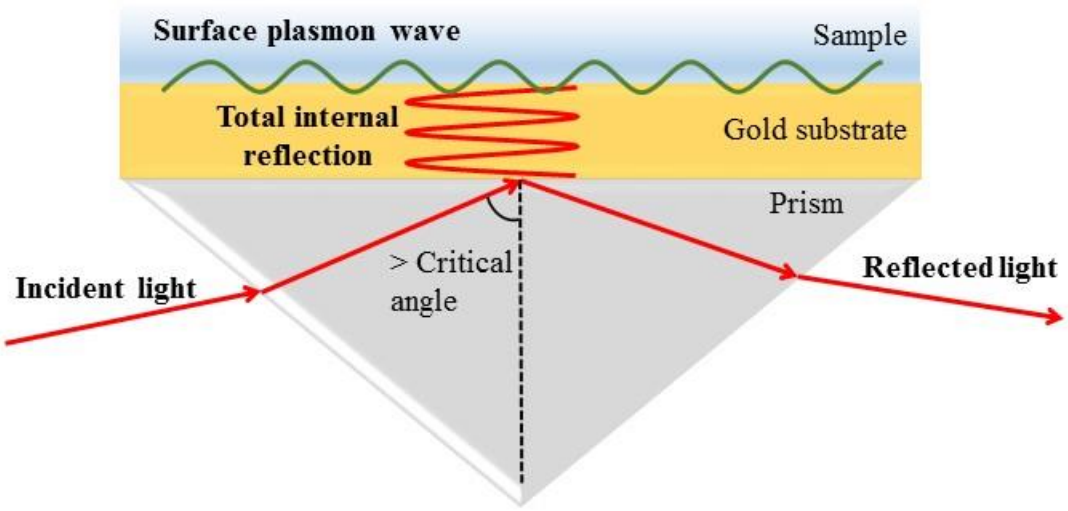

Figure 10 – Schematic representation of the working principle of SPR. Adapted from references[70, 72]

Similarly to QCM, SPR was used to monitor in real time the interaction of lipid vesicles with gold electrodes with distinct surface chemistry. SPR measurements were carried out using a BIOSUPLAR 400 T compact SPR sensor manufactured by Analytical μ-Systems with the help of a peristaltic pump (ISMATEC) which kept the flow rate at 30 μL/min.

SPR has a wide plethora of applications: biomolecular affinity, adsorption kinetics, thermodynamic analysis, concentration assays (e.g. immunosensors), binding stoichiometries, study of interaction mechanisms and others.[69-71, 73] Regarding the field of membrane biophysics the use of SPR has been successfully employed. For example, the application of SPR has helped in the development and characterization of tethered bimolecular lipid membranes[74]. Another crucial application of SPR in this field is the characterization of processes occuring at the membrane level, e.g. to evaluate the interaction of molecules with the lipid bilayer[75] or even protein-lipid interactions, as in the case of α-actinin with a negatively charged lipid bilayer[76] or cholera-toxin with a GM1-containing membrane[77]. Moreover, in experiments using lipid films, SPR has been usd in the assessment of the reaction between antibodies and their biorecognition element[78,79].

2.6. Fluorescence Spectroscopy

Fluorescence spectroscopy comprises a set of techniques often employed in biophysics. In the study of lipid bilayers it allows, for example, to conclude about the nature and amount of lipid phases present, through the use of multiple fluorescent probes with different affinity for the several types of lipid phases/domains. When applied to the study of external molecules with intrinsic fluorescence it gives access directly to the extent of membrane-molecule interaction and, for example, to conclude if this interaction is more superficial or if the molecule inserts deeply into the bilayer.

2.6.1. The Perrin-Jablonski diagram

The Perrin-Jablonski diagram (Figure 11) illustrates some of the processes occurring upon light interaction with matter, from the absorption of light until its emission – photon absorption, internal conversion, fluorescence, intersystem crossing, phosphorescence, delayed fluorescence and triplet–triplet transitions.

Upon absorption of light, which occurs in a time-scale of 10^{-15} s, a fluorophore goes from the fundamental electronic state (S_0) to a singlet electronic state of higher energy (S_1, S_2…) and is now in an excited state. Each electronic state is characterized by different sub-levels of vibrational energy (0, 1, 2...) and excitation can occur to any vibrational state. The energy absorbed upon excitation will, then, be released by different processes. Once excited, most molecules relax rapidly to the lowest vibrational energy level of S_1 through non-radiative processes and the excess of energy can be transferred to solvent through collisions. This process of internal conversion occurs within a time-scale of 10^{-13} to 10^{-11} s. Since the energy gap between S_0 and S_1 is higher than S_2 to S_1 and so on, the transition to the fundamental electronic state, which is usually accomplished by internal conversion may involve the emission of photons, a radiative process. The radiative relaxation from S_1 to S_0 (emission of a photon) is called fluorescence. Additionally, intersystem crossing characterized by a spin conversion from the singlet to the triplet state can occur and the emission of a photon from this state is designated by phosphorescence.[80,81] The processes referred above are of first order which result in an exponential decay of fluorescence intensity.

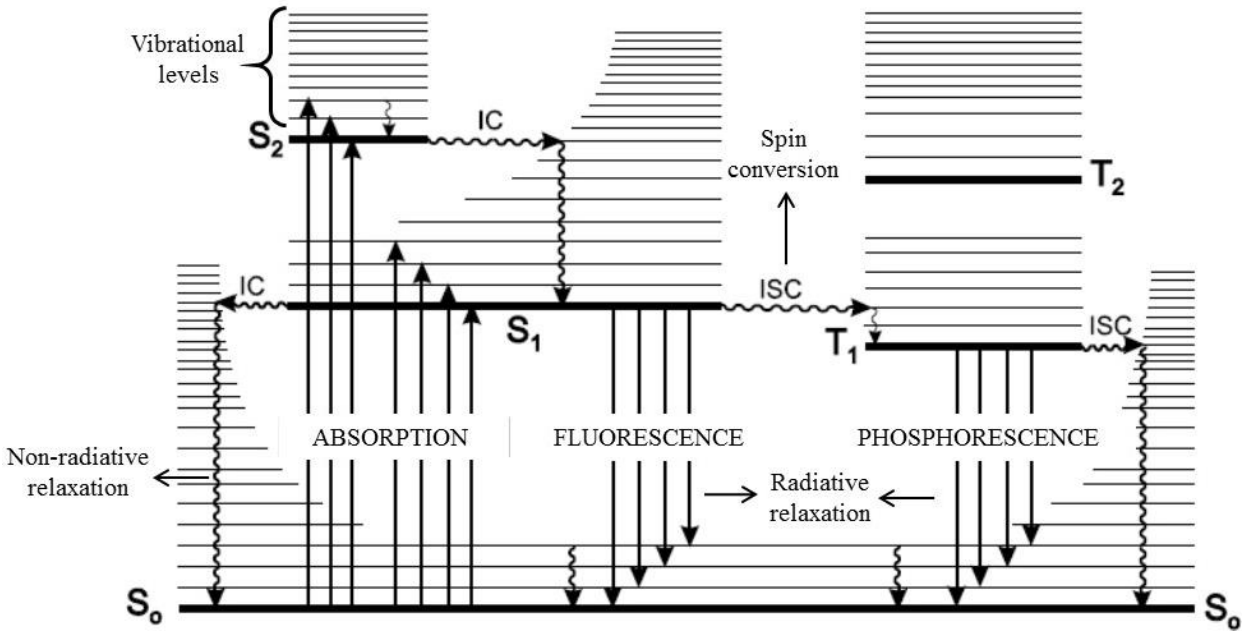

Figure 11 – Perrin-Jablonski diagram. IC – Internal conversion; ISC – Intersystem crossing; S_0, S_1, S_2 – singlet electronic states; T_1, T_2 – Triplet electronic states. Adapted from ref [81].

2.6.2. Steady-state emission and excitation spectra

Steady-state measurements are performed under conditions of continuous illumination with a lamp emitting a constant flow of photons and, as a consequence, the concentration of excited fluorophore remains constant, which means is in a steady-state.

In order to obtain an emission spectrum a fluorophore is excited at a fixed wavelength and then fluorescence intensity is collected for a range of wavelengths (higher than the excitation wavelength). The inverse is done to obtain an excitation spectrum – the fluorophore is excited at various wavelengths and then fluorescence intensity is collected at a fixed wavelength. The maximum of fluorescence emission occurs at a longer wavelength than that of absorption, corresponding to an energy gap known as the Stokes' shift. Emission spectra are usually independent of the excitation wavelength, since as explained above emission occurs from the lowest vibronic level of S_1. However, they can be highly dependent on the polarity of medium. If solvent is polar the dipole of the solvent molecules is on average aligned with the dipole of the fluorophore. As already mentioned, upon excitation the excess of vibrational energy is rapidly lost and the fluorophore relaxes to level S_1. Solvent molecules will realign their dipoles with the one of the excited fluorophore, which is most of the times stronger than that of the ground state, promoting

a further stabilization of the fluorophore and lowering the energy of S_1 level. This process is termed solvent relaxation. When undergoing back to this energy level, dipole alignment will no longer be optimal, meaning that the energy in S_0 is higher than that in the initial situation, before excitation (there will be again solvent relaxation, but this time after the photon has been emitted). Consequently, the energy gap to S_0 is reduced and a red shift in emission, longer wavelength, is verified. If the solvent is non-polar, permanent dipole-dipole interactions are absent, and thus no solvent relaxation will occur.[80,81]

2.6.3. Time-resolved fluorescence spectroscopy

Time-resolved fluorescence spectroscopy, in particular the determination of fluorescence lifetimes, is a technique often used in membrane biophysics that allows to retrieve crucial information about the organization of the membrane, namely the presence of certain types of lipid domains, the packing of the acyl chains or the extent of water penetration[82]. In time-resolved fluorescence spectroscopy the time lapse between the excitation of the sample with a pulsed laser and the arrival of the emitted photon at the detector is measured.

Fluorescence decays are, typically, described by a sum of exponentials[80-83]:

$$i(t) = \sum_i a_i \exp\left(\frac{-t}{\tau_i}\right) \qquad \text{eq.14}$$

where a_i is the normalized pre-exponential (amplitude) and τ_i the lifetime of the decay component *i*. The mean fluorescence lifetime $<\tau>$ (the true mean lifetime of the excited state since it is weighted by the intensity of each component) of a fluorophore exhibiting the fluorescence decay described by eq.15 is defined by[80-82]:

$$< \tau >= \frac{\sum_i a_i \tau_i^2}{\sum_i a_i \tau_i} \qquad \text{eq.15}$$

In some cases, where there is a dependence of the quantum yield with the interaction under studied, the determination of the lifetime weighted quantum yield ($\bar{\tau}$) (also named as amplitude averaged lifetime) becomes more significant[82]. This parameter can be determined as follows[82]:

$$\bar{\tau} = \sum_i a_i \tau_i \qquad \text{eq.16}$$

2.6.4. Steady-state fluorescence anisotropy

In order to perform fluorescence anisotropy (<*r*>) the spectrofluorometer used must be equipped with polarizers, as exemplified in the schematics of Figure 12. Fluorescence anisotropy is an important parameter in biophysics for it is a measure of depolarization of emitted light using a linearly polarized excitation source and thus is highly dependent, among other factors, on the fluorophore rotational dynamics. Fluorescence anisotropy reflects, many times, the environment in which the fluorophore is contained. If it is in a rigid environment it will not freely rotate and then the depolarization of light is not efficient, hence the polarization of emitted light is intimately related with the one of excitation light. Conversely, if the fluorophore is contained in a more fluid medium where it can rotate more freely, emitted light will not exhibited a preferential polarization orientation. Anisotropy can be calculated as follows:[80,81]

$$< r >= \frac{(I_{VV} - G \times I_{VH})}{(I_{VV} + 2 \times G \times I_{VH})} \qquad \text{eq.17}$$

where the different intensities, I_{ij} are the vertical and horizontal components of fluorescence emission in steady-state with vertical (I_{VV} and I_{VH}, respectively) and horizontal (I_{HV} and I_{HH}, respectively) excitation relatively to the emission axis. *G* factor is used to correct the different sensitivity of the detector for the vertical and horizontal polarization and can be determined by the ratio $\frac{I_{HV}}{I_{HH}}$. Steady-state anisotropy ($\bar{r}$), which is measured on continuous illuminations, is a temporal average of the anisotropy decay of a population of excited fluorophores with a fundamental anisotropy (r_0) initial value, as shown by the following equation:

$$\bar{r} = \frac{\int_0^\infty r(t) I(t) \mathrm{d}t}{\int_0^\infty I(t) \mathrm{d}t} \qquad \text{eq.18}$$

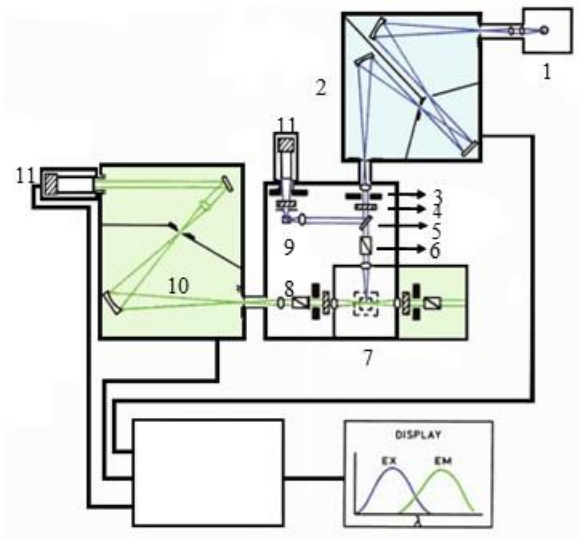

Figure 12 – Schematic representation of the optical pathway in a conventional fluorometer. Light source - Xenon arc lamp (1), excitation double grating monochromator (2), shutter (3), filter holder (4). The beam splitter (5) will reflect part of the excitation light to a reference cell (9) which will produce a signal proportional to the excitation light transmitted by the excitation monochromator and reaches a photomultiplier tube detector (11). The light not reflected by the beam splitter reaches the sample chamber goes (7) (it may go through an excitation polarizer (6), for fluorescence anisotropy measurements). The light emitted by the sample in a direction perpendicular to the incident beam may encounter an emission polarizer (8). The light beam will enter the double grating emission monochromator (10) and finally reaches the photomultiplier tube detector (11). Adapted from reference[80].

As mentioned, the value of anisotropy is affected by the rotational dynamics of the fluorophore and if the local environment is rigid, then the fluorophore will not be able to rotate freely and the anisotropy value will be closer to its fundamental value. The fundamental anisotropy value which is observed in the absence of depolarizing processes, depends on the angle between absorption and emission transition moments (β). If they are collinear r_0 is 0.4. If β is 54.7°, r_0 is 0 and above this angle the fundamental anisotropy becomes negative until a limit of -0.2 for 90°. Curiously, considering a fluorophore that can rotate freely, if its absorption and emission moments are collinear (r_0=0.4) then anisotropy will decrease from its fundamental value as the excited fluorophores rotate. However, if β is 90° (r_0=-0.2) then anisotropy will increase relatively to its fundamental value the more the fluorophore rotates after excitation. In terms of membrane biophysics, a gel phase represents a much more rigid environment than a fluid phase. Thus, a fluorophore with β=0° inserted into the gel will exhibit a higher anisotropy value (typically > 0.3) than when inserted into the fluid.[80,81]

2.6.5. Instrumentation and Biological Applications

Both steady-state fluorescence and time-resolved measurements were performed in a Horiba Jobin Yvon model Tau 3.22 spectrofluorometer equipped with a thermostated sample holder with magnetic stirring. This fluorometer has double grating monochromators in both excitation and emission and the light source for steady-stated acquisitions was a 450 W Xenon short arc lamp (from USHIO, UXL-450S-O). Fluorescence spectra presented throughout this work are already corrected for the blank contribution and with the instrumental correction files. In that sense, they do not exhibit interferences due to light scattering nor do they show any shift due to the non-ideality of the components of the spectrofluorimeter[80, 84]. Further experimental details are described in chapters III and VI.

For the measurements of fluorescence lifetimes the Fluorohub v2.0 module was used for the electronic control of the system that allows obtaining fluorescence decays by the single photon timing technique. This consists in the counting of photons that reached the detector with temporal correlation with the excitation pulse. In these experiments a nanoLED, which emits light pulses of short duration (70 ps) and a repetition rate up to 1 MHz was used as the light source. The nanoLED emits light at a specific wavelength and the one used in each experiment depends on the fluorophore being used and is indicated in each chapter. The fluorescence decay for an infinitesimal excitation pulse is acquired by deconvolution of the experimental decay with the instrument response function, which is obtained using a scatter, colloidal silica Ludox® from Sigma, and appropriate software based on the Levenberg-Marquardt algorithm.

As mentioned, fluorescence spectroscopy is often employed in membrane biophysics and it can be applied in both *in vivo* and *in vitro* studies. It can be used in the characterization of protein-drug interactions[8, 14] or even in the study of the mechanism of virus fusion with lipid membranes[85,86]. Moreover, it has given a crucial contribute in the determination of numerous phase diagrams for diverse lipid mixtures[87-89], as it is also illustrated in chapter III.

2.7. References

1. Gadegaard, N. Atomic force microscopy in biology: technology and techniques. *Biotechnic & Histochemistry* **2006,** *81*, 87-97.
2. Ricci, D.; Braga, P. C. ***Atomic Force Microscopy Biomedical Methods and Applications***. Humana Press: Totowa, 2004; p 3-21.
3. Digital Instruments, *Multimode SPM Instruction Manual* 1999.
4. Murakami, M.; Hirokawa, H.; Hayata, I. Analysis of radiation damage of DNA by atomic force microscopy in comparison with agarose gel electrophoresis studies. *Journal of Biochemical and Biophysical Methods* **2000,** *44*, 31-40.
5. Murakami, M.; Minamihisamatsu, M.; Sato, K.; Hayata, I. Structural analysis of heavy ion radiation-induced chromosome aberrations by atomic force microscopy. *Journal of Biochemical and Biophysical Methods* **2001,** *48*, 293-301.
6. Rivetti, C.; Walker, C.; Bustamante, C. Polymer chain statistics and conformational analysis of DNA molecules with bends or sections of different flexibility. *Journal of Molecular Biology* **1998,** *280*, 41-59.
7. Krautbauer, R.; Pope, L. H.; Schrader, T. E.; Allen, S.; Gaub, H. E. Discriminating small molecule DNA binding modes by single molecule force spectroscopy. *Febs Letters* **2002,** *510*, 154-158.
8. Demoro, B.; de Almeida, R. F. M.; Marques, F.; Matos, C. P.; Otero, L.; Pessoa, J. C.; Santos, I.; Rodriguez, A.; Moreno, V.; Lorenzo, J.; Gambino, D.; Tomaz, A. I. Screening organometallic binuclear thiosemicarbazone ruthenium complexes as potential anti-tumour agents: cytotoxic activity and human serum albumin binding mechanism. *Dalton Trans.* **2013,** *42*, 7131-7146.
9. Willemsen, O. H.; Snel, M. M. E.; Cambi, A.; Greve, J.; De Grooth, B. G.; Figdor, C. G. Biomolecular interactions measured by atomic force microscopy. *Biophysical Journal* **2000,** *79*, 3267-3281.
10. Stolz, M.; Stoffler, D.; Aebi, U.; Goldsbury, C. Monitoring biomolecular interactions by time-lapse atomic force microscopy. *Journal of Structural Biology* **2000,** *131*, 171-180.
11. Ratcliff, G. C.; Erie, D. A. A novel single-molecule study to determine protein-protein association constants. *Journal of the American Chemical Society* **2001,** *123*, 5632-5635.
12. Hane, F.; Drolle, E.; Gaikwad, R.; Faught, E.; Leonenko, Z. Amyloid-beta Aggregation on Model Lipid Membranes: An Atomic Force Microscopy Study. *J. Alzheimers Dis.* **2011,** *26*, 485-494.
13. Drolle, E.; Hane, F.; Lee, B.; Leonenko, Z. Atomic force microscopy to study molecular mechanisms of amyloid fibril formation and toxicity in Alzheimer's disease. *Drug Metab. Rev.* **2014,** *46*, 207-223.
14. Jesus, A. R.; Dias, C.; Matos, A. M.; de Almeida, R. F. M.; Viana, A. S.; Marcelo, F.; Ribeiro, R. T.; Macedo, M. P.; Airoldi, C.; Nicotra, F.; Martins, A.; Cabrita, E. J.; Jimenez-Barbere, J.; Rauter, A. P. Exploiting the Therapeutic Potential of 8-beta-D-Glucopyranosylgenistein: Synthesis, Antidiabetic Activity, and Molecular Interaction with Islet Amyloid Polypeptide and Amyloid beta-Peptide (1-42). *Journal of Medicinal Chemistry* **2014,** *57*, 9463-9472.
15. Casuso, I.; Khao, J.; Chami, M.; Paul-Gilloteaux, P.; Husain, M.; Duneau, J. P.; Stahlberg, H.; Sturgis, J. N.; Scheuring, S. Characterization of the motion of membrane proteins using high-speed atomic force microscopy. *Nat. Nanotechnol.* **2012,** *7*, 525-529.
16. Fritz, M.; Radmacher, M.; Gaub, H. E. GRANULA MOTION AND MEMBRANE SPREADING DURING ACTIVATION OF HUMAN PLATELETS IMAGED BY ATOMIC-FORCE MICROSCOPY. *Biophysical Journal* **1994,** *66*, 1328-1334.
17. Ohnesorge, F. M.; Horber, J. K. H.; Haberle, W.; Czerny, C. P.; Smith, D. P. E.; Binnig, G. AFM review study on pox viruses and living cells. *Biophysical Journal* **1997,** *73*, 2183-2194.
18. Saka, S. K.; Honigmann, A.; Eggeling, C.; Hell, S. W.; Lang, T.; Rizzoli, S. O. Multi-protein assemblies underlie the mesoscale organization of the plasma membrane. *Nat Commun* **2014,** *5*.
19. Scheuring, S.; Sturgis, J. N. Chromatic adaptation of photosynthetic membranes. *Science* **2005,** *309*, 484-487.

20. Legrimellec, C.; Lesniewska, E.; Cachia, C.; Schreiber, J. P.; Defornel, F.; Goudonnet, J. P. IMAGING OF THE MEMBRANE-SURFACE OF MDCK CELLS BY ATOMIC-FORCE MICROSCOPY. *Biophysical Journal* **1994,** *67*, 36-41.
21. Yamashita, H.; Taoka, A.; Uchihashi, T.; Asano, T.; Ando, T.; Fukumori, Y. Single-Molecule Imaging on Living Bacterial Cell Surface by High-Speed AFM. *J. Mol. Biol.* **2012,** *422*, 300-309.
22. Shibata, M.; Uchihashi, T.; Ando, T.; Yasuda, R. Long-tip high-speed atomic force microscopy for nanometer-scale imaging in live cells. *Sci Rep* **2015,** *5*, 7.
23. Alsteens, D.; Dupres, V.; Yunus, S.; Latge, J. P.; Heinisch, J. J.; Dufrene, Y. F. High-Resolution Imaging of Chemical and Biological Sites on Living Cells Using Peak Force Tapping Atomic Force Microscopy. *Langmuir* **2012,** *28*, 16738-16744.
24. Weisenhorn, A. L.; Schmitt, F. J.; Knoll, W.; Hansma, P. K. STREPTAVIDIN BINDING OBSERVED WITH AN ATOMIC FORCE MICROSCOPE. *Ultramicroscopy* **1992,** *42*, 1125-1132.
25. Ira; Johnston, L. J. Sphingomyelinase generation of ceramide promotes clustering of nanoscale domains in supported bilayer membranes. *Biochimica et biophysica acta* **2008,** *1778*, 185-197.
26. Yuan, C. B.; Furlong, J.; Burgos, P.; Johnston, L. J. The size of lipid rafts: An atomic force microscopy study of ganglioside GM1 domains in sphingomyelin/DOPC/cholesterol membranes. *Biophysical Journal* **2002,** *82*, 2526-2535.
27. Li, M.; Chen, M.; Sheepwash, E.; Brosseau, C. L.; Li, H.; Pettinger, B.; Gruler, H.; Lipkowski, J. AFM studies of solid-supported lipid bilayers formed at a Au(111) electrode surface using vesicle fusion and a combination of Langmuir-Blodgett and Langmuir-Schaefer techniques. *Langmuir* **2008,** *24*, 10313-10323.
28. Berquand, A.; Mingeot-Leclercq, M. P.; Dufrene, Y. F. Real-time imaging of drug-membrane interactions by atomic force microscopy. *Biochimica et Biophysica Acta-Biomembranes* **2004,** *1664*, 198-205.
29. Leonenko, Z.; Finot, E.; Cramb, D. AFM study of interaction forces in supported planar DPPC bilayers in the presence of general anesthetic halothane. *Biochimica et Biophysica Acta (BBA) - Biomembranes* **2006,** *1758*, 487-492.
30. Owen, D. M.; Gaus, K. Imaging lipid domains in cell membranes: the advent of super-resolution fluorescence microscopy. *Front. Plant Sci.* **2013,** *4*.
31. Gottesfeld, S. Ellipsometry - Principles and Recent Applications in Electrochemistry. *Electroanalytical Chemistry* **1989,** *15*, 143-265.
32. Tompkins, H. G. *A User's Guide to Ellipsometry*; Dover Publications: Mineola, New York, 2006.
33. Jellison, G. E. Ellipsometry. In *Encyclopedia of spectroscopy and spectrometry* Tranter, G.; Holmes, J.; Lindon, J., Eds.; Elsevier, 2000, pp 402-411.
34. Arwin, H. Spectroscopic ellipsometry and biology: recent developments and challenges. *Thin Solid Films* **1998,** *313*, 764-774.
35. Jarrendahl, K.; Arwin, H. Multiple sample analysis of spectroscopic ellipsometry data of semi-transparent films. *Thin Solid Films* **1998,** *313*, 114-118.
36. Abrantes, L. M.; Correia, J. P.; Savic, M.; Jin, G. Structural modifications during conducting polymer formation - an ellipsometric study. *Electrochim. Acta* **2001,** *46*, 3181-3187.
37. Wang, Z. H.; Viana, A. S.; Jin, G.; Abrantes, L. M. Immunosensor interface based on physical and chemical immunogylobulin G adsorption onto mixed self-assembled monolayers. *Bioelectrochemistry* **2006,** *69*, 180-186.
38. de Almeida, R. F. M.; Loura, L. M. S.; Fedorov, A.; Prieto, M. Nonequilibrium phenomena in the phase separation of a two-component lipid bilayer. *Biophysical Journal* **2002,** *82*, 823-834.
39. Han, X. J.; Achalkumar, A. S.; Bushby, R. J.; Evans, S. D. A Cholesterol-Based Tether for Creating Photopatterned Lipid Membrane Arrays on both a Silica and Gold Surface. *Chem.-Eur. J.* **2009,** *15*, 6363-6370.
40. Ainalem, M. L.; Campbell, R. A.; Khalid, S.; Gillams, R. J.; Rennie, A. R.; Nylander, T. On the Ability of PAMAM Dendrimers and Dendrimer/DNA Aggregates To Penetrate POPC Model Biomembranes. *J. Phys. Chem. B* **2010,** *114*, 7229-7244.

41. Machan, R.; Miszta, A.; Hermens, W.; Hof, M. Real-time monitoring of melittin-induced pore and tubule formation from supported lipid bilayers and its physiological relevance. *Chem. Phys. Lipids* **2010,** *163*, 200-206.
42. Benes, M.; Billy, D.; Benda, A.; Speijer, H.; Hof, M.; Hermens, W. T. Surface-dependent transitions during self-assembly of phospholipid membranes on mica, silica, and glass. *Langmuir* **2004,** *20*, 10129-10137.
43. Richter, R. P.; Brisson, A. R. Following the formation of supported lipid bilayers on mica: A study combining AFM, QCM-D, and ellipsometry. *Biophysical Journal* **2005,** *88*, 3422-3433.
44. Howland, M. C.; Szmodis, A. W.; Sanii, B.; Parikh, A. N. Characterization of physical properties of supported phospholipid membranes using imaging ellipsometry at optical wavelengths. *Biophysical Journal* **2007,** *92*, 1306-1317.
45. Bard, A. J.; Faulkner, L. R. *Electrochemical Methods: Fundamentals and Applications*; 2nd ed.; John Wiley & Sons2001.
46. Brett, C. M. A.; Brett, A. M. O. *Electrochemistry Principles, Methods, and Applications*; Oxford University Press1994.
47. Evans, D. H.; Oconnell, K. M.; Petersen, R. A.; Kelly, M. J. CYCLIC VOLTAMMETRY. *Journal of Chemical Education* **1983,** *60*, 290-293.
48. Kissinger, P. T.; Heineman, W. R. CYCLIC VOLTAMMETRY. *Journal of Chemical Education* **1983,** *60*, 702-706.
49. Mabbott, G. A. AN INTRODUCTION TO CYCLIC VOLTAMMETRY. *Journal of Chemical Education* **1983,** *60*, 697-702.
50. Schneider, T. W.; Buttry, D. A. ELECTROCHEMICAL QUARTZ-CRYSTAL MICROBALANCE STUDIES OF ADSORPTION AND DESORPTION OF SELF-ASSEMBLED MONOLAYERS OF ALKYL THIOLS ON GOLD. *Journal of the American Chemical Society* **1993,** *115*, 12391-12397.
51. Salamon, Z.; Tollin, G. Interfacial Electrochemistry of Cytochrome-C at A Lipid Bilayer Modified Electrode - Effect of Incorporation of Negative Charges Into the Bilayer on Cyclic Voltammetric Parameters. *Bioelectrochemistry and Bioenergetics* **1991,** *26*, 321-334.
52. Zhang, Z.; Nassar, A. E. F.; Lu, Z. Q.; Schenkman, J. B.; Rusling, J. F. Direct electron injection from electrodes to cytochrome P450(cam) in biomembrane-like films. *Journal of the Chemical Society-Faraday Transactions* **1997,** *93*, 1769-1774.
53. Liu, Y. X.; Wel, W. Z. Detection of Cytochrome c at Biocompatible Nanostructured Au-lipid Bilayer-modified Electrode. *Analytical Sciences* **2008,** *24*, 1431-1436.
54. Andersson, M.; Keizer, H. M.; Zhu, C. Y.; Fine, D.; Dodabalapur, A.; Duran, R. S. Detection of single ion channel activity on a chip using tethered bilayer membranes. *Langmuir* **2007,** *23*, 2924-2927.
55. Jeuken, L. J. C.; Weiss, S. A.; Henderson, P. J. F.; Evans, S. D.; Bushby, R. J. Impedance Spectroscopy of Bacterial Membranes: Coenzyme-Q Diffusion in a Finite Diffusion Layer. *Analytical Chemistry* **2008,** *80*, 9084-9090.
56. Marchal, D.; Boireau, W.; Laval, J. M.; Moiroux, J.; Bourdillon, C. Electrochemical Measurement of Lateral Diffusion Coefficients of Ubiquinones and Plastoquinones of Various Isoprenoid Chain Lengths Incorporated in Model Bilayers. *Biophysical Journal* **1998,** *74*, 1937-1948.
57. Becucci, L.; Scaletti, F.; Guidelli, R. Gel-Phase Microdomains and Lipid Rafts in Monolayers Affect the Redox Properties of Ubiquinone-10. *Biophysical Journal* **2011,** *101*, 134-143.
58. Briand, E.; Zach, M.; Svedhem, S.; Kasemo, B.; Petronis, S. Combined QCM-D and EIS study of supported lipid bilayer formation and interaction with pore-forming peptides. *Analyst* **2010,** *135*, 343-350.
59. Wilkop, T.; Xu, D. K.; Cheng, Q. Characterization of pore formation by streptolysin o on supported lipid membranes by impedance spectroscopy and surface plasmon resonance spectroscopy. *Langmuir* **2007,** *23*, 1403-1409.
60. Marx, K. A. Quartz crystal microbalance: A useful tool for studying thin polymer films and complex biomolecular systems at the solution-surface interface. *Biomacromolecules* **2003,** *4*, 1099-1120.

61. Bott, A. W. Characterization of Films Immobilized on an Electrode Surface Using the Electrochemical Quartz Crystal Microbalance. *Current Separations* **1999,** *18*, 5.
62. Bruckenstein, S.; Shay, M. EXPERIMENTAL ASPECTS OF USE OF THE QUARTZ CRYSTAL MICROBALANCE IN SOLUTION. *Electrochimica Acta* **1985,** *30*, 1295-1300.
63. Deakin, M. R.; Buttry, D. A. ELECTROCHEMICAL APPLICATIONS OF THE QUARTZ CRYSTAL MICROBALANCE. *Analytical Chemistry* **1989,** *61*, A1147-&.
64. Reimhult, E.; Hook, F.; Kasemo, B. Intact vesicle adsorption and supported biomembrane formation from vesicles in solution: Influence of surface chemistry, vesicle size, temperature, and osmotic pressure. *Langmuir* **2003,** *19*, 1681-1691.
65. Keller, C. A.; Kasemo, B. Surface specific kinetics of lipid vesicle adsorption measured with a quartz crystal microbalance. *Biophysical Journal* **1998,** *75*, 1397-1402.
66. Wang, X.; Shindel, M. M.; Wang, S. W.; Ragan, R. A Facile Approach for Assembling Lipid Bilayer Membranes on Template-Stripped Gold. In *Langmuir*; American Chemical Society, 2010; Vol. 26, pp 18239-18245.
67. Pfeiffer, I.; Petronis, S.; Koper, I.; Kasemo, B.; Zach, M. Vesicle Adsorption and Phospholipid Bilayer Formation on Topographically and Chemically Nanostructured Surfaces. *Journal of Physical Chemistry B* **2010,** *114*, 4623-4631.
68. Ekeroth, J.; Konradsson, P.; Hook, F. Bivalent-ion-mediated vesicle adsorption and controlled supported phospholipid bilayer formation on molecular phosphate and sulfate layers on gold. *Langmuir* **2002,** *18*, 7923-7929.
69. de Mol, N. J.; Fischer, M. J. E. *Surface Plasmon Resonance Methods and Protocls*; Humana Press2010.
70. Pranveer, S. *Surface Plasmon Resonance*; Nova Science Publishers2014.
71. Olaru, A.; Bala, C.; Jaffrezic-Renault, N.; Aboul-Enein, H. Y. Surface Plasmon Resonance (SPR) Biosensors in Pharmaceutical Analysis. *Critical Reviews in Analytical Chemistry* **2015,** *45*, 97-105.
72. Nguyen, H. H.; Park, J.; Kang, S.; Kim, M. Surface Plasmon Resonance: A Versatile Technique for Biosensor Applications. *Sensors* **2015,** *15*, 10481-10510.
73. Phillips, K. S.; Cheng, Q. Recent advances in surface plasmon resonance based techniques for bioanalysis. *Analytical and Bioanalytical Chemistry* **2007,** *387*, 1831-1840.
74. Sinner, E. K.; Ritz, S.; Naumann, R.; Schiller, S.; Knoll, W. SELF-ASSEMBLED TETHERED BIMOLECULAR LIPID MEMBRANES. In *Advances in Clinical Chemistry, Vol 49*, Makowski, G. S., Ed.; Elsevier Academic Press Inc: San Diego, 2009; Vol. 49, pp 159-179.
75. Yasuda, R.; Toko, K.; Akiyama, H.; Kaneishi, T.; Matsuno, T.; Ezaki, S.; Yamafuji, K. Detection of flavor substances using surface plasmon resonance with lipid LB membranes. *Electron. Commun. Jpn. Pt. II-Electron.* **1997,** *80*, 1-8.
76. Li, A. X.; Ma, Y.; Yang, F.; Yang, X. R. Interaction between alpha-actinin and negatively charged lipids membrane investigated by surface plasmon resonance and electrochemical methods. *Appl. Surf. Sci.* **2007,** *253*, 6103-6108.
77. Terrettaz, S.; Stora, T.; Duschl, C.; Vogel, H. PROTEIN-BINDING TO SUPPORTED LIPID-MEMBRANES - INVESTIGATION OF THE CHOLERA-TOXIN GANGLIOSIDE INTERACTION BY SIMULTANEOUS IMPEDANCE SPECTROSCOPY AND SURFACE-PLASMON RESONANCE. *Langmuir* **1993,** *9*, 1361-1369.
78. Liley, M.; Bouvier, J.; Vogel, H. Incorporation and antibody recognition of a lipid-anchored membrane protein in supported lipid layers. *Journal of Colloid and Interface Science* **1997,** *194*, 53-58.
79. Kurihara, Y.; Sawazumi, T.; Takeuchi, T. Exploration of interactions between membrane proteins embedded in supported lipid bilayers and their antibodies by reflectometric interference spectroscopy-based sensing. *Analyst* **2014,** *139*, 6016-6021.
80. Lakowicz, J. R. *Principles of Fluorescence Spectroscopy*; Third ed.; Springer Science: New York, USA, 2006.
81. Valeur, B.; Berberan-Santos, M. N. *Molecular Fluorescence Principles and Applications*; Second ed.; WILEY-VCH2012. p 569.

82. de Almeida, R. F. M.; Loura, L. M. S.; Prieto, M. Membrane lipid domains and rafts: current applications of fluorescence lifetime spectroscopy and imaging. *Chemistry and Physics of Lipids* **2009,** *157*, 61-77.
83. Bastos, A. E. P.; Scolari, S.; St+Âckl, M.; de Almeida, R. F. M. Chapter Three - Applications of Fluorescence Lifetime Spectroscopy and Imaging to Lipid Domains In Vivo. In *Methods in Enzymology, Imaging and Spectroscopic Analysis of Living Cells Optical and Spectroscopic Techniques*, Volume 504 ed.; conn, P. M., Ed.; Academic Press, 2012, pp 57-81.
84. Marques, J. T.; de Almeida, R. F. M. Application of Ratiometric Measurements and Microplate Fluorimetry to Protein Denaturation: An Experiment for Analytical and Biochemistry Students. *Journal of Chemical Education* **2013,** *90*, 1522-1527.
85. Guillen, J.; de Almeida, R. F. M.; Prieto, M.; Villalain, J. Structural and dynamic characterization of the interaction of the putative fusion peptide of the S2SARS-CoV virus protein with lipid membranes. *Journal of Physical Chemistry B* **2008,** *112*, 6997-7007.
86. Guillen, J.; de Almeida, R. F. M.; Prieto, M.; Villalain, J. Interaction of a peptide corresponding to the loop domain of the S2 SARS-CoV virus protein with model membranes. *Molecular Membrane Biology* **2009,** *26*, 236-248.
87. de Almeida, R. F.; Fedorov, A.; Prieto, M. Sphingomyelin/phosphatidylcholine/cholesterol phase diagram: boundaries and composition of lipid rafts. *Biophysical journal* **2003,** *85*, 2406-2416.
88. Silva, L.; de Almeida, R. F.; Fedorov, A.; Matos, A. P.; Prieto, M. Ceramide-platform formation and -induced biophysical changes in a fluid phospholipid membrane. *Molecular membrane biology* **2006,** *23*, 137-148.
89. De Almeida, R. F. M.; Borst, J.; Fedorov, A.; Prieto, M.; Visser, A. J. W. G. Complexity of lipid domains and rafts in giant unilamellar vesicles revealed by combining imaging and microscopic and macroscopic time-resolved fluorescence. *Biophysical Journal* **2007,** *93*, 539-553.

Chapter III

Phytoceramide interactions with a fluid phospholipid

3.1. Formation and properties of membrane ordered domains by phytoceramide: role of sphingoid base hydroxylation

Formation and properties of membrane ordered domains by phytoceramide: role of sphingoid base hydroxylation

Joaquim T. Marquês[1,§], André M. Cordeiro[1,§], A. S. Viana[1], A. Herrmann[2], H. S. Marinho[1], Rodrigo F. M. de Almeida[1],*

[1] Centro de Química e Bioquímica, Departamento de Química e Bioquímica, Faculdade de Ciências da Universidade de Lisboa, Ed. C8, Campo Grande, 1749-016, Lisboa, Portugal

[2] Department of Biology, Molecular Biophysics, Humboldt University, Berlin, Germany

ABSTRACT

Phytoceramide is the backbone of major sphingolipids in fungi, plants and is essential in several tissues of animal organisms, such as human skin. Its sphingoid base, phytosphingosine, differs from that usually found in mammals by the addition of a hydroxyl group to the 4-ene, which may be a crucial factor for the different properties of membrane microdomains among those organisms and tissues. Recently, sphingolipids hydroxylation in animal cells emerged as a key feature in several physiopathological processes. Hence, the study of the biophysical properties of phytosphingolipids is relevant also in that context, since it helps to understand the effects of sphingolipid hydroxylation. In this work, binary mixtures of *N*-stearoyl-phytoceramide (PhyCer) with palmitoyloleoylphosphatidylcholine (POPC) were studied. Steady-state and time-resolved fluorescence of membrane probes, X-ray diffraction, atomic force microscopy and confocal microscopy were employed. As for other saturated ceramides, highly rigid gel domains start to form with just ~5 mol% PhyCer at 24ºC. However, PhyCer gel-enriched domains in coexistence with POPC-enriched fluid present additional complexity, since their properties (maximal order, shape and thickness) change at specific POPC:PhyCer molar ratios, suggesting the formation of highly stable stoichiometric complexes with their own properties, distinct from both POPC and PhyCer. A POPC/PhyCer binary phase diagram, supported by the different experimental approaches employed, is proposed with complexes of 3:1 and 1:2 stoichiometries, stable at least from ~15 °C to ~55 °C, providing mechanisms for *in vivo* formation of sphingolipid-enriched gel domains, that may account for stable membrane compartments and diffusion barriers in eukaryotic cell membranes.

INTRODUCTION

In recent years several studies have demonstrated that the structural diversity of ceramides, whether alone or as the backbone of complex sphingolipids, affects markedly their biophysical properties, and the effect they exert on cell membrane organization and function[1-3]. Ceramides can affect the order, compactness and phase behavior of the lipid bilayer, domain-formation ability, interact with sterols and alter the patterns of membrane fusion and transmembrane lipid motion[4]. Ceramides are usually present in low amounts in biological membranes, but have strong interactions with complex sphingolipids that are present in larger proportions. These interactions are very important for the lateral organization of the lipids and the properties of the so-called lipid rafts,[5-8] ordered domains that are enriched in both sphingolipids and cholesterol in mammalian cells. It is known that the organization of ordered domains in

the plasma membrane of plants and yeast is quite complex and highly dependent on the sphingolipids[9] with several putative biological roles such as GPI-anchored protein transport in yeast[10]. Indeed, not only ergosterol-enriched liquid ordered domains are present, the counterparts of the mammalian cholesterol-enriched lipid rafts, but also gel occur in significant amounts on the plasma membrane of *Saccharomyces cerevisiae*[11]. These too are ordered domains, but from a different type, as their formation relies solely on the presence of sphingolipids, and they are ergosterol-depleted[11,12]. Such gel domains may act as effective diffusion barriers[13,14] for both lipids and proteins, with vast biological functions, from the formation of stable membrane compartments to the separation of mother and daughter cell components in the budding yeast during division[15].

Structural differences at the ceramide backbone level of sphingolipids, such as the length[7, 16-19] and unsaturation[20,21], or hydroxylation degree, both in the acyl chain[11] and the sphingoid base[1], can have profound consequences in membrane properties. Thus, the exploration of the structural differences between mammalian and yeast sphingolipids will shed light into the differences between the ordered domains found in each type of organism. The importance of the hydroxylation, in particular, has been increasingly recognized[22]. Free hydroxylated fatty acids, namely 2-hydroxyoleic acid, have biophysical[23] and biochemical[24] effects that are remarkably different from those of their non-hydroxylated counterparts. Deoxyceramides, which lack the hydroxyl group at position C1 of the sphingoid base, are less miscible with sphingomyelin than sphingosine-based ceramides[2]. Phytoceramide (PhyCer), has one hydroxyl group instead of a double bond at C-4 of the sphingoid base, phytosphingosine. The major sphingolipid species in many important taxonomic groups such as plant and fungi are phytoceramide-based[25]. PhyCer is also present in several human tissues, such as the stratum corneum of the epidermis[26,27]. It has much stronger effect on the thermal stability of ordered domains rich in cholesterol than the sphingosine-based ceramide [28]. The absence of an hydroxyl group in position C-4 of the sphingoid base leads to a strong decrease in fluidity of the membrane in living yeast cells[1]. On the other hand, in model systems an additional hydroxylation in position C-4 of sphingomyelin (phytosphingomyelin) leads to a membrane with a higher gel/fluid melting temperature[29]. It is thus important to study PhyCer biophysical properties to understand its role and that of PhyCer-based lipids in the organization and function of membranes in animals, plants and fungi. To this end, it is of high relevance to study the behavior of PhyCer in the presence of a fluid phospholipid and to compare it with the behavior of ceramides with the same or similar acyl chain.

In this work we present a thorough biophysical characterization of mixtures of N-stearoyl-phytosphingosine (N-stearoyl-phytoceramide) mixed with 1-palmitoyl-2-oleoyl-*sn*-glycero-3-phosphocholine (POPC), one of the most abundant phospholipids in the plasma membrane of many eukaryotic organisms,[30,31] using a variety of techniques. Fluorescence spectroscopy of different membrane probes incorporated into lipid vesicles yields results from the whole suspension and not each vesicle in particular. AFM is capable of probing a small area of a supported lipid bilayer (SLB) with outstanding lateral and axial resolution. Confocal fluorescence microscopy allows confirming the presence of microdomains that exclude fluorescent probes and X-ray diffraction provides structural data that can be directly related to molecular organization. PhyCer effects on the fluid membrane, its gel-domain formation ability and the composition and biophysical properties of those gel domains, are presented. Rather than a typical gel phase, our data strongly suggests that PhyCer can form stable stoichiometric complexes with two different stoichiometries when mixed with POPC, giving rise to a phase diagram clearly distinct from those previously proposed for POPC mixed with sphingosine based ceramides. Importantly, the PhyCer-enriched

domains studied in this work share many biophysical properties with the gel domains found in the plasma membrane of living yeast.

METHODS

Chemicals

POPC, *N*-octadecanoyl(2*S*,3*S*,4*R*)-2-amino-1,3,4-octadecanetriol (phytoceramide from *S. cerevisiae*), and *N*-(lyssamine rhodamine B sulfonyl)-1,2-dioleoyl-*sn*-3-phosphatidylehanolamine ammonium salt (Rhod-DOPE) were purchased from Avanti Polar Lipids (Alabaster, AL). Ludox (colloidal silica diluted to 50 weight % in water) was purchased from Sigma. *t*-PnA was purchased from Santa Cruz Biotechnology (Santa Cruz, CA, USA), and DPH and di-4-ANEPPS from Invitrogen (Madrid, Spain). Solvents for lipid and probe stock solutions were spectroscopic grade. All other reagents were of the highest purity available.

Preparation of Multilamellar Vesicles and Giant Unilamellar Vesicles

Multilamellar vesicles (MLVs) containing the appropriate lipids, DPH and *t*-PnA were prepared by standard procedures e.g.[32]. Briefly, adequate volumes of lipid stock solutions were added to a tube to have the desired lipid mole fractions. The solvent was slowly vaporized by a mild flow of nitrogen, forming a thin layer of lipid in the bottom of the tube. The lipid was hydrated by the addition of 1 mL of PBS buffer (2.71 mM K_2HPO_4, 1.54 mM NaH_2PO_4, 154 mM NaCl, pH 7.4), previously heated above the main transition temperature (T_m) of the lipids. The samples were then progressively vortex-stirred and submitted to freeze/thaw cycles. The probe, at a concentration of less than 1 % (v/v), was then added from an ethanol stock solution to the desired lipid/probe ratio followed by 1h incubation and further freeze/thawing. Afterwards, they were slowly cooled and kept in the dark at 4°C. Before measurements, they were slowly brought to room temperature, or to the lowest temperature used in temperature-dependence studies.

For fluorescence spectroscopy, the probe/lipid ratio used was 1:200 (mol/mol) for DPH and 1:500 (mol/mol) for *t*-PnA with 0.2 mM total lipid to avoid incomplete hydration of ceramide (e.g.,[33]).

Giant unilamellar vesicles (GUVs) were prepared by the electroformation method as described previously with minor modifications[34]. Adequate volumes of lipids and probe (Rhod-DOPE) stock solutions were mixed to have the desired lipid mole fractions and lipid/probe ratio, a final lipid concentration of 1 mM, and a chloroform/methanol ratio of 2:1 (v/v). The mixture was homogenized by vortexing, and a volume of 25 μL of solution was spread on the titanium GUV formation chamber with a gas-tight syringe. The traces of organic solvent were removed through vacuum desiccation for 30 min. The titanium chambers were filled with 700 μL of sucrose buffer (250 mM sucrose solution, 15 mM NaN_3) 280 mOsm/kg in MilliQ water (>18 MΩ), sealed and connected to the signal generator. A sinusoidal signal with a peak-to-peak voltage of 0.4 V and 10 Hz was applied and the voltage was increased to 2.0 V and maintained overnight. Then, the frequency was decreased to 4 Hz and the voltage increased to 2.6 V for 20min. Finally, the signal generator was turned off. For PhyCer-containing mixtures, the chambers were in a block heater at 60°C (a temperature above which no gel domains are detected from the fluorescence of *t*-PnA at the PhyCer mole fractions used), and the sucrose buffer was previously heated to that temperature. The vesicle suspension was kept at room temperature (24 °C) in the dark until use. The probe:lipid ratio used was 1:500 (mol/mol).

POPC concentrations in stock solutions (chloroform) were determined by phosphorus analysis[35]. Probe concentrations were determined spectrophotometrically as in ref [5]. PhyCer concentrations in stock solutions made in chloroform/methanol 2:1 (v/v) were determined by gravimetry.

The preparation of Small Unilamellar Vesicles (SUVs) is described under "Supported Lipid Bilayers" for atomic force microscopy (AFM) studies.

Absorption and Fluorescence Measurements and Data Analysis

The spectrophotometric absorption measurements were performed on a Jasco V-560 (Tokyo, Japan) double beam spectrophotometer and the fluorescence measurements were carried out on a Spex Fluorolog 3-22/Tau 3 spectrofluorometer equipped with double grating monochromators in both excitation and emission light paths from Horiba Jobin Yvon at 24°C as described previously[11].

For steady-state measurements (450 W Xe arc lamp light source), the samples were under constant magnetic stirring, and the excitation / emission wavelengths were 358nm / 430nm for DPH and 303nm / 404 nm for *t*-PnA. The steady-state anisotropy (*r*) was calculated according to,

$$r = (I_{VV} - G \times I_{VH})/(I_{VV} + 2G \times V_H) \quad \text{(Eq.1)}$$

in which *G* is the instrumental correction factor . Subscripts V and H represent the vertical and horizontal orientations of the polarizers and the order of the subscripts corresponds to the excitation and emission. An adequate blank was subtracted from each intensity reading. The set of the four intensity components for each sample was measured seven times.

For time-resolved measurements by the single photon counting technique, nanoLED N-320 (Horiba Jobin Yvon) was used for the excitation of *t*-PnA, and emission wavelength was 404 nm; nanoLED N-370 with a cut-of filter UGI-370 for DPH with emission set at 450 nm. The resolution of the detection system was 50 ps. The number of counts on the peak channel was 20,000. The number of channels per curve used for the analysis was ~1000. The time scale was 0.05552 ns/channel for both probes, and for *t*-PnA timescales of 0.1114 and 0.22231 ns/channel were frequently used. Ludox was used as the scatter to obtain the instrumental response function. The program TRFA Data Processor v.1.4 (Scientific Software Technologies Center, Minsk, Belarus) was used for the analysis of the experimental fluorescence decays.

For a fluorescence intensity decay described by a sum of exponentials, i.e.,

$$I(t) = \sum_{i=1}^{n} \alpha_i exp(-t/\tau_i) \quad \text{(Eq.2)}$$

where α_i and τ_i are the normalized amplitude and lifetime of component i, respectively. The (intensity-weighted) mean fluorescence lifetime is given by

$$\langle\tau\rangle = \sum \alpha_i \tau_i^2 / \sum \alpha_i \tau_i \quad \text{(Eq.3)}$$

and the amplitude-weighted average fluorescence lifetime is defined as

$$\tau_{av} = \sum \alpha_i \tau_i \quad \text{(Eq.4)}$$

In general, two exponentials were required to describe DPH fluorescence intensity decays, whereas for *t*-PnA, three or four components were necessary depending on the complexity of the lipid mixture. The quality of fit was judged by a reduced-χ^2 value close to 1 and random distribution of weighted residuals and residuals autocorrelation.

The background (obtained with the blank sample) was subtracted from the decay.

All the data represents the mean ± standard deviation of at least 3 independent samples.

Confocal microscopy of GUVs

Intensity images were taken using an Olympus Fluoview 1000 (Olympus, Tokyo, Japan) equipped with a X60 (1.35 N.A.) oil immersion objective. Rhod-DOPE was excited at 543 nm using the HeNe laser and was detected in the range of 570-670 nm. Images with a frame size of 512 X 512 pixels were acquired.

Supported Lipid Bilayer Preparation

MLVs were prepared as described above, except for the hydration buffer which in the present case was10 mM Hepes, 150 mM NaCl, pH 7.4 (total lipid concentration 1 mM). Small unilamellar vesicles (SUV) were originated by power sonication (Hielscher, UP200S) 140 W dutty cycle 0.75 followed by centrifugation for 20 minutes at 6800 g of the suspension. The supernatant was recovered to which $CaCl_2$ was added to a final concentration of 5 mM (from a 100 mM $CaCl_2$ stock solution)[32]. 150 µL of this suspension was deposited on freshly cleaved mica (Veeco) and incubated for 30 minutes at 60 °C. After this incubation step the samples were left at room temperature to cool for 1 h and SLB were washed several times with buffer 10 mM Hepes, 150 mM NaCl, pH 7.4 at room temperature (23 ±1 °C).

AFM imaging

AFM *in-situ* measurements, i.e. with the sample immersed in buffer recurring to a liquid cell, were performed at room temperature using a Multimode Nanoscope IIIa Microscope (Digital Instruments, Veeco). Topographic images were taken with a scan rate of ca. 1.8 Hz in *tapping* mode. Under these conditions, tip scanning has no effect on the height, shape and domain organization of the lipid bilayer[32].

Before each experiment, the glass block holding the cantilever was washed several times with water and ethanol. The cantilevers used were made of silicon nitride (NPS, ca. 0.35 N/m of spring constant, Bruker) with a resonance frequency in liquid of about 26 kHz. The samples were initially covered with 80 µL of buffer 10 mM Hepes, 150 mM NaCl, pH 7.4.

The images presented in this study are representative of each mixture (the observations are uniform for the whole sample); at least 2 independent experiments on freshly prepared SLB were performed for each lipid system. To obtain the thickness values (or thickness differences), at least 5

different profiles were drawn in each image, and the median value taken. The values for the thickness in Table S1 are the mean ± standard deviation of the values from all the experiments, and the most representative profiles were selected for the figures shown. The estimation of the area corresponding to the different types of domains was performed using the software ImageJ. All the domains of a specific thickness were added to obtain the total phase area.

X-ray Scattering

For x-ray diffraction measurements, MLVs with a final lipid concentration of 3.5mM were prepared as described above. Samples were, then, centrifuged at 11300 g for 30 min, and the pellets (with an estimated volume of ca. 1/10 of the initial volume) were stored at 4°C. To perform the measurements, the pellets were transferred to a glass capillary. Small and wide-angle x-ray scattering (SAXS and WAXS) were performed at 20°C, using a Philips Analytical PW 3050/60 X'Pert PRODiffractometer, operating with a Cu-$K\alpha$ radiation and previously calibrated using a Si standard, from 0.68° to 65° with 0.03° steps.

The anhydrous bilayer thickness can be determined from the small angle region according to the equation[36]:

$$d_{100} = d_l \left[1 + \left(\frac{v_w}{v_l}\right).n_w\right] \quad (5)$$

where d_{100} corresponds to the reflection, d_l is the effective thickness of the bilayer, v_w and v_l are the molecular volumes of water and lipid, respectively and n_w stands for the water/lipid mole ratio.

From the wide angle region, the chain-to-chain spacing (a) can be calculated according to the following expression, where s is the observed reflection, considering that in a gel phase the acyl chains occupy a hexagonal lattice[36]:

$$a = \frac{2}{\sqrt{3}}s \quad (6)$$

The area per molecule, S_0, can be retrieved using the following equation:

$$S_0 = \frac{4}{\sqrt{3}}s^2 \quad (7)$$

RESULTS AND DISCUSSION

Fluorescence spectroscopy of trans-parinaric acid at room temperature: formation of phytoceramide-enriched gel-phases

It has been shown for several ceramide species that these molecules when mixed with fluid phase phospholipids are able to induce the formation of gel or solid ordered domains[21, 33]. Therefore, *t*-PnA, a probe with a partition coefficient and fluorescence quantum yield favorable to the gel (or solid ordered) phase has proved invaluable in the study of the biophysical changes induced by the presence of ceramide in fluid phospholipid bilayers. As a first step in the characterization of the binary system POPC/PhyCer we determined steady-state and time-resolved (Figure 1) fluorescence properties of *t*-PnA as a function of PhyCer mole fraction at 24 °C .

In previous studies we found that the long lifetime component of *t*-PnA fluorescence intensity decay in this system rises abruptly in the 5 to 10 mol % composition range, reaching a value of ~40-42 ns.[11] In the present study, this behavior was confirmed, and for PhyCer compositions above 30 mol % till 90 % PhyCer a value ca. 40-42 ns is kept after a maximum of 45 ns that occurs for 25 mol % PhyCer (Figure S1). The very high values of the long lifetime component, confirm the formation of a PhyCer-enriched gel phase.

The trend of steady-state fluorescence anisotropy is complex. After 5 mol % of PhyCer, it starts to increase markedly, displaying a maximum around 20-25 mol %, being reasonably stable between ~30-50 mol % and presenting another local maximum around 60 – 70 mol % PhyCer (Figure 1a). Finally, for very high PhyCer levels (equal or above 70 mol %) the anisotropy slightly decreases, which is indicative of some exclusion of the probe from the gel domains or of aggregation of the probe, both of which could be explained by the formation of a very rigid and compact solid phase enriched in PhyCer.

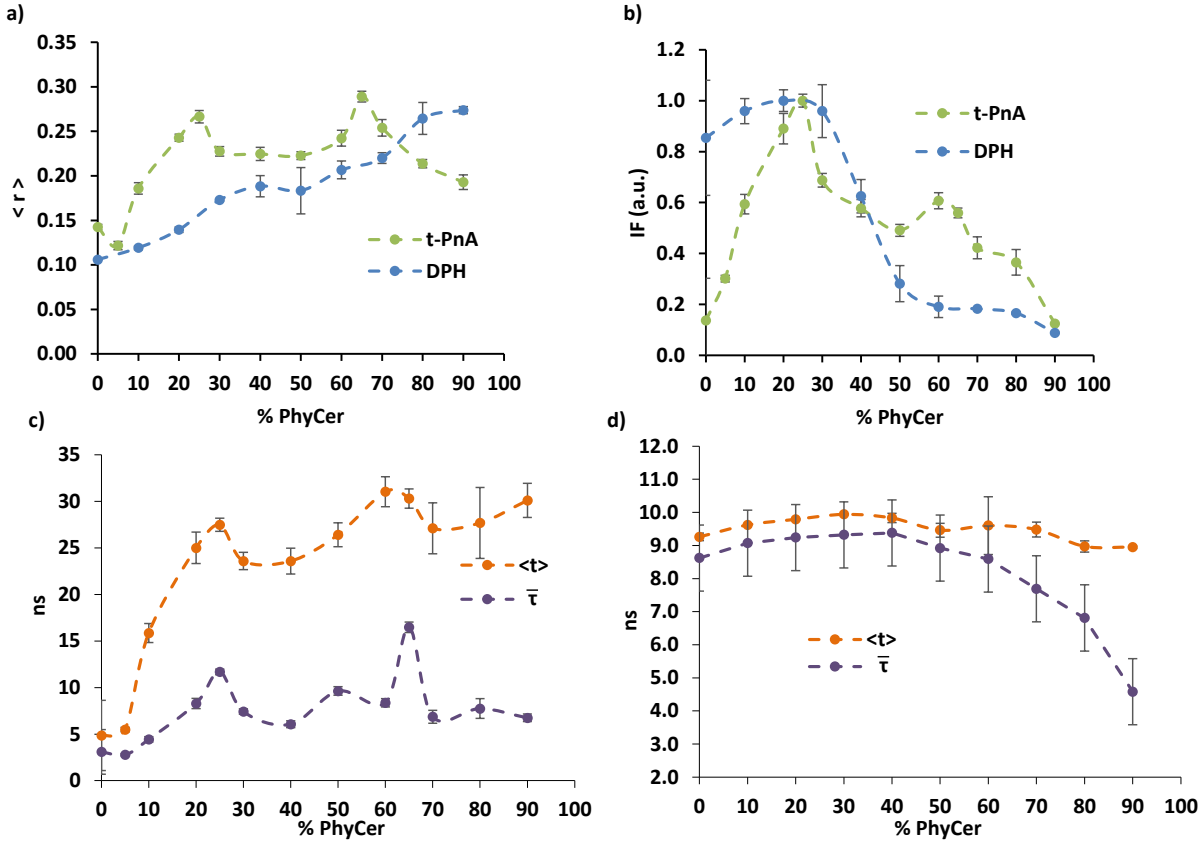

Figure 1 - Steady-state fluorescence at 24ºC in POPC/PhyCer MLVs as a function of PhyCer mole fraction. a) Steady-state fluorescence anisotropy and b) Steady-state fluorescence intensity of *t*-PnA and DPH; and time-resolved fluorescence at 24ºC in POPC/PhyCer MLVs as a function of PhyCer mole fraction. Intensity-weighted average fluorescence lifetime (orange line) and amplitude-weighted mean fluorescence lifetime (purple line) of c) *t*-PnA and d) DPH. Data represents the mean ± standard deviation of at least 3 independent samples.

Noteworthy is the fact that the maximum anisotropy value obtained is ~0.29 for 65 mol % of PhyCer, and that for all other compositions it is well below the typical values found in ceramide gel phases

(≥ 0.3) whether in the presence or not of sphingomyelin and cholesterol.[5, 21, 33] This suggests differences in the organization between PhyCer and sphingosine-based Cer-rich phases.

To further understand this behavior, the steady-state fluorescence intensity of *t*-PnA was also measured as a function of composition at 24 °C (Figure 1b). This parameter increases ~several-fold between pure POPC and ca. 25 mol % PhyCer, reporting the formation of a highly ordered gel phase. Above 25 mol% PhyCer the fluorescence intensity decreases, a behavior that supports the formation of a new gel phase. There is also a local maximum around 65 mol % PhyCer, but for higher concentrations of PhyCer the fluorescence intensity decreases to values found in the absence of gel domains. However, from the long fluorescence lifetime component of *t*-PnA lifetime values that are fingerprints of the gel phase are obtained (Figure S1). Thus, the gel phase formed by PhyCer above 65 mol % is so rigid that even *t*-PnA, the only known fluorescent membrane probe that has a clear preference for gel phases, is excluded. For the highest concentrations of PhyCer achievable the system is completely in a gel phase, thus exclusion of *t*-PnA from the gel is in fact segregation of the probe from the membrane to the aqueous milieu, where *t*-PnA has negligible quantum yield, leading to a decrease of fluorescence intensity.

The average fluorescence lifetimes of *t*-PnA as a function of PhyCer molar fraction at 24 °C (Figure 1c) corroborates this interpretation. They increase markedly for PhyCer fractions ≥5 mol %, attaining a first maximum at 25 %, and a second maximum at ~65 mol %. For these parameters and the fluorescence anisotropy, which reflect the compactness and order of the acyl chains/sphingoid base, the absolute maximum occurs at ~65 mol % and not at ~ 25 mol % as observed for the steady-state fluorescence intensity. We surmise that the fluorescence quantum yield for the probe that repartitions to the aqueous phase is quite low (essentially it does not fluoresce) and thus it contributes to a decrease in the steady-state intensity for higher PhyCer fractions, not affecting strongly the other parameters. The fact that both fluorescence lifetimes and anisotropy have local maxima confirms that for those PhyCer compositions (~ 25 and 65 mol %) the system is particularly well ordered and compact.

Fluorescence spectroscopy of DPH at room temperature: rigidity of phytoceramide-enriched gel-phases

DPH displays a different lipid domain partition behavior than *t*-PnA. Typically it distributes equally among gel and fluid phases[37]. Therefore, its use in the characterization of binary lipid mixtures, such as PhyCer/POPC provides complementary information to *t*-PnA. However, in the case of Cer-containing samples, the formation of Cer-rich gel phases can lead to a strong[33] or moderate[21] exclusion of the probe from the membrane. In Figure 1a, the steady-state anisotropy of DPH at 24 °C is shown. As PhyCer levels increase, so does the anisotropy of DPH. This increase is, however, gradual and monotonic in opposition to that observed for *t*-PnA. DPH seems to be sensitive only to the global ordering of the membrane as PhyCer levels increase. The steady-state fluorescence intensity of DPH at 24 °C was also plotted versus PhyCer mole fraction (Figure 1b). This parameter has a slight increase for low PhyCer mole fractions and it decreases sharply for PhyCer fraction above ~30 mol %, pointing to an exclusion by PhyCer stronger than for *t*-PnA, as expected.

The fluorescence intensity decays of DPH up to 60 – 70 mol % PhyCer are described by the sum of two exponentials, with lifetime components of 3 – 5.5 ns and 9.5 – 10.5 ns, respectively (not shown). These values are similar to others usually found in membrane model systems, since DPH fluorescence lifetime is less sensitive to changes in the lipid phase when compared to its anisotropy[5, 37]. The average fluorescence lifetime and the amplitude-weighted average fluorescence lifetime of DPH at 24 °C are represented in Figure 1d. As expected, no strong variations are observed for those parameters as a function of PhyCer mole fraction. The slight increase observed for low PhyCer concentrations is probably due to an ordering

of the acyl chains of lipids in the fluid phase, because steady-state fluorescence intensity (Figure 1b) also increases in this composition range. For high concentrations of PhyCer (> 60 mol%) the decrease in the amplitude-weighted average fluorescence lifetime, which is a measurement of fluorescence quantum yield, is probably due to an exposure of the lipid-interacting probe to the aqueous milieu, that results from its difficulty to accommodate within an even more compact phase. An increased hydration of DPH microenvironment is reflected by a short lifetime component[38], which affects mainly this parameter, and affects much less the intensity-weighted mean fluorescence lifetime, from Eqs. 3 and 4. The fact that the steady-state fluorescence intensity trend is not analogous to that of the amplitude-weighted mean fluorescence lifetime points to a population of probe which is not fluorescent, and is probably due to probe aggregates completely segregated into the aqueous phase, justifying the low values of fluorescence intensity between ~30 mol % and ~60 mol % PhyCer, but not of the average lifetime.

Thermotropic behavior of POPC/PhyCer binary systems from *t*-PnA and DPH fluorescence anisotropy

In order to understand the effect of temperature on the solid ordered (gel) phases formed by PhyCer, and ultimately to obtain a partial phase diagram for the POPC/PhyCer system, the steady-state fluorescence anisotropy of *t*-PnA was measured as a function of temperature. The results are shown in Figure 2. As predicted, the values for that parameter decrease with the increase in temperature of the system, as it becomes less ordered and/or the gel domains are melting. For 100 mol % POPC, the results are in agreement with those previously reported.[21, 33] The T_m for this lipid is -2.9 °C[39], and therefore this system is fluid at all temperatures scanned. The decrease in anisotropy observed is in agreement with the curves previously obtained for pure POPC liposomes[21, 33, 40], and also to a decrease in the order of the fluid phase itself. For ≥ 10 mol % PhyCer, three regimes are detected; a first regime at low temperatures with high anisotropy reflecting the predominance of gel domains. A second regime, with a steep decrease of anisotropy for intermediate temperatures, where the probe is essentially detecting the melting of ordered domains, and a third one, for high temperatures where low anisotropy values are observed. To describe these regions quantitatively, straight lines were fitted to each of the three regimes. With this method, an initial melting temperature (T_i), and a final melting temperature (T_f) are obtained. The procedure for obtaining these parameters is exemplified in Supplementary Material of ref[11]. For 5 mol % PhyCer, it was possible to retrieve only the value of T_f. In agreement with a visual inspection of the curves in Figure 2, the thermal stability of the ordered domains increases as the levels of PhyCer in the membrane become higher, and then it stabilizes, or even has a slight tendency to decrease for sphingolipid mole fractions higher than 60 mol%. The temperatures T_f were used to build a partial phase diagram for the binary POPC/PhyCer mixture. The values of T_f correspond to the complete melting of the gel domains for which *t*-PnA has a preferential partition. The T_i value is distorted by that preference and, therefore, was not used for the phase diagram. However, the fact that its value is almost independent of composition (between 10 and 80 mol % of PhyCer) indicates that a horizontal line should be present in the lower temperature range of a putative phase diagram POPC/PhyCer, ascertaining the presence of several immiscible/low miscibility gel-like phases.

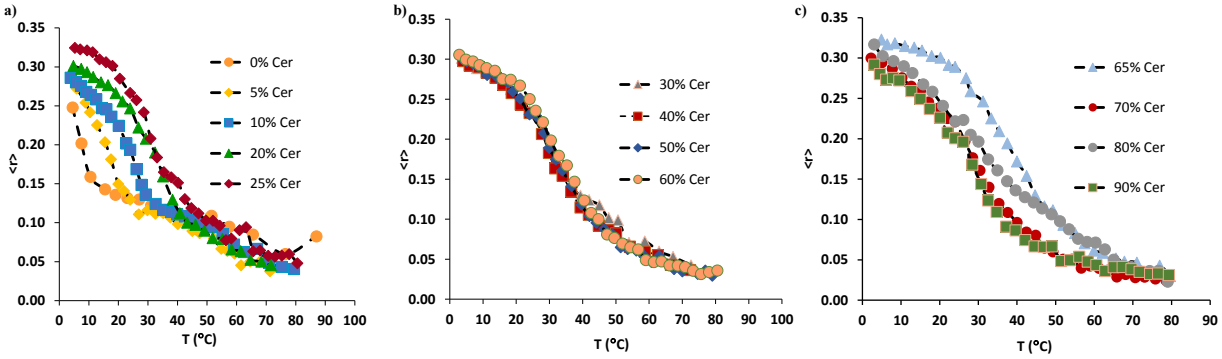

Figure 2 - Steady-state fluorescence anisotropy of *t*-PnA as a function of temperature in POPC/PhyCer MLVs with 0, 5, 10, 20, 30, … mol% PhyCer. Data represents the median of at least 3 independent samples.

A different way of representing these data is given in Figure 3, i.e., steady-state fluorescence anisotropy as a function of composition for a given temperature. The curve obtained at 15 °C shows the appearance of a significant fraction of gel domains for low PhyCer mole fractions, as observed at 24 °C. A similar trend with two maxima around 0.31 is attained, typical of a gel phase (≥0.3). The two local maxima occur for the same PhyCer mole fraction as observed for 24 °C. Furthermore, these maxima persist for higher temperatures, at least 45 °C for the maximum at X_{PhyCer} = 25 mol%, and for ~55 °C for X_{PhyCer} = 65 mol %. This behavior strongly suggests that at or near those PhyCer compositions the system has unique properties, until the temperatures at which the sharp peaks fade are reached.

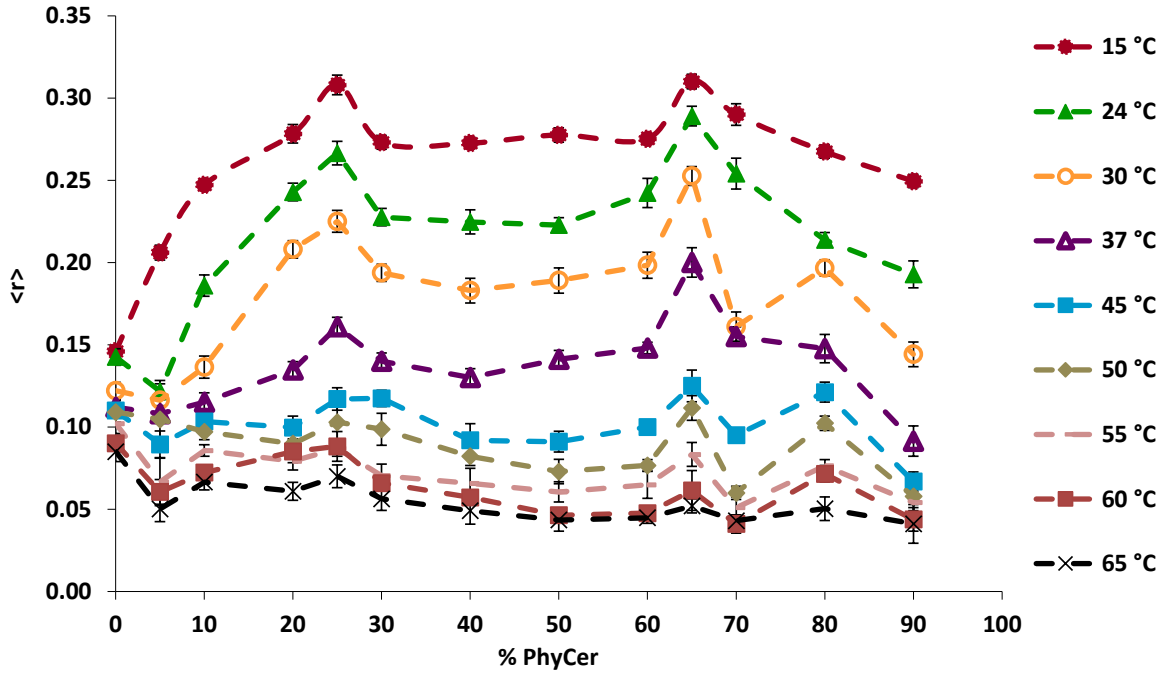

Figure 3 - Steady-state fluorescence anisotropy of *t*-PnA in POPC/PhyCer MLVs as a function of PhyCer mole fraction for a wide range of temperatures. Data represents the mean ± standard deviation of at least 3 independent samples.

A similar experiment was performed with DPH, and the results are shown in Figure 4a. At 37 °C, the behavior is similar to the one observed at 24 °C, except that the anisotropy values are smaller, as expected. Thus, it seems that a gel phase starts forming at ~5-10 mol % PhyCer at both temperatures. At ~30 mol % growth of this phase is terminated, because the anisotropy of DPH becomes approximately constant for that PhyCer concentration, until ~50 mol % is reached. Then, the anisotropy restarts rising. At 65 °C the anisotropy values show that the membrane should be in a fluid state, until an increase is observed for mole fractions of PhyCer higher than 60 mol %. The fluorescence intensity of DPH as a function of PhyCer content (Figure 4b) shows an expected decrease with the temperature and at both 24°C and 37 °C exclusion of the probe by PhyCer containing phases or its exposure to the aqueous environment is clearly observed.

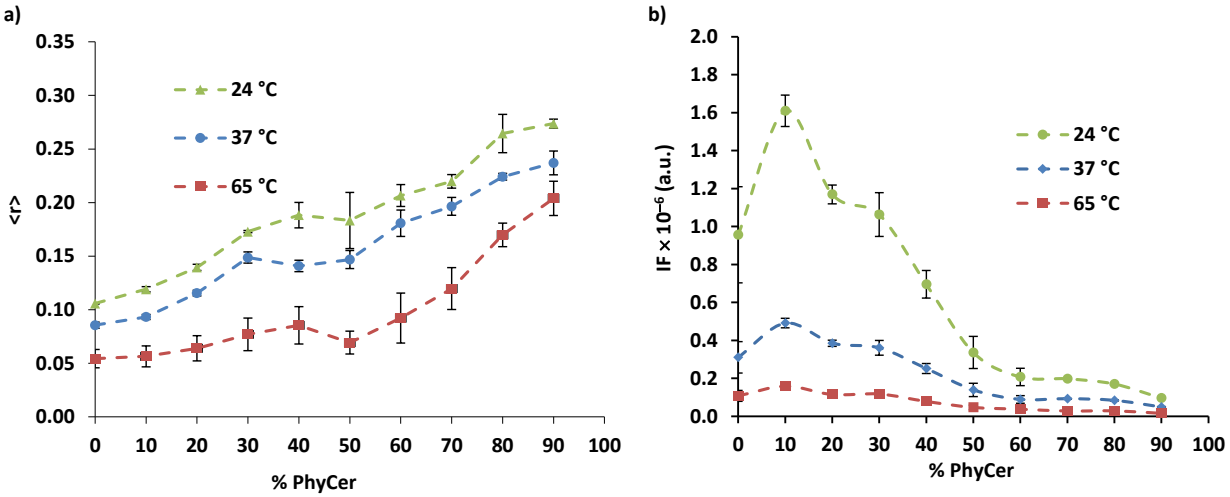

Figure 4 - Steady-state fluorescence a) anisotropy and b) intensity of DPH in POPC/PhyCer MLVs as a function of PhyCer mole fraction for 24, 37 and 65 °C. Data represents the mean ± standard deviation of at least 3 independent samples.

X-ray diffraction of a POPC:PhyCer mixture: compound or superstructure formation

Both SAXS and WAXS were employed in order to obtain structural information concerning pure POPC and POPC:PhyCer 4:1 (mol/mol) mixture (Figure 5). SAXS diffractograms of POPC MLVs reveal a single and symmetric peak, corresponding to a repeat distance of ~ 53 Å (Figure 5a). This value is in agreement with the one previously reported for a pure POPC MLV suspension[36]. In the presence of 20 mol % of PhyCer, besides the reflection at ~ 53 Å, a second peak at ~ 44 Å, in the small-angle region, was detected (Figure 5b). The presence of an additional reflection in this region indicates the formation of a new phase at this lipid composition. Interestingly, a lamellar repeat distance of 45 Å has been determined for PhyCer/water mixtures at 20°C[41]. The reflection observed by us at 44 Å can be unequivocally assigned to a phase with a strong structural influence of PhyCer.

In the wide-angle region no clear reflection was detected for the pure POPC system which can be attributed to the highly disordered nature of POPC acyl chains. However, for the system containing 20 mol % of PhyCer two reflections were observed (Figure 5c). The one at ~ 3.7 Å is related to the chain-to-chain spacing (*a* in eq. 6). A value of 4.2 Å is obtained for the chain-to-chain spacing, and of ~ 32 Å^2 (eq. 7) for the molecular area. The values obtained for both chain-to-chain spacing and area per molecule are

characteristic of a compact and ordered membrane reflecting the presence of a PhyCer rich phase at 20 mol % of this lipid. Such compactness is higher than the one found for other ceramide-rich gel phases as in the case of nervonoylceramide (NCer) gel phase (40.7 Å^2 molecular in the binary mixture POPC:NCer, and 35.1 Å^2 for the pure NCer gel phase[21]). Moreover, for the palmitoylsphingomyelin / cholesterol / palmitoylceramide (54:23:23) system a molecular area of 38.8 Å^2 [6] was retrieved at 20 °C. The very compact nature of the PhyCer enriched phase suggests a distinctive organization of the lipid molecules comprising this phase. Yet, another reflection at ~ 7.3 Å was observed. When a and S_0 are calculated for this reflection, anomalously large values are obtained (a = 8.4 Å, S_0 = 123 Å^2). Hence, this reflection stems from the repetition of a larger unit along the surface.

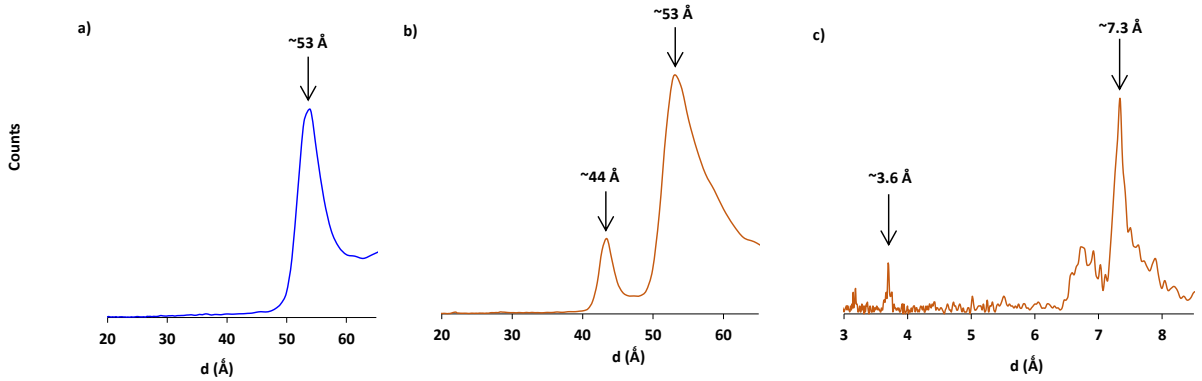

Figure 5 – Small-angle X-ray scattering of a suspension of MLV composed by (a) POPC and (b) 20 mol % POPC / 80 mol % PhyCer. On panel (c) the diffractogram for the wide angle region of the same POPC/PhyCer mixture is shown.

Confocal fluorescence microscopy in GUVs: PhyCer-rich microdomains

In order to characterize the microscale domain organization of POPC/PhyCer systems, GUVs labeled with Rhod-DOPE, a fluid phase probe, were prepared and observed by confocal fluorescence microscopy. The composition range spanned was just 0 to 40 mol % PhyCer, because higher amounts of this type of sphingolipids do not allow the formation of giant vesicles in a reproducible way[42]. In Figure 6, the 3D projections of the confocal slices of representative GUVs are shown. For 100 % POPC, the GUVs display a homogeneous fluid phase, as expected. For 10 mol % PhyCer, while in some GUVs, no gel domains (dark domains, from which the probe is excluded) could be observed, for other GUVs small gel domains could be detected. This is probably due to the fact that the fraction of gel domains is small for that PhyCer concentration. Furthermore, the packing density of the gel phase is much higher than that of the fluid phase, as shown above and, consequently, the area fraction of the vesicle occupied by the gel phase is even smaller. Both these factors justify the fact that in some vesicles the observation of gel domains is difficult. The gel domains become detectable in every GUV, and have a higher fractional area when PhyCer content was increased to 20 (not shown) and to 40 mol % (Figure 6c). The dark areas had a negligible fluorescence intensity demonstrating an almost complete exclusion of the probe, in agreement with the results previously shown. Also of note is the change in the shape of PhyCer-rich domains (dark areas) that was observed from the lower to the higher PhyCer mole fraction employed, which may indicate a different type of organization at the molecular level. An important aspect is that no tubular structures were observed in any of the samples examined. This contrasts with observations made on GUVs consisting of

POPC/ceramide binary mixtures for which at about 30 mol % of ceramide (C24:0, C24:1 or C16+C24:1) strong morphological alterations and other tubular structures are present[40].

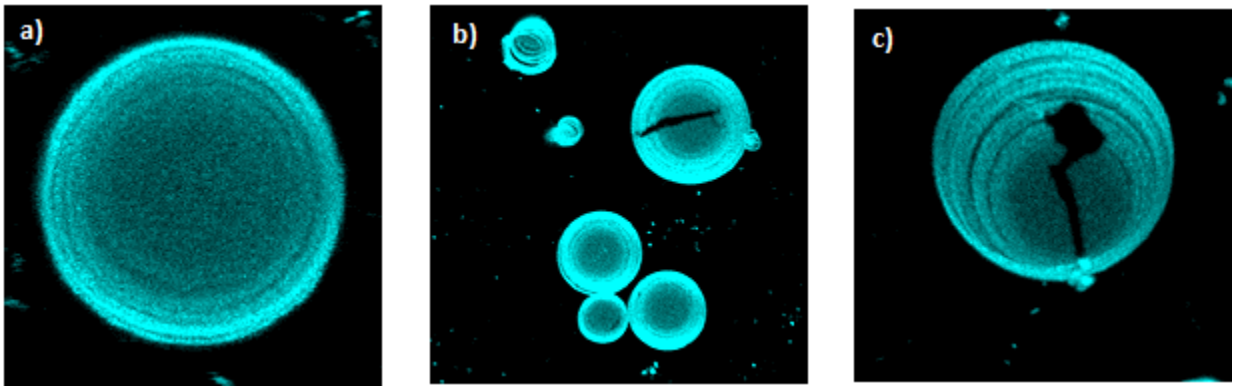

Figure 6 - Lipid domain formation as observed by confocal fluorescence microscopy: 3D projection images obtained from confocal sections of GUV labelled with Rho-DOPE (0.2 mol %) at 24 °C. GUV were prepared from (a) POPC and mixtures of POPC/PhyCer(b) (8:2) and (c) (6:4).

Atomic force microscopy: PhyCer-rich domain nanoscale structure and thickness

AFM imaging of supported lipid bilayers on mica offers a complementary approach to characterize the biophysical properties of the POPC/PhyCer binary system. This imaging technique is probe-free and allows visualizing lateral details of the lipid bilayer with nanometer resolution, giving quantitative information on the thickness of the different phases in the bilayer. This important biophysical property allows discriminating between multiple lipid phase coexistence situations.

SLB with different POPC:PhyCer molar proportions were prepared and observed by *in situ* AFM. The results are summarized in Table S1, and the different types of organization observed shown in Figure 7. For the lower PhyCer proportion studied the lipid bilayer was composed by two distinct phases, which differ in thickness by ~1.1 nm forming round-shaped domains (Figure 7a). The height of the thicker phase was ~5.4 nm whereas the other was ~4.3 nm. These values are in excellent agreement with the ones obtained by X-ray diffraction in which two phases displaying a total thickness of ~5.3 nm (POPC-rich) and ~4.4 nm (PhyCer-enriched) were identified for the mixture containing 20 mol % of PhyCer. The PhyCer-enriched phase occupied almost 80 % of the bilayer area, meaning that this phase was actually composed mainly of POPC, a crucial feature to be accounted for in a POPC/PhyCer phase diagram. At equimolar proportions of the two lipids (Figure 7b), the topographic AFM images revealed a lipid bilayer displaying flower-like percolativedomains. Moreover, the phase with 4.3 nm thickness could also be found, but not the POPC-enriched fluid phase with 5.4 nm. Rather, a new phase with a height of ~6.1 nm was detected (Figure 7b). Also, an expected increase in the area fraction of this phase was observed with increment in PhyCer fraction to 60 %. Interestingly, at 70% PhyCer (Figure 7c) the outer shape of the lipid domains remained unaltered. However, the percolative-like structure observed for intermediate PhyCer concentrations was no longer observed, and the height gap between the two observed phases was reduced to 1.2 nm, which points to a new type of phase coexistence.

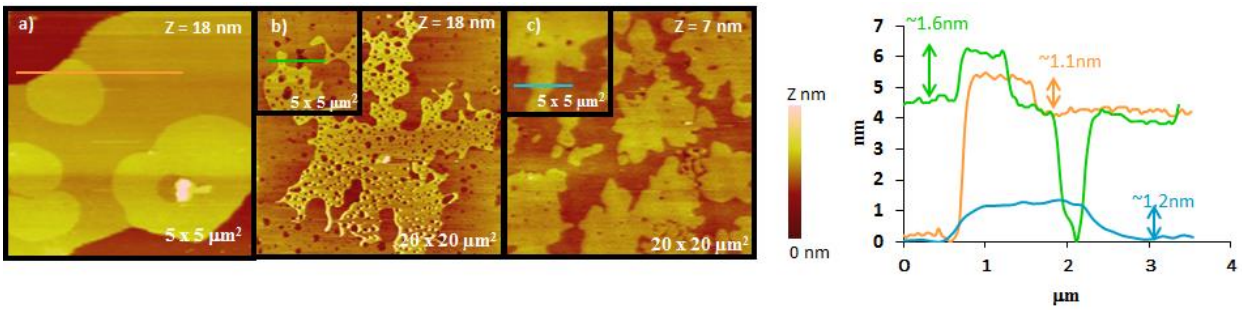

Figure 7 – *Tapping mode* AFM images of supported lipid bilayers formed on mica and composed by the binary mixture POPC:PhyCer at different molar proportions: a) 7:3, b) 1:1 and c) 3:7. Image size and z scale are indicated in each panel. Topographical profiles correspond to the colored lines drawn in each image.

Building the POPC/PhyCer phase diagram

The properties of lipid bilayers containing hydroxylated ceramides as well as the relevance of sphingoid base hydroxylation have not been widely explored in the literature. In this work, a thorough biophysical study of POPC/PhyCer mixtures has been carried out, in order to understand the importance of PhyCer and PhyCer backbone in complex sphingolipids for the formation and properties of ordered domains in different organisms. By using the experimental results here described to build a phase diagram for the POPC/PhyCer system, a direct comparison with other POPC/Cer systems is established, and reveal the differences in molecular organization, both quantitative and qualitative.

The results suggest an elaborated phase diagram (Figure 8) for the binary system POPC:PhyCer, with several important pieces of evidence corroborating the formation of two different stoichiometric complexes "superordered" structures. Of particular interest was the presence of anomalies of fluorescence anisotropy obtained for *t*-PnA (Figure 3) i.e. the two maxima that were constantly observed for 25 and 65% of PhyCer at all scanned temperatures until 45°C, for the 25 mol %, and ~60°C for 60 mol %. The formation of one single complex has been proposed to occur in mixtures of cholesterol with phospholipids or sphingolipids in monolayers [43-45] and free-standing bilayers[46,47]. Here, the two main anomalies identified in the trends of fluorescence anisotropy of *t*-PnA can, certainly, be correlated with the sharp minima (cusp) of the average molecular area observed for the cholesterol/phospholipid and cholesterol/sphingolipid monolayer phase diagrams[44,45]. These cusps represent equivalence points which correspond to a defined composition where there is neither an excess of one component nor the other, in this case, POPC and PhyCer. Thus, these equivalence points help to determine the stoichiometries of the proposed complexes. Considering that the two cusps appear at ~ 25 mol % and ~ 65 mol % of PhyCer (Figures 1 and 3), we suggest that two distinct complexes are formed, one with a stoichiometry of 3 POPC : 1 PhyCer and the other with stoichiometry of 1 POPC : 2 PhyCer. The formation of complexes is also supported by the X-ray diffraction data. The individual lipid molecules are highly condensed into a very packed gel phase (32.1 $Å^2$/molecule), and thus are tightly bound through strong interactions. The reflection at 7.3 Å reports a rather large area per molecule which could be explained by the formation of a supra-structure, in this case corresponding to the area of each unit of the complex and consistent with a $(POPC)_3$PhyCer compound (123 $Å^2$). The formation of these complexes is effectively supported by AFM results which show the formation of three different types of domains differing in shape and thickness, attesting the formation of structures which are not simply POPC enriched fluid or PhyCer enriched gel

phases. Moreover, for 20 mol% PhyCer, the thickness of the domains observed by AFM match the two bilayer repeat distances obtained from the WAXS peaks.

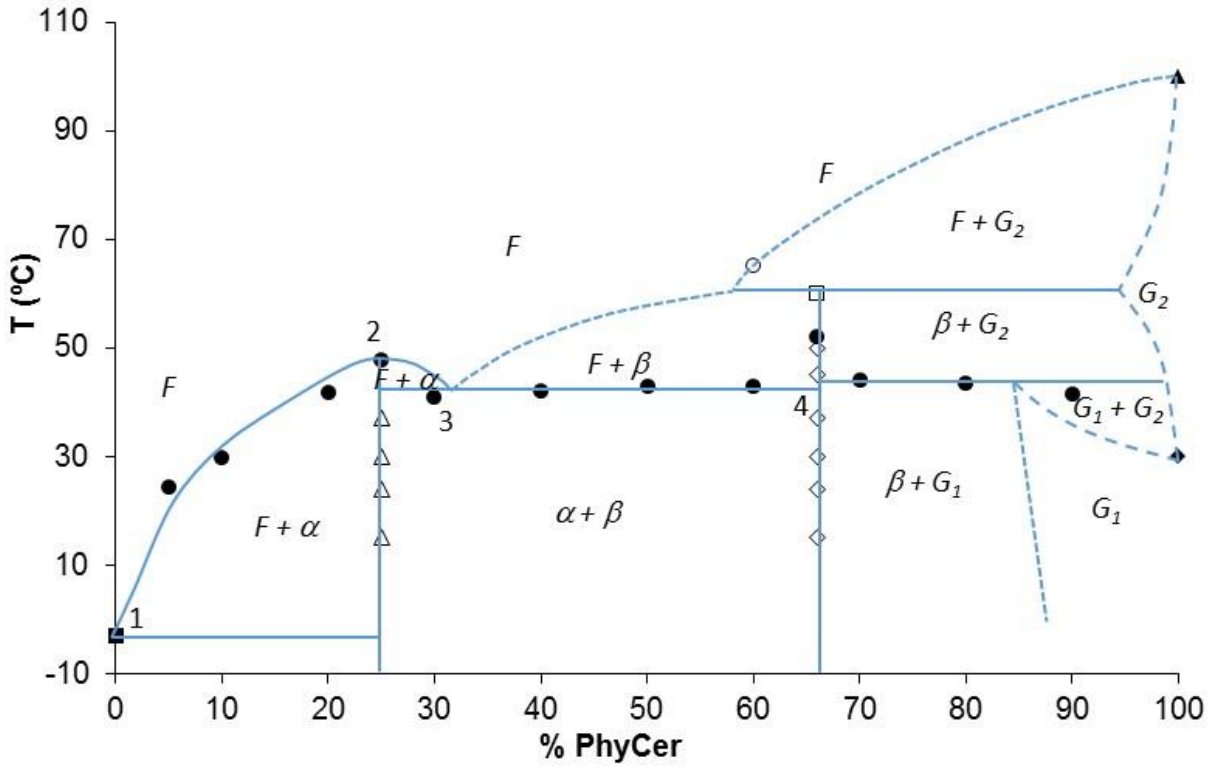

Figure 8 – Phase diagram for the binary mixture POPC:PhyCer.

The POPC/PhyCer binary phase diagram shown in Figure 8 is consistent with both the experimental data here presented and thermodynamic rules. The full lines are supported by experimental data, whereas the dotted lines are mainly derived from the experimental lines, thermodynamic considerations, and phase diagrams of similar lipid mixtures[21, 33]. The phase diagram is of the meritectic type and contains various two-phase regions. All the T_f values retrieved from the analysis of the steady-state fluorescence anisotropy of *t*-PnA as a function of temperature (Figure 2) are represented as solid black circles. These points represent a melting transition detected by *t*-PnA, most likely of one of the complexes, because the other complex still persists above those temperatures, and also because it excludes the probe from the membrane. The phase transition temperature of POPC (main transition,-2.9 °C)[39] (solid square) and PhyCer (pre-transition at 30°C – solid diamond, and main transition at ~100° - solid triangle)[41, 48], taken from the literature, are also plotted, and they are consistent with the T_f values obtained from *t*-PnA. The analysis of Figure 4 also enabled to add another point (open circle) to the top part of the phase diagram which helped clarifying the boundaries of regions coexisting at higher temperatures. This point corresponds to the curve of DPH steady-state anisotropy at 65 °C, which clearly starts to increase above 60 mol % PhyCer.

In other binary systems, either lipidic[43-45, 47], metallic[49] or ionic liquid + aromatic compound[50], stoichiometric complexes or intermediate phases have been described. In this work we advance with the possibility for the formation of more than one complex with different stoichiometries, in a biologically relevant binary lipid system and within a physiologically relevant temperature range. In particular, they occur at 25 and at 66.7 mol % PhyCer, defining the vertical lines in the phase diagram (data from Figures 2 and 3 - open triangles for complex α and diamonds for complex β). The open square is taken from Figure 3, which shows that the peak observed repeatedly at 65 mol % PhyCer disappears for a temperature close to 60 °C.

From the exposed above, it is clear that the properties of the system is very rich and highly dependent on composition and temperature range within analysis. Until 25 mol % of PhyCer, it is possible to observe that the first complex (α) [compound $(POPC)_3PhyCer$] starts to form at low PhyCer concentrations. Moreover, with temperature increase α melts and only a fluid phase is present, which is shown by the lines 1-2. Above 25 mol % until ~ 66.7 mol % of PhyCer and below ~42 °C a coexistence of both complexes is observed. In addition to lines 2-3, 3-4 also corresponds to the melting of α. Above this line a fluid phase and complex β [compound $POPC(PhyCer)_2$] coexist. For higher temperatures this complex also melts and only a fluid phase is present. For PhyCer concentrations higher than 66.7% only β is stable, persisting until ~ 80-90 mol % PhyCer for temperatures below 43 °C. This complex coexists with two distinct gel phases below (G_1) or above (G_2) ~43 °C. These two gel states appear because pure PhyCer has a pre-transition and has itself two gel phases, below the pre-transition, and between the pre-transition and the main transition temperature (solid diamond and solid triangle, respectively). Below 43°C, for very high PhyCer fractions (> 90%) a region of G1-G2 is expected on thermodynamic grounds. Above ~60°C the complex β melts and a region of fluid – gel (G_2) coexistence is present until the gel also melts. In this diagram, the two complexes are considered immiscible. Complex β and Cer-rich gel phases are, however, partially miscible. Complex β, by excluding very efficiently both probes, only allows its melting to be detected when the system has a composition very close to its stoichiometry, and the system virtually corresponds to complex where the probes are then forced to accommodate. This explains the sharp maxima observed for this composition in several photophysical parameters. In the region of α+β coexistence, *t*-PnA possibly accommodates more in defect regions between the domains formed by each complex, where the packing and order of the bilayer are weaker and water penetration is deeper. It is interesting that DPH anisotropy (Figure 4A) is able to detect the formation of G_1 (at 24 °C and 37 °C) and G_2 (at 65 °C), meaning that these phases although richer in PhyCer than complex β are not so efficient in excluding the probe (as reflected in the trend of it fluorescence intensity (Figure 4B). This is further evidence of compound or stoichiometric complex formation.

A previous phase diagram, of the peritectic type, has already been published for the binary system PCer-POPC [33] and NCer-POPC[21]. Some similarities can be found between both phase diagrams. In both cases, for ceramide proportions higher than 50%, the complete melting occurs at temperatures close or higher than 60 °C, which reflects the high membrane order induced by both ceramide species. Moreover, both phase diagrams predict several two-phase coexisting regions and the formation of different gel phases. The main difference might be, in fact, the formation of complexes for the PhyCer-POPC system. Nonetheless, these molecular entities might also be formed for the PCer-POPC system since the particularities found by us for PhyCer data around 25 mol % and 65 mol % are observed for PCer and NCer mole fractions around 50 mol % as noted by Quinn[46]. The huge difference in T_m and headgroup structure both contribute to a strong non-ideality of Cer-POPC mixtures and leads to large gel-fluid separation where the mutual solubility of POPC on Cer-rich gel and Cer on PC-enriched fluid are small. However, for PhyCer,

the presence of an additional hydroxyl group (added to a double bond) provides an additional way for headgroup-headgroup interactions. This additional hydroxyl group is sufficiently small not to disrupt the main interaction between PC molecules. However, through stabilization of acyl chain packing and headgroup H-bonding involving the 4-OH group, probably it is possible to stably trap one PhyCer molecule between 3 POPC molecules, or conversely 1 POPC molecule between 2 PhyCer molecules. The fact that PhyCer itself is not as densely packed (due to the 4-OH) is an essential feature for this kind of behavior to take place because, otherwise, a Cer gel excluding most of the POPC would simply occur, a fact known from liquid clathrates[51]. In sum, the possibility of an additional H-bond, i.e., directional interaction may account for the stability of the complexes, as recently demonstrated for ionic liquid-benzene mixtures where the formation of an inclusion crystal (or liquid clathrate) was reported and the corresponding phase diagram shows an anomaly in the trend of the melting curve, which is a consequence of the compound formed[50]. The relevance of hydrogen bonding regarding membrane organization has recently been invoked to explain the higher tendency of ceramides to form ordered domains in a POPC matrix as compared to diacylglycerols[20] and the formation of highly regular supramolecular structures by synthetic bolapolyphiles[52]. Moreover, the higher stability of raft-like domains containing PhyCer instead of Cer[28] also accounts for the possible ability of PhyCer to form particular molecular entities, which, in turn shall be a direct consequence of the extra hydroxylation in position C-4. Other data that might point for the hypothesis presented above is the formation of flower-like domains in a Cer (porcine brain)/POPC supported lipid bilayer for a Cer proportion as low as 16.6%[42]. In the present work for such PhyCer proportion only round domains were observed, which shows that a higher surface tension exists between POPC and ceramide than between POPC and PhyCer. Such results shows that, at low fractions, the ability of PhyCer to establish interactions with POPC is higher than that of a sphingosine-based ceramide, and that this ability is conferred by the presence of an additional hydroxylation.

With this work we were able to generate the phase diagram for the POPC:PhyCer binary mixture which shows several regions of two phase coexistence and, more importantly, it predicts the formation of two distinct stoichiometric complexes. The formation of such compounds could be inferred from the joint analysis of the different analytical techniques employed in this work. As the condensed complexes of cholesterol and phospholipids or sphingolipids find their biological relevance in a possible facilitation of the formation of specialized domains such as lipid rafts[43,44], also the complexes described in this work could be related with the formation of stable compartments or signaling platforms that are believed to occur *in vivo*[46, 53], where changes on hydroxylation levels occur concomitantly with membrane microdomain reorganization in cellular adaptive processes[22].

CONCLUSIONS

Minimalistic models containing PhyCer might be a first step in the comprehension and in the characterization of the main properties of the domains often formed in plant and fungal biomembranes, since phytosphingosine is the main sphingoid base found in plants and fungi. The recent discovery of the existence of gel domains in yeast[11], which are sphingolipid enriched and ergosterol depleted, gives strength to the use of PhyCer as a first approach into understanding the dynamics of the biomembranes of the living beings comprising these two kingdoms. The phases formed by PhyCer such as the complexes with POPC described in this work are probably the most straightforward way of mimicking yeast sphingolipid rich gel domains. In this respect, it is of particular relevance the remarkable similarity between the steady-state anisotropy and fluorescence lifetimes of *t*-PnA when labeling POPC/PhyCer complexes in

binary mixture (this work) and the plasma membrane in living *S. cerevisiae* wild type cells[11] (at 24 °C, ~0.28 and ~26 ns).

Several evidence concerning the formation of microdomains with distinct properties from mammalian cells that do not fit the lipid raft definition,[54] both in plants and fungi, has been reported, and recently reviewed[9]. These include the presence of temporally and spatially stable compartments identified by fluorescence microscopy and fractions of immobile proteins during long periods of time that may reach hours or even during all the cell cycle[9, 55]. A certain degree of low mobility of some protein clusters in mammalian cells has also been found, and currently the different mechanisms whereby diffusion of proteins and lipids may be restricted in cell membranes are considered of high biological relevance[56]. In this work, it was shown that the additional hydroxyl group in the sphingoid base of PhyCer may be a crucial structural aspect in order to promote the formation of stable complexes with fluid phospholipids. As mentioned above, these complexes exhibit some of the biophysical properties already described for the stable gel domains identified in yeast cells and under physiological conditions[11,12]. Thus it is conceivable that the abundance of sphingolipids with PhyCer backbone might be, at least in part, responsible for the stability of these gel domains *in vivo*, rendering them detectable with *t*-PnA fluorescence. This has, so far, not been reported for mammalian cells[37, 54]. Interactions involving the 4-OH group of phytosphingosine would therefore contribute significantly to the different microdomain organization in those organisms, not only because they would contain higher abundance/more stable gel domains, but also because these gel domains may represent a natural barrier to the mobility and diffusion of membrane proteins (and other lipids) and thus they might be an important mechanism for the spatiotemporal stability of membrane compartments in yeast and other organisms, and for other biological processes involving membrane diffusion barriers. The changes in ordered domain organization and properties with increasing PhyCer fractions described in the present work can also provide a basis for the ability of the gel microdomains to undergo fast reorganization observed upon depolarizing events in living yeast cells[57].

The present work provides a molecular explanation for the finding of stable gel domains in living yeast cells under physiological conditions, since it is found that the sphingoid base hydroxylation gives the ability to form different types of highly ordered and rigid stoichiometric complexes that are stable under a large range of compositions and temperatures.

ASSOCIATED CONTENT

Supporting Information

Additional information showing the fluorescence lifetime components of *t*-PnA and the respective fraction of emitted light in MLV with different proportions of POPC and PhyCer and table resuming the information retrieved by AFM is presented in supporting information. This material is available free of charge via the Internet at http://pubs.acs.org.

AUTHOR INFORMATION

Corresponding author:

*Tel.: +351217500925. E-mail: rodrigo.almeida@fc.ul.pt;

Author Contributions

§ Equally contributing authors

Notes

The authors declare no competing financial interest.

ACKNOWLEDGMENTS

Fundação para a Ciência e a Tecnologia (FCT), Portugal is acknowledged for PTDC/QUI-BIQ/104311/2008, PEst 2015-2020 (UID/Multi/00612/2013), and IF2012/2013 initiatives (POPH, Fundo Social Europeu). J.T.M. acknowledges a PhD. scholarship SFRH/BD/64442/2009. Dr. Jorg Nikolaus and Dr. Silvia Scolari are acknowledged for their assistance in the GUV preparation and confocal microscopy observations in Berlin. We are thankful for the kind assistance of Dr. Olinda Monteiro in the acquisition of the X-ray scattering data.

REFERENCES

1. Uemura, S.; Shishido, F.; Tani, M.; Mochizuki, T.; Abe, F.; Inokuchi, J.-i. Loss of hydroxyl groups from the ceramide moiety can modify the lateral diffusion of membrane proteins in S. cerevisiae. *Journal of Lipid Research* **2014,** *55*, 1343-1356.
2. Jimenez-Rojo, N.; Sot, J.; Busto, J. V.; Shaw, W. A.; Duan, J. J.; Merrill, A. H.; Alonso, A.; Goni, F. M. Biophysical Properties of Novel 1-Deoxy-(Dihydro)ceramides Occurring in Mammalian Cells. *Biophys. J.* **2014,** *107*, 2850-2859.
3. Björkbom, A.; Ohvo-Rekilä, H.; Kankaanpää, P.; Nyholm, T. K. M.; Westerlund, B.; Slotte, J. P. Characterization of membrane properties of inositol phosphorylceramide. *Biochimica et Biophysica Acta (BBA) - Biomembranes* **2010,** *1798*, 453-460.
4. Goni, F. M.; Alonso, A. Biophysics of sphingolipids I. Membrane properties of sphingosine, ceramides and other simple sphingolipids. *Biochimica et biophysica acta* **2006,** *1758*, 1902-1921.
5. Castro, B. M.; de Almeida, R. F.; Silva, L. C.; Fedorov, A.; Prieto, M. Formation of ceramide/sphingomyelin gel domains in the presence of an unsaturated phospholipid: a quantitative multiprobe approach. *Biophys.J.* **2007,** *93*, 1639-1650.
6. Busto, J. V.; Garcia-Arribas, A. B.; Sot, J.; Torrecillas, A.; Gomez-Fernandez, J. C.; Goni, F. M.; Alonso, A. Lamellar Gel (L-beta) Phases of Ternary Lipid Composition Containing Ceramide and Cholesterol. *Biophysical Journal* **2014,** *106*, 621-630.
7. Nybond, S.; Bjorkqvist, Y. J.; Ramstedt, B.; Slotte, J. P. Acyl chain length affects ceramide action on sterol/sphingomyelin-rich domains. *Biochimica et biophysica acta* **2005,** *1718*, 61-66.
8. Silva, L. C.; de Almeida, R. F.; Castro, B. M.; Fedorov, A.; Prieto, M. Ceramide-domain formation and collapse in lipid rafts: membrane reorganization by an apoptotic lipid. *Biophysical journal* **2007,** *92*, 502-516.
9. Malinsky, J.; Opekarova, M.; Grossmann, G.; Tanner, W. Membrane microdomains, rafts, and detergent-resistant membranes in plants and fungi. *Annual review of plant biology* **2013,** *64*, 501-529.
10. Watanabe, R.; Funato, K.; Venkataramam, K.; Futerman, A. H.; Riezman, H. Sphingolipids are required for the stable membrane association of glycosylphosphatidylinositol-anchored proteins in yeast. *Journal of Biological Chemistry* **2002,** *277*, 49538-49544.
11. Aresta-Branco, F.; Cordeiro, A. M.; Marinho, H. S.; Cyrne, L.; Antunes, F.; de Almeida, R. F. Gel domains in the plasma membrane of Saccharomyces cerevisiae: highly ordered, ergosterol-free, and sphingolipid-enriched lipid rafts. *J.Biol.Chem.* **2011,** *286*, 5043-5054.
12. Vecer, J.; Vesela, P.; Malinsky, J.; Herman, P. Sphingolipid levels crucially modulate lateral microdomain organization of plasma membrane in living yeast. *FEBS Letters* **2014,** *588*, 443-449.
13. Ratto, T. V.; Longo, M. L. Obstructed diffusion in phase-separated supported lipid bilayers: A combined atomic force microscopy and fluorescence recovery after photobleaching approach. *Biophysical Journal* **2002,** *83*, 3380-3392.
14. Almeida, P. F. F.; Vaz, W. L. C.; Thompson, T. E. Lateral Diffusion and Percolation in 2-Phase, 2-Component Lipid Bilayers - Topology of the Solid-Phase Domains Inplane and Across the Lipid Bilayer. *Biochemistry* **1992,** *31*, 7198-7210.
15. Clay, L.; Caudron, F.; Denoth-Lippuner, A.; Boettcher, B.; Frei, S. B.; Snapp, E. L.; Barral, Y. A sphingolipid-dependent diffusion barrier confines ER stress to the yeast mother cell. *Elife* **2014,** *3*.
16. Chiantia, S.; Kahya, N.; Schwille, P. Raft domain reorganization driven by short- and long-chain ceramide: a combined AFM and FCS study. *Langmuir : the ACS journal of surfaces and colloids* **2007,** *23*, 7659-7665.
17. Sot, J.; Aranda, F. J.; Collado, M. I.; Goni, F. M.; Alonso, A. Different effects of long- and short-chain ceramides on the gel-fluid and lamellar-hexagonal transitions of phospholipids: a calorimetric, NMR, and x-ray diffraction study. *Biophysical journal* **2005,** *88*, 3368-3380.

18. Maula, T.; Artetxe, I.; Grandell, P.-M.; Slotte, J. P. Importance of the Sphingoid Base Length for the Membrane Properties of Ceramides. *Biophysical Journal* **2012,** *103*, 1870-1879.
19. Sot, J.; Goni, F. M.; Alonso, A. Molecular associations and surface-active properties of short- and long-N-acyl chain ceramides. *Biochimica et biophysica acta* **2005,** *1711*, 12-19.
20. Ekman, P.; Maula, T.; Yamaguchi, S.; Yamamoto, T.; Nyholm, T. K. M.; Katsumura, S.; Slotte, J. P. Formation of an ordered phase by ceramides and diacylglycerols in a fluid phosphatidylcholine bilayer — Correlation with structure and hydrogen bonding capacity. *Biochimica et Biophysica Acta (BBA) - Biomembranes* **2015,** *1848*, 2111-2117.
21. Pinto, S. N.; Silva, L. C.; de Almeida, R. F.; Prieto, M. Membrane domain formation, interdigitation, and morphological alterations induced by the very long chain asymmetric C24:1 ceramide. *Biophysical journal* **2008,** *95*, 2867-2879.
22. Pedroso, N.; Matias, A. C.; Cyrne, L.; Antunes, F.; Borges, C.; Malhó, R.; de Almeida, R. F.; Herrero, E.; Marinho, H. S. Modulation of plasma membrane lipid profile and microdomains by H2O2 in Saccharomyces cerevisiae. *Free Radic.Biol.Med.* **2009,** *46*, 289-298.
23. Khmelinskaia, A.; Ibarguren, M.; de Almeida, R. F. M.; Lopez, D. J.; Paixao, V. A.; Ahyayauch, H.; Goni, F. M.; Escriba, P. V. Changes in Membrane Organization upon Spontaneous Insertion of 2-Hydroxylated Unsaturated Fatty Acids in the Lipid Bilayer. *Langmuir* **2014,** *30*, 2117-2128.
24. Martin, M. L.; Barcelo-Coblijn, G.; de Almeida, R. F. M.; Noguera-Salva, M. A.; Teres, S.; Higuera, M.; Liebisch, G.; Schmitz, G.; Busquets, X.; Escriba, P. V. The role of membrane fatty acid remodeling in the antitumor mechanism of action of 2-hydroxyoleic acid. *Biochimica Et Biophysica Acta-Biomembranes* **2013,** *1828*, 1405-1413.
25. Bure, C.; Cacas, J. L.; Mongrand, S.; Schmitter, J. M. Characterization of glycosyl inositol phosphoryl ceramides from plants and fungi by mass spectrometry. *Analytical and Bioanalytical Chemistry* **2014,** *406*, 995-1010.
26. Bouwstra, J. A.; Ponec, M. The skin barrier in healthy and diseased state. *Biochimica Et Biophysica Acta-Biomembranes* **2006,** *1758*, 2080-2095.
27. Iwai, I.; Han, H. M.; den Hollander, L.; Svensson, S.; Ofverstedt, L. G.; Anwar, J.; Brewer, J.; Bloksgaard, M.; Laloeuf, A.; Nosek, D.; Masich, S.; Bagatolli, L. A.; Skoglund, U.; Norlen, L. The Human Skin Barrier Is Organized as Stacked Bilayers of Fully Extended Ceramides with Cholesterol Molecules Associated with the Ceramide Sphingoid Moiety. *J. Invest. Dermatol.* **2012,** *132*, 2215-2225.
28. Megha; Sawatzki, P.; Kolter, T.; Bittman, R.; London, E. Effect of ceramide N-acyl chain and polar headgroup structure on the properties of ordered lipid domains (lipid rafts). *Biochimica Et Biophysica Acta-Biomembranes* **2007,** *1768*, 2205-2212.
29. Jaikishan, S.; Slotte, J. P. Stabilization of sphingomyelin interactions by interfacial hydroxyls - A study of phytosphingomyelin properties. *Biochimica Et Biophysica Acta-Biomembranes* **2013,** *1828*, 391-397.
30. Guan, X. L.; Wenk, M. R. Mass spectrometry-based profiling of phospholipids and sphingolipids in extracts from Saccharomyces cerevisiae. *Yeast* **2006,** *23*, 465-477.
31. Stillwell, W. *An Introduction to Biological Membranes*; First ed.; Elsevier Science: San Diego, 2013.
32. Marques, J. T.; Viana, A. S.; de Almeida, R. F. Ethanol effects on binary and ternary supported lipid bilayers with gel/fluid domains and lipid rafts. *Biochim.Biophys.Acta* **2011,** *1808*, 405-414.
33. Silva, L.; de Almeida, R. F.; Fedorov, A.; Matos, A. P.; Prieto, M. Ceramide-platform formation and -induced biophysical changes in a fluid phospholipid membrane. *Molecular membrane biology* **2006,** *23*, 137-148.
34. Stöckl, M.; Nikolaus, J.; Herrmann, A. Visualization of Lipid Domain-Specific Protein Sorting in Giant Unilamellar Vesicles. 2010; Vol. 606, pp 115-126.
35. Mcclare, C. W. F. Accurate and Convenient Organic Phosphorus Assay. *Analytical Biochemistry* **1971,** *39*, 527-&.

36. Marsh, D. *Handbook of Lipid Bilayers*; CRC Press, Taylor & Francis Group2013.
37. Bastos, A. E. P.; Scolari, S.; St+Âckl, M.; de Almeida, R. F. M. Chapter Three - Applications of Fluorescence Lifetime Spectroscopy and Imaging to Lipid Domains In Vivo. In *Methods in Enzymology, Imaging and Spectroscopic Analysis of Living Cells Optical and Spectroscopic Techniques*, Volume 504 ed.; conn, P. M., Ed.; Academic Press, 2012, pp 57-81.
38. Guillen, J.; de Almeida, R. F. M.; Prieto, M.; Villalain, J. Structural and dynamic characterization of the interaction of the putative fusion peptide of the S2SARS-CoV virus protein with lipid membranes. *Journal of Physical Chemistry B* **2008,** *112*, 6997-7007.
39. Koynova, R.; Caffrey, M. Phases and phase transitions of the phosphatidylcholines. *Biochimica et Biophysica Acta (BBA) - Reviews on Biomembranes* **1998,** *1376*, 91-145.
40. Pinto, S. N.; Silva, L. C.; de Almeida, R. F. M.; Prieto, M. Ceramide Gel Domain Formation in a Phospholipid Bilayer: The Impact of Ceramide Acyl Chain. *Biophysical Journal* **2010,** *98*, 664A-664A.
41. Raudenkolb, S.; Wartewig, S.; Neubert, R. H. H. Polymorphism of ceramide 3. Part 2: a vibrational spectroscopic and X-ray powder diffraction investigation of N-octadecanoyl phytosphingosine and the analogous specifically deuterated d35 derivative. *Chemistry and Physics of Lipids* **2003,** *124*, 89-101.
42. Fidorra, M.; Duelund, L.; Leidy, C.; Simonsen, A. C.; Bagatolli, L. A. Absence of fluid-ordered/fluid-disordered phase coexistence in ceramide/POPC mixtures containing cholesterol. *Biophysical journal* **2006,** *90*, 4437-4451.
43. McConnell, H. M.; Radhakrishnan, A. Condensed complexes of cholesterol and phospholipids. *Biochimica Et Biophysica Acta-Biomembranes* **2003,** *1610*, 159-173.
44. Radhakrishnan, A.; Anderson, T. G.; McConnell, H. M. Condensed complexes, rafts, and the chemical activity of cholesterol in membranes. *Proceedings of the National Academy of Sciences of the United States of America* **2000,** *97*, 12422-12427.
45. Radhakrishnan, A.; Li, X. M.; Brown, R. E.; McConnell, H. M. Stoichiometry of cholesterol-sphingomyelin condensed complexes in monolayers. *Biochimica Et Biophysica Acta-Biomembranes* **2001,** *1511*, 1-6.
46. Quinn, P. J. A lipid matrix model of membrane raft structure. *Progress in Lipid Research* **2010,** *49*, 390-406.
47. Quinn, P. J. Structure of Sphingomyelin Bilayers and Complexes with Cholesterol Forming Membrane Rafts. *Langmuir* **2013,** *29*, 9447-9456.
48. Garidel, P. Structural organisation and phase behaviour of a stratum corneum lipid analogue: ceramide 3A. *Physical Chemistry Chemical Physics* **2006,** *8*, 2265-2275.
49. John, V. B. *Understanding Phase Diagrams*; Macmillan: Bristol, 1974.
50. Lachwa, J.; Bento, I.; Duarte, M. T.; Lopes, J. N. C.; Rebelo, L. P. N. Condensed phase behaviour of ionic liquid-benzene mixtures: congruent melting of a emim NTf2 center dot C6H6 inclusion crystal. *Chemical Communications* **2006**, 2445-2447.
51. Holbrey, J. D.; Reichert, W. M.; Nieuwenhuyzen, M.; Sheppard, O.; Hardacre, C.; Rogers, R. D. Liquid clathrate formation in ionic liquid-aromatic mixtures. *Chem. Commun.* **2003**, 476-477.
52. Werner, S.; Ebert, H.; Lechner, B.-D.; Lange, F.; Achilles, A.; Baerenwald, R.; Poppe, S.; Blume, A.; Saalwaechter, K.; Tschierske, C.; Bacia, K. Dendritic Domains with Hexagonal Symmetry Formed by X-Shaped Bolapolyphiles in Lipid Membranes. *Chem.-Eur. J.* **2015,** *21*, 8840-8850.
53. Joly, E. Hypothesis: could the signalling function of membrane microdomains involve a localized transition of lipids from liquid to solid state? *Bmc Cell Biology* **2004,** *5*.
54. de Almeida, R. F. M.; Joly, E. Crystallization around solid-like nanosized docks can explain the specificity, diversity, and stability of membrane microdomains. *Front. Plant Sci.* **2014,** *5*, 14.
55. Martiniere, A.; Runions, J. Protein diffusion in plant cell plasma membranes: the cell-wall corral. *Front. Plant Sci.* **2013,** *4*.

56. Trimble, W. S.; Grinstein, S. Barriers to the free diffusion of proteins and lipids in the plasma membrane. *J. Cell Biol.* **2015,** *208*, 259-271.
57. Herman, P.; Vecer, J.; Opekarova, M.; Vesela, P.; Jancikova, I.; Zahumensky, J.; Malinsky, J. Depolarization affects the lateral microdomain structure of yeast plasma membrane. *Febs J.* **2015,** *282*, 419-434.

Table of Contents

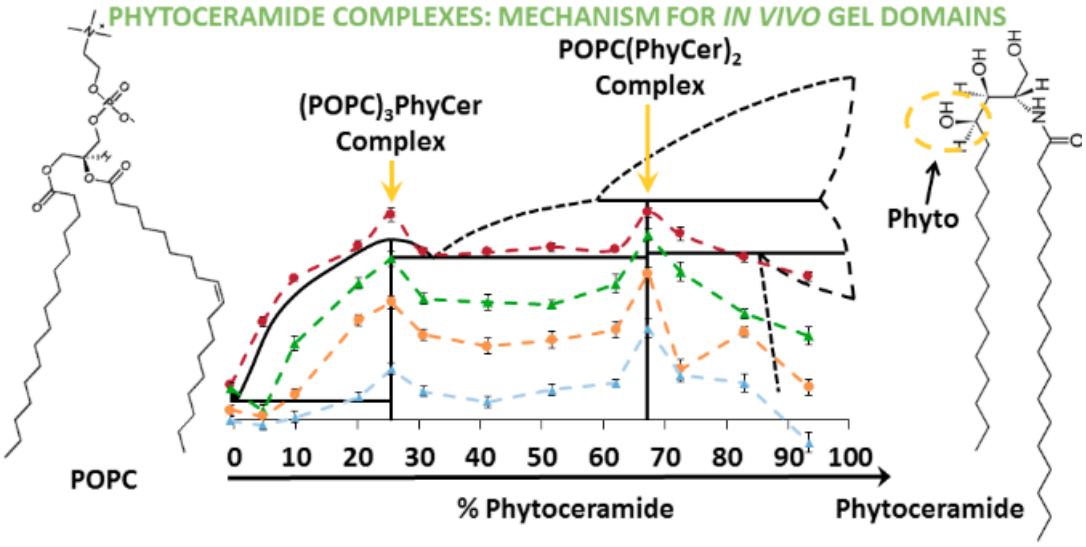

3.2. Supporting Information

Supporting Information

Formation and properties of membrane ordered domains by phytoceramide: role of sphingoid base hydroxylation

Joaquim T. Marquês[1,§], André M. Cordeiro[1,§], Ana. S. Viana[1], Andreas. Herrmann[2], H. Susana. Marinho[1], Rodrigo F. M. de Almeida[1],*

[1] Centro de Química e Bioquímica, Departamento de Química e Bioquímica, Faculdade de Ciências da Universidade de Lisboa, Ed. C8, Campo Grande, 1749-016, Lisboa, Portugal

[2] Department of Biology, Molecular Biophysics, Humboldt University, Berlin, Germany

[§] Equally contributing authors

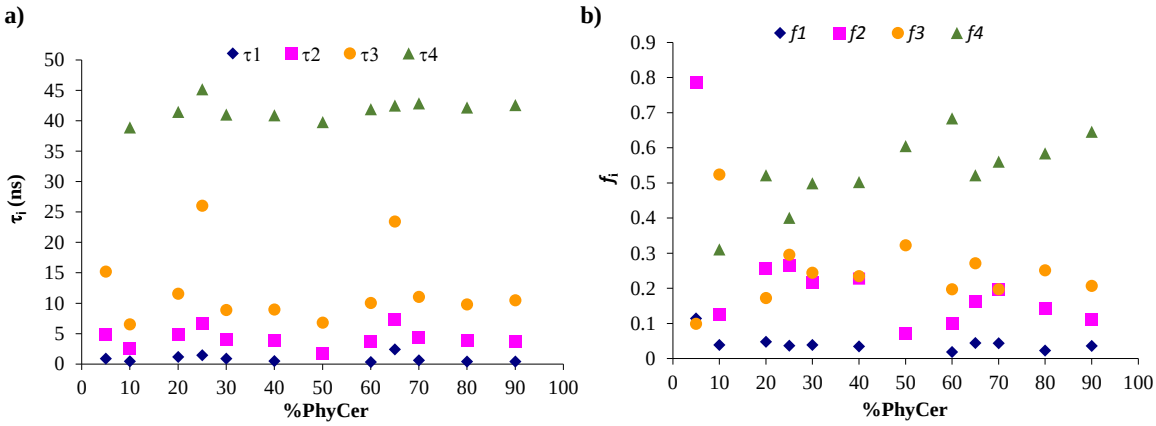

Figure S1 – Fluorescence lifetime components of *t*-PnA (*a*) and respective fraction of emitted light (*b*) as a function of PhyCer mole fraction. The values were retrieved from the analysis of the experimental fluorescence intensity decays of the probe at 24 °C as described under the experimental section. In (*a*) it can be observed that in addition to the longest component, also other components, particularly the second longest, has pronounced maxima at 25 and 65 mol% PhyCer corroborating the formation of complexes involving also the POPC molecules near these compositions. Regarding the fractions of light (*b*), the trend with pronounced maxima extends to the second shortest component, further showing that all the membrane is involved in the formation of a specific highly ordered phase, once again supporting the presence of stoichiometric complexes.

Table S1 - Summary of AFM observations for the POPC / Phytoceramide System (supported lipid bilayers on mica).

Composition (POPC:PhyCer mol:mol)	Main Observations	Domains shape	Domains Height difference (nm)	Lipid phases fraction (in area)
90-75:10-25	• Two distinct phases with a height difference around 1.1 nm	Round	1.1±0.14	81:19
50:50	• Bilayers formed at lower extent • Increased height gap • Higher segregation – larger domains • Percolated domains	Flower-like	1.67±0.13	68:32
40:60	• Thicker domains 1.4 – 1.9nm thicker • High segregation – large domains	Flower-like	1.63±0.22	56:44
30:70	• Height gap in the range between 1.2-1.4nm • High segregation – large domains • Percolated domains not identified	Flower-like	1.23±0.10	45:55

Chapter IV

Membrane lateral organization on ethanol effects

4.1. Ethanol effects on binary and ternary supported lipid bilayers with gel/fluid domains and lipid rafts

Biochimica et Biophysica Acta 1808 (2011) 405–414

Contents lists available at ScienceDirect

Biochimica et Biophysica Acta

journal homepage: www.elsevier.com/locate/bbamem

Ethanol effects on binary and ternary supported lipid bilayers with gel/fluid domains and lipid rafts

Joaquim T. Marquês, Ana S. Viana, Rodrigo F.M. De Almeida *

Centro de Química e Bioquímica, Faculdade de Ciências da Universidade de Lisboa, Ed. C8, Campo Grande 1749-016, Lisboa, Portugal

ARTICLE INFO

Article history:
Received 14 July 2010
Received in revised form 8 October 2010
Accepted 12 October 2010
Available online 15 October 2010

Keywords:
Ethanol–membrane interactions
Liquid AFM
Liquid ordered liquid disordered
Bilayer expansion
Silicon
Sphingomyelin

ABSTRACT

Ethanol–lipid bilayer interactions have been a recurrent theme in membrane biophysics, due to their contribution to the understanding of membrane structure and dynamics. The main purpose of this study was to assess the interplay between membrane lateral heterogeneity and ethanol effects. This was achieved by *in situ* atomic force microscopy, following the changes induced by sequential ethanol additions on supported lipid bilayers formed in the absence of alcohol. Binary phospholipid mixtures with a single gel phase, dipalmitoylphosphatidylcholine (DPPC)/cholesterol, gel/fluid phase coexistence DPPC/dioleoylphosphatidylcholine (DOPC), and ternary lipid mixtures containing cholesterol, mimicking lipid rafts (DOPC/DPPC/cholesterol and DOPC/sphingomyelin/cholesterol), i.e., with liquid ordered/liquid disordered (ld/lo) phase separation, were investigated. For all compositions studied, and in two different solid supports, mica and silicon, domain formation or rearrangement accompanied by lipid bilayer thinning and expansion was observed. In the case of gel/fluid coexistence, low ethanol concentrations lead to a marked thinning of the fluid but not of the gel domains. In the case of ld/lo all the bilayer thins simultaneously by a similar extent. In both cases, only the more disordered phase expanded significantly, indicating that ethanol increases the proportion of disordered domains. Water/bilayer interfacial tension variation and freezing point depression, inducing acyl chain disordering (including opening and looping), tilting, and interdigitation, are probably the main cause for the observed changes. The results presented herein demonstrate that ethanol influences the bilayer properties according to membrane lateral organization.

1. Introduction

In the last decades, the importance of the lipid components of the bilayer, especially their lateral organization into microdomains with different physical properties, was established [1,2]. Currently, it is widely accepted that the plasma membrane of many cell types is highly compartmentalized and organized into domains in different time and length scales, with differentiated lipid–lipid interactions [3]. The most widely investigated domains are the sphingolipid/cholesterol-enriched domains known as lipid rafts [4–7]. It was also established from biophysical studies that to model the properties of these domains it is necessary to use a ternary lipid mixture of cholesterol and two other lipids (phospho or sphingolipids) differing significantly in their main transition temperature (T_m) [8–10]. More recently, the formation of high T_m sphingolipid-enriched domains with properties similar to the lipid gel phase that is commonly found in model systems has been gaining strength [11]. It is thus important in studies of membrane related phenomena to account for the dynamic role of membrane lipid composition and organization into nano or microdomains.

One significant area of study with lipid bilayers has been their interaction with ethanol. Understanding ethanol–lipid interactions has helped to unravel membrane biophysical properties and elucidate the mechanism of action of other small molecules with anaesthetic properties [12–14]. This subject is also relevant for human health, e.g. [15–17], and for a significant number of experiments which require the addition of external components, such as probes or drugs, in ethanol solutions to liposomes or cells [18]. Moreover, it is necessary to the understanding of the adaptation of organisms performing alcoholic fermentation to high ethanol levels in the growing medium [19].

Most biophysical studies of ethanol–bilayer interactions have been conducted using bulk techniques, such as X-ray scattering [20,21], differential scanning calorimetry (DSC) [21–23], fluorescence spectroscopy [22,24–26], NMR [27,28], and EPR [29]. Importantly, it was determined that ethanol binds to the lipid–water interface [28] and promotes the disordering of the acyl chains [27]. Furthermore, the induction of bilayer thickness reduction has been reported, which may occur mainly by three processes—disordering [21,30,31], tilt angle change [21,32] or interdigitation of phospholipid acyl chains [20,21]. This last mechanism is characterized by the interpenetration of the acyl chains from one bilayer leaflet into the other with the consequent bilayer

* Corresponding author. Tel.: +351 217500924; fax: +351 217500088.
E-mail address: rodrigo.almeida@fc.ul.pt (R.F.M. De Almeida).

0005-2736/$ – see front matter © 2010 Elsevier B.V. All rights reserved.
doi:10.1016/j.bbamem.2010.10.006

thinning. The increase of the mean molecular area results in a lateral expansion of the bilayer [20,33]. In addition, phospholipid/ethanol phase diagrams were established, which show that below the phospholipid T_m, i.e., in the gel phase, it is possible to have coexistence of an interdigitated and a non-interdigitated phase [21]. The ethanol/DPPC phase diagrams indicate that the threshold for interdigitated domain formation should be between 3.2% [21] and 5% [33] ethanol, and that the bilayer should be fully interdigitated for 10–12% of this alcohol. However, more recently, it was shown by atomic force microscopy (AFM) that overnight incubation of a fluid phospholipid bilayer with ethanol also promoted the formation of height-reduced domains coexisting with unchanged portions of the bilayer [12]. The use of AFM also helped to elucidate the events by which some anaesthetics, such as halothane and ethanol, or antibiotics exert their actions [12,34].

Detailed studies of the effect of ethanol on lipid mixtures are scarce despite the evidence suggesting that the outcome should be highly dependent on the phase behaviour of the system [35–37]. It was found by DSC and fluorescence spectroscopy that cholesterol in small concentration (2 mol%) enhances ethanol effects [22], whereas in high concentrations (20 mol%) cholesterol has a protective action, preventing interdigitation [24]. These studies were conducted in binary mixtures with no lipid phase separation. Recently, an AFM study reported a similar effect for DPPC/ergosterol bilayers [38]. To the best of our knowledge, a study of ethanol interaction with lipid raft-forming bilayers, i.e., ternary lipid mixtures with liquid ordered (lo)/liquid disordered (ld) phase separation, was not yet performed, whereby the role of lipid domains on ethanol-induced effects remains undisclosed. Considering the vital functions associated with lipid rafts, such as protein sorting, signal transduction and internalization of pathogens [39–41], it is significant to establish the interactions between ethanol and raft-forming bilayers.

In the present work, the interactions of ethanol with distinct lipid bilayers containing no domains, gel/fluid domains, and lipid rafts models were studied. *In situ* tapping-mode AFM using a liquid cell was performed in order to follow in real time the dynamic morphological changes of the supported lipid bilayer (SLB) induced by increasing ethanol concentrations. SLBs were prepared on two different substrates, mica and silicon. Mica is a well-known substrate for successful lipid deposition and AFM imaging [42–44] and silicon is much less explored, despite its unique optical properties [45,46]. In addition, many of the technologies currently used and in development are silicon based, and the improvement of the deposition of lipid bilayers in silicon and their characterization offer potentially new applications for SLB (e.g. [47–49]). Additionally, the use of two distinct solid supports stems from the possibility that membrane–substrate interactions may affect the formation and dynamics of lipid domains [44]. Regarding the effect of ethanol on silicon SLBs, Miszta et al. [50] did not detect ethanol-induced thinning in fluid bilayers composed of DOPC, DLPC and DOPC/DOPS using conventional ellipsometry. However, Gedig et al. [51] used imaging ellipsometry and they were able to observe ethanol-induced thickness reduction in gel and fluid phase dimiristoylphosphatidylcholine (DMPC) bilayers deposited on silicon.

The results here presented show the lateral reorganization of the lipid bilayer from the nano to the microscale, and the alterations in the height of the domains at a sub-nanometer scale. The changes observed are highly dependent on the previous organization and nature of the lipid domains or rafts. The contributions of water/bilayer interfacial tension reduction, freezing point depression, disordering/tilting of acyl chains and interdigitation in relation to the domain (re) organization of the bilayer are discussed.

2. Materials and methods

2.1. Chemicals

1,2-Dipalmitoyl-*sn*-glycero-3-phosphocholine (DPPC), 1,2-dioleoyl-*sn*-Glycero-3-phosphocholine (DOPC) and *N*-palmitoyl-D-*erythro*-sphingosylphosphorylcholine or *N*-palmitoyl-sphingomyelin (PSM) were purchased from Avanti Polar Lipids (Alabaster, AL); cholesterol was purchased from Sigma (St. Louis, MO). Other reagents were of the highest purity available.

Three buffers were used for hydration of lipid mixtures and AFM imaging: buffer A—10 mM Hepes, 150 mM NaCl, pH 7.4; buffer B—10 mM Hepes, 150 mM NaCl, 3 mM $CaCl_2$, pH 7.4; buffer C—2.71 mM K_2HPO_4, 1.54 mM NaH_2PO_4, 154 mM NaCl, pH 7.4.

2.2. Phospholipid and cholesterol quantification

The phospholipid concentration was determined gravimetrically and by inorganic phosphate quantification [52]. Cholesterol quantification was made by gravimetry.

2.3. Preparation of supported lipid bilayers on mica and silicon

Lipid stock solutions and lipid mixtures were prepared with spectroscopic grade chloroform from Merck (Darmstadt, Germany). The solvent was evaporated first under a mild flow of nitrogen, followed by overnight vacuum. The lipids were hydrated with buffer A, for mica, or C for silicon, which were shown to be the most appropriate buffers to form SLBs on those substrates ([53] and [45], respectively). To confirm this literature result, other buffers were essayed, including using buffer A for silicon and buffer C for mica, and the quality of the SLBs obtained was inferior (data not shown). The lipid was suspended by vortex stirring and freeze-thaw cycles (total lipid concentration 10 mg/mL). Small unilamellar vesicles (SUV) were made by power sonication (Hielscher, UP200S). For deposition on mica, 10 μL of SUV suspension was diluted in 140 μL buffer B [54] and deposited on freshly cleaved mica (Veeco) and incubated for 30 min at 70 °C. After this incubation step the samples were left at room temperature to cool for 1 h and SLB were washed several times with buffer A at room temperature (20 °C).

Silicon oxide wafers (provided by Institute of Mechanics, Beijing, PRC) were washed in a freshly prepared piraña solution (sulfuric acid and hydrogen peroxide 3:1) for ca. 5 min and maintained in water until use. Before lipid deposition the silicon wafers were dried under a nitrogen flow. Large unilamellar vesicles (LUV) were prepared by extrusion in an Avanti Mini-extruder at 60 °C using polycarbonate filters with 100 nm pore diameter (Whatman). LUV suspension (100 μL) was added to the silicon oxide wafer and incubated for 30 min at 60 °C. Again, after this incubation step the samples were left at room temperature to cool for 1 h and SLB was washed by immersion in buffer C at 20 °C.

2.4. AFM imaging

The procedure was identical for both mica and silicon substrates. AFM *in situ* measurements, i.e., with the sample immersed in buffer recurring to a liquid cell, were performed at room temperature using a Multimode Nanoscope IIIa Microscope (Digital Instruments, Veeco). Topographic images were taken with a scan rate of ca. 2 Hz in tapping mode, where the use of an oscillating probe drastically reduces the force applied to the sample during the scanning [42], as compared to the measurements performed in contact mode [55], since the cantilever only touches the surface after one oscillation cycle. A sequence of different scanned areas containing the same bilayer region was included in Supplementary Fig. S1, in order to demonstrate that tip scanning had no effect on the height, shape and domain organization of the lipid bilayer.

Before each experiment, the glass block holding the cantilever was washed several times with water and ethanol. The cantilevers used were made of silicon nitride (NPS, ca. 0.58 N/m of spring constant, Veeco) with a resonance frequency in liquid of about 9 kHz. The samples were initially covered with 45 μL of buffer A for mica SLBs or buffer C for silicon SLBs.

When a stable image in a region of interest of the SLB in a buffered solution was obtained, successive additions of ethanol were performed and the same region was imaged between each addition. In many cases, regions where the coverage by lipid was incomplete, and where the lipid bilayer has a distinctive shape were chosen on purpose, in order to easily identify the changes in lateral organization of the membrane upon successive additions of ethanol. To fully appreciate bilayer expansion, it was necessary to have images where the area coverage was around 50% before ethanol addition. The images presented in this study are representative of each sample (the observations are uniform for the whole sample); at least 3 independent experiments on freshly prepared SLB have been performed for each lipid system. To obtain the thickness values (or thickness differences) for each sample, at least 10 different profiles were drawn, and the median value taken. The values of thickness in Table 1 are the average ± standard deviation of the values from all the experiments, and the most representative profiles were selected for the figures shown. The estimation of the area corresponding to the different types of domains was performed using the software ImageJ. All the domains of a specific thickness were added to obtain the total phase area.

3. Results

3.1. Interaction of ethanol with lipid bilayers displaying gel/fluid phase coexistence

At room temperature, the binary lipid system DOPC/DPPC displays a range of compositions for which a gel phase rich in DPPC coexists with a fluid phase rich in DOPC [56,57]. Accordingly, DOPC/DPPC (1:1 mol:mol) bilayers deposited on mica were used to address the influence of gel/fluid domains on ethanol-induced membrane changes. In Fig. 1, panel a, the phase coexistence is clearly observed by AFM, since the lipid bilayer is heterogeneous, presenting domains with distinct thickness. The height of thicker (6.4 nm) and thinner (5.2 nm) domains in coexistence is very similar to the respective thickness of the phases formed by the two pure lipids DPPC (6.4 nm) and DOPC (5.3 nm) as shown in the topographical profiles of Supplementary Fig. S2a and b, respectively. Since the T_m of DPPC is 41 °C, the lipid bilayer is in the gel phase [58]. The T_m of DOPC is −22 °C [59]; thus at room temperature, the lipid bilayer formed is clearly in the fluid phase [56]. This allows unambiguous assignment of the thicker and thinner domains observed in the binary mixture to the gel and to the fluid, respectively. The thickness gap between coexisting domains in DOPC/DPPC is thus 1.2 nm, as also found by other authors [34,60]. The thickness of the bilayers with or without phase coexistence, and height differences, are summarized in Table 1. The area fraction of gel/fluid phases was also calculated (Table 2), and is in agreement with the molar fractions predicted by the DOPC/DPPC (24% gel, 76% fluid) phase diagram according to the lever rule, after correction for the different mean molecular area of each phase [56].

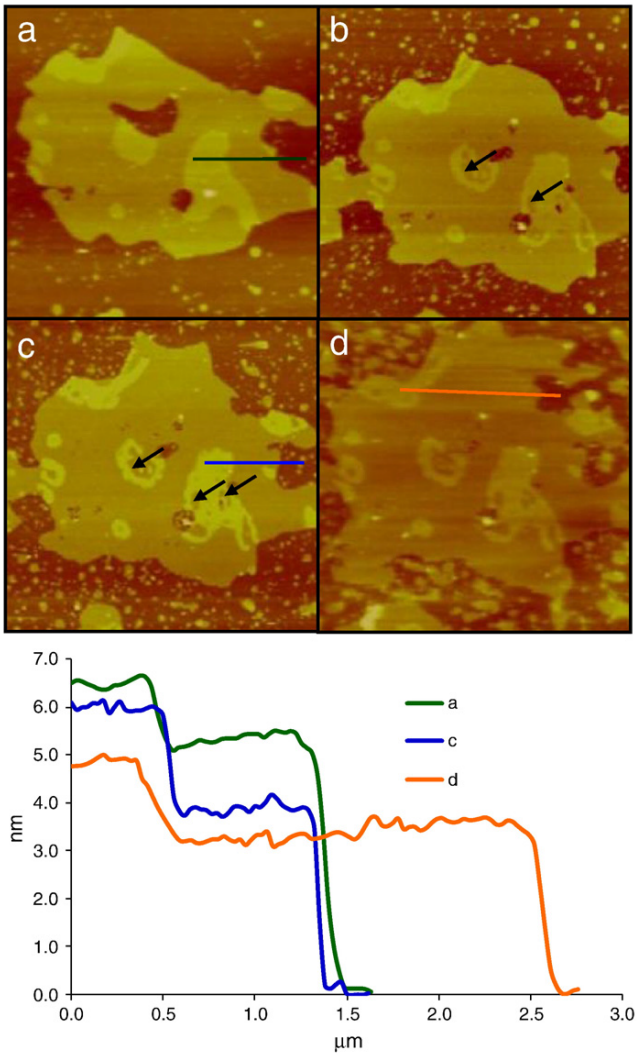

Fig. 1. Ethanol interactions with a bilayer with gel/fluid phase coexistence. AFM image of an SLB composed of DOPC/DPPC (1:1) deposited on mica, (a) in the absence of ethanol, and after successive additions of ethanol to a final concentration of (b) 11%, (c) 22%, and (d) 34% (v/v) in Hepes buffer. The images were obtained in a liquid cell at room temperature. The inset shows the topographical profiles corresponding to the colored lines in panels a–d. The images correspond to an area of 5 μm × 5 μm. $Z = 24$ nm. The black arrows indicate fluid domains that form inside gel domains.

Table 1
Bilayer thickness values for different lipid systems deposited on mica and silicon before and after final ethanol (EtOH) addition. When different types of domains coexist, their height differences are also indicated. The data presented correspond to the average ± standard deviation, obtained as described under Materials and Methods. Chol stands for cholesterol.

	Lipid system	Bilayer thickness	Domain height difference	Height reduction after EtOH addition
Mica	DPPC/Chol (98:2)	6.4 ± 0.3		1.9 ± 0.2
	DOPC/DPPC (1:1)[a]	6.4 ± 0.3 (g)	1.2 ± 0.2	0.4 + 1.1 = 1.5 ± 0.2 (g)[b]
		5.2 ± 0.2 (f)		1.3 + 0.3 = 1.6 ± 0.2 (f)[b]
	DOPC/DPPC/Chol (40:40:20)[c]	6.5 ± 0.3 (lo)	1.2 ± 0.2	1.1 ± 0.2
		5.3 ± 0.2 (ld)		
	DOPC/PSM/Chol (40:40:20)[c]	6.0 ± 0.3 (lo)	1.0 ± 0.2	1.0 ± 0.2
		5.0 ± 0.2 (ld)		1.2 ± 0.2
Silicon	DPPC	6.2 ± 0.3		1.8 ± 0.2
	DOPC/PSM/Chol (40:40:20)[c]	6.6 ± 0.3 (lo)	1.1 ± 0.2	1.3 ± 0.2
		5.5 ± 0.2 (ld)		

[a] Gel (g)/fluid (f) phases.
[b] First thickness reduction + second thickness reduction.
[c] Liquid ordered (lo)/liquid disordered phases (ld) (lipid rafts).

Sequential additions of ethanol to the mixed DOPC/DPPC SLB on mica were performed in the liquid cell. When 11% (v/v) ethanol is reached the only detectable change is the appearance of fluid patches within the former gel domains, whereas in the presence of 22% (v/v) of ethanol (Fig. 1b and c), the thickness of both fluid and gel domains decreased, as illustrated in the topographical profile of panel c (the corresponding profile for panel b (not shown) is identical to the one for panel a). However, the height of the gel decreased only by ~0.4 nm, whereas that of the fluid decreased by 1.3 nm. Under such conditions, the height difference between gel and fluid phases is maximal, with a value of ~2.1 nm. The lower height effect on the gel has been observed for all the scanned regions and is in agreement

Table 2
Estimation of bilayer area and volume for lipid phases of SLBs deposited on mica, unless otherwise stated. Initial area (A_i) and volume (V) refers to the values before ethanol addition. Final area values were experimentally obtained ($A_{f\ Exp}$) or calculated considering volume conservation ($A_{f\ Calc}$). f, fluid; g, gel; ld, liquid disordered; lo, liquid ordered. All the calculations were performed based on 400 μm^2 AFM images except for DOPC/DPPC and DOPC/PSM/cholesterol deposited on silicon for which the calculations were based on 64 μm^2 and 9 μm^2 images, respectively. Chol stands for cholesterol.

Lipid system			A_i (nm^2)×10^7	Area fraction	V (nm^3)×10^7	A_f (nm^2)×10^7		$A_{f\ Exp}/A_i$
						Calc.	Exp.	
DOPC/DPPC		f	1.3	0.80	6.8	1.8	2.0 (34% EtOH)	1.5
		g	0.3	0.20	2.1	0.4	0.3 (34% EtOH)	0.9
DOPC/DPPC/Chol		ld	10.0	0.68	54.0	11.2	15.2 (13% EtOH)	1.5
							34.9 (25% EtOH)	3.5
		lo	4.5	0.32	30.0	5.5	5.2 (13% EtOH)	1.2
							4.6 (25% EtOH	1.0
DOPC/PSM/Chol		ld	13.7	0.57	73.7	15.5	22.4 (13% EtOH)	1.7
		lo	10.7	0.43	69.5	11.8	11.5 (13% EtOH)	1.1
	Silicon	ld	0.5	0.92	2.7	0.6	0.6 (13% EtOH)	1.3
		lo	0.04	0.08	0.3	0.05	0.03 (13% EtOH)	0.9

with a previous observation by Vierl et al. [21]. In that study, X-ray diffraction was used to investigate ethanol-induced interdigitation in DPPC liposome suspension. The authors observed a 0.2 nm reduction of the lamellar repeat distance, which was attributed to an alteration of the tilt angle of the acyl chains in relation to the bilayer normal.

In addition, the fraction of fluid domains in relation to gel ones increased, because fluid domains appear within regions that in the absence of ethanol (panel a) were occupied by gel phase (arrows in panels b and c; Table 2; see also Supplementary Fig. S3). Finally, with 34% (v/v) of ethanol, the gel becomes much thinner, and the fluid phase also presents a more extensive thickness reduction, originating a gel/fluid height gap of ~1.3 nm which is similar to the one in the absence of ethanol. A marked expansion of the fluid phase can be also observed (see Table 2 for quantification), while gel domains maintain their identity.

The fact that the fluid undergoes a more significant thickness reduction before the gel is in agreement with the need for a lower ethanol concentration to induce the formation of thinned domains in pure DOPC than in pure DPPC, as reported in the literature. In a previous study, it was shown that domains of reduced thickness appeared in DOPC bilayers for concentrations of alcohol that had no effect on DPPC [12].

An interesting observation is that the site of formation of thinned domains depends on lipids proportion and domain arrangement. In Fig. 1 described above, the bilayer is composed of gel domains in a continuous fluid, and the thinned fluid domains form within the gel domains. In Fig. 2, an image of the DOPC/DPPC mixture is shown, in this case with a molar ratio of 8:92. In opposition to the mixture shown in Fig. 1, the majority of the bilayer is now in the gel phase, which is the continuous phase, surrounding fluid phase domains. The thickness reduction of fluid domains is observed first in the interface between gel and fluid regions of the bilayer. The formation of those domains gives rise to "islands" of unmodified fluid, and generates topographical profiles as the one shown in Fig. 2.

The observations described above seem to be in contradiction with the hydrophobic matching principle, since an increased height difference at the domain interface implies a higher exposure of the hydrophobic portion of the gel phase lipids to the water phase [61]. However, such behavior could be explained by an accumulation of ethanol molecules in interfacial regions, thereby protecting the acyl chains of gel phase lipids from exposure to water.

3.2. Ethanol-induced membrane effects in a binary single-phase bilayer

It was previously shown, through a fluorescence spectroscopy method used in liposome suspensions, that cholesterol at low concentrations can have a facilitating effect regarding ethanol interaction in the system DPPC/cholesterol (98:2 mol:mol) [22]. In the present study, SLBs with the same composition were prepared on mica, and the effect of ethanol followed by AFM. A result concurrent with the literature was obtained, as described in Fig. 3. It is shown that i) in the absence of ethanol the thickness of the bilayer is similar to that of pure DPPC (see Supplementary Fig. S2); ii) 11% (v/v) of ethanol induces the thickness reduction by approximately 2 nm of a substantial fraction of the bilayer and its expansion. The effect was much more pronounced than the ones observed for DOPC-enriched fluid and even more so for DPPC-enriched gel in the DOPC/DPPC mixtures described above. Thus, the facilitating effect previously reported [22] is also observed for SLBs of the same composition. This promotion probably stems from the perturbation that a small amount of cholesterol induces in the gel phase, which becomes less compact or more defective allowing for a better penetration of small molecules such as ethanol. Interestingly, ergosterol apparently does not have this enhancing effect at low concentrations [38].

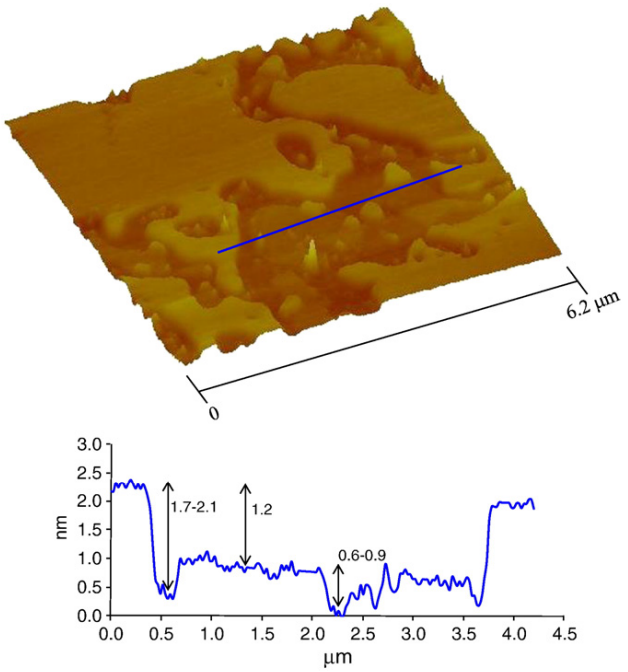

Fig. 2. The topology of gel/fluid domains modulates ethanol interactions with the lipid bilayer. AFM image of an SLB composed of DOPC/DPPC (8:92 mol:mol) deposited on mica, after successive additions of ethanol to a final concentration of 18% (v/v) in Hepes buffer. The image was obtained in a liquid cell at room temperature. The inset shows the topographical profile corresponding to the colored line in the main panel. $Z = 10$ nm. The numbers indicated next to the arrows correspond to a height difference.

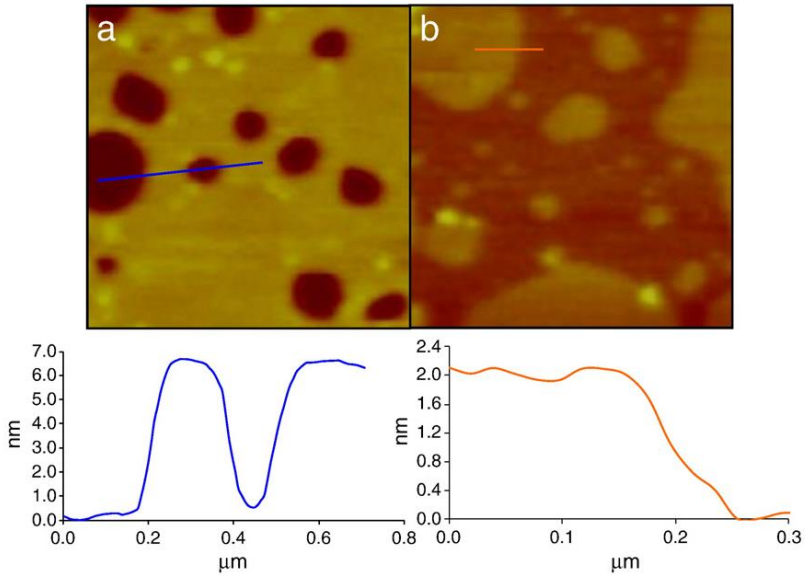

Fig. 3. Effect of cholesterol in small amounts on the alterations induced by ethanol in a gel phase bilayer. Top row: AFM images of DPPC/cholesterol 98:2 SLB on mica with 1.4 μm × 1.4 μm obtained in Hepes buffer at room temperature: (a) in the absence of ethanol, and (b) after addition of ethanol 11% (v/v). $Z = 15$ nm (a); $Z = 20$ nm (b). Bottom row: topographical profiles corresponding to the colored lines in the top row images. From the blue line it is possible to determine the original bilayer thickness; from the orange line it is possible to determine the height difference between interdigitated and non-interdigitated domains. The bright round features correspond to incompletely fused vesicles, and not to lipid domains.

3.3. Interaction of ethanol with raft-forming ternary lipid mixtures

Ternary lipid mixtures displaying lo/ld phase separation are good models of the lipid domains known as lipid rafts that occur in many cellular membranes as described in the Introduction section. In the present study, two ternary mixtures were used: DOPC/DPPC/cholesterol and DOPC/PSM/cholesterol both with molar ratios of 40:40:20. According to the ternary phase diagrams reported for these mixtures [56,62], for that molar ratio, the systems lay in the lo/ld coexistence region, with ca. 40% mol fraction of lo phase. The lo phase corresponds to the high T_m lipid/cholesterol-enriched domains (lipid rafts) and the ld phase to the rest of the membrane, rich in the low T_m lipid (in both cases, DOPC).

Fig. 4 shows AFM images recorded in the liquid cell of a DOPC/DPPC/cholesterol SLB deposited on mica, in the absence of ethanol, and after successive additions of ethanol. In the pristine bilayer (panel

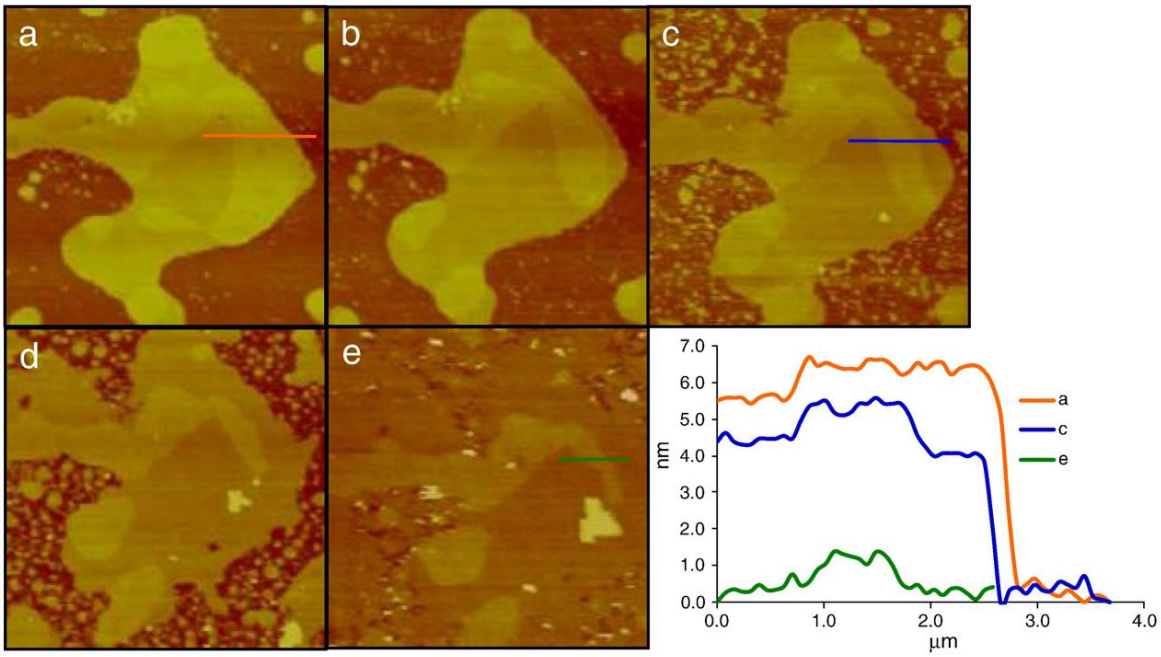

Fig. 4. Ethanol interactions with a bilayer displaying ld/lo phase separation (lipid rafts) on mica. AFM image of an SLB composed of DOPC/DPPC/cholesterol (40:40:20 mol:mol:mol) deposited on mica, a) in the absence of ethanol, and after successive additions of ethanol to a final concentration of b) 8%; c) 13%; d) 20%; and f) 25% (v/v) in Hepes buffer. The images were obtained in a liquid cell at room temperature. The inset shows the topographical profiles corresponding to the colored lines in panels a–e. The images correspond to an area of 11 μm × 11 μm. $Z = 15$ nm.

a), the coexistence of ld and lo domains with a height difference of 1.2 nm is clearly observed (Table 1). For this lipid system the area fraction of lo domains (Table 2) is similar to the one predicted by the phase diagram [56]. Upon addition of ethanol to a concentration of 8% (v/v) (Fig. 4b), the topography of the system remained essentially unchanged. However, when the concentration of ethanol reached 13% (v/v) (Fig. 4c), both ld and lo domains became thinner by ~1.1 nm, as demonstrated by the topographical profiles of Fig. 4 and Table 1. The whole bilayer has undergone thickness reduction simultaneously, to a similar height value as the fluid phase in DOPC/DPPC mixtures for high ethanol concentration (22%). This behavior is completely distinct from the one observed for the gel/fluid coexistence (Figs. 1 and 2), and shows how the membrane composition and lateral organization strongly influence ethanol-induced alterations. With successive additions of ethanol other effects become apparent: with 20% (v/v) ethanol (Fig. 4d), the area fraction occupied by thinner (more disordered) domains becomes larger; for higher concentrations of ethanol (Fig. 4e), pronounced bilayer expansion is observed.

Fig. 5 shows the results of a similar study where the high T_m lipid is PSM instead of DPPC. Through the comparison of the results obtained for this system with those described in the previous paragraph, it will be possible to understand if the type of ordered domains present in the membrane is the ruling factor determining ethanol-induced effects, or if these are highly dependent on the particular high T_m lipid. Again, the clear coexistence of ld and lo domains is observed in Fig. 5a, and the ld/lo area fractions (Table 2) are in good accordance with the phase diagram [62]. The height difference between the domains is 1.0 nm (see also inset with topographical profile in Fig. 5 and Table 1), in agreement with a previous study of an analogous system [63]. Upon addition of ethanol to a final concentration of 4% (v/v) (Fig. 5b), no significant changes were detected. However, at 13% (v/v) of ethanol (Fig. 5c) the whole bilayer undergoes a reduction of its thickness around 1.2 nm for ld domains and 1.0 nm for lo domains. Thus, the system DOPC/PSM/cholesterol behaves in a similar manner as the DOPC/DPPC/cholesterol. Further additions of ethanol cause an increase of the area fraction occupied by ld domains since only this portion of the bilayer expands significantly as a result of the interaction with ethanol (Fig. 5d, Table 2).

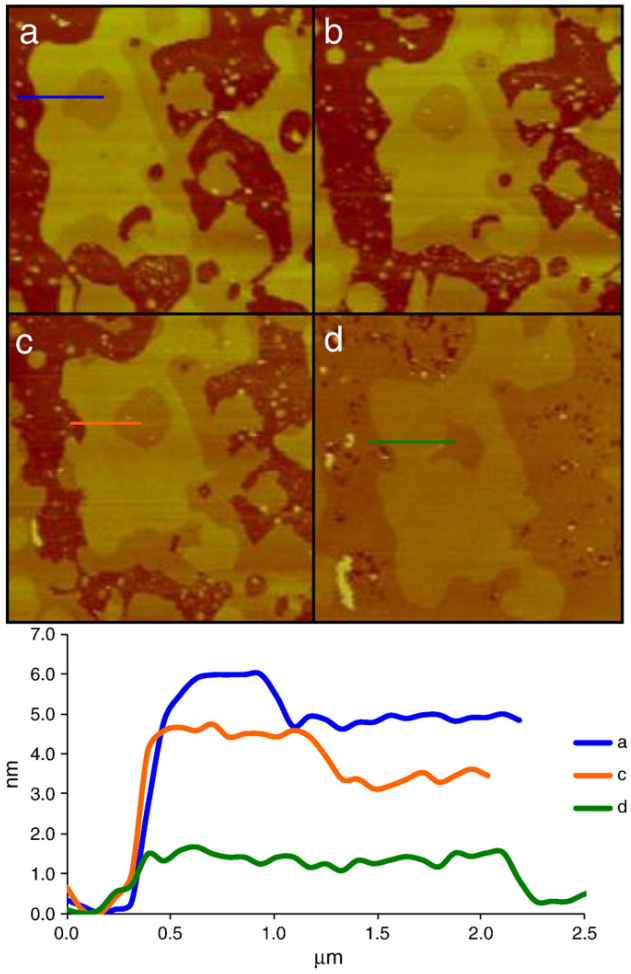

Fig. 5. Ethanol interactions with a bilayer containing sphingomyelin and with ld/lo phase separation (lipid rafts) on mica. AFM image of an SLB composed of DOPC/PSM/cholesterol (40:40:20 mol:mol:mol) deposited on mica, (a) in the absence of ethanol, and after successive additions of ethanol to a final concentration of (b) 4%, (c) 13%, and (d) 25% (v/v) in Hepes buffer. The images were obtained in a liquid cell at room temperature. The inset shows the topographical profiles corresponding to the colored lines in panels a–d. The images correspond to an area of 11 μm×11 μm. $Z=15$ nm.

3.4. Lipid bilayers deposited on silicon

The influence of ethanol on DPPC bilayers was studied using silicon as substrate (Fig. 6). As mentioned in the Introduction, ethanol–DPPC interactions were thoroughly addressed in the literature using mica as a substrate, but not silicon. In the absence of ethanol the DPPC bilayer thickness on silicon (~6.2 nm; panel a) is close to the one observed for mica surfaces (Supplementary Fig. S2a) and for low ethanol concentrations, no significant alterations were observed. At 20% (v/v) ethanol concentration (Fig. 6b) some portions of the bilayer become thinner and the difference between thin domains and unmodified bilayer is similar to the one obtained on mica (Table 1). Furthermore, for high ethanol concentrations (30%, v/v) bilayer expansion with almost complete coverage of the observation area also happened (Fig. 6c). The final height reduction observed in pure DPPC is close to 2 nm, as reported by several authors for DPPC bilayers on mica [12,64]. This height reduction is similar to the one observed for DPPC-enriched gel domains in DOPC/DPPC bilayers. However, in the binary gel domains, a significant expansion of the gel as detected in pure DPPC bilayers was not observed, pointing to a role for gel/fluid coexistence in the outcome of ethanol effects.

The effect of ethanol in PSM-containing lipid rafts was also performed for bilayers deposited on silicon (Fig. 7). With this substrate, ld/lo phase separation was also observed for the DOPC/PSM/cholesterol (40:40:20) mixture (Fig. 7a). However, the area fraction of ordered phase is smaller than for SLB of the same composition deposited in mica (Table 2). Recently, a similar behavior was observed with DOPC/1,2-distearoyl-sn-glycero-3-phosphocholine (DSPC)/cholesterol bilayers supported in silica xerogel where the fraction of the ordered domains was lower than the one expected from the phase diagram and observed on mica. The authors attributed this difference to curvature-induced mechanisms [65]. The average size and shape of the domains is also influenced by the substrate, since it can be clearly seen that they are different when a bilayer of the same composition is formed on mica (Fig. 5). In Fig. 7 it is shown that upon successive ethanol additions to DOPC/PSM/cholesterol SLB on silicon, the following effects were observed: simultaneous thickness reduction for both ld and lo domains (panels b and c) of 1.3 nm, and bilayer expansion of ld domains with respective increased fractional area of these domains (panels c and d), i.e., qualitatively the same behavior as noticed in mica (Fig. 5). The extent of expansion (Table 2) was comparable to the one observed in mica for intermediate ethanol concentrations (13%). It was not possible to obtain good quality images of SLB in silicon for higher ethanol concentrations.

4. Discussion

In this work, the interaction of ethanol with lipid bilayers presenting different lipid number and/or types of lipid phases was

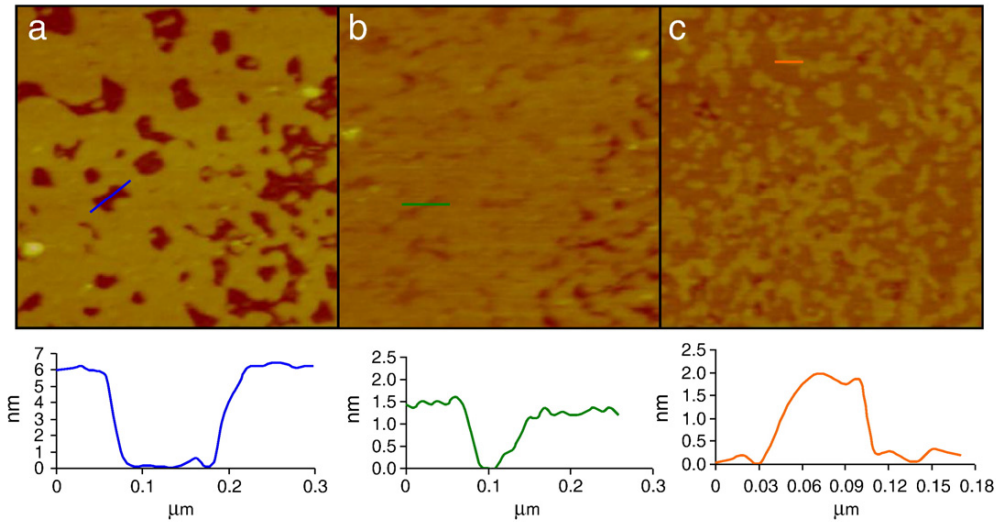

Fig. 6. Ethanol interactions with a bilayer in the gel phase deposited on silicon. AFM image of an SLB composed of DPPC deposited on silicon, after successive additions of ethanol to a final concentration of (a) 0%, (b) 20%, and (c) 30% (v/v) in PBS buffer. The images were obtained in a liquid cell at room temperature. The insets show the topographical profiles corresponding to the colored lines in panels a–c. The images correspond to an area of 1.5 µm × 1.5 µm. $Z = 20$ nm.

studied by AFM. The main goal of this work was to determine to what extent the presence and type of lipid domains, namely gel/fluid domains, and ld/lo domains (lipid rafts) modulate the ethanol-induced membrane changes. In addition, it was also intended to determine the consequences of progressively increase ethanol concentration in the hydration medium of the lipids.

In general, the observations here reported can be correlated with previously published studies [20–22] of ethanol–bilayer interactions, using single-phase lipid bilayers, either free-standing or on solid supports, mica and silicon. This was confirmed by studying the role of small amounts of cholesterol in the promotion of interdigitation of gel phase bilayers shown in the present work on mica SLBs (Fig. 3), and previously reported for silicon SLBs studied by ellipsometry [51]. Moreover, the phase mole fractions obtained in mica in phase separating mixtures are coincident with the published phase diagrams for free-standing bilayers [56,62].

On silicon, bilayer thickness reduction was observed for gel phase SLB (DPPC, Fig. 6), and for ternary fluid bilayers of DOPC/PSM/cholesterol (Fig. 7), being this latter a better model for the lipid composition of the outer leaflet of mammalian plasma membrane. Similar effects were observed for this ternary mixture deposited on mica. Although the solid support has an influence on bilayer organization, possibly due to surface effects such as frictional coupling [66], the substrate used is not determining the outcome of ethanol–bilayer interactions, except for high ethanol concentrations, because in this case the ternary lipid bilayer becomes unstable when supported on silicon. However, the substrate may influence the amounts of ethanol necessary for observing the same effect as in free-standing bilayers [38], as discussed below, and also the ld/lo phase fractions and domain morphology, since on silicon they are different from those on mica [65] and giant vesicles [62].

DPPC is one of the few cases where ethanol-induced interdigitation has been unequivocally observed from the analysis of the electron density profiles obtained by X-ray diffraction [21]. The height and area alterations reported there are in agreement with the results obtained in the present AFM study for both ethanol–DPPC on silicon, and for the gel phase DPPC/cholesterol (98:2) on mica (Tables 1 and 2). The height difference between tilted liquid expanded and upright liquid condensed DPPC monolayers or bilayers is ~0.6 nm [32], indicating that the ~2 nm height reduction induced by ethanol on gel phase SLBs (Table 1) is not explained solely by tilting.

In the present study, even for high ethanol concentrations, the gel phase SLB is not fully interdigitated, which is not in agreement with the established phase diagrams [21,33,38]. However, it should be pointed out that in the present study ethanol was added sequentially to pre-formed SLBs, requiring the use of higher ethanol concentrations in order to observe similar effects. This has been previously described, and recently it was shown that incubating the vesicles with ethanol above the phospholipid T_m is necessary for quantitative agreement between SLBs and free-standing bilayers [38,51]. Note that in most studies with free-standing bilayers, the lipid is hydrated with ethanol/water mixtures and subjected to heating/cooling cycles. To this respect, the results of the present work are in agreement with the typical SLB behavior.

The study of the mixture DOPC/DPPC revealed the presence of gel domains coexisting with fluid domains, separated by a height difference of ~1.2 nm (Table 1), as previously described [34,60]. When interacting with this mixture ethanol induces a first bilayer thickness reduction, that is larger for the fluid domains, and only at higher concentrations the second thickness reduction is larger for the gel domains (Fig. 1). The membrane partitioning of ethanol is less propitious into saturated/ordered bilayers than into unsaturated/disordered ones [67]. Moreover, the increase of fluid phase fraction relatively to gel fraction was observed as a consequence of the fluid phase expansion in response to ethanol interaction while gel domains maintain their total area (Table 2). The area calculated considering volume conservation is very similar to the one experimentally observed. If the reduction in gel phase fraction is also taken into consideration in the estimated areas, then volume conservation is verified. In this case it is possible to quantitatively compare the results with those obtained by micropipette aspiration in SOPC fluid bilayers in the presence of ethanol [68,69]. The authors observed a thickness reduction and area increase up to 10–15% due to water/bilayer interfacial tension reduction, which leads to an expansion of the lipid bilayer because the lipid headgroups are less tightly packed [68], possibly becoming more disordered and/or more tilted. However, the first height reduction observed for the fluid in the present work was much higher (~1.3 nm), hence an additional mechanism should be accountable. DOPC has a very low T_m and therefore at room temperature the degree of disorder is already quite large. In addition, for very disordered acyl chains it is difficult to infer on tilting, due to their high mobility and lack of organization. It is possible that,

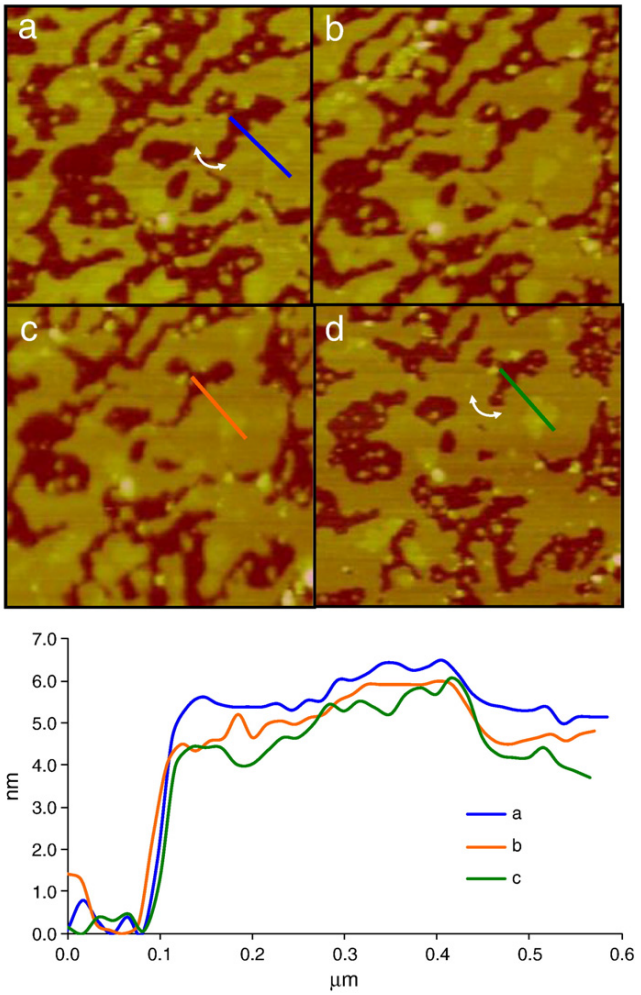

Fig. 7. Ethanol interactions with a bilayer containing sphingomyelin displaying ld/lo phase separation (lipid rafts) on silicon. AFM image of an SLB composed of DOPC/PSM/cholesterol (40:40:20 mol:mol:mol) deposited on silicon, before (a) and after successive additions of ethanol to a final concentration of (b) 4%, (c) 8%, and (d) 13% (v/v) in Hepes buffer. The images were obtained in a liquid cell at room temperature. The inset shows the topographical profiles corresponding to the colored lines in panels a–d. The images correspond to an area of 2.0 μm×2.0 μm. $Z=15$ nm. The curved white arrows highlight bilayer expansion as seen by increased substrate coverage.

together with disordering or tilting, a partial interpenetration of the acyl chains from one leaflet to the other is occurring, which is different from the interdigitation reported for gel phase in pure DPPC. The formation of partially interdigitated phases does not affect significantly the lateral mobility of the phospholipids [70], which is compatible with a fluid phase, particularly with highly disordered unsaturated chains [71]. A similar mechanism has been proposed for pure DOPC bilayer expansion and thinning induced by an increase of the temperature from 40 to 50 °C as determined by AFM in liquid [72]. Recent molecular dynamics simulations predicted the formation of interdigitated structures in fluid bilayers in the presence of moderately high ethanol concentrations [73]. Regarding the gel domains, due to its significant fraction decrease, it is not possible to offer a unique molecular description of the process. However, it should be noted that the thickness reduction (1.8 nm) is similar to the one observed for pure DPPC reported in the literature [12,64] and in the present work for DPPC on silicon (1.8 nm) and DPPC/cholesterol 98:2 in mica (1.9 nm) (Figs. 6 and 3, respectively). In the gel phase the phospholipid acyl chains are arranged in a hexagonal packing as a consequence of *trans*-configuration of the phospholipid acyl chains which results in the almost complete absence of free volume inside of the bilayer [74,75]. The effects of ethanol on DPPC-enriched gel may thus be explained by interdigitation, concomitantly with a large decrease of gel phase fraction, thereby maintaining the gel phase area. However, this interdigitation occurs only for very high ethanol concentrations due to the preferential interaction of ethanol with the fluid, and thus it should have limited biological significance. The tilting that is probably responsible for the first 0.4 nm thinning of the gel domains is much more plausible to occur in very ordered domains in biological systems.

Finally, one more worth noting observation in the DOPC/DPPC mixture is that the region where the first thickness reduction domains start to form depends on the domain organization. Thinner fluid domains appear inside gel domains when these are discontinuous and the fluid phase is prominent (Fig. 2), whereas they appear at the gel-fluid interface surrounding fluid domains when these are discontinuous and minor (Fig. 1). There is both theoretical [61] and experimental [18,76,77] evidence that the dynamic wetting layer effects at gel/fluid interfaces become less influential when the gel phase fraction is increased, particularly when it becomes the continuous phase, and that the interfacial lipid is maximal near phase coexistence boundaries. Accordingly, ethanol would act more easily inside the gel domains at the corrugation defects in the 1:1 mixture, whereas the less rigid and more prevalent gel/fluid interfaces would be the preferential targets for ethanol in the gel-enriched mixture. The observed increase of fluid domains fraction (Table 2) is related to the fact that ethanol interacts preferentially with this phase, enhancing its stability relatively to the gel phase. While this can be partially explained by a freezing point depression (see e.g. [30]), the more complex effects relating the sites of first thickness reduction to which domains are discontinuous cannot be fully accounted by this single thermodynamic consideration.

The use of lipid raft-forming ternary mixtures provided additional evidence for the importance of membrane domain organization on the interaction with ethanol. In the case of ld/lo phase separation, in two different systems (DOPC/DPPC/cholesterol and DOPC/PSM/cholesterol), thickness reduction occurred for a relatively low ethanol concentration and to a similar extent for both ordered and disordered domains (Figs. 4 and 5), a behavior distinct from the one observed for the gel/fluid DOPC/DPPC mixture. This is a reflex of the fluid nature of both phases present in the ternary mixtures. To better understand ethanol effects on those mixtures, area and volume calculations were also performed (Table 2). Similarly to what was detected for DOPC/DPPC, it is clear that the disordered phase has undergone expansion, while ordered domains, in this case lo phase, did not experience significant area variations (Table 2). Thus, a clear increase of the disordered fraction occurred. Since there was no detectable change in the area of the ordered domains, despite the height reduction of this fraction, plausibly due to disordering/tilting of the acyl chains and partial interdigitation, as described for DOPC-enriched fluid phase in DOPC/DPPC bilayers, it is implied that part of the lipids of lo domains were transferred to the ld phase. With 13% ethanol, the changes in the disordered phase are comparable to those described above in the case of gel/fluid coexistence. However, for higher ethanol concentration, a much larger expansion took place, which cannot be solely explained by means of disordering, tilting or partial interpenetration. The degree of expansion observed could be justified by the opening of the acyl chains of each phospholipid, similarly to the reported extended lipid conformation [78,79] or through their looping, as described for other lipids [80]. In the case of DOPC/PSM/cholesterol, the interaction between ethanol and the lipid bilayer follows the trends discussed above, except that the estimated final expansion (Table 2) was smaller. However, a total coverage of the substrate was reached for both ternary mixtures, in contrast to the observed for the binary gel/fluid system. The second height reduction of the fluid phase in DOPC/

DPPC is only of 0.3 nm. However, this takes place when significant fluid phase expansion occurs in that system. Thus, an opening of the acyl chains may be occurring, but more limited than in the ternary lipid mixtures, possibly due to the presence of cholesterol.

Ethanol affects bilayer thickness and also the domain organization of the membrane, thus its biological effects can be exerted by affecting the functions associated with membrane proteins whose location and activity are dependent on bilayer thickness and also on domain structure [81–83].

Finally, bilayer expansion was always observed for high ethanol concentrations, suggesting that this can be a useful strategy for an improved lipid coating of solid substrates that can be used either to better study membrane related phenomena, or to design technological devices based on lipid–water interfaces [84,85]. To this respect the observation of bilayer expansion leading to increased surface coverage in silicon is particularly relevant.

5. Conclusions

The present work demonstrates the ability of AFM to unravel details from the nano to the micro scale of the interaction between ethanol and complex lipid systems. The study of binary and ternary lipid systems has shown that this alcohol interacts preferentially with the most disordered phase, promoting an increase of its fraction. The thickness reduction of the fluid phase with increasing ethanol concentrations in the absence of cholesterol can be explained by an interfacial tension reduction for low ethanol concentrations, accompanied by additional disordering/tilting and/or partial interdigitation (~1.3 nm) and then by a slight aperture of the acyl chains (0.3 nm and more pronounced expansion). In the lipid rafts-mimicking ternary mixtures, these effects play a role also for lower ethanol concentrations (~1 nm thickness reduction) and for higher alcohol levels a dramatic bilayer expansion, possibly involving acyl chain extended conformations or looping, occurs. It was also shown that ethanol effects were similar on both ternary lipid systems studied (lo/ld coexistence), whereas gel/fluid and lo/ld bilayers present a different behavior in response to ethanol. As a consequence ethanol action should be more dependent on the type of domains present than on the type of lipid.

Finally, qualitatively similar ethanol effects were observed for bilayers deposited on mica and silicon, demonstrating that the major effects are not dependent on the substrate used for the formation of SLB. However, the domain organization is clearly different and ethanol effects are not completely comparable at a quantitative level.

Supplementary materials related to this article can be found online at doi:10.1016/j.bbamem.2010.10.006.

Acknowledgements

A.S.V. and R.F.M.D. acknowledge funding from F.C.T., Portugal, received through the Centre of Chemistry and Biochemistry and research grant PTDC/QUI/66612/2006. J.T.M. acknowledges PhD scholarship SFRH/BD/64442/2009.

References

[1] R.F.M. de Almeida, L.M.S. Loura, M. Prieto, Membrane lipid domains and rafts: current applications of fluorescence lifetime spectroscopy and imaging, Chem. Phys. Lipids 157 (2009) 61–77.
[2] A. Kusumi, C. Nakada, K. Ritchie, K. Murase, K. Suzuki, H. Murakoshi, R.S. Kasai, J. Kondo, T. Fujiwara, Paradigm shift of the plasma membrane concept from the two-dimensional continuum fluid to the partitioned fluid: high-speed single-molecule tracking of membrane molecules, Annu. Rev. Biophys. Biomol. Struct. 34 (2005) 351-U54.
[3] R.G.W. Anderson, K. Jacobson, Cell biology—a role for lipid shells in targeting proteins to caveolae, rafts, and other lipid domains, Science 296 (2002) 1821–1825.
[4] R.F.M. de Almeida, A. Fedorov, M. Prieto, Sphingomyelin/phosphatidylcholine/cholesterol phase diagram: boundaries and composition of lipid rafts, Biophys. J. 85 (2003) 2406–2416.
[5] M. Stockl, A.P. Plazzo, T. Korte, A. Herrmann, Detection of lipid domains in model and cell membranes by fluorescence lifetime imaging microscopy of fluorescent lipid analogues, J. Biol. Chem. 283 (2008) 30828–30837.
[6] C.D. Blanchette, W.C. Lin, C.A. Orme, T.V. Ratto, M.L. Longo, Domain nucleation rates and interfacial line tensions in supported bilayers of ternary mixtures containing galactosylceramide, Biophys. J. 94 (2008) 2691–2697.
[7] P.E. Milhiet, C. Domec, M.C. Giocondi, N. Van Mau, F. Heitz, C. Le Grimellec, Domain formation in models of the renal brush border membrane outer leaflet, Biophys. J. 81 (2001) 547–555.
[8] R.F.M. de Almeida, L.M.S. Loura, A. Fedorov, M. Prieto, Lipid rafts have different sizes depending on membrane composition: a time-resolved fluorescence resonance energy transfer study, J. Mol. Biol. 346 (2005) 1109–1120.
[9] M.C. Giocondi, P.E. Milhiet, P. Dosset, C. Le Grimellec, Use of cyclodextrin for AFM monitoring of model raft formation, Biophys. J. 86 (2004) 861–869.
[10] A. Bunge, P. Muller, M. Stockl, A. Herrmann, D. Huster, Characterization of the ternary mixture of sphingomyelin, POPC, and cholesterol: support for an inhomogeneous lipid distribution at high temperatures, Biophys. J. 94 (2008) 2680–2690.
[11] L.C. Silva, R.F.M. de Almeida, B.M. Castro, A. Fedorov, M. Prieto, Ceramide-domain formation and collapse in lipid rafts: membrane reorganization by an apoptotic lipid, Biophys. J. 92 (2007) 502–516.
[12] Z.V. Leonenko, D.T. Cramb, Revisiting lipid - general anesthetic interactions (I): thinned domain formation in supported planar bilayers induced by halothane and ethanol, Can. J. Chem. Rev. Can. Chim. 82 (2004) 1128–1138.
[13] L.G. Shamrakov, D.T. Cramb, Induced structural changes of a supported planar bilayer after exposure to halothane—a real-time atomic force microscopy study, Can. J. Chem. Rev. Can. Chim. 83 (2005) 1190–1194.
[14] Z. Leonenko, E. Finot, D. Cramb, AFM study of interaction forces in supported planar DPPC bilayers in the presence of general anesthetic halothane, Biochim. Biophys. Acta (BBA)-Biomembr. 1758 (2006) 487–492.
[15] F. Schroeder, T. Hubbell, S.M. Colles, W.G. Wood, Expression of liver fatty-acid-binding protein in L-cells - plasma-membrane response to ethanol, Arch. Biochem. Biophys. 316 (1995) 343–352.
[16] D.M. Lovinger, Alcohols and neurotransmitter gated ion channels: past, present and future, Naunyn-Schmiedebergs Arch. Pharmacol. 356 (1997) 267–282.
[17] F. Schroeder, S.M. Colles, G.P. Kreishman, C.E. Heyliger, W.G. Wood, Synaptic Plasma-membrane structure and polarity of long-sleep and short-sleep mice, Arch. Biochem. Biophys. 309 (1994) 369–376.
[18] R.F.M. de Almeida, L.M.S. Loura, A. Fedorov, M. Prieto, Nonequilibrium phenomena in the phase separation of a two-component lipid bilayer, Biophys. J. 82 (2002) 823–834.
[19] G.P. Casey, W.M.M. Ingledew, Ethanol tolerance in yeasts, CRC Crit. Rev. Microbiol. 13 (1986) 219–280.
[20] S.A. Simon, T.J. Mcintosh, Interdigitated hydrocarbon chain packing causes the biphasic transition behavior in lipid alcohol suspensions, Biochim. Biophys. Acta 773 (1984) 169–172.
[21] U. Vierl, L. Lobbecke, N. Nagel, G. Cevc, Solute effects on the colloidal and phase behavior of lipid bilayer membranes: ethanol–dipalmitoylphosphatidylcholine mixtures, Biophys. J. 67 (1994) 1067–1079.
[22] M.F.N. Rosser, H.M. Lu, P. Dea, Effects of alcohols on lipid bilayers with and without cholesterol: the dipalmitoylphosphatidylcholine system, Biophys. Chem. 81 (1999) 33–44.
[23] T.J. Mcintosh, H.N. Lin, S.S. Li, C.H. Huang, The effect of ethanol on the phase transition temperature and the phase structure of monounsaturated phosphatidylcholines, Biochim. Biophys. Acta-Biomembr. 1510 (2001) 219–230.
[24] H. Komatsu, E.S. Rowe, Effect of cholesterol on the ethanol-induced interdigitated gel phase in phosphatidylcholine—use of fluorophore pyrene-labeled phosphatidylcholine, Biochemistry 30 (1991) 2463–2470.
[25] F. Schroeder, W.J. Morrison, C. Gorka, W.G. Wood, Transbilayer effects of ethanol on fluidity of brain membrane leaflets, Biochim. Biophys. Acta 946 (1988) 85–94.
[26] H.E. Schueler, R.J. Hitzemann, R.A. Harris, G.P. Kreishman, Ethanol-induced differential disordering of the surface of synaptic plasma membranes from mice selected for genetic differences in ethanol intoxication, Prog. Clin. Biol. Res. 292 (1989) 425–434.
[27] J.A. Barry, K. Gawrisch, Direct Nmr evidence for ethanol binding to the lipid–water interface of phospholipid-bilayers, Biochemistry 33 (1994) 8082–8088.
[28] L.L. Holte, K. Gawrisch, Determining ethanol distribution in phospholipid multilayers with MAS-NOESY spectra, Biochemistry 36 (1997) 4669–4674.
[29] J.H. Chin, D.B. Goldstein, Drug tolerance in biomembranes—spin label study of effects of ethanol, Science 196 (1977) 684–685.
[30] T. Heimburg, A.D. Jackson, The thermodynamics of general anesthesia, Biophys. J. 92 (2007) 3159–3165.
[31] J.A. Barry, K. Gawrisch, Effects of ethanol on lipid bilayers containing cholesterol, gangliosides, and sphingomyelin, Biochemistry 34 (1995) 8852–8860.
[32] C.W. Hollars, R.C. Dunn, Submicron structure in L-alpha-dipalmitoylphosphatidylcholine monolayers and bilayers probed with confocal, atomic force, and near-field microscopy, Biophys. J. 75 (1998) 342–353.
[33] K.J. Tierney, D.E. Block, M.L. Longo, Elasticity and phase behavior of DPPC membrane modulated by cholesterol, ergosterol, and ethanol, Biophys. J. 89 (2005) 2481–2493.
[34] A. Berquand, M.P. Mingeot-Leclercq, Y.F. Dufrene, Real-time imaging of drug-membrane interactions by atomic force microscopy, Biochim. Biophys. Acta-Biomembr. 1664 (2004) 198–205.

[35] E.S. Rowe, Induction of lateral phase separations in binary lipid mixtures by alcohol, Biochemistry 26 (1987) 46–51.
[36] C. Trandum, P. Westh, K. Jorgensen, O.G. Mouritsen, Association of ethanol with lipid membranes containing cholesterol, sphingomyelin and ganglioside: a titration calorimetry study, Biochim. Biophys. Acta-Biomembr. 1420 (1999) 179–188.
[37] C. Trandum, P. Westh, K. Jorgensen, O.G. Mouritsen, A thermodynamic study of the effects of cholesterol on the interaction between liposomes and ethanol, Biophys. J. 78 (2000) 2486–2492.
[38] J.M. Vanegas, R. Faller, M.L. Longo, Influence of ethanol on lipid/sterol membranes: phase diagram construction from AFM imaging, Langmuir 26 (2010) 10415–10418.
[39] L.J. Pike, Lipid rafts: heterogeneity on the high seas, Biochem. J. 378 (2004) 281–292.
[40] P. Sengupta, B. Baird, D. Holowka, Lipid rafts, fluid/fluid phase separation, and their relevance to plasma membrane structure and function, Semin. Cell Dev. Biol. 18 (2007) 583–590.
[41] D.A. Brown, E. London, Functions of lipid rafts in biological membranes, Annu. Rev. Cell Dev. Biol. 14 (1998) 111–136.
[42] M.P. Mingeot-Leclercq, M. Deleu, R. Brasseur, Y.F. Dufrene, Atomic force microscopy of supported lipid bilayers, Nat. Protoc. 3 (2008) 1654–1659.
[43] M.C. Giocondi, D. Yamamoto, E. Lesniewska, P.E. Milhiet, T. Ando, C. Le Grimellec, Surface topography of membrane domains, Biochim. Biophys. Acta (BBA)-Biomembr. 1798 (2010) 703–718.
[44] C. Leidy, T. Kaasgaard, J.H. Crowe, O.G. Mouritsen, K. Jorgensen, Ripples and the formation of anisotropic lipid domains: imaging two-component supported double bilayers by atomic force microscopy, Biophys. J. 83 (2002) 2625–2633.
[45] M.C. Howland, A.W. Szmodis, B. Sanii, A.N. Parikh, Characterization of physical properties of supported phospholipid membranes using imaging ellipsometry at optical wavelengths, Biophys. J. 92 (2007) 1306–1317.
[46] M. Sundh, S. Svedhem, D.S. Sutherland, Influence of phase separating lipids on supported lipid bilayer formation at SiO2 surfaces, Phys. Chem. Chem. Phys. 12 (2010) 453–460.
[47] I. Pfeiffer, B. Seantier, S. Petronis, D. Sutherland, B. Kasemo, M. Zach, Influence of nanotopography on phospholipid bilayer formation on silicon dioxide, J. Phys. Chem. B 112 (2008) 5175–5181.
[48] A.P. Quist, A. Chand, S. Ramachandran, C. Daraio, S. Jin, R. Lal, Atomic force microscopy imaging and electrical recording of lipid bilayers supported over microfabricated silicon chip nanopores: lab-on-a-chip system for lipid membranes and ion channels, Langmuir 23 (2007) 1375–1380.
[49] R. Zeineldin, J.A. Last, A.L. Slade, L.K. Ista, P. Bisong, M.J. O'Brien, S.R.J. Brueck, D.Y. Sasaki, G.P. Lopez, Using bicellar mixtures to form supported and suspended lipid bilayers on silicon chips, Langmuir 22 (2006) 8163–8168.
[50] A. Miszta, B. van Deursen, R. Schoufs, M. Hof, W.T. Hermens, Absence of ethanol-induced interdigitation in supported phospholipid bilayers on silica surfaces, Langmuir 24 (2008) 19–21.
[51] M. Gedig, S. Faiss, A. Janshoff, Melting and interdigitation of microstructured solid supported membranes quantified by imaging ellipsometry, Biointerphases 3 (2008) FA51–FA58.
[52] C.W.F. Mcclare, Accurate and convenient organic phosphorus assay, Analytical Biochemistry 39 (1971) 527–530.
[53] M. Benes, D. Billy, A. Benda, H. Speijer, M. Hof, W.T. Hermens, Surface-dependent transitions during self-assembly of phospholipid membranes on mica, silica, and glass, Langmuir 20 (2004) 10129–10137.
[54] I. Reviakine, A. Brisson, Formation of supported phospholipid bilayers from unilamellar vesicles investigated by atomic force microscopy, Langmuir 16 (2000) 1806–1815.
[55] R.L. McClain, J.J. Breen, The image-based observation of the L beta I-to-L-beta ' phase transition in solid-supported lipid bilayers, Langmuir 17 (2001) 5121–5124.
[56] R.F.M. de Almeida, J. Borst, A. Fedorov, M. Prieto, A.J.W.G. Visser, Complexity of lipid domains and rafts in giant unilamellar vesicles revealed by combining imaging and microscopic and macroscopic time-resolved fluorescence, Biophys. J. 93 (2007) 539–553.
[57] B.R. Lentz, Y. Barenholz, T.E. Thompson, Fluorescence depolarization studies of phase-transitions and fluidity in phospholipid bilayers. 2. Two-component phosphatidylcholine liposomes, Biochemistry 15 (1976) 4529–4537.
[58] E.S. Rowe, Lipid chain-length and temperature-dependence of ethanol phosphatidylcholine interactions, Biochemistry 22 (1983) 3299–3305.
[59] D. Marsh, Thermodynamic analysis of chain-melting transition temperatures for monounsaturated phospholipid membranes: dependence on cis-monoenoic double bond position, Biophys. J. 77 (1999) 953–963.
[60] S. Morandat, K. El Kirat, Solubilization of supported lipid membranes by octyl glucoside observed by time-lapse atomic force microscopy, Colloids Surf., B 55 (2007) 179–184.
[61] K. Jorgensen, O.G. Mouritsen, Phase separation dynamics and lateral organization of two-component lipid membranes, Biophys. J. 69 (1995) 942–954.
[62] S.L. Veatch, S.L. Keller, Miscibility phase diagrams of giant vesicles containing sphingomyelin, Phys. Rev. Lett. 94 (2005).
[63] C.B. Yuan, J. Furlong, P. Burgos, L.J. Johnston, The size of lipid rafts: an atomic force microscopy study of ganglioside GM1 domains in sphingomyelin/DOPC/cholesterol membranes, Biophys. J. 82 (2002) 2526–2535.
[64] J.X. Mou, J. Yang, C. Huang, Z.F. Shao, Alcohol induces interdigitated domains in unilamellar phosphatidylcholine bilayers, Biochemistry 33 (1994) 9981–9985.
[65] E.I. Goksu, M.L. Longo, Ternary lipid bilayers containing cholesterol in a high curvature silica xerogel environment, Langmuir 26 (11) (2010) 8614–8624. doi: 10.1021/la9046885.
[66] Y. Kaizuka, J.T. Groves, Structure and dynamics of supported intermembrane junctions, Biophys. J. 86 (2004) 905–912.
[67] E. Terama, O.H.S. Ollila, E. Salonen, A.C. Rowat, C. Trandum, P. Westh, M. Patra, M. Karttunen, I. Vattulainen, Influence of ethanol on lipid membranes: from lateral pressure profiles to dynamics and partitioning, J. Phys. Chem. B 112 (2008) 4131–4139.
[68] H.V. Ly, M.L. Longo, The influence of short-chain alcohols on interfacial tension, mechanical properties, area/molecule, and permeability of fluid lipid bilayers, Biophys. J. 87 (2004) 1013–1033.
[69] H.V. Ly, D.E. Block, M.L. Longo, Interfacial tension effect of ethanol on lipid bilayer rigidity, stability, and area/molecule: a micropipet aspiration approach, Langmuir 18 (2002) 8988–8995.
[70] V. Schram, T.E. Thompson, Interdigitation does not affect translational diffusion of lipids in liquid crystalline bilayers, Biophys. J. 69 (1995) 2517–2520.
[71] M. Mihailescu, K. Gawrisch, The structure of polyunsaturated lipid bilayers important for rhodopsin function: a neutron diffraction study, Biophys. J. 90 (2006) L04–L06.
[72] Z.V. Leonenko, E. Finot, H. Ma, T.E.S. Dahms, D.T. Cramb, Investigation of temperature-induced phase transitions in DOPC and DPPC phospholipid bilayers using temperature-controlled scanning force microscopy, Biophys. J. 86 (2004) 3783–3793.
[73] A.N. Dickey, R. Faller, How alcohol chain-length and concentration modulate hydrogen bond formation in a lipid bilayer, Biophys. J. 92 (2007) 2366–2376.
[74] P.F.F. Almeida, W.L.C. Vaz, T.E. Thompson, Lateral diffusion in the liquid-phases of dimyristoylphosphatidylcholine cholesterol lipid bilayers—a free-volume analysis, Biochemistry 31 (1992) 6739–6747.
[75] P.F.F. Almeida, W.L.C. Vaz, T.E. Thompson, Lipid diffusion, free area, and molecular dynamics simulations, Biophys. J. 88 (2005) 4434–4438.
[76] G. Leidy, W.F. Wolkers, K. Jorgensen, O.G. Mouritsen, J.H. Crowe, Lateral organization and domain formation in a two-component lipid membrane system, Biophys. J. 80 (2001) 1819–1828.
[77] K. Jorgensen, A. Klinger, R.L. Biltonen, Nonequilibrium lipid domain growth in the gel-fluid two-phase region of a DC16PC-DC22PC lipid mixture investigated by Monte Carlo computer simulation, FT-IR, and fluorescence spectroscopy, J. Phys. Chem. B 104 (2000) 11763–11773.
[78] J.P. Mattila, K. Sabatini, P.K.J. Kinnunen, Interaction of cytochrome c with 1-palmitoyl-2-azelaoyl-sn-glycero-3-phosphocholine: evidence for acyl chain reversal, Langmuir 24 (2008) 4157–4160.
[79] E. Kalanxhi, C.J.A. Wallace, Cytochrome c impaled: investigation of the extended lipid anchorage of a soluble protein to mitochondrial membrane models, Biochem. J. 407 (2007) 179–187.
[80] A. Chattopadhyay, E. London, Parallax method for direct measurement of membrane penetration depth utilizing fluorescence quenching by spin-labeled phospholipids, Biochemistry 26 (1987) 39–45.
[81] T.K.M. Nyholm, S. Ozdirekcan, J.A. Killian, How protein transmembrane segments sense the lipid environment, Biochemistry 46 (2007) 1457–1465.
[82] M.C. Giocondi, F. Besson, P. Dosset, P.E. Milhiet, C. Le Grimellec, Remodeling of ordered membrane domains by GPI-Anchored intestinal alkaline phosphatase, Langmuir 23 (2007) 9358–9364.
[83] E. Sparr, W.L. Ash, P.V. Nazarov, D.T.S. Rijkers, M.A. Hemminga, D.P. Tieleman, J.A. Killian, Self-association of transmembrane alpha-helices in model membranes - Importance of helix orientation and role of hydrophobic mismatch, J. Biol. Chem. 280 (2005) 39324–39331.
[84] M.I. Fisher, T. Tjarnhage, Structure and activity of lipid membrane biosensor surfaces studied with atomic force microscopy and a resonant mirror, Biosens. Bioelectron. 15 (2000) 463–471.
[85] E. Reimhult, K. Kumar, Membrane biosensor platforms using nano- and microporous supports, Trends Biotechnol. 26 (2008) 82–89.

4.2. Supporting Information

SUPPORTING INFORMATION

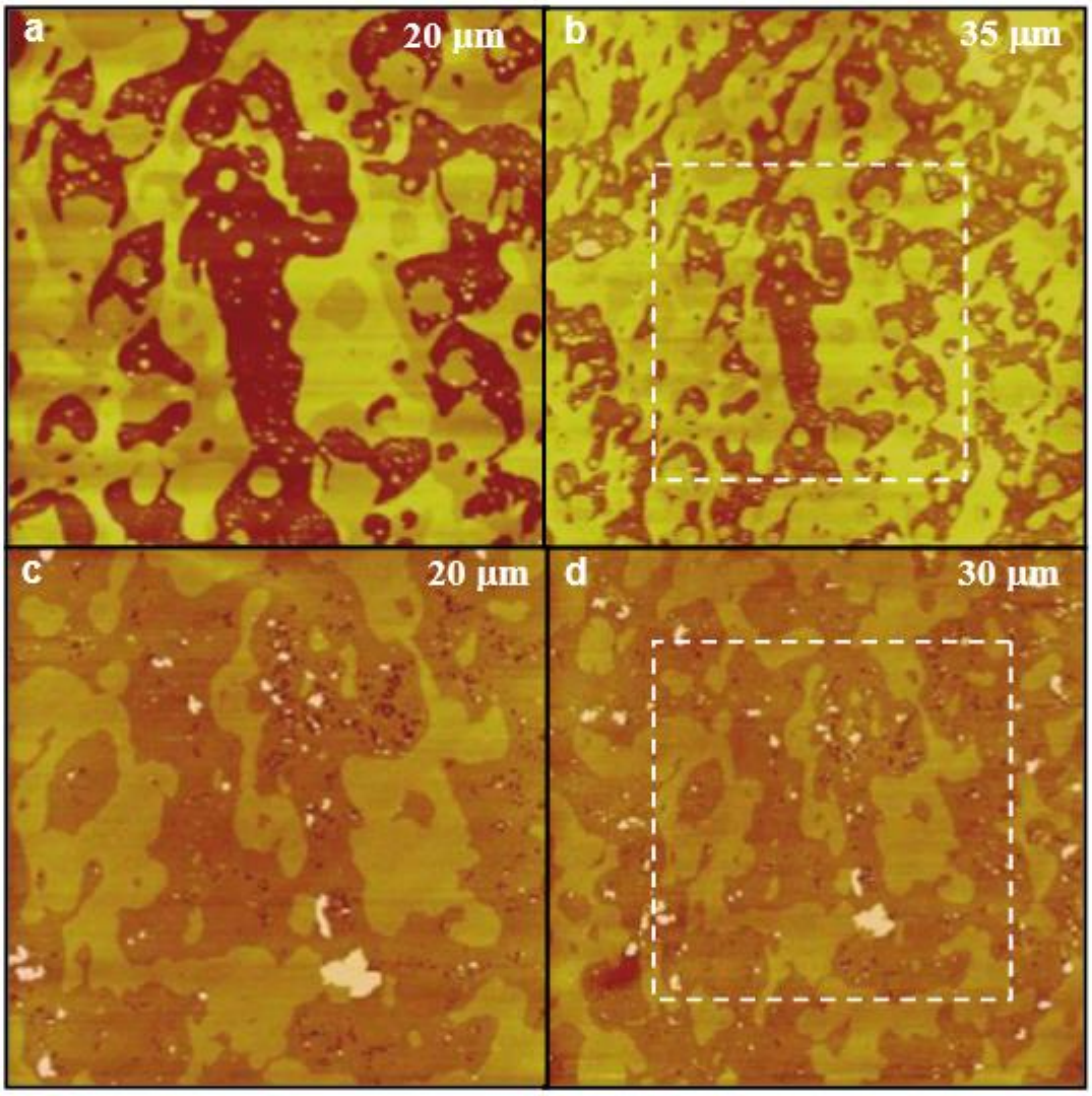

Figure S1 – *The repeated scanning of a selected area has no influence on ethanol-bilayer interactions*. AFM images of a SLB composed by DOPC/PSM/Chol (40:40:20) deposited on mica a), b) in the absence of ethanol and c), d) in the presence of 13% (v/v) of ethanol in Hepes buffer. The images were obtained in liquid at room temperature. Z = 15 nm. The white dashed squares shown in the larger area images demonstrate the previously scanned areas.

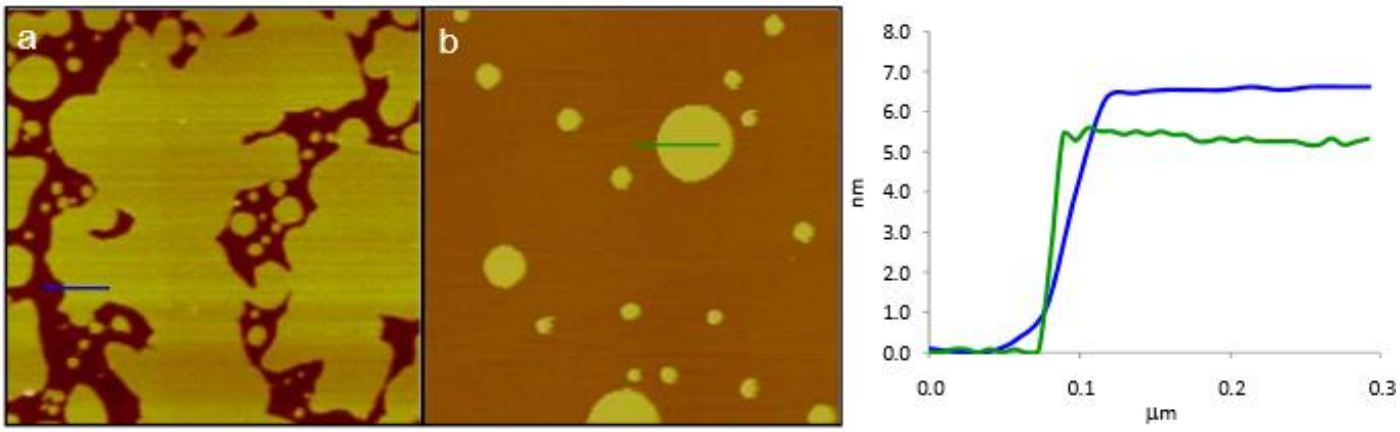

Figure S2 – *Formation of DPPC gel SLB (a) and DOPC fluid SLB (b) on mica and determination of the lipid bilayer thickness.* AFM topographical images with 3.5 µm × 3.5 µm obtained in Hepes buffer at room temperature. Z = 15 nm. Topographical profiles corresponding to the colored lines in the AFM images are shown on the right.

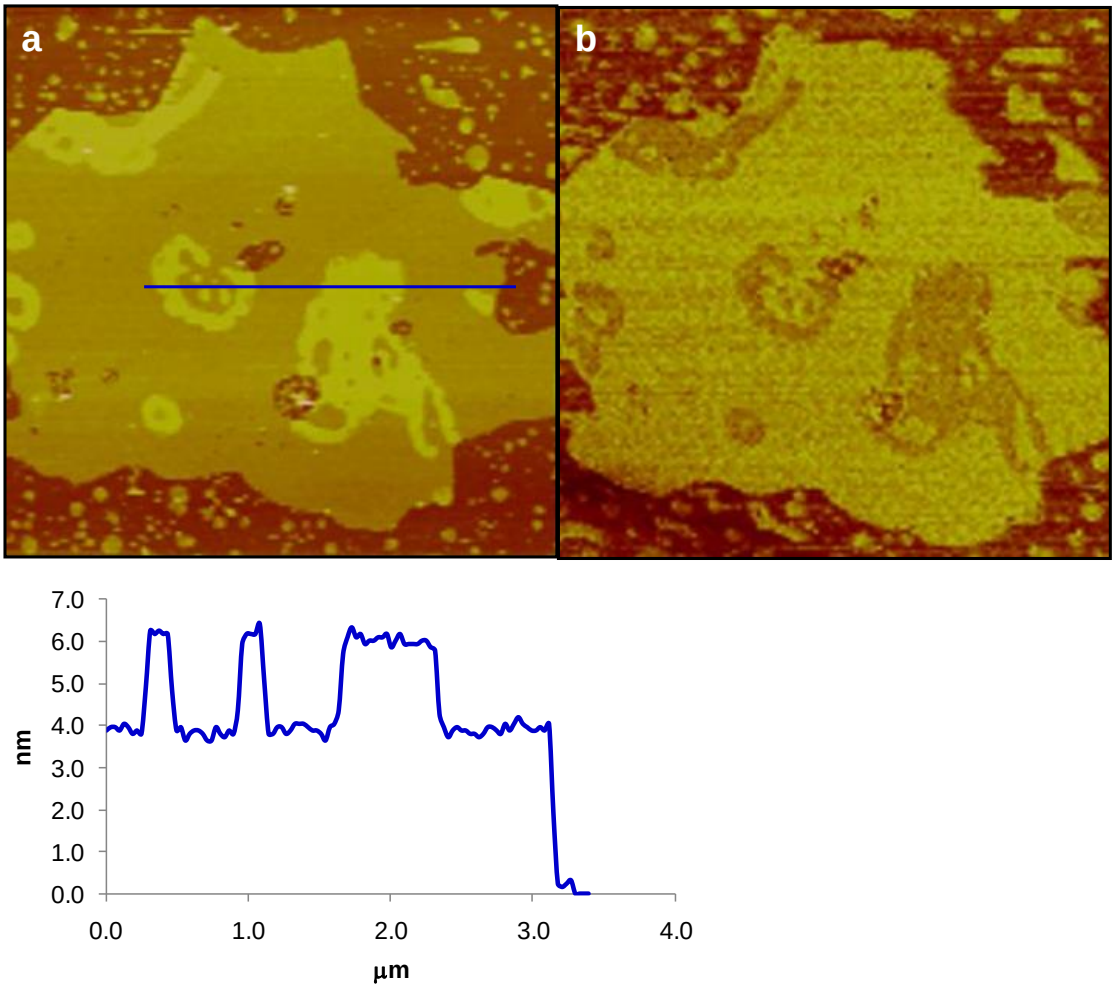

Figure S3 – *Patches formed within gel domains after ethanol addition are in the fluid phase.* Interaction of ethanol with a bilayer presenting gel/fluid coexistence induces the formation of small fluid domains of reduced thickness within the original gel domains. The profile drawn in the topographic image (a) clearly shows that these new fluid domains exhibit the same height than the fluid phase surrounding the original gel domains. A phase image is also presented (b), where the assignment of the fluid and gel phases is possible due to their different material properties (namely viscoelasticity). From the phase image is thus possible to identify the patches that form within gel domains as fluid, since they present the same color as the remaining fluid phase

.

Chapter V

Building lipid rafts on bare gold

5.1. Biomimetic membrane rafts stably supported on unmodified gold

Soft Matter

Dynamic Article Links

Cite this: *Soft Matter*, 2012, **8**, 2007

www.rsc.org/softmatter

PAPER

Biomimetic membrane rafts stably supported on unmodified gold†

Joaquim T. Marquês, Rodrigo F. M. de Almeida* and Ana S. Viana*

Received 13th September 2011, Accepted 24th November 2011
DOI: 10.1039/c2sm06738b

The formation of lipid bilayers on bare gold containing gel/fluid and liquid disordered/liquid ordered domains (lipid rafts), essential for the functioning of biological membranes, is reported here for the first time. Such binary and ternary lipid mixtures deposited on gold are improved biomimetic platforms. However, gold's hydrophobic nature has been an obstacle for direct deposition, and most studies rely on previous modification of its surface. In this work, lipid mixtures were deposited under different experimental conditions, including those commonly used for other solid supports such as mica, which are known to yield planar and organized bilayers. Atomic force microscopy imaging was used to study the topography of the lipid films at the nanoscale. The coverage, continuity and packing were addressed by ellipsometry and cyclic voltammetry, taking advantage of gold optical/electrical properties. A high quality bilayer displaying well organized lipid rafts is obtained by small or large unilamellar vesicle fusion in 10 mM Hepes buffer without added salt, while the presence of NaCl inhibits the formation of a lipid bilayer and leads to tubular structures. The raft-containing bilayer is stable over a wide range of potential sweep, enabling the development of new lipid raft based biosensing interfaces.

Introduction

Biomimetic platforms with a controlled number of key components of biomembranes provide model systems, in which an environment close to the biological one is recreated, allowing biomembrane-related processes to be addressed.[1,2] In this context, the adsorption of lipids at solid supports, forming supported lipid bilayers (SLBs), has been widely explored.[3–7] The most widely used solid support for lipid bilayer assembly and characterization is mica due to its surface properties which encompass hydrophilicity, negative charge at neutral pH and atomic flatness.[6] In fact, SLB formation on hydrophilic surfaces by the method of vesicle fusion has been thoroughly characterized and crucial parameters such as the presence of calcium ions, vesicle size, incubation time and temperature were established.[3,8–10] However, the use of conductive substrates, such as hydrophobic gold, has been gaining importance due to the potential technological applications that may emerge in diverse fields such as nanotechnology and biomaterials and in the search for new and more biocompatible devices.[11,12] Indeed, SLBs are proper biomimetic interfaces, and much effort has been involved in the development of lipid-based biosensors with electrochemical transduction.[11] In opposition to hydrophilic surfaces, the conditions that lead to the complete fusion and spreading of vesicles with the formation of well organized lipid bilayers on gold are not so well defined and are more difficult to achieve due to its hydrophobicity. In many cases the simple adsorption of vesicles without rupture or even the formation of a monolayer was described.[13,14] In order to overcome these difficulties, many lipid-based platforms involve the use of thiolipids which establish a strong and stable interaction with gold.[1,12,15] Another common strategy consists of modifying the gold[16] surface with self-assembled monolayers (SAMs) containing a hydrophilic terminal group.[17,18] However, the strong interaction/coupling between the bottom leaflet of the bilayer and the gold surface (in the case of thiolipids) or electrical blocking by the modifying agent (in the case of SAM) hinders the dynamics or electrochemical response of the bilayers, respectively. These handicaps can be surpassed by the direct formation of SLB on bare gold. Lipkowski's group was the first to report the formation of SLB on bare gold using vesicle fusion.[16,19,20] In their series of works, it was shown that the use of sonicated vesicles, gold with a predominant (111) orientation, and the presence of sodium fluoride were important conditions for the formation of a lipid bilayer.

In those studies, single-phase lipid systems were characterized, namely, DMPC, DMPC/cholesterol, and DOPC.[19,20] This paved the way for the study of more complex systems that mimic better the environment provided by biological membranes. One of the key tenets of the current paradigm of biomembranes is the existence of domains. In particular, the small (10–200 nm), heterogeneous, highly dynamic, sterol- and sphingolipid-enriched domains known as lipid rafts compartmentalize cellular processes and are necessary for the appropriate location,

Centro de Química e Bioquímica, Faculdade de Ciências da Universidade de Lisboa, Ed. C8, Campo Grande, 1749-016 Lisboa, Portugal. E-mail: anaviana@fc.ul.pt; rodrigo.almeida@fc.ul.pt; Fax: +351 217 500 088; Tel: + 351 217 500 000 (ext. 28255 or 28444)

† Electronic supplementary information (ESI) available. See DOI: 10.1039/c2sm06738b

interaction and activity of many membrane proteins.[21] In order to prepare model systems containing domains resembling lipid rafts, a ternary mixture of a low main-transition temperature (T_m) lipid, a high T_m lipid and cholesterol is required. In certain proportions, such mixtures lead to the presence of two phases, the liquid disordered (l_d) phase, which is enriched with the lower T_m lipid, and the liquid ordered (l_o) phase enriched with higher T_m lipid and cholesterol.[22–24] In addition, gel domains such as those formed in binary DOPC/DPPC mixtures have recently emerged as important biomembrane feature[25] situations.

Thus the main purpose of this work was the formation of a lipid bilayer displaying lipid rafts—l_o/l_d coexistence—and gel domains directly on a gold substrate. To characterize the topography, continuity and surface coverage of the different lipid structures formed on bare and modified gold, atomic force microscopy (AFM), ellipsometry and cyclic voltammetry (CV) were employed.

Materials and methods

Chemicals

1,2-Dipalmitoyl-*sn-glycero*-3-phosphocholine (DPPC), 1,2-dioleoyl-*sn-glycero*-3-phosphocholine (DOPC) and ganglioside G_{M1} (GM1), from ovine brain, were purchased from Avanti Polar Lipids (Alabaster, AL). Cholesterol (Chol), minimum 99%, was obtained from Sigma (St Louis, MO). For lipid structures see Fig. 1a. Potassium ferricyanide [$K_3Fe(CN)_6$], minimum 99%, was acquired from Merck and 11-mercaptoundecanoic acid (MUA), 95%, from Sigma. Other reagents were of the highest purity available.

Four different buffers, prepared with ultrapure Milli-Q water at 18.2 MΩ, were used for hydration of lipid mixtures, deposition of vesicles and AFM imaging: buffer A—10 mM Hepes, 150 mM NaCl; buffer B—10 mM Hepes, 150 mM NaCl, 5 mM $CaCl_2$, pH 7.4; buffer C—10 mM Hepes, pH 7.4; buffer D—10 mM Hepes, 5 mM $CaCl_2$, pH 7.4.

Preparation of gold surface for lipid deposition

The gold slides used were manufactured by Arrandee™ and consist of a thin film (200 nm) of gold on glass (1.1 × 1.1 cm^2) with a chromium undercoat (2–4 nm). Before each experiment, the surface was cleaned by immersion in piranha solution for a few minutes, followed by thorough rinse with ethanol and ultrapure water, and drying under a nitrogen flow. The gold surface was then flame-annealed by focusing a butane–O_2 flame on the surface until the gold starts to get incandescent and then retreat the flame with five repetitions. This leads to the formation of large grains where the surface is very flat and organized in triangularly shaped monoatomic terraces (Fig. 2a), separated by 0.24 nm. This last step is crucial because it produces a locally flat

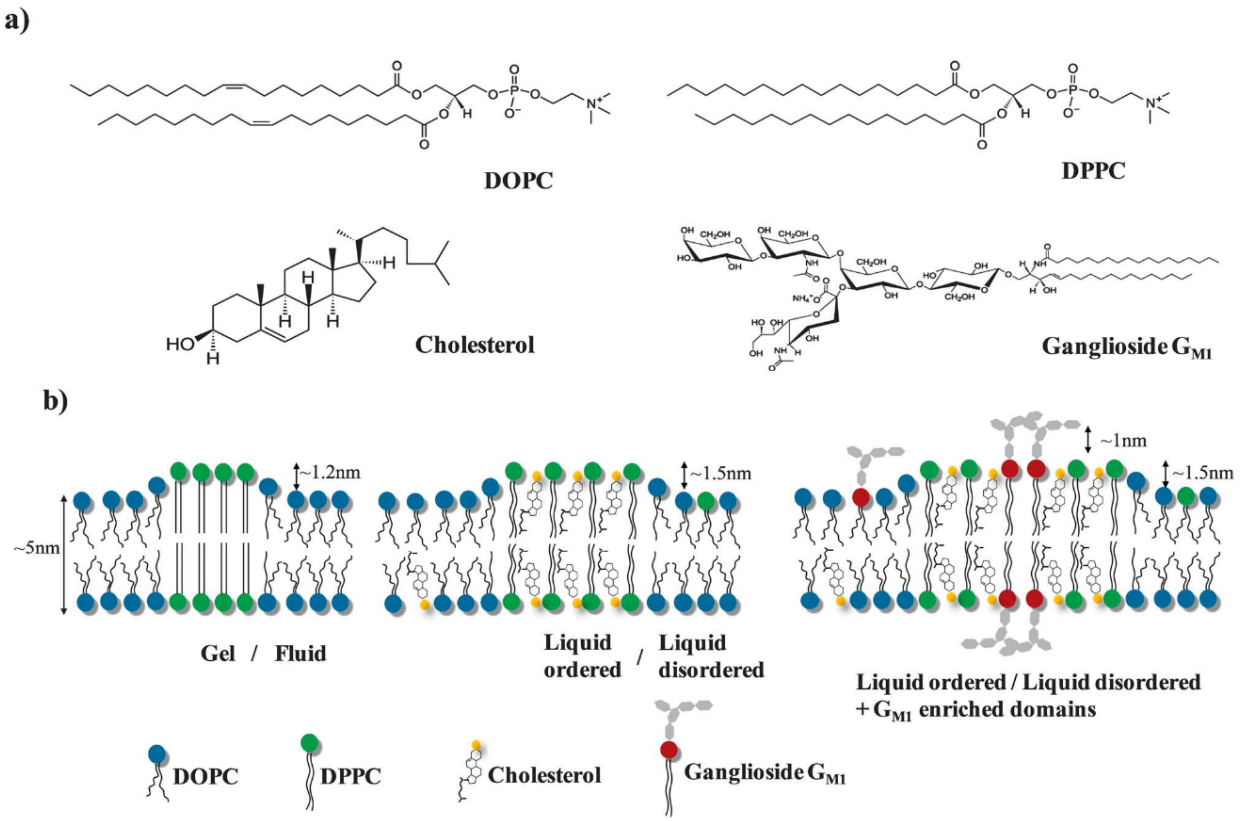

Fig. 1 Schematic representation (a) of the structure of the lipid molecules used in this work and (b) of the different lipid domains formed when lipids are mixed in certain proportions. Gel/fluid—DOPC/DPPC (1 : 1); liquid ordered/liquid disordered—DOPC/DPPC/Chol (2 : 2 : 1); and liquid ordered/liquid disordered + 10% of GM1—DOPC/DPPC/Chol (2 : 2 : 1) + 10% GM1.

surface, enabling identification of morphological details of the deposited lipid layers, including lipid rafts and domains.

Modification of the gold surface with 11-mercaptoundecanoic acid

The formation of a SAM composed of 11-mercaptoundecanoic acid (MUA) was achieved by immersion of the gold slides in 1 mM solution of MUA in ethanol for 18 hours. After this incubation period the gold slides were abundantly rinsed with ethanol and Milli-Q water in order to remove the MUA molecules that did not establish a strong interaction with the gold surface.

Preparation of supported lipid bilayers

The phospholipid concentration was determined gravimetrically and by inorganic phosphate quantification.[26] Cholesterol and GM1 quantification were made by gravimetry.

Lipid stock solutions and lipid mixtures were prepared with spectroscopic grade chloroform from Merck (Darmstadt, Germany). The solvent was evaporated first under a mild flow of nitrogen, followed by overnight vacuum. According to the objective of each experiment lipids were hydrated with buffer A or C followed by vortexing and freeze–thaw cycles (total lipid concentration 1 mM). SUVs were made by power sonication (Hielscher, UP200S) followed by centrifugation for 30 minutes at 10 000 rpm of the suspension. LUVs were prepared by extrusion (Avanti Mini-Extruder) at 60 °C of the multilamellar vesicle suspension through polycarbonate filters with 100 nm diameter pores (Nuclepore, Whatman). When required, $CaCl_2$ was added to a final concentration of 5 mM to the SUV or LUV suspension. For deposition on gold, 150 µL of SUV or LUV suspension were deposited on a gold surface and incubated for 45 minutes at 45 °C. After this incubation the samples were left at room temperature to cool for 1 h and SLBs were washed several times at room temperature (21 °C) with the buffer used for hydration.

AFM imaging

AFM measurements were performed in liquid at room temperature using a Multimode Nanoscope IIIa Microscope (Digital Instruments, Veeco). To avoid any kind of contamination, before each experiment, the glass block holding the cantilever was washed several times with water and ethanol. Topographic images were obtained in *tapping mode* at a scan rate close to 2 Hz. For this purpose silicon nitride cantilevers (NPS and NLS, *ca.* 0.58 N m^{-1} of spring constant, Veeco) were used in a liquid with a resonance frequency of about 9 kHz for NPS and 26 kHz for NLS. Images and the profile associated to each image, and thus the height differences shown, are representative of the behavior of the system. A large number of profiles were traced and several images obtained for each sample. Software ImageJ was used to estimate the area fraction corresponding to the different domains on at least two independent samples.

Ellipsometry

Ellipsometric measurements were performed at 70° using a SE 400 Ellipsometer (Sentech Instruments) equipped with a He–Ne laser (632.8 nm). The thickness of the lipid layers was estimated from the variation of the ellipsometric parameters (Ψ and Δ) before and after vesicle deposition, using a three-phase model.[27,28] The thickness of lipid films was estimated by fixing the real part of the refractive index at 1.5, a value frequently employed for hydrocarbon layers and determined to be the refractive index for gel lipids,[29] which are expected to be nearly transparent, with very low extinction coefficients at the working wavelength.

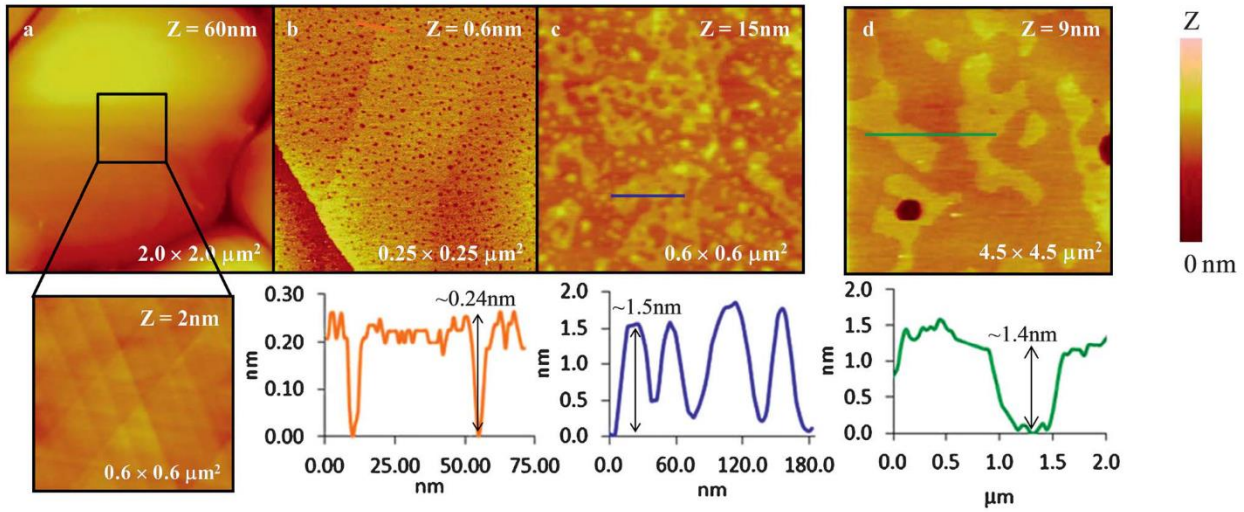

Fig. 2 *Tapping mode* AFM images of Au (111) after flame annealing, exhibiting monoatomic terraces (~0.24 nm high) (a). Scanning tunneling microscopy of Au (111) modified with SAM of MUA showing the typical pits one gold atom deep (~0.24 nm) (b). DOPC/DPPC/Chol (2 : 2 : 1) lipid bilayers formed on a previously MUA-modified gold surface (c), and on mica (d), with similar height gaps between thinner (l_d) and thicker (l_o) domains. The vesicles deposition was performed using buffer B. Image size and *z*-scale are indicated in each panel. The topographical profiles below correspond to the colored line drawn on the images.

Cyclic voltammetry

Electrochemical assays were conducted using a Parstat 2263 electrochemical station (Ametek, Princeton Applied Research). A three electrode Teflon cell was used to carry out cyclic voltammetric measurements using a gold slide as working electrode, a saturated calomel electrode (SCE) as reference electrode and a platinum foil as counter-electrode. The geometric area of the working electrode was determined to be 0.57 cm^2. The electrolyte solution, 1 mM $K_3Fe(CN)_6$ in 50 mM Hepes buffer, pH 7.4, was degassed with pure nitrogen before each experiment.

Results and discussion

The influence of using different saline conditions and lipid vesicles with various compositions and sizes—SUVs and LUVs—was evaluated in the process of bilayer formation by performing vesicles deposition on gold using Hepes buffer containing or not NaCl and/or $CaCl_2$. Table S1† summarizes the different experimental conditions tested throughout this work, including the lipid mixtures that were investigated. Three different lipid systems were studied—DOPC/DPPC (1 : 1) and DOPC/DPPC/Chol (2 : 2 : 1) with 0 or 10% of GM1. According to the phase diagrams[30,31] and AFM studies on mica[10] gel/fluid phase separation is expected for DOPC/DPPC and liquid disordered (l_d)/liquid ordered (l_o) phase separation for DOPC/DPPC/Chol. The composition and structural features of these phases in coexistence are depicted in Fig. 1b.

AFM is an imaging technique with unique nanoscale axial and horizontal resolution especially suitable for analysing the topography of SLB containing domains, while ellipsometry is an optical technique often employed to determine the mean thickness of a film on a surface. Cyclic voltammetry was used to evaluate the blocking effect of the SLB formed towards the redox process of a reversible system such as $Fe(CN)_6^{3-}/Fe(CN)_6^{4-}$, thus complementing the information obtained by ellipsometry and AFM.

Formation of a SLB on a previously modified gold surface with a SAM

The formation of a SLB depends on the surface hydrophilicity at the moment of vesicles deposition[5] and this parameter is difficult to control on bare gold. Thus, electrode modification with a mercaptoundecanoic acid (COOH terminated) SAM (Fig. 2b) was performed in order to confer hydrophilicity and negative charge at pH 7.4 upon the gold surface (Fig. 2a). The adsorption of thiol groups onto the Au (111) surface typically generates one gold atom deep depressions (Fig. 2b), with lateral sizes usually varying from 2 to 10 nm, which are fully covered with ordered thiol monolayers.[32] The origin of such pits is still controversial but it is believed to be caused by the strength of the S–Au linkage which makes the underlying Au–Au bonds more labile and induces the movement of the Au atoms or Au–S entities from the surface terraces to the step edges.[33] The presence of pits is therefore a fingerprint of ordered self-assembled monolayers of thiols on gold. After such modification gold surface properties become closer to those of mica, and thus the conditions used for the formation of a SLB on mica (Table S1†) were employed to generate a planar lipid bilayer on a SAM-modified gold surface (Fig. 2c). The lipid bilayer so formed exhibited phase separation, namely, thinner (l_d) and thicker (l_o) domains with a height difference close to 1.5 nm (Fig. 2c), as depicted in Fig. 1b. The topography observed and the height gap between domains are similar to the ones detected on mica (Fig. 2d), which proves that the modification of the gold surface and the conditions commonly used for mica are suitable to promote the formation of a planar SLB with lipid rafts on this metal. The following step was to evaluate if those conditions were also appropriate for domain-containing SLBs directly deposited on a gold surface.

Lipid deposition directly on gold in the presence of NaCl and $CaCl_2$: formation of tubular structures

The deposition of lipid mixtures on unmodified gold was initially performed under the same conditions as used above for mica (Table S1†). The results obtained for both binary DOPC/DPPC (Fig. 3a) and ternary DOPC/DPPC/Chol (Fig. 3d) mixtures show the formation of lipid tubules with a diameter that resembles that of intact vesicles (*ca.* 40 nm), along with globular features clearly depicted for the DOPC/DPPC/Chol system, that correspond to unfused vesicles adsorbed onto the surface. The lipid tubular structures are probably a result of an incomplete and unidirectional fusion of vesicles as suggested by other authors who also identified lipid tubules with similar diameter using 1,2-dimyristoyl-*sn-glycero*-3-phosphocholine (DMPC) and electron microscopy.[34] When composed of cationic lipids these structures may be applied in gene therapy due to their ability to form complexes with DNA.[35] At the cellular level, lipid tubular structures may be involved in the formation of the cisternae of Golgi apparatus, in cellular traffic and also in establishing contact between the membranes of different organelles.[36,37] *N*-Nervonoylceramide, the ceramide species predominant in nerve tissues, has a strong propensity to induce tubule formation.[38] Thus, the result here obtained may be of importance as a potential new method to prepare lipid tubules.

Lipid deposition directly on gold in the presence of $CaCl_2$ and in the absence of NaCl

As a planar lipid bilayer was not obtained under the conditions above described, the vesicles deposition was then carried out in the absence of NaCl, as it has been shown that ionic strength plays an important role in the formation of a planar lipid bilayer.[5] The same lipid mixtures were used (Table S1†), and in both cases, a planar lipid bilayer was formed (Fig. 3b and e) which should be continuous in the planar regions of the electrode since it was not possible to discriminate areas corresponding to bare gold, in opposition to mica, preventing the determination of the bilayer thickness directly by AFM imaging. For the binary mixture, a lipid bilayer showing undulations, with a periodicity of 9.5 nm and observed height of ~0.6 nm, was obtained, which must correspond to previously reported lipid corrugations[20] (Fig. 3b). These periodic undulations can be considered a benchmark for the formation of a single lipid bilayer on bare gold, as will be discussed in detail below. However, gel/fluid phase separation, *i.e.*, lipid domains with distinct heights, was not clearly identified for this mixture. Concerning the ternary mixture DOPC/DPPC/Chol elevated features are observed,

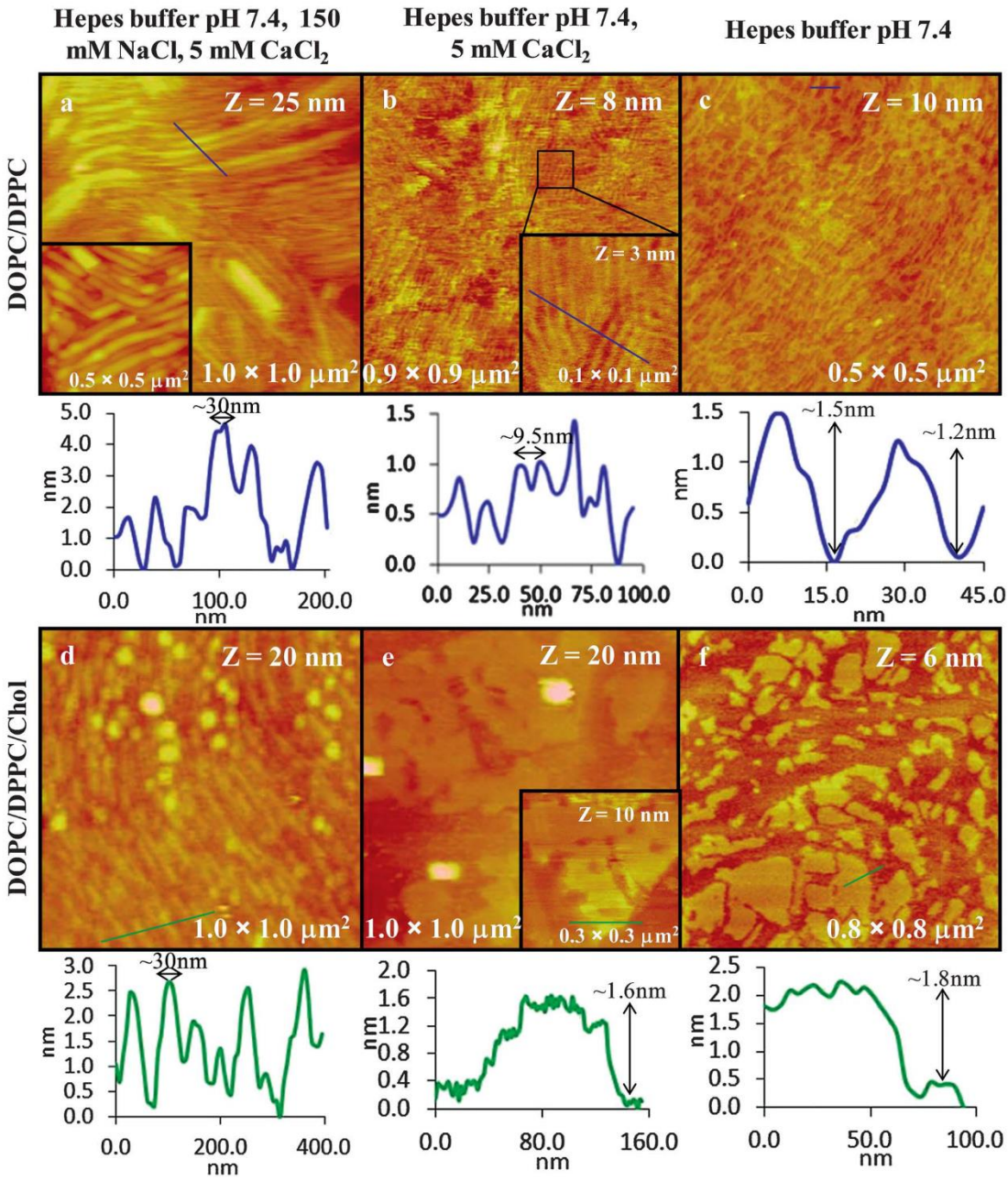

Fig. 3 AFM images of the Au (111) surface after the deposition of DOPC/DPPC (1 : 1) (upper row) and DOPC/DPPC/Chol (2 : 2 : 1) (bottom row) SUV using Hepes buffer with 150 mM of NaCl and 5 mM of $CaCl_2$ (left column), Hepes buffer containing 5 mM $CaCl_2$ (middle column) or Hepes buffer with no salt (right column). Image size and *z*-scale are indicated in each panel. For each image the topographical profile corresponding to the colored line drawn is shown below.

which according to the height difference (~1.6 nm) and taking into account the composition of the lipid mixture (Fig. 1b) may be assigned to l_d/l_o lipid domains (Fig. 3e). Also, unfused intact vesicles on top of the surface are detected.

Lipid deposition directly on gold in the absence of both $CaCl_2$ and NaCl

As already shown, the presence of salt interferes with a complete fusion of vesicles on a gold surface and thus, lipid deposition was carried out using only Hepes 10 mM. For the binary mixture, a planar lipid bilayer exhibiting corrugation and phase-separation is observed (Fig. 3c), with a difference in thickness between the two phases estimated to be ~1.4 nm, which is in agreement with the separation between gel and fluid phases observed on mica.[10] However, the domain size and arrangement are markedly distinct from those which are formed in mica using the same lipid mixture (Fig. S1†). On the other hand, for the ternary mixture a planar bilayer with domains differing in height by ~1.8 nm from the surrounding bilayer is clearly observed, unequivocally

showing that the conditions used are suitable for the formation of ternary lipid mixtures on bare gold (Fig. 3f). The presence of corrugations in the l_d phase is also detected (Fig. 4a). To confirm that the patches observed indeed correspond to lipid domains, gel/fluid in the binary mixture, and l_d/l_o domains (lipid rafts) in the ternary, the deposition of the pure lipids, DOPC and DPPC, was also performed, maintaining the other experimental conditions (Table S1†). As shown in ESI Fig. S2†, neither DOPC nor DPPC alone leads to the formation of domain-containing bilayers, and therefore, the height differences observed in the lipid mixtures can be safely assigned to the presence of gel/fluid and l_d/l_o domains. It was previously shown that in two other substrates, mica and silicon, both pure DOPC and pure DPPC lead to the formation of bilayers where lipid domains are absent.[10] Regarding the proportion of each phase, the area fraction of the l_o phase is close to 23%, which is distant from the molar fraction predicted by the phase diagram for this mixture (43%)[31] and also from the one obtained for lipid bilayers composed of this mixture supported on mica (32%).[10] In a pure DMPC bilayer on gold (111), the T_m is lowered by approximately 2 °C, when compared to freestanding bilayers, probably due to stress caused by the reduced coupling between the bilayer leaflets.[20] In the case of coexistence between an ordered and a disordered phase, the outcome of such a bilayer stress is expectedly the reduction of the ordered phase fraction. Furthermore, it cannot be ruled out that the mean molecular area of each lipid phase for a lipid bilayer on gold is different from those on mica and freestanding bilayers. In fact, when lipids are displayed in a corrugated arrangement their mean molecular area tends to be superior and thus the area fraction of l_d (the phase exhibiting undulations) should be increased compared to freestanding bilayers. Also the morphology of the domains on gold is distinct from those observed in freestanding bilayers[31] and SLBs on mica and silicon,[10] because the boundaries of lipid phase domains tend to align with the edges of gold (111) triangular monoatomic terraces (Fig. 3f and 2a, respectively).

The formation of a lipid bilayer with raft-like domains on unmodified gold was achieved by removing 150 mM NaCl from the buffer solution, and clearly improved by further removing $CaCl_2$. The influence of NaCl (and $CaCl_2$) may be explained by the negative charge that phosphatidylcholine lipid vesicles tend to exhibit under saline conditions due to the binding of anions, namely chloride ion, to the trimethylammonium group of choline.[39] In these circumstances the presence of calcium is of extreme importance if a negative substrate, such as mica or gold modified with a COO^- terminated SAM, is used for the deposition of lipids (Fig. 2). Calcium will then mediate the interaction between the negative groups of the substrate and the negatively charged moiety (PO_4^-). However, when using an unmodified gold substrate, which is neutral, calcium will not have such a pivotal role. In addition, the use of NaCl is known to stabilize the bilayers in suspension,[40] rendering their fusion and spreading more difficult. This is corroborated by the results presented in Fig. 3a and d, which reveal the formation of tubular structures (incomplete vesicle fusion). Moreover, the observed effect should be specifically related to the use of chloride ions, since a planar bilayer of 1,2-dimyristoyl-*sn-glycero*-3-phosphocholine (DMPC) using NaF at 100 mM has been reported.[20] To further confirm this assumption, a DMPC bilayer was prepared in the absence of both NaCl and NaF, resulting also in a planar bilayer with corrugations (Fig. S3†). Such behavior may be explained by the more effective binding of chloride to the lipids headgroup than fluoride. In fact, the effectiveness of halogen binding to the trimethylammonium ion increases along the lyotropic series, *i.e.*, as the halogen ionic radius becomes larger.[39] In addition the chloride ion tends to chemisorb on gold[41] which, in turn, may also prevent the adsorption of lipid vesicles onto the Au (111) surface and thus the formation of a lipid bilayer.

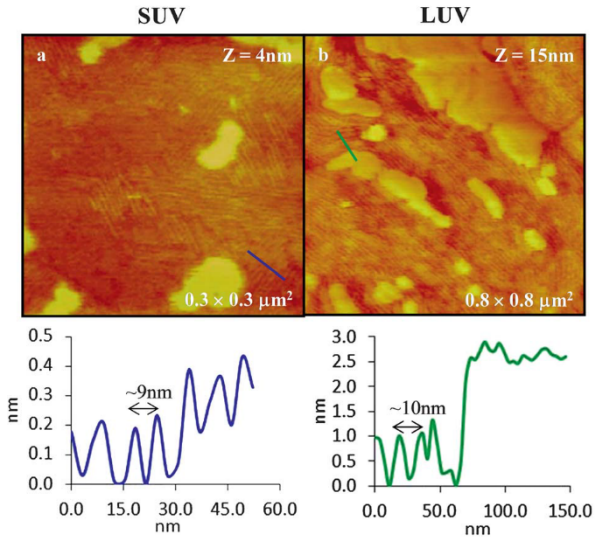

Fig. 4 AFM images of DOPC/DPPC/Chol (2 : 2 : 1) ternary lipid bilayers prepared from SUV (a), and LUV (b), deposited on Au (111) using Hepes buffer. Image size and *z*-scale are indicated in each panel. For each image the topographical profile, corresponding to the colored line drawn, is shown below.

Small unilamellar vesicles *versus* large unilamellar vesicles

In addition to salting effects, the size of lipid vesicles is also critical for the formation of a lipid bilayer on solid supports.[42] Therefore, this effect was investigated by depositing LUV of the ternary mixture DOPC/DPPC/Chol on bare gold, instead of SUV. AFM images reveal the presence of a lipid bilayer exhibiting phase separation with a height difference between l_o and l_d domains close to 1.6 nm (Fig. 4b). Moreover a corrugation with a periodicity (~10 nm) similar to the one obtained for the SUV-generated bilayer is observed (Fig. 4a). Thus, no remarkable differences were detected by AFM whether using SUV or LUV. It should be pointed out that the origin of this periodic arrangement is not due to gold surface reconstruction since the periodicity of the undulation is 8 to 10 nm (Fig. 4a and b) while the reconstruction of gold generates a corrugation with a typical separation of ~6.7 nm.[43] It was experimentally demonstrated that a DMPC lipid bilayer exhibits a corrugation both on reconstructed and unreconstructed Au (111) annealed surfaces.[20] Therefore, such undulated structure is intrinsic to the lipid bilayer and independent of the possible underlying gold periodic corrugation. It can be also concluded that the observed phenomenon does not correspond to the formation of the pseudo-lamellar lipid ripple phase which, on freestanding

bilayers, only forms below the lipid T_m[44] and for SLB on mica, it was solely identified on the top bilayer of a double bilayer array.[45,46] In the present work, corrugations were present in DOPC-rich fluid phases, *i.e.*, well above the lipid T_m (−20 °C[47]), and in a previous study of DMPC bilayers the corrugation was found both above and below the T_m of DMPC.[20] In addition, previous results with the same lipid mixtures as used in this work, using mica and silicon, as substrate, did not show the formation of corrugated patterns.[10] In the case of a SLB deposited on unmodified gold, and as pointed out by Li *et al.* 2008, the formation of a corrugated phase is a consequence of the interaction between the gold surface and the phosphorylcholine headgroups which leads to a tilt and splay deformation causing a spontaneous curvature controlled by the elastic properties of the membrane. It has been demonstrated that this spontaneous curvature together with an asymmetric environment between the two bilayer leaflets leads to undulations.[48] Because corrugations are due to interaction between the inner leaflet and the substrate, their presence is a direct indication that a SLB has been formed, *i.e.*, it is neither a lipid monolayer nor a multibilayer.

As mentioned above, these structures were not detected on liquid ordered domains suggesting that in these regions there is a similar hydration environment of both bilayer leaflets in opposition to the l_d domains. This assumption should elucidate the larger height separation consistently obtained between l_d/l_o on gold (*ca.* 1.8 nm) relative to that occurring for the same ternary lipid bilayer on mica (*ca.* 1.2 nm).

Formation of a DOPC/DPPC/Chol bilayer with 10% of GM1 on mica and gold

GM1 is associated with the most ordered regions of membranes, namely with naturally occurring and model lipid rafts, and is co-localized with other "raft markers" namely glycosylphosphatidylinositol-anchored proteins.[49] Due to its large polar headgroup and tendency to locate in ordered regions it allows, in certain circumstances, the clear visualization of domains as height differences.[50] Thus, raft-forming ternary lipid mixtures containing GM1 were also used for SLB formation on bare gold.

The formation of a DOPC/DPPC/Chol (2 : 2 : 1) bilayer containing 10% of GM1 was first assessed on mica (Table S1†) because this is the substrate usually used to observe lipid domains, as explained in the Introduction. A lipid bilayer with three distinct heights is formed (Fig. 5a), as schematically depicted in Fig. 1b. The thicker areas (~8 nm) correspond to GM1-enriched domains, since this molecule tends to be found in the most ordered regions of the membrane and thus is co-located/segregates in l_o domains.[51] However, on gold a lipid film exhibiting pores with a depth of ~6 to 7 nm (Fig. 5b) was obtained and therefore the lipid organization observed on mica was not possible to discriminate on this substrate. In this specific situation, the negative charge introduced by the ganglioside may be pointed out as the reason that explains the disparate results obtained using as solid support mica or gold. On mica the negative charge of the surface can play an adjuvant role as the presence of calcium will mediate electrostatic interactions with the large and negatively charged polar head of GM1. In opposition, on gold, which has a neutral surface, a different

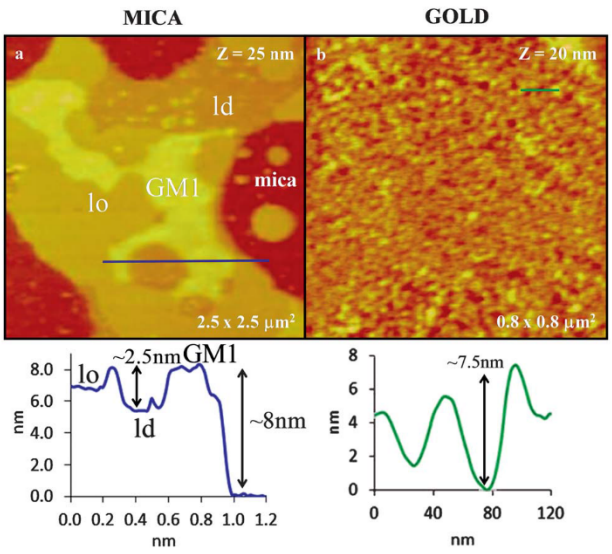

Fig. 5 AFM images of a quaternary DOPC/DPPC/Chol (2 : 2 : 1)/GM1 (10%) lipid bilayer, deposited from SUV on mica, using buffer B (a), and on gold, using buffer C (b). Image size and *z*-scale are indicated in each panel. For each image the topographical profile, corresponding to the colored line drawn, is shown below.

interaction should be established and the lateral organization and compactness of the bilayer, identified on mica, are prevented.

Ellipsometric and electrochemical characterization of DOPC/DPPC/Chol lipid films on gold

In order to characterize to a larger extent the distinct DOPC/DPPC/Chol lipid films prepared under different conditions (Table S1†), ellipsometry and cyclic voltammetry were employed to infer on the coverage of the gold surface, the blocking properties as well as the integrity and compactness (presence of (pin) holes and defects) of the lipid films formed. Four different systems were analyzed: lipid tubules, planar SUV and LUV generated bilayers, and lipid bilayer formed onto a SAM-modified gold surface.

Ellipsometry is an optical technique often used to determine the thickness of thin films formed on a substrate.[28,52] This technique analyses a larger area of the sample when compared to AFM, and so the data will be affected by discontinuities/defects in the bilayer, or even by the presence of intact vesicles. As a consequence, only an average value dependent on surface coverage may be obtained, and not the real thickness of the lipid bilayers. Notwithstanding, the relative optical differences of the distinct supported bilayers provide valuable and complementary information to the AFM imaging.

It is common to use an electroactive compound, such as potassium ferricyanide, with reversible redox behaviour to probe the blocking properties of a film formed on an electrode surface. A decrease in the intensity of both oxidation and reduction peak currents is expected if a partial blocking to the electron transfer is occurring. Moreover a total blocking, corresponding to a continuous, very well organised and highly packed layer, should suppress any electrochemical process. It is worth noting

Table 1 Average ellipsometric parameters (Ψ, Δ) and estimated thickness (d) and extinction coefficient (k) for DOPC/DPPC/Chol SLB on Au (111) prepared under different conditions, as described in the Experimental section. Oxidation peak current densities (i_p^{ox}) obtained by cyclic voltammetry are also presented

System	Ψ/°	Δ/°	d/nm	k	i_p^{ox}/mA cm^{-2}
Bare gold	43.1 ± 0.4	106.5 ± 0.6	—	—	57.2
Tubules	43.1 ± 0.4	95.9 ± 4.1	9.1 ± 3.3	0.09 ± 0.03	31.6
SUV, no salt	42.8 ± 0.4	102.7 ± 1.5	3.7 ± 0.9	0.09 ± 0.04	38.3
LUV, no salt	43.4 ± 0.1	100.6 ± 0.9	5.3 ± 1.0	0.06 ± 0.01	31.7
LUV on SAM	42.9 ± 0.3	101.6 ± 1.8	4.7 ± 1.2	0.14 ± 0.08	—

that the presence of pores is enough to create a dispersed arrangement of microelectrodes, which may oxidise and reduce redox species in solution, with a distinct kinetics (radial diffusion) than bare planar electrodes with large uncovered regions (linear diffusion), originating a sigmoidal type voltammogram.[53–55]

Table 1 compiles average ellipsometric parameters, Ψ and Δ, obtained for bare gold and after vesicle deposition, as well as average film thickness values and extinction coefficients fitted as described in the Experimental section (for a reasonably fixed film refractive index). The peak current intensity for ferricyanide oxidation was measured by cyclic voltammetry (Fig. 6) and is also presented in Table 1.

Lipid tubules yield the highest mean thickness (~9.1 nm) which corresponds approximately to a double bilayer, corroborating the AFM topographic images. Moreover the estimated thickness is in agreement with the breakthrough distance (8.9 nm) obtained by force spectroscopy for 1-palmitoyl-2-oleoyl-*sn-glycero*-3-phosphocholine (POPC) lipid vesicles adsorbed onto a template-stripped Au surface.[56] Thus, in the present work, the data suggest that the lipid tubular structures are arranged in a double bilayer as a result of the incomplete and unidirectional fusion of vesicles. In addition, the decrease in peak current intensities was more pronounced for this sample together with an LUV generated bilayer (Table 1 and Fig. 6). The values obtained for the mean thicknesses of planar bilayers formed from SUV and LUV are close to the one determined for a pure POPC lipid bilayer deposited directly on gold (~4 nm).[56] The mean thickness of a lipid bilayer with the same DOPC/DPPC/Chol composition on mica, taking into account the l_d/l_o thicknesses and area fractions, is ~5.7 nm.[10] This value is slightly higher than those on gold, which can be explained by the presence of a thinner water cushion between the latter substrate and lipid, as recently proposed by Laredo *et al.*[57] LUV generated bilayers exhibit a larger mean thickness (5.3 nm, Table 1) than those formed from SUV, which should be a consequence of a higher coverage of the electrode. Cyclic voltammetric results presented in Fig. 6 corroborate such ellipsometric data, since a greater decrease in peak current intensity of ferricyanide was obtained for the LUV generated bilayer in comparison to the SUV bilayer (Table 1). As a consequence, a larger area fraction of the gold substrate should be covered when comparing LUV and SUV bilayers. The fact that the blocking ability towards the redox process is only partial, but that no uncovered substrate was observed on gold terraces by AFM, strongly indicates that most uncovered regions should be as expected localized within the grain boundaries of the substrate crystallites originated during flame-annealing (Fig. 2a).

Lipid deposition on gold under different conditions also results in differently shaped voltammograms. In the case of tubular structures, although the peak current is strongly reduced, a linear diffusion current response is obtained, similarly to bare gold (Fig. 6). For SUV and LUV derived planar bilayers the sigmoidal-like appearance of the voltammograms (Fig. 6)

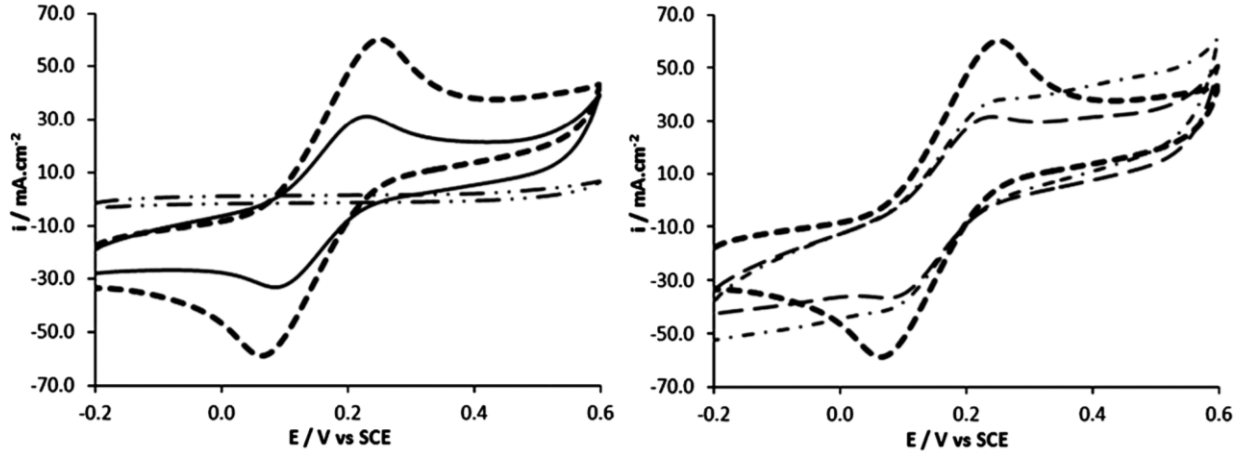

Fig. 6 Cyclic voltammograms of bare gold and gold modified with DOPC/DPPC/Chol lipid mixtures prepared under different conditions: bare gold (---), tubules (—), LUV on SAM (—··—), SUVs no salt (-··-) and LUVs no salt (– – –) in 50 mM Hepes buffer with 1 mM $K_3Fe(CN)_6$, recorded at 50 mV s^{-1}.

suggests the presence of a compact film with pinholes contributing to a hemispherical diffusion of the electroactive species towards the electrode surface, in addition to the linear diffusion.

When analysing the lipid bilayer formed on a previously modified gold surface with a SAM, a smaller value of mean thickness was obtained when compared to the LUV bilayer, indicating that the coverage may not be complete. A total blocking effect to the ferricyanide redox process was achieved in this situation; however, this outcome is due to the very compact nature of the underlying SAM and not to the lipid film itself, since the SAM alone caused the same blocking effect (not shown).

Finally, it was observed that the lipid film containing GM1 was unstable upon the potential sweep during cyclic voltammetry since an increase of the oxidation peak current intensity was observed during the experiment (Fig. S4†). This may be a consequence of the negative charge of GM1 that may lead to desorption of the lipid film with the exposure of a higher fraction of the electrode surface.

Conclusions

In this work, an approach to obtain biomimetic platforms based on the formation of lipid rafts containing bilayers directly on gold was developed. The formation of planar, continuous and organized ternary lipid bilayers with domains on unmodified gold was possible using Hepes buffer at pH 7.4 in the absence of salt. Moreover, the SLBs obtained are stable within the potential range applied during voltammetric experiments, making them suitable for building electrochemical lipid-based biosensing platforms. By presenting well-defined l_o/l_d domains, they provide an organization close to biological membranes, and a proper environment for the incorporation and activity of membrane proteins, increasing their biocompatibility. In contrast, vesicles deposition at high saline concentration leads to the formation of lipid tubules, thus the optimal conditions to form a SLB on mica (150 mM NaCl, $CaCl_2$) or onto gold modified by a hydrophilic SAM are not suitable for the formation of a lipid bilayer directly on gold. Still, these may be useful to address biological processes related to lipid tubular structures. Additionally, both SUV and LUV-derived SLBs possibly contain small pores responsible for non-linear diffusion of ferricyanide during cyclic voltammetric experiments, in agreement with the absence of uncovered areas on gold monoatomic terraces as observed by AFM. The SLB made from larger vesicles covers a larger fraction of the substrate as shown by ellipsometry and sustained by the higher blocking effect obtained. In sum, the observation that it is possible to form planar and stable lipid bilayers directly on gold containing lipid rafts mimicking biomembrane domains opens new possibilities not only to study raft-related phenomena, as well as to find new applications for lipid-on-gold biomimetic devices.

Acknowledgements

The authors acknowledge funding from F.C.T., Portugal, received through PTDC/QUI/66612/2006, PEst-OE/QUI/UI0612/2011 and Ciência2007. J.T.M. acknowledges PhD scholarship SFRH/BD/64442/2009.

References

1 I. Koper, *Mol. BioSyst.*, 2007, **3**, 651 657.
2 C. Rossi and J. Chopineau, *Eur. Biophys. J.*, 2007, **36**, 955 965.
3 I. Reviakine and A. Brisson, *Langmuir*, 2000, **16**, 1806 1815.
4 Z. V. Leonenko, A. Carnini and D. T. Cramb, *Biochim. Biophys. Acta, Biomembr.*, 2000, **1509**, 131 147.
5 R. P. Richter, R. Berat and A. R. Brisson, *Langmuir*, 2006, **22**, 3497 3505.
6 E. I. Goksu, J. M. Vanegas, C. D. Blanchette, W. C. Lin and M. L. Longo, *Biochim. Biophys. Acta, Biomembr.*, 2009, **1788**, 254 266.
7 J. Lipkowski, *Phys. Chem. Chem. Phys.*, 2010, **12**, 13874 13887.
8 M. Benes, D. Billy, A. Benda, H. Speijer, M. Hof and W. T. Hermens, *Langmuir*, 2004, **20**, 10129 10137.
9 M. P. Mingeot-Leclercq, M. Deleu, R. Brasseur and Y. F. Dufrene, *Nat. Protoc.*, 2008, **3**, 1654 1659.
10 J. T. Marques, A. S. Viana and R. F. M. De Almeida, *Biochim. Biophys. Acta, Biomembr.*, 2011, **1808**, 405 414.
11 E. Reimhult and K. Kumar, *Trends Biotechnol.*, 2008, **26**, 82 89.
12 W. Knoll, I. Koper, R. Naumann and E. K. Sinner, *Electrochim. Acta*, 2008, **53**, 6680 6689.
13 C. A. Keller and B. Kasemo, *Biophys. J.*, 1998, **75**, 1397 1402.
14 J. Ekeroth, P. Konradsson and F. Hook, *Langmuir*, 2002, **18**, 7923 7929.
15 J. K. R. Kendall, B. R. G. Johnson, P. H. Symonds, G. Imperato, R. J. Bushby, J. D. Gwyer, C. van Berkel, S. D. Evans and L. J. C. Jeuken, *ChemPhysChem*, 2010, **11**, 2191 2198.
16 M. H. Chen, M. Li, C. L. Brosseau and J. Lipkowski, *Langmuir*, 2009, **25**, 1028 1037.
17 B. P. Oberts and G. J. Blanchard, *Langmuir*, 2009, **25**, 2962 2970.
18 S. Ip, J. K. Li and G. C. Walker, *Langmuir*, 2010, **26**, 11060 11070.
19 I. Zawisza, X. M. Bin and J. Lipkowski, *Bioelectrochemistry*, 2004, **63**, 137 147.
20 M. Li, M. Chen, E. Sheepwash, C. L. Brosseau, H. Li, B. Pettinger, H. Gruler and J. Lipkowski, *Langmuir*, 2008, **24**, 10313 10323.
21 L. J. Pike, *J. Lipid Res.*, 2006, **47**, 1597 1598.
22 M. C. Giocondi, P. E. Milhiet, P. Dosset and C. Le Grimellec, *Biophys. J.*, 2004, **86**, 861 869.
23 R. F. M. De Almeida, L. M. S. Loura, A. Fedorov and M. Prieto, *J. Mol. Biol.*, 2005, **346**, 1109 1120.
24 A. Bunge, P. Muller, M. Stockl, A. Herrmann and D. Huster, *Biophys. J.*, 2008, **94**, 2680 2690.
25 F. Aresta-Branco, A. M. Cordeiro, H. S. Marinho, L. Cyrne, F. Antunes and R. F. M. De Almeida, *J. Biol. Chem.*, 2011, **286**, 5043 5054.
26 C. W. F. Mcclare, *Anal. Biochem.*, 1971, **39**, 527.
27 S. Gottesfeld, *Electroanal. Chem.*, 1989, **15**, 143 265.
28 Z. H. Wang, A. S. Viana, G. Jin and L. M. Abrantes, *Bioelectrochemistry*, 2006, **69**, 180 186.
29 R. F. M. De Almeida, L. M. S. Loura, A. Fedorov and M. Prieto, *Biophys. J.*, 2002, **82**, 823 834.
30 S. L. Veatch and S. L. Keller, *Phys. Rev. Lett.*, 2005, **94**, 148101.
31 R. F. M. De Almeida, J. Borst, A. Fedorov, M. Prieto and A. J. W. G. Visser, *Biophys. J.*, 2007, **93**, 539 553.
32 J.-B. D. Green, C. A. McDermott, M. D. Porter, *Imaging of Surfaces and Interfaces (Frontiers of Electrochemistry)*, Wiley-VCH, 1999.
33 F. T. Arce, M. E. Vela, R. C. Salvarezza and A. J. Arvia, *Electrochim. Acta*, 1998, **44**, 1053 1067.
34 U. Lauf, A. Fahr, K. Westesen and A. S. Ulrich, *ChemPhysChem*, 2004, **5**, 1246 1249.
35 S. Chesnoy and L. Huang, *Annu. Rev. Biophys. Biomol. Struct.*, 2000, **29**, 27 47.
36 G. van Meer, *EMBO Rep.*, 2005, **6**, 418 419.
37 B. Sorre, A. Callan-Jones, J. B. Manneville, P. Nassoy, J. F. Joanny, J. Prost, B. Goud and P. Bassereau, *Proc. Natl. Acad. Sci. U. S. A.*, 2009, **106**, 5622 5626.
38 S. N. Pinto, L. C. Silva, R. F. de Almeida and M. Prieto, *Biophys. J.*, 2008, **95**, 2867 2879.
39 S. A. Tatulian, *Biochim. Biophys. Acta, Biomembr.*, 1983, **736**, 189 195.
40 M. M. A. E. Claessens, B. F. van Oort, F. A. M. Leermakers, F. A. Hoekstra and M. A. C. Stuart, *Biophys. J.*, 2004, **87**, 3882 3893.
41 Z. C. Shi and J. Lipkowski, *J. Electroanal. Chem.*, 1996, **403**, 225 239.
42 V. P. Zhdanov and B. Kasemo, *Langmuir*, 2001, **17**, 3518 3521.

43 M. H. Dishner, J. C. Hemminger and F. J. Feher, *Langmuir*, 1997, **13**, 2318 2322.
44 E. J. Luna and H. M. Mcconnell, *Biochim. Biophys. Acta, Biomembr.*, 1977, **466**, 381 392.
45 Y. Fang and J. Yang, *J. Phys. Chem.*, 1996, **100**, 15614 15619.
46 C. Leidy, T. Kaasgaard, J. H. Crowe, O. G. Mouritsen and K. Jorgensen, *Biophys. J.*, 2002, **83**, 2625 2633.
47 R. N. A. H. Lewis, B. D. Sykes and R. N. Mcelhaney, *Biochemistry*, 1988, **27**, 880 887.
48 W. Helfrich, *Z. Naturforsch., C: J. Biosci.*, 1974, **29**, 692 693.
49 E. G. Hofman, M. O. Ruonala, A. N. Bader, D. van den Heuvel, J. Voortman, R. C. Roovers, A. J. Verkleij, H. C. Gerritsen and P. M. P. V. Henegouwen, *J. Cell Sci.*, 2008, **121**, 2519 2528.
50 C. B. Yuan, J. Furlong, P. Burgos and L. J. Johnston, *Biophys. J.*, 2002, **82**, 2526 2535.
51 Y. Ohta, S. Yokoyama, H. Sakai and M. Abe, *Colloids Surf., B*, 2004, **34**, 147 153.
52 A. S. Viana, L. M. Abrantes, G. Jin, S. Floate, R. J. Nichols and M. Kalaji, *Phys. Chem. Chem. Phys.*, 2001, **3**, 3411 3419.
53 H. O. Finklea, D. A. Snider, J. Fedyk, E. Sabatani, Y. Gafni and I. Rubinstein, *Langmuir*, 1993, **9**, 3660 3667.
54 D. Garcia-Raya, R. Madueno, J. M. Sevilla, M. Blbzquez and T. Pineda, *Electrochim. Acta*, 2008, **53**, 8026 8033.
55 C. Amatore, J. M. Saveant and D. Tessier, *J. Electroanal. Chem.*, 1983, **147**, 39 51.
56 X. Wang, M. M. Shindel, S. W. Wang and R. Ragan, *Langmuir*, 2010, **26**, 18239 18245.
57 T. Laredo, J. R. Dutcher and J. Lipkowski, *Langmuir*, 2011, **27**, 10072 10087.

5.2. Supporting Information

Electronic Supplementary Material (ESI) for Soft Matter

Table S1 – Summary of the different experimental conditions tested throughout this work, including the lipid mixtures that were investigated and the main observations obtained for each system studied.

Lipid System	Hepes 10mM, pH 7.4	Vesicles size	Solid support	Lipid film
DOPC/DPPC (1:1)	+ 150mM NaCl, 5mM $CaCl_2$	SUV's	Unmodified gold	Tubules
	+ 5mM $CaCl_2$	SUV's	Unmodified gold	Planar bilayer, no lipid domains
	No salt	SUV's	Unmodified gold	Planar bilayer with lipid domains
DOPC/DPPC/Chol (2:2:1)	+ 150mM NaCl, 5mM $CaCl_2$	SUV's	Unmodified gold	Tubules
	+ 5mM $CaCl_2$	SUV's	Unmodified gold	Planar bilayer with lipid domains, presence of vesicles
	No salt	SUV's	Unmodified gold	Planar bilayer with lipid domains, undulations
			Mica	Planar bilayer with lipid domains
		LUV's	Unmodified gold	Planar bilayer with lipid domains, undulations
			MUA modified gold	Planar bilayer with lipid domains
DOPC/DPPC/Chol (2:2:1) + 10% GM_1	+ 150mM NaCl, 5mM $CaCl_2$	SUV's	Mica	Planar bilayer with three types of domains
	No salt		Unmodified gold	Planar bilayer with pores

Electronic Supplementary Material (ESI) for Soft Matter

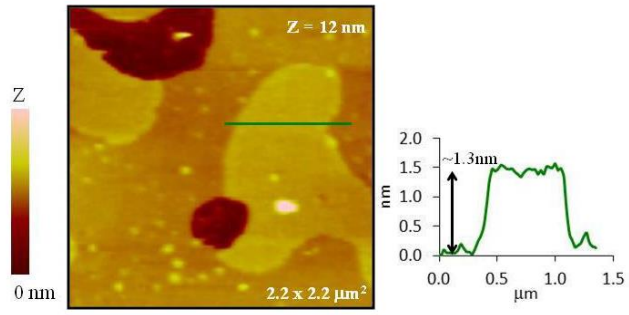

Fig. S1 - AFM image of a DOPC/DPPC (1:1) lipid bilayer on mica with gel (thicker) and fluid (thinner) domains, differing in height by approximately 1.3 nm. The image was obtained by *tapping mode* AFM in buffer solution at room temperature and the topographical profile shown corresponds to the colored line drawn.

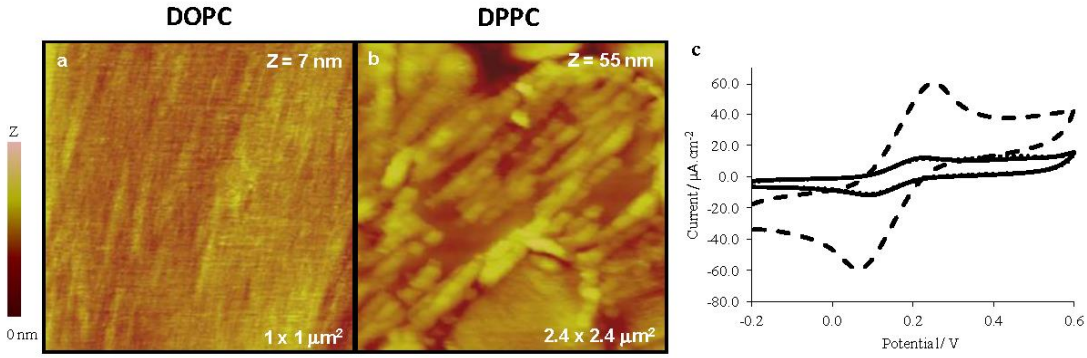

Fig. S2 - AFM images of pure DOPC a) and DPPC b) lipid films deposited on gold from SUV, using hepes buffer without added salt. DOPC (fluid at room temperature, T_m = - 20 ºC) forms a continuous and planar lipid film with a corrugation pattern assignable to a single lipid bilayer, while DPPC (gel at room temperature, T_m = 41 ºC) generates mostly lipid tubules surrounded by planar regions. In neither situation phase separation is observed. These studies highlight the importance of having binary or ternary lipid mixtures to be able to form stable bilayers directly on unmodified gold, containing ordered lipid domains. The blocking effect to the $K_3Fe(CN)_6$ redox process is also shown for pure lipid films in c). An almost complete suppression of the $K_3Fe(CN)_6$ redox signal indicates a high coverage of the gold electrode for both systems. – – – Bare gold — DPPC ····· DOPC.

Electronic Supplementary Material (ESI) for Soft Matter

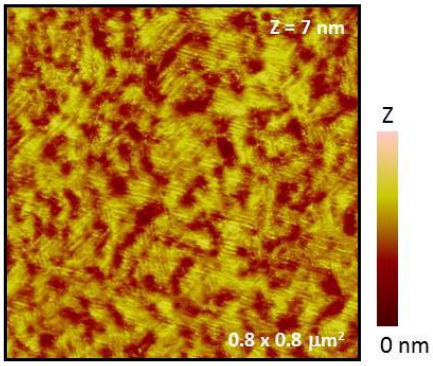

Fig. S3 - *Tapping mode* AFM image (obtained in a liquid cell) of a DMPC bilayer on Au (111), prepared from SUV deposition in Hepes buffer with no salt. Corrugations, with an average periodicity of ~5.3 nm, are clearly depicted. The observed heterogeneity corresponds probably to gel and fluid coexistence as the imaging was performed at room temperature (21°C) within the main phase transition temperature-range of DMPC SLB.

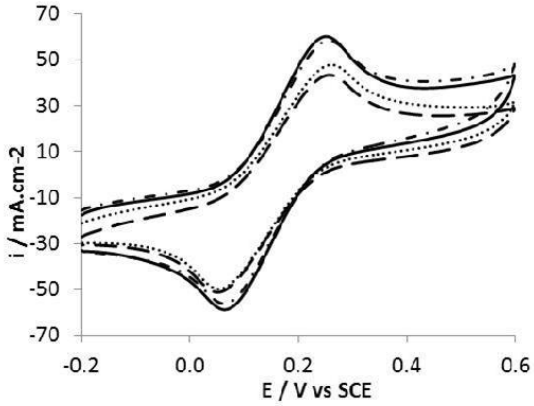

Fig. S4 – Successive cyclic voltammograms recorded at 50 mVs^{-1} of 1 mM $K_3Fe(CN)_6$ in 50 mM Hepes buffer on gold modified with lipid films of DOPC/DPPC/Chol (2:2:1)/GM1 (10%) prepared in Hepes buffer in the absence of salt. With the successive scans the lipid film is detached from the gold surface which becomes more exposed leading to an increase of the peak current intensity. — Bare gold – – – first scan ····· second scan –·– third scan.

Chapter VI

Lipid bilayers on gold to study electroactive molecules

6.1. A Biomimetic Platform to Study the Interactions of Bioelectroactive Molecules with Lipid Nanodomains

Langmuir

Article

pubs.acs.org/Langmuir

A Biomimetic Platform to Study the Interactions of Bioelectroactive Molecules with Lipid Nanodomains

Joaquim T. Marquês, Ana S. Viana,* and Rodrigo F. M. de Almeida*

Centro de Química e Bioquímica, Faculdade de Ciências, Universidade de Lisboa, Ed. C8, Campo Grande, 1749-016 Lisboa, Portugal

Supporting Information

ABSTRACT: In this work, we developed a biomimetic platform where the study of membrane associated redox processes and high-resolution imaging of lipid nanodomains can be both performed, based on a new functional gold modification, L-cysteine self-assembled monolayer. This monolayer proved to be ideal for the preparation of defect-free planar supported lipid bilayers (SLBs) where nanodomains with height difference of ~1.5 nm are clearly resolved by atomic force microscopy. Single and multicomponent lipid compositions were used, leading to the formation of different phases and domains mimicking the lateral organization of cellular membranes, and in all cases stable and continuous bilayers were obtained. These platforms were tested toward the interaction with bioelectroactive molecules, the antioxidant quercetin, and the hormone epinephrine. Despite the weak interaction detected between epinephrine and lipid bilayers, our biomimetic interface was able to sense the redox process of membrane-bound epinephrine, obtain its surface concentration (9.36×10^{-11} mol/cm^2 for a fluid bilayer), and estimate a mole fraction membrane/water partition coefficient (K_p) from cyclic voltammetric measurements (1.13×10^4 for a fluid phase membrane). This K_p could be used to quantitatively describe the minute changes observed in the photophysical properties of epinephrine intrinsic fluorescence upon its interaction with liposome suspensions. Moreover, we showed that the lipid membrane stabilizes epinephrine structure, preventing its oxidation, which occurs in neutral aqueous solution, and that epinephrine partition and mobility in membranes depends on lipid phase, expanding our knowledge on hormone membrane interactions.

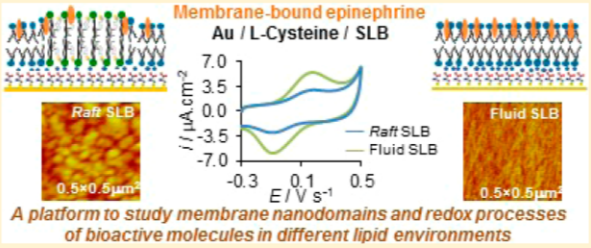

A platform to study membrane nanodomains and redox processes of bioactive molecules in different lipid environments

INTRODUCTION

In search for improved biomimetic platforms, supported lipid bilayers (SLBs) prepared on gold or other metal surfaces are gaining considerable importance whether it is in the development of lipid-based biosensor interfaces[1−5] or in the study of biomembrane-related cellular processes.[6−10] Despite the well established fact that biological membranes are characterized by a complex matrix of lipids and proteins organized into laterally distinct domains,[11] many studies conducted on gold employ single-component or single-phase lipid bilayers.[2−4,12−15] So far, only a few studies were dedicated to complex lipid mixtures that demonstrably lead to the formation of domains in order to better mimic the lateral compartmentalization of biological membrane.[6,16,17] In eukaryotic organisms, lipid rafts are an important type of lipid domains due to their role in intracellular distribution of proteins and lipids, signal transduction, and many other cellular functions.[11,18] In order to mimic the presence of lipid rafts, membrane model systems, such as SLBs, should have at least three different lipids: cholesterol and two other lipids, phospholipids or sphingolipids differing significantly in their main phase transition temperature (T_m).[19,20] For certain proportions, these ternary lipid mixtures lead to the coexistence of liquid ordered (l_o) domains, which mimic lipid rafts, and liquid disordered (l_d) phase, that simulates the more fluid surrounding membrane.[21,22] Besides its biological relevance, the presence of this kind of domain, with a typical height difference of ~1.5 nm, can be used as a fingerprint to identify the presence of a planar and organized lipid bilayer.

Gold-supported lipid bilayers bring together in the same device the biocompatibility and the advantageous conductive and optical properties characteristic of gold, which allow the application of, for example, electrochemical techniques, ellipsometry, and surface plasmon resonance (SPR). Recently, our group has shown that lipid bilayers displaying l_o/l_d (lipid rafts) or gel/fluid phase separation can be formed on bare gold. Moreover, the topography of theses domains can be assessed by atomic force microscopy and the blocking properties of these lipid bilayers evaluated by cyclic voltammetry.[23] It was found that, due to the gold hydrophobic nature, which does not favor the adsorption of lipids through their polar heads, the direct formation of raft-mimicking SLBs[23] on bare gold surfaces requires very stringent conditions. Additionally, bare gold surfaces hampered the formation of stable SLB containing ganglioside G_{M1} (GM1), an important raft marker[24] and cellular receptor, and the lipid bilayers formed on these surfaces presumably exhibited small pores/defects.[23] Fortunately, it is

Received: August 1, 2014
Revised: September 26, 2014
Published: September 30, 2014

possible to tailor the interfacial properties of gold required for a given application by surface modification typically with organosulfur compounds. In this context, thiolipids[14,25,26] and self-assembled monolayers (SAMs)[13,16,17,27] of functionalized alkanethiols with hydrophilic groups have been used to modify the surface prior to lipid bilayer deposition. However, thiolipids may hamper both the lateral diffusion of lipids and the incorporation of large proteins in a functional manner.[28,29] It has been accepted that long chain thiol derivatives, namely, 11-mercaptoundecanoic acid (MUA) that forms tightly packed monolayers on gold, are required for the stable assembly of a compact and continuous SLB.[16,23] In addition, MUA also contains a terminal COOH group that makes the surface hydrophilic and negatively charged (at physiological pH), which are crucial for a stable interaction with the lipids polar head. However, due to its very compact nature, the electronic access of electroactive species to the gold surface is severely hindered,[23] which limits its application to directly monitor redox reactions occurring at the membrane.

In the present work, we develop a new and functional lipid based interface using a short monolayer. We have chosen to modify the surface with a small molecule, L-cysteine, which contains a thiol anchor, and the amine and carboxylic hydrophilic groups. We predicted that such modification would allow simultaneous (1) strong and stable linkage to gold; (2) charge and hydrophilicity required for stable SLB formation; (3) electron transfer from the substrate to bioelectroactive molecules interacting with the lipid bilayer; (4) high-resolution topographical imaging of nanodomains in the lipid bilayer. The observation of these nanostructures will greatly enhance the ability to establish the relations between their organization, SLB properties, and membrane−biomolecule interactions, all very active research topics.[11,30]

To illustrate the wide applicability of this platform, we followed the redox process of two different electroactive compounds: quercetin, a bioactive flavonoid,[31,32] and epinephrine, a catecholamine hormone, both having a well-known range of important biological activities.[33,34] For the former, the interaction with lipid bilayers is well established,[35−38] whereas the interaction of epinephrine, or any member of its class for that matter, with lipid membranes is missing in the literature. According to the "membrane as a catalyst for hormone−receptor interactions hypothesis",[39] these endocrine messengers should be able to interact with the lipid moiety of the membrane which is much wider than the specific receptor binding pocket, but in fact this catecholamine is not particularly hydrophobic, nor it is positively charged, the features that are usually found in membrane interacting messengers. The adsorption to the lipid bilayer would concentrate the hormone (which must exert its activity at very low concentrations) in the membrane and induce a change in conformation due to the hydrophobic nature of the medium, both facilitating the interaction with its receptor.

Here, we use the newly designed platform to detect with high sensitivity and quantify the epinephrine molecules which are effectively bound to different types of lipid bilayer membranes and show that its stability is greatly enhanced when compared to the molecule in solution.

MATERIALS AND METHODS

Chemicals. 1,2-Dioleoyl-*sn*-glycero-3-phosphocholine (DOPC), 1,2-dipalmitoyl-*sn*-glycero-3-phosphocholine (DPPC), and ganglioside G_{M1} from ovine brain mainly acylated with C16:1 and C18 hydrocarbon chains were purchased from Avanti Polar Lipids (Alabaster, AL). Cholesterol (Chol), minimum 99%, and all other reagents, analytical grade, were acquired from Sigma.

Buffer solutions used throughout this work were prepared with ultrapure Milli-Q water at 18.2 MΩ. The buffer used for hydration and deposition of lipid mixtures was HEPES 10 mM at pH 7.4 containing 150 mM NaCl or 5 mM $CaCl_2$ or both. Each condition is discriminated along the text. Sodium chloride is added in order to meet biological requirements while the role of calcium chloride is to mediate the electrostatic bridge between the lipids polar headgroup and the modified gold surface.

Preparation of Gold Surfaces for Lipid Deposition. Two different types of gold surfaces differing in their crystallography, morphology, and roughness were used depending on the analytical technique used. For quartz crystal microbalance (QCM) assays, the gold electrodes consisted of a thin film of gold (100 nm), evaporated on quartz with a prelayer of 10 nm of titanium (CH Instrumenst). For SPR experiments, a thin layer of gold 50 nm thick deposited on glass (Analytical μ-Systems) was used. Both gold surfaces are very uniformly constituted by small grains with a diameter of ca. 15−20 nm and a root-mean-square (rms, R_q) roughness close to 1 nm (for an area of 0.6×0.6 μm^2).[40] For atomic force microscopy (AFM), ellipsometry, and cyclic voltammetric experiments, gold substrates manufactured by Arrandee consisting of a thin film (200 nm) of gold on borosilicate glass (1.1×1.1 cm^2) with a chromium undercoat (2-4 nm) were used. The electrodes were cleaned in piranha solution, thoroughly rinsed with ultrapure water and ethanol, cleaned in a UV-ozone chamber for ∼40 min, and rinsed with ultrapure water. Before the UV-ozone cleaning, the Arrandee gold substrates were flame-annealed, as previously described[23] to achieve atomically flat terraces with a predominant (111) orientation (for a 0.6×0.6 μm^2 area R_q is ca. 0.5 nm). This step is crucial because the flat gold regions enable one to identify morphological details of the SLB, including lipid rafts and domains.

Modification of the Gold Surfaces with 11-Mercaptoundecanoic Acid and L-Cysteine. The formation of SAMs of MUA or Cys was achieved by immersion of the gold slides in a 1 mM solution of MUA in ethanol or 1 mM solution of Cys in water for 18 h. After this incubation period, the gold slides were abundantly rinsed with ethanol and Milli-Q water in order to remove the MUA or Cys molecules that did not establish a strong interaction with the gold surface.

Preparation of Large Unilamellar Vesicle (LUV) Suspensions and Supported Lipid Bilayers. The phospholipid concentration was determined gravimetrically and by inorganic phosphate quantification.[41] Cholesterol and GM1 quantification was made by gravimetry. The lipid systems, whether single or multicomponent, differing in their composition and phase behavior, studied throughout this work were as follows: DPPC (gel), DOPC (fluid), DOPC/DPPC 1:1 (molar proportions, fluid/gel), DOPC/DPPC/Chol 2:2:1 (l_o/l_d), and DOPC/DPPC/Chol 2:2:1 with 10% GM1. The ternary system DOPC/DPPC/Chol 1:11:8 (l_o) was also employed but only in the fluorescence spectroscopy studies.

All lipid stock solutions and lipid mixtures were prepared with spectroscopic grade chloroform from Merck (Darmstadt, Germany), kept at −20 °C in dark under N_2 atmosphere. The required stock solution volume was added to a vial, and the solvent evaporated first under a mild flow of nitrogen, followed by overnight vacuum. In conformity with the requirements of each experiment, lipids were hydrated (total lipid concentration 1 mM) with buffer containing NaCl or not, depending on whether it was meant for deposition on MUA or Cys modified gold, respectively. The hydration was followed by vortexing and freeze−thaw cycles. Large unilamellar vesicles were formed by extrusion (Avanti Mini-extruder) at 60 °C, by forcing the multilamellar vesicle suspension 21 times through polycarbonate filters with 400 nm diameter pores (Nuclepore, Whatman). When required (in the case of modified gold electrodes), $CaCl_2$ was added to a final concentration of 5 mM to the LUV suspension. For SLB formation, 150 μL of LUV suspension was added to the surface and incubated for 1 h at 60 °C. After this incubation step, the samples were left at room

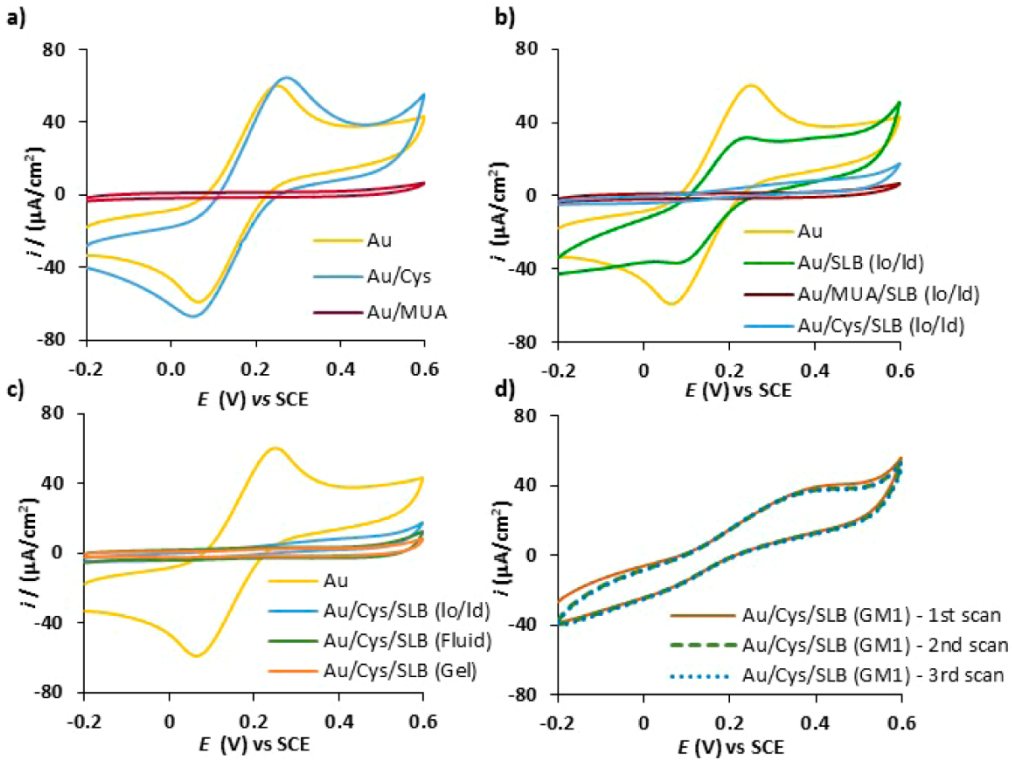

Figure 1. Cyclic voltammograms acquired at 50 mV/s of 1 mM $Fe(CN)_6^{3-}/Fe(CN)_6^{4-}$ in 50 mM HEPES buffer, pH 7.4, on different gold surfaces: (a) bare and modified gold with MUA and Cys SAMs; (b) bare and modified gold with MUA and Cys SAMs containing DOPC/DPPC/Chol SLB; (c) Cys modified gold containing three different SLBs; and (d) gold modified with a Cys SAM containing a SLB with 10% GM1.

temperature to cool for 1 h and SLBs were then washed several times at room temperature (23 °C) with the buffer used for lipid hydration.

Incubation of Quercetin and Epinephrine with SLB. Quercetin or epinephrine was allowed to interact with the lipid bilayers by incubating the SLB for 1 h with 150 μL of a 1 mM quercetin or epinephrine solution. The SLB was then rinsed thoroughly with HEPES buffer, in order to remove non-membrane-bound electroactive molecules. Cyclic voltammograms were recorded after this procedure.

Quartz Crystal Microbalance. The gravimetric experiments were conducted in a 420 model CH Instruments electrochemical QCM.[42] The adsorption was carried out at 23 ± 1 °C onto an 8 MHz AT-cut quartz crystal coated with 100 nm of gold fitted in a one-compartment Teflon cell (CH Instruments).

Surface Plasmon Resonance. SPR measurements were carried out using a BIOSUPLAR 400T compact SPR sensor manufactured by Analytical μ-Systems. The real-time monitoring of lipid adsorption and interaction is obtained using slope mode with the help of a peristaltic pump (ISMATEC) which kept the flow rate at 30 μL/min.

Cyclic Voltammetry. Electrochemical assays were conducted using a Parstat 2263 electrochemical station (Ametek, Princeton Applied Research) and a three-electrode Teflon cell fitted with the gold slide as working electrode, a saturated calomel electrode (SCE) as reference electrode, and a platinum foil as secondary electrode. The geometric area of the working electrode was determined to be 0.50 cm^2. The electrolyte solutions were degassed with pure nitrogen before each experiment.

Surface concentration of adsorbed electroactive species was determined by integrating the area under the oxidation (for quercetin and epinephrin) or reduction (MUA and Cys) peak, after subtracting the charging current baseline:[43]

$$\Gamma = \frac{Q}{nFA} \quad (1)$$

where Γ (mol/cm^2) is the surface coverage, Q is the charge in coulombs, n is the number of electrons transferred, F is Faraday's constant, and A is the electrode area.

Atomic Force Microscopy. AFM measurements were performed in liquid at 23 ± 2 °C using a Multimode Nanoscope IIIa microscope (Digital Instruments, Veeco). Topography images were obtained in tapping mode at a scan rate close to 1.8 Hz. For this purpose, silicon nitride cantilevers (SNL, ca. 0.35 N/m spring constant, Bruker) with a resonance frequency of about 26 kHz in liquid were used. AFM images and the topographical profiles shown are representative of the behavior of each system. For each system, three or more independent samples were studied.

Ellipsometry. Ellipsometric measurements were performed at 70° using a SE 400 ellipsometer (Sentech Instruments) equipped with a He−Ne laser (632.8 nm). The thickness of the lipid layers was estimated from the variation of the ellipsometric parameters (Ψ and Δ) before and after vesicle deposition, using a three-phase model.[44,45] The thickness of lipid films was estimated by fixing the real part of the refractive index at 1.5, a value frequently employed for hydrocarbon layers and determined to be the refractive index for gel lipids,[46] which are expected to be nearly transparent, with very low extinction coefficients at the working wavelength.

Fluorescence Spectroscopy. A battery of LUV samples differing in their lipid compositions (pure fluid, pure gel, fluid/gel, l_o/l_d, and l_o systems at final lipid concentration of 1 mM and 3 mM) was prepared in 10 mM HEPES buffer, and the interaction of epinephrine with each of them was evaluated by fluorescence spectroscopy, making use of epinephrine intrinsic fluorescence. Epinephrine was prepared in HEPES buffer, and its concentration was first determined spectrophotometrically. Epinephrine was added to lipid solutions to a final concentration of ~0.11 mM. To carry out fluorescence spectroscopy measurements, a Horiba Jobin Yvon Fluorolog Tau 3-22 spectrofluorimeter was used. The experiments were conducted at 23 ± 1 °C. For steady-state measurements, the excitation and emission

dx.doi.org/10.1021/la503086a | Langmuir 2014, 30, 12627−12637

wavelengths were fixed at 279 and 309 nm, respectively, or scanned in the case of excitation and emission spectra acquisition. The steady-state anisotropy ($\langle r \rangle$) was determined as in ref 46. The bandwidths were 3 nm for spectral acquisition and of 6.5 nm for fluorescence anisotropy measurements in both excitation and emission. An adequate blank was subtracted from each intensity reading. For time-resolved measurements by the single photon counting technique, a nanoLED N-280 light source (Horiba Jobin Yvon) was used for the excitation of epinephrine at 279 nm and emission wavelength was set to 309 nm with a bandwidth of 6 nm and a time scale of 0.05552 ns/channel. The individual analysis (after subtraction of a blank decay) of the fluorescence decays was performed using a sum of 2 exponentials. Further details on the measurement and analysis of fluorescence decays can be found in ref 47.

RESULTS

Formation of Cys SAM on Gold Surfaces. Gold surfaces become rapidly hydrophobic when exposed to air, and thus, the relative hydrophilicity created by the cleaning procedure is only active for a short period of time. In order to generate hydrophilic surfaces stable over time, MUA and Cys were employed here as modifying agents. These two molecules will predictably generate SAMs differing in their compactness as suggested by their chemical structure, namely, the length of their hydrocarbon chain, and consequently with different ability to block the access of redox species to the metal. Hence, the blocking effect of each monolayer to the redox process of the $Fe(CN)_6^{3-}/Fe(CN)_6^{4-}$ system was evaluated by cyclic voltammetry (Figure 1a). MUA totally suppresses the redox signal by hindering the access of ferricyanide to the electrode surface, which shows that it is a highly dense and compact monolayer. Conversely, the Cys-based monolayer does not appear to influence the process of electronic exchange. The electrochemical reductive desorption of sulfur from both SAMs shows that MUA detaches from the surface at a more negative potential than do Cys molecules (Figure S1a, Supporting Information). This is explained by lateral van der Waals interactions established between the hydrocarbon chains of adjacent attached molecules, which stabilize the monolayer. The integration of the reductive desorption peaks from Figure S1a allows computing the surface coverage (eq 1) of each monolayer. The values retrieved from these calculations are $\sim 6.5 \times 10^{-10}$ mol/cm^2 for MUA and $\sim 4.5 \times 10^{-10}$ mol/cm^2 for Cys, showing that MUA generates a more compact and dense monolayer, in total agreement with the blocking behavior toward the redox process of ferricyanide discussed above.

The redox process of the positively charged $Ru(NH_3)_6^{3+}/Ru(NH_3)_6^{2+}$ on a Cys-modified gold surface was also studied (Figure S1b). As for the negatively charged ferricyanide, the electrochemical process was not affected, indicating a surface that should be globally neutral (zwitterionic). In fact, considering the pK_a of the carboxylic (~2.05) and amine (~10.25) groups, L-cysteine is globally neutral at pH 7.4 despite its negative and positive charges. In nature, membrane lipids are either zwitterionic or anionic. Thus, the zwitterionic nature of the surface in Cys-modified gold might be an extremely important feature for the formation of stable SLBs containing both zwitterionic and anionic lipids, as will be shown later in this work for the biologically relevant lipid ganglioside GM1.

The fact that gold modification with Cys does not suppress the redox processes at the electrode surface matches one of the fundamental requisites for a biomimetic platform for redox studies of bioactive molecules, in opposition to the previously employed SAM of MUA.[16,23] At this stage, it is crucial to evaluate if it is possible to form a planar and continuous SLB with phase separation on top of Cys modified gold surfaces.

Forming Multicomponent SLB with Nanodomains onto Cys Modified Gold Electrodes. A flat gold surface with predominant (111) orientation was used to test the ability to form planar and continuous raft-containing SLB. The ternary lipid mixture DOPC/DPPC/Chol 2:2:1 was used, and the formation of SLB on each modified gold surface was characterized by AFM, cyclic voltammetry, and ellipsometry.

AFM is entirely suitable to depict details in lipid film topography[12,48] such as nano/microdomains. In Figure 2, AFM images of the lipid mixture deposited on either Cys- or MUA-modified gold are shown. In both cases, continuous and uniform lipid films containing lateral heterogeneities with a height difference of about 1.5−1.8 nm are clearly observed. This height difference is the one expected for l_o versus l_d membrane lipid domains, in agreement with the ones found for other SLB formed on gold[23] or other substrate, such as mica.[48] The ordered domains on both SAMs correspond to the bilayer regions of higher thickness, clearly depicted in both images, indicating that the formation of SLB with phase separation mimicking cell lipid rafts was successfully achieved.

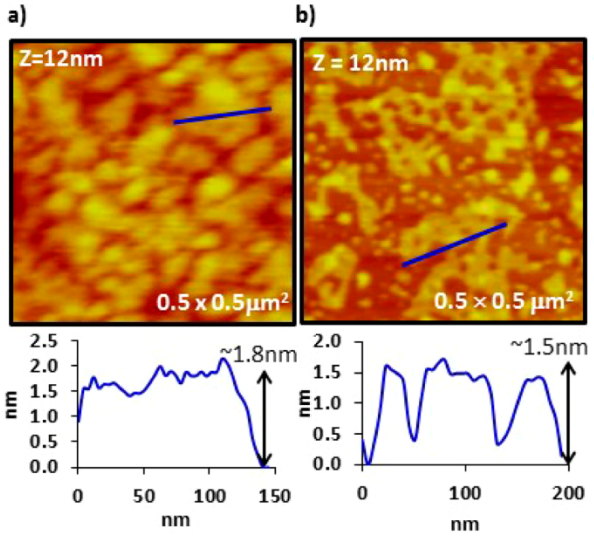

Figure 2. AFM topographic images of DPPC/DOPC/Chol (2:2:1 mol ratio) SLB onto (a) Cys- and (b) MUA-modified gold surfaces. AFM was performed in tapping mode and in HEPES buffer solution. Topographic profiles correspond to the colored line drawn in each figure.

AFM characterization allows the detailed examination of small areas of the sample. To acquire large scale information in terms of surface coverage, blocking properties, integrity, and compactness, ellipsometry and cyclic voltammetry were employed. Ellipsometry is an optical technique often used to determine the thickness of thin films formed on an optically active substrate such as gold.[23,45,49] Ellipsometry probes a large area of the sample, and thus, the thickness value retrieved represents an average of the bilayer. Ellipsometric data, compiled in Table 1, revealed a mean bilayer thickness of almost 5 nm, for both fluid/gel and l_o/l_d SLBs formed on top of MUA- and Cys-modified gold. This value lies in the range expected for a bilayer, which may vary between 4 and 6 nm in

Table 1. Average Ellipsometric Parameters (Ψ, Δ), Estimated Thickness (d), and Extinction Coefficient (k) for Single- And Multicomponent SLB on Differently Modified Au(111) Electrodes Prepared under Different Conditions, As Described in the Materials and Methods[a]

system	Ψ/deg	Δ/deg	d/nm	k
bare	43.1 ± 0.4	106.5 ± 0.6		
MUA/SLB (l_o/l_d)	42.9 ± 0.3	101.6 ± 1.8	4.7 ± 1.2	0.14 ± 0.08
Cys/SLB (l_o/l_d)	42.5 ± 0.1	101.4 ± 1.0	4.6 ± 0.9	0.22 ± 0.05
Cys/SLB (GM1)	43.1 ± 0.1	101.9 ± 1.1	5.0 ± 1.1	0.08 ± 0.06
Cys/SLB (fluid/gel)	43.0 ± 0.1	102.8 ± 1.4	4.3 ± 1.6	0.15 ± 0.03
Cys/SLB (gel)	43.2 ± 0.14	101.4 ± 1.6	6.3 ± 1.4	0.09 ± 0.02
Cys/SLB (fluid)	43.3 ± 0.16	103.4 ± 0.8	3.9 ± 0.5	0.09 ± 0.06

[a]The bilayer containing GM1 has the following composition: DOPC/DPPC/Chol (2:2:1 mol ratio) with 10% GM1.

most cases,[12,23,48,50] suggesting the formation of a continuous bilayer spread throughout the electrode.

The ellipsometric data are in fine agreement with our previous AFM results.[23,48] The thickest bilayer corresponds to pure DPPC gel, for which a value of 6.2 nm has been reported,[48] due to the high order of saturated acyl chains. Mean thicknesses in Table 1 follow the expected order, with the fluid bilayer being the thinnest, reflecting the disordered unsaturated chains of fluid DOPC. Gel/fluid and l_o/l_d bilayers have intermediate values, with the latter being consistent with the domain thicknesses measured by AFM (Figure 2a). The l_o/l_d lipid bilayer containing 10% GM1 has a mean thickness slightly higher than that of the same SLB without the ganglioside, which expresses the contribution of tetraglycosyl headgroup of GM1 for the average thickness of the lipid film.

The redox process of the reversible system $Fe(CN)_6^{3-}/Fe(CN)_6^{4-}$ was followed by cyclic voltammetry as a means to evaluate the blocking properties of the lipid film formed on the electrode surface. The formation of a continuous, well organized, and highly packed SLB should exert a total blocking, suppressing the redox signal.[15,23,27] For the lipid bilayer formed on top of a MUA-modified surface, a total blocking effect was observed (Figure 1b, red curve). However, in this situation, and as previously mentioned, the very compact nature of the SAM per se leads to a similar blocking (Figure 1a, red curve). As noted before, this is a limitation of MUA-modified gold for SLB properties evaluation and application in redox studies of electroactive biomolecules (and presumably of any other very compact SAM modification).

A different behavior was observed for the SLB on Cys SAM (Figure 1b, blue curve). This SLB also hinders the redox process; however, since the Cys SAM alone did not have any blocking effect (Figure 1a, blue curve), the changes in the current intensity of both oxidation and reduction peaks in the presence of the SLB can be safely assigned to the lipid bilayer itself. In fact, the almost complete inhibition of the redox signal obtained suggests that the bilayer is organized, compact, and spread throughout the entire electrode surface, all crucial features in the development of improved biomimetic platforms. One aspect that should be noted is that an SLB of the same lipid composition formed directly on bare gold (Figure 1b, green curve) has a much weaker barrier effect on the redox process of $Fe(CN)_6^{3-}/Fe(CN)_6^{4-}$. This shows the importance of modifying the gold surface in order to favor the spreading of a lipid bilayer on top of the metal.

The pure fluid and gel lipid bilayers on Cys-modified gold exhibited a strong blocking to the ferricyanide redox process (Figure 1c, green and orange curves, respectively), which shows that these SLBs are also organized, continuous, and spread throughout the electrode, corroborating the mean thicknesses estimated by ellipsometry. The slightly lower blocking properties observed for the ternary lipid bilayer should be due to its lateral heterogeneities resembling lipid rafts, and not to defects on the bilayer, as once more supported by ellipsometric data. Furthermore, the data reveals the ability of cysteine SAMs to sustain lipid bilayers of all the different phases and phase coexistence that are biologically relevant, constituting a new tool to advance biomembrane research.

Gangliosides are an important family of sphingolipids, acting as cellular receptors and markers of functional membrane domains, and they all have negative net charge due to sialic acid residues (the common structural feature to all gangliosides).[51] GM1, in particular, is an important raft marker used in many biomembrane studies in both model[52] and cellular membranes.[53] A serious limitation of raft-containing SLBs on bare gold is their instability in the presence of GM1. Our previous results using bare gold as a substrate for deposition with a DOPC/DPPC/Chol 2:2:1 SLB containing 10% GM1 have shown a detachment of the SLB formed directly on gold with the successive voltammetric scans.[23] This was attributed to the negative charge of GM1 which was unfavorable for the interaction of the bilayer with hydrophobic gold. Hence, we have now conducted an experiment with the ternary SLB also containing 10% GM1 assembled on a Cys-modified surface. In this case, the SLB deposited on Cys SAM was stable over the potential range during successive cyclic voltammetry runs (Figure 1d), contrary to the case of bare gold. Cys modification is thus playing a pivotal role by contributing to the stability of a SLB containing GM1, possibly through the electrostatic bridge between the negative carboxylic group of L-cysteine and GM1 mediated by Ca^{2+}.

The affinity and kinetics of vesicle adsorption onto a short and not very compact Cys monolayer is the same as that for a compact long MUA monolayer, as shown by QCM and SPR experiments (Supporting Information, section II). The joint application of AFM, ellipsometry, and cyclic voltammetry provided the evidence for the formation of stable multicomponent SLB with nanodomains on Cys-modified (111) gold electrodes, which are planar, continuous, compact and organized structures.

Interactions of Quercetin with Supported Lipid Bilayers. Quercetin is a flavonoid and a powerful antioxidant. It has been shown that quercetin establishes hydrogen bonds with lipid polar head regions, leading to a decrease in packing.[35] It also promotes a fluidization of the hydrophobic core of the membrane,[35,37] leading to a decrease of the main phase transition temperature.[38] It has been reported that quercetin increases lipid bilayer conductance and capacitance[37] and

dx.doi.org/10.1021/la503086a | Langmuir 2014, 30, 12627−12637

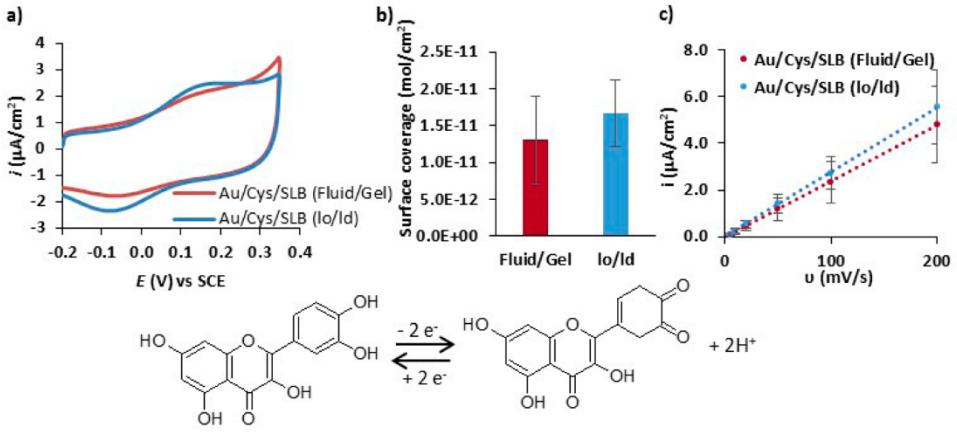

Figure 3. (a) Cyclic voltammograms for the redox process of membrane-bound quercetin in Au(111)/Cys/SLB in HEPES buffer 50 mM, pH 7.4, at a scan rate of 50 mV/s. (b) Surface coverage of quercetin interacting with lipid membranes of different composition, and the respective (c) graphical representation of peak current density versus scan rate for quercetin in a fluid/gel ($i = 0.0238\upsilon$ μA/cm^2; $R^2 = 0.9996$) and l_o/l_d ($i = 0.0277\upsilon$ μA/cm^2; $R^2 = 0.9996$) environment. Data in panels (b) and (c) come from six independent experiments, and the mean values are shown with the respective standard deviation.

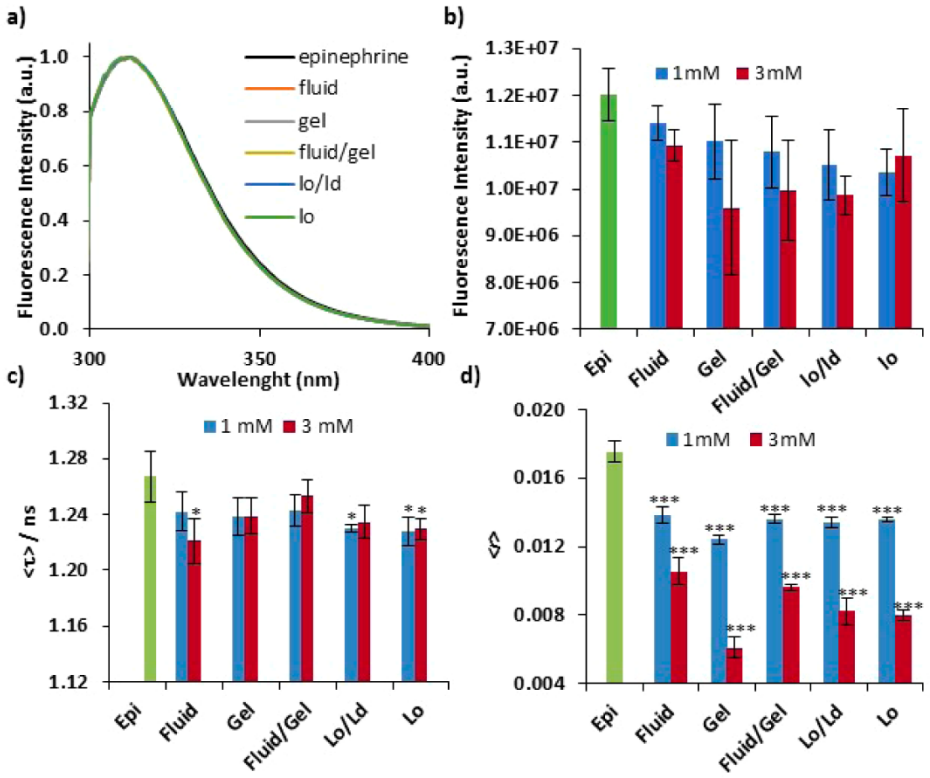

Figure 4. Fluorescence spectroscopy of epinephrine in different lipid environments: HEPES buffer in the absence and in the presence of LUVs with total lipid concentrations of 1 and 3 mM, with different lipid phases, as indicated. For the corresponding lipid compositions, see Materials and Methods. Normalized emission spectra (λ_{ex} = 279 nm) of epinephrine are shown in panel (a). Changes in steady-state fluorescence intensity and anisotropy (λ_{ex} = 279 nm; λ_{em} = 309 nm) and in fluorescence mean lifetime (λ_{ex} = 278 nm; λ_{em} = 309 nm) are shown in panels (b)−(d), respectively (average of at least three independent samples; error bars = standard deviation). Experiments were carried out at room temperature (23 ± 1 °C). Student's t test significance values compare each system with epinephrine in the absence of lipid bilayers (green bar): $^*p < 0.05$, $^{***}p < 0.001$.

promotes the formation of pores or defects in SLBs.[36] Here, it is intended to assess the redox process of membrane bound quercetin in two different lipid environments: fluid/gel phase separation and l_o/l_d phase separation. Quercetin was allowed to interact, and after incubation with the lipid bilayers all the non-membrane-bound quercetin was removed from the system as described in the Materials and Methods. Cyclic voltammograms of quercetin incorporated into different lipid environments are shown in Figure 3a. The electrochemical studies conducted on the modified electrodes show that the number of quercetin

dx.doi.org/10.1021/la503086a | Langmuir 2014, 30, 12627−12637

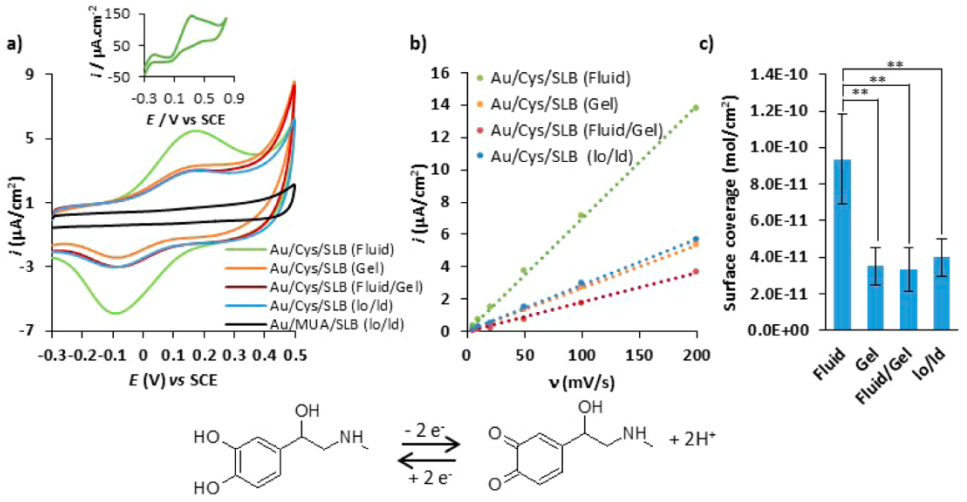

Figure 5. (a) Cyclic voltammograms for the redox process of membrane-bound epinephrine in Au(111)/Cys/SLB in HEPES buffer 50 mM, pH 7.4, at a scan rate of 50 mV/s. (b) Graphical representation of peak current density versus scan rate of epinephrine interacting with lipid membranes of different composition: fluid ($i = 0.070\upsilon$ µA/cm^2; $R^2 = 0.9991$); gel ($i = 0.027\upsilon$ µA/cm^2; $R^2 = 0.9976$); fluid/gel ($i = 0.018\upsilon$ µA/cm; $R^2 = 0.9931$); l_o/l_d ($i = 0.029\upsilon$ µA/cm^2; $R^2 = 0.9993$); and the respective (c) surface coverage of epinephrine in the same conditions. Values in panel (c) are the mean ± standard deviation of at least four independent experiments. Student's t test significance: $^{**}p < 0.01$.

molecules bound to each lipid bilayer is similar, and thus, no significant difference was observed between a membrane with fluid/gel (surface coverage (Γ) = $1.3 \times 10^{-11} \pm 0.6 \times 10^{-11}$ mol/cm^2) coexistence and one with l_o/l_d ($\Gamma = 1.7 \times 10^{-11} \pm 0.5 \times 10^{-11}$ mol/cm^2) phase separation (Figure3b). However, when inserted into a membrane environment, the redox process of quercetin is not as reversible (redox peak separation, ΔE_p, is ~0.23 V for both fluid/gel and l_o/l_d systems) as the one observed for free quercetin in solution ($\Delta E_p \sim 0.10$ V).

The representation of the oxidation peak current versus the potential sweep rate yields a linear relationship (Figure 3b), in accordance to equation 2:[54]

$$i_p = \frac{n^2F^2A\Gamma\nu}{4RT} \quad (2)$$

where i_p stands for current density, n is the number of electrons involved in the redox process, F is the Faraday constant, A is the electrode area, Γ is the surface coverage of the electroactive species, and ν is the sweep rate. This equation describes a system where the electroactive species are immobilized close to the surface and therefore the electron transfer process is not controlled by diffusion, thus proving that the multicomponent SLBs can accommodate quercetin. Also, it demonstrates that our platform is suitable to follow the redox process of membrane-interacting bioelectroactive molecules.

Evidence for Epinephrine Interaction with Different Membrane Environments. To the best of our knowledge, there are no studies/evidence for a direct epinephrine–lipid bilayer interaction. Thus, we evaluated the interaction of epinephrine with lipid vesicles in suspension, using well established biophysical methods in membrane–biomolecule interaction studies. In this case, using epinephrine intrinsic fluorescence, it was possible to carry out this study by fluorescence spectroscopic techniques without the use of any added probe. Two final lipid concentrations were employed: a "typical" 1 mM and a higher concentration of 3 mM to enhance the possible interaction. Figure 4a displays the normalized emission spectra for epinephrine, obtained in the presence of different lipid environments. Such representation allows one to easily inspect eventual spectral shifts of epinephrine emission. Such shifts were not observed regardless of the lipid composition used. Moreover, only a slight decrease in fluorescence intensity was observed (Figure 4b). Also, the mean fluorescence lifetime of epinephrine (Figure 4c) becomes slightly shorter in the presence of the lipid bilayers, confirming that the interaction induces a small decrease of the fluorescence quantum yield of epinephrine. The changes in fluorescence anisotropy (Figure 4c) also indicate that epinephrine is able to interact, although not very strongly, with lipid bilayers exhibiting distinct compositions and phases. Fluorescence anisotropy is usually used as a measure of the rotational motions of fluorophores, and of their immobilization in the membrane. However, in the present case, the small anisotropy value (0.018) of free epinephrine becomes even smaller in the presence of lipid vesicles. This unusual behavior cannot be interpreted as a restricted rotational dynamics of the hormone, which would lead to a higher anisotropy. Instead, taken together with the decrease in quantum yield, the results suggest that there is a change in the lowest energy electronic transition upon incorporation in the membrane, which is probably due to the less polar environment surrounding the molecule. The interaction is more effective at the highest lipid concentration (3 mM) revealing that at 1 mM lipid concentration a significant portion of the hormone still remains in solution.

Using the New Biomimetic Platform to Detect Membrane-Immobilized Epinephrine with Increased Redox Stability. The fluorescence spectroscopy experiments have shown that epinephrine and lipid membranes interact, although weakly. However, it was not possible to demonstrate epinephrine immobilization in the membrane. Thus, the Cys-SAM/SLB was used as a biomimetic interface to conduct redox studies of epinephrine in a membrane environment, either single-phase or containing domains. These studies with epinephrine were carried out exactly as for quercetin, to guarantee that before cyclic voltammetric experiments all the unbound epinephrine had been removed. The results are

dx.doi.org/10.1021/la503086a | Langmuir 2014, 30, 12627–12637

shown in Figure 5. For all the Au/Cys/SLB systems studied, the two electron, two proton redox conversion of hydroquinone to quinone forms of epinephrine was detected (Figure 5a). The oxidation peak potentials (ca. 0.165 V) are very similar to those reported for covalently attached catecholamine on modified gold at pH 7,[55] proving that this interface exhibits a high performance for the detection of electroactive molecules interacting with the SLB. For epinephrine adsorbed to a ternary lipid bilayer formed on top of a MUA modified electrode, no redox process could be detected (Figure 5a, black line). The absence of signal is due to the blocking effect of the very compact MUA monolayer as described above for ferricyanide.

Considering the biological importance of membrane lipid composition and phase behavior, we made a thorough examination of epinephrine redox behavior in different lipid environments: fluid (DOPC), gel (DPPC), fluid/gel coexistence (DOPC/DPPC 1:1), and l_o/l_d coexistence (DOPC/DPPC/Chol 2:2:1). This was only possible due to the versatility of this biomimetic platform, which can support stable and high quality SLBs with varied phase behavior (Table 1 and Figure 1). For all the systems, the representation of the maximum current of the oxidation peak versus the scan rate yields a linear relationship, which means that, as observed for quercetin, the electroactive species is immobilized close to the surface, proving that both the single and multicomponent SLB can accommodate epinephrine (Figure 5b). It should be remembered that such immobilization could not be demonstrated from the fluorescence anisotropy results. Furthermore, this linear relationship also proves the stability of the different SLB under the potential range studied and with the consecutive potential sweep. The highest surface concentration of membrane-bound epinephrine was obtained for the pure fluid bilayer (9.3×10^{-11} mol/cm^2), and significantly differed from all the others (Figure 5c). This effect is not due to the presence of a bilayer with defects, because this SLB has totally suppressed the $Fe(CN)_6^{3-}/Fe(CN)_6^{4-}$ redox signal (Figure 1c).

As depicted from the inset of Figure 5a, the redox process of free epinephrine in solution (pH 7.4) is not reversible within the studied potential range. Such electrochemical behavior is attributed to epinephrine instability at neutral pH which oxidizes and tends to cyclize and/or form polymers.[56] In fact, covalently attached epinephrine to modified gold trough amine linkage exhibits a very reversible redox behavior, since the compound is no longer able to cyclize.[57,58] Returning to membrane-bound epinephrine (Figure 5a), it is clear that the redox process is more reversible in this potential range with a redox peak potential ($E_{1/2} \sim 0$ V) identical in all lipid environments and $\Delta E_p \sim 0.25$ V. This shows the important role played by the SLB in preventing epinephrine oxidative degradation, pointing to a possible role of the membrane to promote catecholamine stability. Thus, the lipid-based platform not only creates a biomimetic environment suitable to detect and study bioelectroactive molecules but also in this specific situation it stabilizes the molecule.

Globally, it was possible to obtain a very clear electrochemical signal of a molecule that, according to the fluorescence spectroscopic measurements, interacts very weakly with lipid bilayers. To detect appreciable changes in a fluorescence parameter, a concentration of 3 mM for the lipid had to be used. In the novel biomimetic platform, only a planar lipid bilayer covering the electrode was present; that is, the amount of lipid is about 3 orders of magnitude lower. In addition, there was an extensive washing step, implying that the unbound hormone was not present. Yet, the membrane bound epinephrine could still be detected, Taking into account the amount of epinephrine adsorbed on the SLB, it is possible to estimate a mole-fraction partition coefficient of epinephrine (K_p) (Supporting Information, section III) for the different membrane environments, which in the case of SLB in the l_d phase yielded the highest value ($K_p = 1.13 \times 10^4$). The possibility of estimating a membrane/water partition coefficient from cyclic voltammetric data offered by this platform allows one to interrelate quantitatively electrochemical and fluorescence spectroscopy data (Supporting Information, section III). Ultimately, and considering that a large amount of epinephrine remains in a free state (in fluorimetric experiments), this correlation allows one to infer a negative anisotropy value for epinephrine in its membrane-bound state for all lipid environments studied, suggesting that the decrease in quantum yield is indeed due to a different electronic transition with a transition moment approximately perpendicular to the one in aqueous solution.

DISCUSSION

Building lipid bilayers on gold surfaces, whether modified or not, is still a challenge. Although the formation of single-phase[12] and multiple-phase[23] SLBs directly on gold has been achieved, these assemblies did not meet an important requirement for biomimetic purposes: a spatial separation between the gold and the lipid bilayer in order to reduce the hydrophobic influence of the metal surface, thus enabling, for example, the functional incorporation of membrane proteins or other biomolecules. In order to overcome such a limitation, several surface modifications have been developed.[13,16,17,25,27,59] However, many of those modifications, as it is in the case of thiolipids,[25,59] may hamper the incorporation of large proteins in a functional manner and also affect lateral diffusion of lipids. Additionally, as demonstrated in this work, surface modifications that will originate a compact SAM (as a result of the relatively long hydrocarbon chain of the modifying agent), such as MUA, tend to inhibit any electronic transfer. Therefore, one of our main goals was to develop a perfectly functional surface modification that would prevent direct interaction of the lipids with the metal surface but still allowing electron transfer processes of electroactive species interacting with the membrane. In addition, it would be essential that stable, planar, compact, organized, continuous SLBs covering the electrode could be assembled. L-Cysteine as a gold modifying agent promoted the formation of SLBs with those features, made from a variety of lipid compositions and phases. Moreover, in opposition to MUA, L-cysteine did not hamper any of the electronic transfer processes studied which renders it suitable for the development of biomimetic interfaces with the purpose of biosensing or study redox processes of bioactive molecules in cellular membrane-like environment. In addition, in the case of a ternary-component SLB exhibiting lateral phase separation onto a Cys-modified gold surface, it was possible to directly image the nanodomains differing in height by about 1.5 nm using AFM. The principles governing the formation of lipid domains in cells is still an active field of research,[60] and therefore, this platform can be used for future studies concerning lipid rafts and membrane domains.

To obtain fundamental information relating the influence of the lipid membrane in the redox process of biological electroactive molecules, the applicability of the platform was

dx.doi.org/10.1021/la503086a | Langmuir 2014, 30, 12627−12637

first established for a well characterized compound, quercetin, and afterward, we addressed the undisclosed interaction of the hormone epinephrine with lipid bilayers. For the latter, the fluorescence spectroscopy studies showed that there is a weak interaction which is difficult to detect and even more so to quantify. The use of the platform allowed us to obtain the amount of membrane-immobilized epinephrine molecules, and determine for which type of lipid bilayer it has a stronger affinity. These results are a contribution for our understanding of hormone−membrane interactions. Moreover, electrochemical and fluorimetric data can be correlated, and the determination of a partition coefficient of epinephrine for membrane from surface coverage values allowed us to deduce a negative anisotropy value for membrane-bound epinephrine. The transition from a positive, in the free state, to a negative value, when membrane-bound, in epinephrine anisotropy, most likely, reports a large reorientation of the transition dipole moment. However, the major finding was that the membrane confers stability to epinephrine molecules, preventing their chemical degradation at the physiological pH. Moreover, properties important for the kinetic and thermodynamic control of redox processes, such as lateral diffusion and transversal location in the lipid bilayer, might be strongly influenced by the lipid composition. Guidelli and coworkers have recently shown how distinct lipid compositions and domains (fluid/gel, DOPC/palmitoylsphingomyelin (PSM); l_o/l_d, DOPC/PSM/Chol) have a profound influence both in the redox properties of ubiquinone-10 (UQ10) and in its distribution throughout the membrane.[9]

One of the main applications of bilayer assemblies on metal surfaces is the study of redox processes involving membrane-associated small molecules, such as UQ10,[6,9] flavonoids, and cathecolamine hormones or proteins, such as cytochrome *c* and P450,[7,8] and myoglobin.[7] The platform developed in this work has the required sensitivity to develop such studies.

CONCLUSIONS

The work presented shows that a short and not completely packed L-cysteine monolayer is a suitable gold modification to investigate lipid bilayer properties and to conduct redox studies concerning electroactive molecules. The SLBs are stable, under potential cycling, even when containing an anionic lipid, such as the paradigmatic raft-marker ganglioside GM1. The possibility to build high quality SLBs with varied physical properties (e.g., gel, fluid, l_o/l_d) is certainly advantageous when working with membrane proteins in order to create the perfect match between the hydrophobic moieties of the lipid bilayer and the protein, maximizing its activity.

We have also demonstrated the ability of epinephrine to interact, although weakly, with lipid membranes in suspension. However, epinephrine immobilization in the membrane could only be clearly detected and quantified on the Cys-Au based biomimetic platform. Moreover, the chemical stability of the hormone in a lipid environment versus in aqueous solution was also demonstrated. Thus, this study has also contributed to the "lipid bilayer as a catalyst of hormone−receptor interaction" hypothesis, which thus far did not consider the interaction with the membrane as a possible means of maintaining the hormone integrity, and will potentially contribute to clarify other relevant biological questions.

ASSOCIATED CONTENT

Supporting Information

Electrochemical reductive desorption of MUA and Cys monolayers; electrochemical behavior of negatively or positively charged redox probes on a Cys SAM; determination of QCM adsorbing masses; estimation of the mass and number of molecules of an SLB deposited on a 1 cm^2 electrode; epinephrine membrane/water partition coefficient and its quantitative relation to fluorescence spectroscopic measurements. This material is available free of charge via the Internet at http://pubs.acs.org.

AUTHOR INFORMATION

Corresponding Authors

*E-mail: anaviana@fc.ul.pt.
*E-mail: rodrigo.almeida@fc.u.pt.

Notes

The authors declare no competing financial interest.

ACKNOWLEDGMENTS

This work was financed by Portuguese national funds through FCT: Ph.D. Fellowship SFRH/BD/64442/2009, Grant PEst-OE/QUI/UI0612/2013, and IF2012 and 2013 initiatives (POPH, Fundo Social Europeu).

REFERENCES

(1) Reimhult, E.; Kumar, K. Membrane biosensor platforms using nano- and microporous supports. *Trends Biotechnol.* **2008**, *26*, 82−89.
(2) Zheng, L.; Xiong, L.; Zheng, D.; Li, Y.; Liu, Q.; Han, K.; Liu, W.; Tao, K.; Yang, S.; Xia, J. Bilayer lipid membrane biosensor with enhanced stability for amperometric determination of hydrogen peroxide. *Talanta* **2011**, *85*, 43−48.
(3) Michaloliakos, A. L; Nikoleli, G. P.; Siontorou, C. G.; Nikolelis, D. P. Rapid flow injection electrochemical detection of Aroclor 1242 using stabilized lipid membranes with incorporated sheep anti-PCB antibody. *Electroanalysis* **2012**, *24*, 495−501.
(4) Fritzen-Garcia, M. B.; Zoldan, V. C.; Oliveira, I. R. W. Z.; Soldi, V.; Pasa, A. A.; Creczynski-Pasa, T. B. Peroxidase immobilized on phospholipid bilayers supported on Au(111) by DTT self-assembled monolayers: Application to dopamine determination. *Biotechnol. Bioeng.* **2013**, *110*, 374−382.
(5) Peng, Z. Q.; Tang, J. L.; Han, X. J.; Wang, E. K.; Dong, S. J. Formation of a supported hybrid bilayer membrane on gold: A sterically enhanced hydrophobic effect. *Langmuir* **2002**, *18*, 4834−4839.
(6) Jeuken, L. J. C.; Weiss, S. A.; Henderson, P. J. F.; Evans, S. D.; Bushby, R. J. Impedance spectroscopy of bacterial membranes: Coenzyme-Q diffusion in a finite diffusion layer. *Anal. Chem.* **2008**, *80*, 9084−9090.
(7) Rusling, J. F. Enzyme bioelectrochemistry in cast biomembrane-like films. *Acc. Chem. Res.* **1998**, *31*, 363−369.
(8) Liu, Y. X.; Wei, W. Z. Detection of cytochrome *c* at biocompatible nanostructured Au-lipid bilayer-modified electrode. *Anal. Sci.* **2008**, *24*, 1431−1436.
(9) Becucci, L.; Scaletti, F.; Guidelli, R. Gel-phase microdomains and lipid rafts in monolayers affect the redox properties of ubiquinone-10. *Biophys. J.* **2011**, *101*, 134−143.
(10) Ma, W.; Li, D.-W.; Sutherland, T. C.; Li, Y.; Long, Y.-T.; Chen, H.-Y. Reversible redox of NADH and NAD(+) at a hybrid lipid bilayer membrane using ubiquinone. *J. Am. Chem. Soc.* **2011**, *133*, 12366−12369.
(11) Lingwood, D.; Simons, K. Lipid rafts as a membrane-organizing principle. *Science* **2010**, *327*, 46−50.
(12) Li, M.; Chen, M.; Sheepwash, E.; Brosseau, C. L.; Li, H.; Pettinger, B.; Gruler, H.; Lipkowski, J. AFM studies of solid-supported lipid bilayers formed at a Au(111) electrode surface using vesicle

fusion and a combination of Langmuir-Blodgett and Langmuir-Schaefer techniques. *Langmuir* **2008**, *24*, 10313−10323.
(13) Ekeroth, J.; Konradsson, P.; Hook, F. Bivalent-ion-mediated vesicle adsorption and controlled supported phospholipid bilayer formation on molecular phosphate and sulfate layers on gold. *Langmuir* **2002**, *18*, 7923−7929.
(14) Wang, X.; Shindel, M. M.; Wang, S. W.; Ragan, R. A facile approach for assembling lipid bilayer membranes on template-stripped gold. *Langmuir* **2010**, *26*, 18239−18245.
(15) Oberts, B. P.; Blanchard, G. J. Formation of air-stable supported lipid monolayers and bilayers. *Langmuir* **2009**, *25*, 2962−2970.
(16) Ip, S.; Li, J. K.; Walker, G. C. Phase segregation of untethered zwitterionic model lipid bilayers observed on mercaptoundecanoic-acid-modified gold by AFM imaging. *Langmuir* **2010**, *26*, 11060−11070.
(17) Kycia, A. H.; Wang, J. P.; Merrill, A. R.; Lipkowski, J. Atomic force microscopy studies of a floating-bilayer lipid membrane on a Au(111) surface modified with a hydrophilic monolayer. *Langmuir* **2011**, *27*, 10867−10877.
(18) Malinsky, J.; Opekarova, M.; Grossmann, G.; Tanner, W. Membrane microdomains, rafts, and detergent-resistant membranes in plants and fungi. *Annu. Rev. Plant Biol.* **2013**, *64*, 501−529.
(19) de Almeida, R. F. M.; Fedorov, A.; Prieto, M. Sphingomyelin/phosphatidylcholine/cholesterol phase diagram: Boundaries and composition of lipid rafts. *Biophys. J.* **2003**, *85*, 2406−2416.
(20) Bunge, A.; Muller, P.; Stockl, M.; Herrmann, A.; Huster, D. Characterization of the ternary mixture of sphingomyelin, POPC, and cholesterol: Support for an inhomogeneous lipid distribution at high temperatures. *Biophys. J.* **2008**, *94*, 2680−2690.
(21) Veatch, S. L.; Keller, S. L. Miscibility phase diagrams of giant vesicles containing sphingomyelin. *Phys. Rev. Lett.* **2005**, *94*.
(22) de Almeida, R. F.; Borst, J.; Fedorov, A.; Prieto, M.; Visser, A. J. Complexity of lipid domains and rafts in giant unilamellar vesicles revealed by combining imaging and microscopic and macroscopic time-resolved fluorescence. *Biophys. J.* **2007**, *93*, 539−553.
(23) Marques, J. T.; De Almeida, R. F. M.; Viana, A. S. Biomimetic membrane rafts stably supported on unmodified gold. *Soft Matter* **2012**, *8*, 2007−2016.
(24) Inoue, M.; Digman, M. A.; Cheng, M.; Breusegem, S. Y.; Halaihel, N.; Sorribas, V.; Mantulin, W. W.; Gratton, E.; Barry, N. P.; Levi, M. Partitioning of NaPi cotransporter in cholesterol-, sphingomyelin-, and glycosphingolipid-enriched membrane domains modulates NaPi protein diffusion, clustering, and activity. *J. Biol. Chem.* **2004**, *279*, 49160−49171.
(25) Schiller, S. M.; Naumann, R.; Lovejoy, K.; Kunz, H.; Knoll, W. Archaea analogue thiolipids for tethered bilayer lipid membranes on ultrasmooth gold surfaces. *Angew. Chem., Int. Ed.* **2003**, *42*, 208−+.
(26) Kendall, J. K. R.; Johnson, B. R. G.; Symonds, P. H.; Imperato, G.; Bushby, R. J.; Gwyer, J. D.; van Berkel, C.; Evans, S. D.; Jeuken, L. J. C. Effect of the structure of cholesterol-based tethered bilayer lipid membranes on ionophore activity. *ChemPhysChem* **2010**, *11*, 2191−2198.
(27) Oberts, B. P.; Blanchard, G. J. Headgroup-dependent lipid self-assembly on zirconium phosphate-terminated interfaces. *Langmuir* **2009**, *25*, 13918−13925.
(28) Junghans, A.; Koper, I. Structural analysis of tethered bilayer lipid membranes. *Langmuir* **2010**, *26*, 11035−11040.
(29) Kunze, J.; Leitch, J.; Schwan, A. L.; Faragher, R. J.; Naumann, R.; Schiller, S.; Knoll, W.; Dutcher, J. R.; Lipkowski, J. New method to measure packing densities of self-assembled thiolipid monolayers. *Langmuir* **2006**, *22*, 5509−5519.
(30) Elson, E. L.; Fried, E.; Dolbow, J. E.; Genin, G. M. Phase separation in biological membranes: Integration of theory and experiment. *Annu. Rev. Biophys.* **2010**, *39*, 207−226.
(31) Beekmann, K.; Actis-Goretta, L.; van Bladeren, P. J.; Dionisi, F.; Destaillats, F.; Rietjens, I. A state-of-the-art overview of the effect of metabolic conjugation on the biological activity of flavonoids. *Food Funct.* **2012**, *3*, 1008−1018.
(32) Guerra-Araiza, C.; Alvarez-Mejia, A. L.; Sanchez-Torres, S.; Farfan-Garcia, E.; Mondragon-Lozano, R.; Pinto-Almazan, R.; Salgado-Ceballos, H. Effect of natural exogenous antioxidants on aging and on neurodegenerative diseases. *Free Radical Res.* **2013**, *47*, 451−462.
(33) Bonen, A.; Megeney, L. A.; McCarthy, S. C.; McDermott, J. C.; Tan, M. H. Epinephrine administration stimulates glut4 translocation but reduces glucose-transport in muscle. *Biochem. Biophys. Res. Commun.* **1992**, *187*, 685−691.
(34) Halliwill, J. R. Hypoxic regulation of blood flow in humans - Skeletal muscle circulation and the role of epinephrine. In *Hypoxia: Through the Lifecycle*; Roach, R. C., Wagner, P. D., Hackett, P. H., Eds.; Kluwer Academic/Plenum Publishers: New York, 2003; Vol. *543*, pp 223−236.
(35) Cieslik-Boczula, K.; Maniewska, J.; Grynkiewicz, G.; Szeja, W.; Koll, A.; Hendrich, A. B. Interaction of quercetin, genistein and its derivatives with lipid bilayers - An ATR IR-spectroscopic study. *Vib. Spectrosc.* **2012**, *62*, 64−69.
(36) Lu, X.; Liao, T.; Ding, L.; Liu, X.; Zhang, Y.; Cheng, Y.; Du, J. Interaction of quercetin with supported bilayer lipid membranes on glassy carbon electrode. *Int. J. Electrochem. Sci.* **2008**, *3*, 797−805.
(37) Movileanu, L.; Neagoe, I.; Flonta, M. L. Interaction of the antioxidant flavonoid quercetin with planar lipid bilayers. *Int. J. Pharm.* **2000**, *205*, 135−146.
(38) Sinha, R.; Gadhwal, M. K.; Joshi, U. J.; SrivaStava, S.; Govil, G. Interaction of quercetin with DPPC model membrane: Molecular dynamic simulation, DSC and multinuclear NMR studies. *J. Indian Chem. Soc.* **2011**, *88*, 1203−1210.
(39) Sargent, D. F.; Schwyzer, R. Membrane lipid phase as catalyst for peptide receptor interactions. *Proc. Natl. Acad. Sci. U. S. A.* **1986**, *83*, 5774−5778.
(40) Marques, J. T.; de Almeida, R. F. M.; Viana, A. S. Lipid bilayers supported on bare and modified gold - Formation, characterization and relevance of lipid rafts. *Electrochim. Acta* **2014**, *126*, 139−150.
(41) McClare, C. W. An accurate and convenient organic phosphorus assay. *Anal. Biochem.* **1971**, *39*, 527−530.
(42) Viana, A. S.; Kalaji, M.; Abrantes, L. M. Electrochemical quartz crystal microbalance study of self-assembled monolayers and multilayers of ferrocenylthiol derivatives on gold. *Langmuir* **2003**, *19*, 9542−9544.
(43) Viana, A. S.; Kalaji, M.; Abrantes, L. M. Self-assembled monolayers of vitamin B-12 disulphide derivatives on gold. *Electrochim. Acta* **2002**, *47*, 1587−1594.
(44) Gottesfeld, S. Ellipsometry - Principles and recent applications in electrochemistry. *Electroanaly. Chem.* **1989**, *15*, 143−265.
(45) Wang, Z. H.; Viana, A. S.; Jin, G.; Abrantes, L. M. Immunosensor interface based on physical and chemical immunoglobulin G adsorption onto mixed self-assembled monolayers. *Bioelectrochemistry* **2006**, *69*, 180−186.
(46) de Almeida, R. F. M.; Loura, L. M. S.; Fedorov, A.; Prieto, M. Nonequilibrium phenomena in the phase separation of a two-component lipid bilayer. *Biophys. J.* **2002**, *82*, 823−834.
(47) Aresta-Branco, F.; Cordeiro, A. M.; Marinho, H. S.; Cyrne, L.; Antunes, F.; de Almeida, R. F. Gel domains in the plasma membrane of Saccharomyces cerevisiae: highly ordered, ergosterol-free, and sphingolipid-enriched lipid rafts. *J. Biol. Chem.* **2011**, *286*, 5043−5054.
(48) Marques, J. T.; Viana, A. S.; de Almeida, R. F. Ethanol effects on binary and ternary supported lipid bilayers with gel/fluid domains and lipid rafts. *Biochim. Biophys. Acta* **2011**, *1808*, 405−414.
(49) Viana, A. S.; Abrantes, L. M.; Jin, G.; Floate, S.; Nichols, R. J.; Kalaji, M. Electrochemical, spectroscopic and SPM evidence for the controlled formation of self-assembled monolayers and organised multilayers of ferrocenyl alkyl thiols on Au(111). *Phys. Chem. Chem. Phys.* **2001**, *3*, 3411−3419.
(50) Leonenko, Z. V.; Cramb, D. T. Revisiting lipid - general anesthetic interactions (I): Thinned domain formation in supported planar bilayers induced by halothane and ethanol. *Can. J. Chem.* **2004**, *82*, 1128−1138.
(51) Lacomba, R.; Salcedo, J.; Alegria, A.; Lagarda, M. J.; Barbera, R.; Matencio, E. Determination of sialic acid and gangliosides in biological

samples and dairy products: A review. *J. Pharm. Biomed. Anal.* **2010**, *51*, 346−357.
(52) Sasahara, K.; Morigaki, K.; Shinya, K. Effects of membrane interaction and aggregation of amyloid beta-peptide on lipid mobility and membrane domain structure. *Phys. Chem. Chem. Phys.* **2013**, *15*, 8929−8939.
(53) Sanghera, N.; Correia, B.; Correia, J. R. S.; Ludwig, C.; Agarwal, S.; Nakamura, H. K.; Kuwata, K.; Samain, E.; Gill, A. C.; Bonev, B. B.; Pinheiro, T. J. T. Deciphering the molecular details for the binding of the prion protein to main ganglioside GM1 of neuronal membranes. *Chem. Biol.* **2011**, *18*, 1422−1431.
(54) Bard, A. J. F.; Larry R. *Electrochemical Methods: Fundamentals and Applications*, 2nd ed.; Wiley: New York, 2001, p 864.
(55) Cabrita, J. F.; Abrantes, L. M.; Viana, A. S. N-hydroxysuccinimide-terminated self-assembled monolayers on gold for biomolecules immobilisation. *Electrochim. Acta* **2005**, *50*, 2117−2124.
(56) Chen, S. M.; Chen, J. Y.; Vasantha, V. S. Electrochemical preparation of epinephrine/Nafion chemically modified electrodes and their electrocatalytic oxidation of ascorbic acid and dopamine. *Electrochim. Acta* **2006**, *52*, 455−465.
(57) Almeida, L; Cascalheira, A. C.; Viana, A. S. One step gold (bio)functionalisation based on CS2-amine reaction. *Electrochim. Acta* **2010**, *55*, 8686−8695.
(58) Almeida, L; Ferreira, V. C.; Montemor, M. F.; Abrantes, L. M.; Viana, A. S. One-pot approach to modify nanostructured gold surfaces through in situ dithiocarbamate linkages. *Electrochim. Acta* **2012**, *83*, 311−320.
(59) Jeuken, L. J. C.; Daskalakis, N. N.; Han, X. J.; Sheikh, K.; Erbe, A.; Bushby, R. J.; Evans, S. D. Phase separation in mixed self-assembled monolayers and its effect on biomimetic membranes. *Sens. Actuators, B* **2007**, *124*, 501−509.
(60) Shlomovitz, R.; Maibaum, L.; Schick, M. Macroscopic phase separation, modulated phases, and microemulsions: A unified picture of rafts. *Biophys. J.* **2014**, *106*, 1979−1985.

dx.doi.org/10.1021/la503086a | *Langmuir* 2014, 30, 12627−12637

6.2. Supporting Information

Supporting Information

A Biomimetic Platform to Study the Interactions of Bioelectroactive Molecules with Lipid Nanodomains

Joaquim T. Marquês, Ana S. Viana*, Rodrigo F. M. de Almeida*

Centro de Química e Bioquímica, Faculdade de Ciências, Universidade de Lisboa, Ed. C8, Campo Grande, 1749-016 Lisboa, Portugal

I. Reductive desorption of MUA and Cys monolayers and assessment of Cys SAM global charge

Surface coverage of both MUA and Cys SAM was determined by reductive desorption and the electrochemical behavior of two differently charged redox probes, $[K_3Fe(CN)_6]$ and $[Ru(NH_3)_6]Cl_3$, was employed to assess the global charge of the Cys SAM.

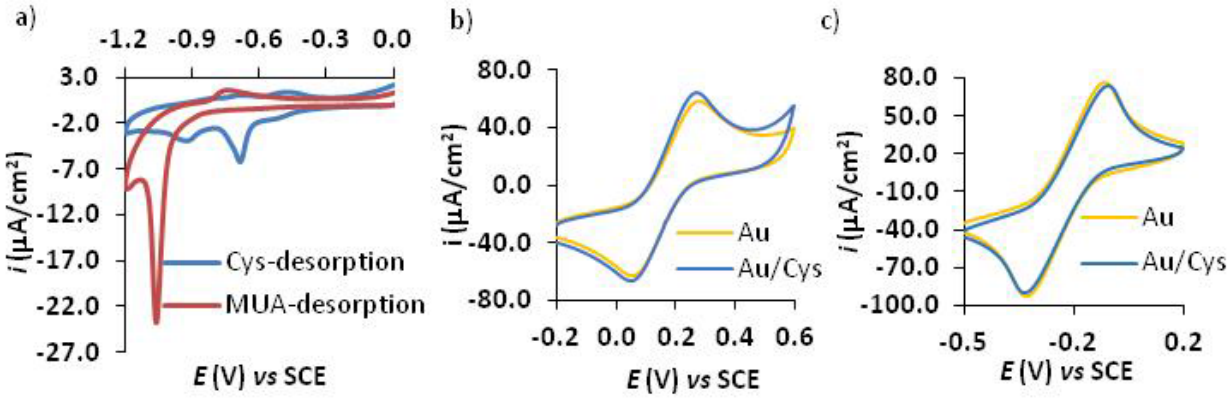

Figure S1 – a) Reductive desorption of L-cysteine and 11-mercaptoundecanoic acid self-assembled on Au (111) performed in 0.1 M NaOH at a scan rate of 20 mV/s. b) $[K_3Fe(CN)_6]$ redox process on a bare and Cys-modified gold surface and c) $[Ru(NH_3)_6]Cl_3$ redox process on a bare and Cys-modified gold surface measured in HEPES buffer 50 mM, pH 7.4, at a scan rate of 50 mV/s.

II. a) Real-time monitoring of lipid vesicles adsorption on modified gold surfaces.

With the purpose of assessing if modified electrodes with Cys are effective towards lipids' polar head group adsorption, we followed the real-time adsorption of lipid vesicles composed of DOPC/DPPC/Chol (2:2:1) on modified gold surfaces. Taking into account that substrate roughness is one of the factors playing an important role in terms of SLB formation[1], and both QCM and SPR electrodes present a higher roughness compared to Au (111) it is most likely that substrate topography will affect vesicle fusion or rupture required for planar SLB formation. Therefore, for the intended purpose of evaluating the extension and kinetics of vesicles adsorption, both QCM and SPR are quite suitable techniques. The two experimental approaches revealed that lipid vesicles interact to a similar extent with both MUA and Cys modified gold surface considering that an identical amount of lipid material is being adsorbed on top of each

electrode surface (Figure S2). Moreover, both QCM (Figure S2a) and SPR (Figure S2b) revealed that the interaction occurs with almost coincident kinetics for each SAM. Thus it is shown that a long compact monolayer is not necessary for efficient vesicle adsorption. Single lipid bilayer formation could not be detected on top of any of the electrodes used whether for QCM or SPR. The total mass adsorbing on QCM gold electrode was ~2.41 × 10^{-6} g/cm^2 and ~2.42 × 10^{-6} g/cm^2 for the MUA and Cys modified electrodes, respectively, whereas a mass of 4.4 × 10^{-7} g/cm^2 would be expected for the formation of a single lipid bilayer arrangement, as discribed in detail in section II.b). The difference between the calculated and measured values clearly shows that most probably a large amount of intact vesicles is being adsorbed on the surface. For both surface modifications, the presence of calcium in the buffer containing the lipid vesicles in suspension was required, since in its absence no significant adsorption to the surface took place (data not shown). More importantly, for the type of gold used in these experiments, a previous surface modification with SAM proved to be crucial to drive a favorable interaction between the lipid and the surface, as in bare Au only the deposition of a sub-monolayer (1.79 × 10^{-7} g/cm^2) was detected (Figure S2a).

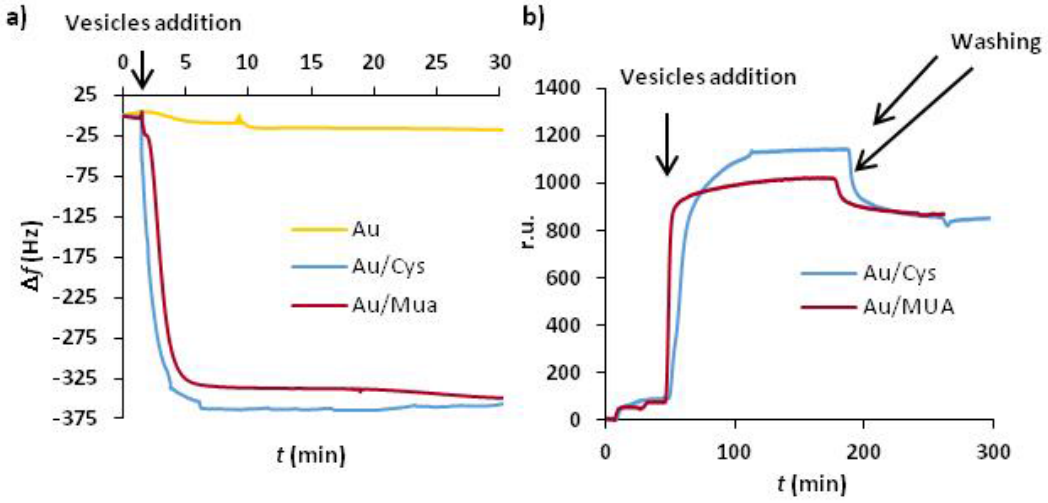

Figure S2 – Real-time monitoring of lipid vesicles adsorption onto bare, Cys- and MUA- modified gold surfaces by a) Quartz Crystal Microbalance and b) Surface Plasmon Resonance. The experiments were conducted in HEPES buffer containing 150 mM NaCl and 5 mM $CaCl_2$ or containing only 5mM $CaCl_2$ for MUA or Cys modified gold surfaces, respectively. The experiments were carried out with DPPC/DOPC/chol (2:2:1 mol ratio) lipid vesicles.

b) Determination of adsorbed mass by Quartz Crystal Microbalance

The amount of lipid deposited on top of bare and modified QCM electrodes was computed using the change in frequency of the quartz crystal upon a given mass variation which is given by Sauerbrey's equation[2],

$$\Delta f = -\frac{2f_0^2}{A\sqrt{\rho_q \mu_q}}\Delta m \qquad \text{(Eq. S1)}$$

where Δf is the frequency variation in Hz, f_0^2 stands for the resonant frequency, which in the present case was determined by the manufacturer to be 8 MHz, A is the piezoelectroative area of the crystal, ρ_q corresponds to the density of quartz which is 2.648 g/cm^3, $\mu_q$is the shear modulus of quartz for an AT-cut crystal which has a value of 2.947x10^{11} g/cm/s^2 and Δm expresses the

change in mass. Considering all the parameters stated above, our QCM exhibits a sensitivity of 6.9 x 10^{-9} g/Hz. Below, in table S1, a compilation of all the values calculated from QCM data is presented.

Table S1 – QCM frequency shift (Δf) and mass change (Δm and Δm/A) for bare and MUA- and Cys modified gold electrodes. The estimated values for the formation of a ternary lipid bilayer are also shown.

System	Δf (Hz)	Δm (g)	Δm/A (g/cm^2)	Lipid arrangement
Au	-26	3.5 x 10^{-8}	1.8 x 10^{-7}	Sub-monolayer
Au/MUA	-348	4.7 x 10^{-7}	2.4 x 10^{-6}	Vesicles
Au/Cys	-350	4.7 x 10^{-7}	2.4 x 10^{-6}	Vesicles
Theoretical Au/SLB	-64	8.6 x 10^{-8}	4.4 x 10^{-7}	Planar bilayer

In table S1 the value estimated for the mass of lipid for a planar and continuous lipid bilayer arrangement on the gold surface is also presented. This value was obtained taking into account both the molar proportion and the area per molecule (A) of each lipid and lipid phase– liquid ordered (l_o) and liquid disordered (l_d). The mol fraction and composition of each phase were taken from the phase diagram for this mixture and the tie-line containing the 2:2:1 molar proportion[3]. The phase l_o corresponds to ~40 mol % of the system with a lipid composition of ca. 63% DPPC, 33% Chol and 4% DOPC (mol%), while the remaining 60 mol% are in the l_d phase with a lipid composition of 65% DOPC, 25% DPPC and 10% Chol. For these lipid proportions, in l_o the area per lipid is around 43 Å^2 [4] while in l_d the area per lipid is close to 60 Å^2 [5]. Considering the following definitions:

$$a_{ld} = \frac{A_{ld}}{N_{ld}}$$

$$a_{lo} = \frac{A_{lo}}{N_{lo}}$$

$$A_t = A_{ld} + A_{lo}$$

$$N_{ld} = \frac{3}{2} N_{lo}$$

where A_t is the total area, a_{ld} and a_{lo} are the area per lipid, A_{ld} and A_{lo} stand for the total area, and N_{ld} and N_{lo} express the total number of molecules in the l_d and l_o phase, respectively, we estimated that the area fraction for the l_o phase is close to 32% while for the l_d is 68%, as shown next. Admitting a total electrode area (A_t) of 1 cm^2:

$$1 - A_{lo} = A_{ld} \Leftrightarrow 1 - A_{lo} = a_{ld} \times \frac{3}{2} N_{lo} \Leftrightarrow \frac{1 - A_{lo}}{\frac{3}{2}\left(\frac{A_{lo}}{a_{lo}}\right)} = a_{ld} \Leftrightarrow a_{lo} = \frac{3}{2} a_{ld} A_{lo} + A_{lo} a_{lo} \Leftrightarrow$$

$$\Leftrightarrow A_{lo} = \frac{a_{lo}}{\frac{3}{2} a_{ld} + a_{lo}} \Leftrightarrow A_{lo} = 0.32 \text{ cm}^2$$

Consequently, $A_{ld} = 0.68$ cm^2

Knowing that,

M (DOPC) = 786.15 g/mol
M (DPPC) = 734.05 g/mol
M (Chol) = 386.66 g/mol:

$N_{ld} = \frac{A_{ld}}{a_{ld}} \Leftrightarrow N_{ld} = \frac{6.8\times10^{15}}{60} = 1.13 \times 10^{14}$ molecules.

$n = \frac{1.13\times10^{14}}{6.022\times10^{23}} = 1.88 \times 10^{-10}$ mol.

$m_{ld} = 1.88 \times 10^{-10} \times \big((0.9 \times 786.15) + (0.1 \times 386.66)\big) = 1.4 \times 10^{-7}$ g

$N_{lo} = \frac{A_{lo}}{a_{lo}} \Leftrightarrow N_{lo} = \frac{3.2\times10^{15}}{43} = 7.44 \times 10^{13}$ molecules of l_o.

$n = \frac{7.44\times10^{13}}{6.022\times10^{23}} = 1.23 \times 10^{-10}$ mol of l_o.

$m_{lo} = 1.24 \times 10^{-10} \times \big((0.7 \times 734.05) + (0.3 \times 386.66)\big) = 7.9 \times 10^{-8}$ g

For a bilayer arrangement the actual mass would be the double of those values and hence the total mass would correspond to, approximately, $4.4\text{x}10^{-7}$ g/cm^2.

III. Determination of partition coefficient of epinephrine and its membrane-bound state anisotropy

Epinephrine surface coverage, determined in cyclic voltammetric experiments, and the total number of lipid moles present in an area of 1 cm^2 were used to estimate the mole-fraction partition coefficient[6] of epinephrine (K_p):

$$K_p = \frac{\frac{n_L^E}{n_L}}{\frac{n_W^E}{n_W}} \qquad \text{(Eq. S2)}$$

where n_W and n_L are the amount (in mole) of water and lipid in each sample, and n_i^E is the amount of epinephrine molecules present in each phase (i = w, aqueous phase; i = L, lipid phase, respectively). Considering the surface coverage of epinephrine for the fluid system (Γ = 9.36×10^{-11} mol/cm^2) and the amount of DOPC (molar volume at 20ºC taken from[7]) in 1 cm^2 (4.48×10^{-10} mol), K_p = 1.13×10^4. For a gel phase DPPC membrane (molar volume taken from[7]) K_p will be 2.8×10^3.

With these K_p estimations it is, then, possible to calculate a fraction of epinephrine bound to the membrane[6] (x_L) in the fluorescence spectroscopy studies, both for the 1 mM and 3 mM lipid experiments:

$$x_w = \frac{[W]}{[W] + K_p[L]} \qquad \text{(Eq. S3)}$$

where $[L]$ and $[W]$ are the lipid and water concentration, respectively. In the case of fluid DOPC for 1 mM of lipid $x_w = 0.827$ and for 3 mM of lipid $x_w = 0.615$. Since the total concentration o epinephrine was the same in every sample:

$$I = \sum x_i I_i \qquad \text{(Eq. S4)}$$

where I is the steady-state fluorescence intensity of epinephrine, I_i is the limiting value characteristic of either free or membrane-bound states and x_i is the fractional population of each species in a sample (i = w, aqueous phase; i = L, lipid phase)[6]. Thus, plotting the fluorescence intensity data obtained for epinephrine in each condition (solution, 1 mM and 3 mM of lipid – Figure 4b in the main article) *versus* mole fraction in solution we can find the fluorescence intensity for epinephrine when totally bound to the membrane, which corresponds to the extrapolation of such representation to zero (only membrane-bound form). The R^2 of this data is 0.99, yielding $I_L = 9.1 \times 10^6$. The fraction of light (f_i) coming from epinephrine in its free and membrane-bound states can be retrieved from the following equation:

$$f_i = \frac{x_i I_i}{I} \qquad \text{(Eq. S5)}$$

The steady-state anisotropy, $<r>$, of epinephrine can, then, be expressed as a function of the contribution of the anisotropy from free, $<r>_w$, and membrane-bound, $<r>_L$, epinephrine weighted by the fraction of light coming from both free (f_w) and membrane-bound (f_L) forms (Weber's and Jablonski's additivity law of anisotropy[8]):

$$< r > = < r >_w f_w + < r >_L f_L \qquad \text{(Eq. S6)}$$

From the data in Figure 4, for the fluid system $I_w = 1.2 \times 10^7$ and $<r>_w = 0.0175$. Using the anisotropy values experimentally determined for 1mM and 3 mM of lipid, it is possible to retrieve $<r>_L$. The values obtained are 0.01387 and 0.01056, respectively. Thus the anisotropy of epinephrine bound to a fluid membrane is -0.0075. For the other systems the uncertainty is larger due to the lower partition coefficients. However, it was clear that in all those cases a negative value of anisotropy for membrane bound epinephrine can be estimated and the values range between -0.1 and -0.2. These are within the range of physically feasible values for steady-state fluorescence anisotropy for a fluorophore with perpendicular absorption and emission transition dipole moments[9]. Moreover, these values are more negative than for the fluid DOPC, in agreement with the fact that the fraction of epinephrine in the membrane bound form is lower (smaller K_p) and the decrease in anisotropy is more pronounced. This shows that the hormone is more immobilized in these systems as compared to the fluid DOPC bilayer membrane, which is expected taking into account that the DOPC bilayer is the most disordered among the different lipid systems studied.

References

1. Marquês, J. T.; de Almeida, R. F. M.; Viana, A. S. Lipid bilayers supported on bare and modified gold – Formation, characterization and relevance of lipid rafts. *Electrochimica Acta*. **2014**, *126*, 139-150.

2. Bott, A. W. Characterization of Films Immobilized on an Electrode Surface Using the Electrochemical Quartz Crystal Microbalance. *Current Separations* **1999,** *18*, 5.
3. de Almeida, R. F.; Borst, J.; Fedorov, A.; Prieto, M.; Visser, A. J. Complexity of lipid domains and rafts in giant unilamellar vesicles revealed by combining imaging and microscopic and macroscopic time-resolved fluorescence. *Biophys.J.* **2007,** *93*, 539-553.
4. Edholm, O.; Nagle, J. F. Areas of molecules in membranes consisting of mixtures. *Biophysical Journal* **2005,** *89*, 1827-1832.
5. Alwarawrah, M.; Dai, J. A.; Huang, J. Y. A Molecular View of the Cholesterol Condensing Effect in DOPC Lipid Bilayers. *J. Phys. Chem. B* **2010,** *114*, 7516-7523.
6. Loura, L. M. S.; de Almeida, R. F. M.; Coutinho, A.; Prieto, M. Interaction of peptides with binary phospholipid membranes: application of fluorescence methodologies. *Chem. Phys. Lipids* **2003,** *122*, 77-96.
7. Marsh, D. *Handbook of Lipid Bilayers*; Second ed.; CRC Press/Taylor & Francis Group: Boca Raton, 2013.
8. Jameson, D. M. In *New Trends in Fluorescence Spectroscopy*, Valeur, B.; Brochon, J.-C., Eds.; Springer/Verlag: Berlin, 2001; pp 35-58.
9. Valeur, B.; Berberan-Santos, M. N. *Molecular Fluorescence: Principles and Applications*; Second ed.; Wiley/VCH: New York, 2012; pp 569-571.

Chapter VII

Concluding remarks

Over the last decade the field of membrane biophysics has met several important developments, though the complete picture of membrane properties, organization and function is not fully elucidated yet. For instance, the generally accepted concept that biological membranes are two-dimensional liquid structures, where lipid rafts (liquid ordered domains) play an important role, and no rigid gel domains are present has been reviewed in the last few years in light of the discovery of gel domains in eukaryotic organisms under physiological conditions.[1] In fact, the topic of membrane organization is broadly discussed in the view of the new developments in this field.[2-4]

The work developed during this thesis was focused on three main goals – understand how sphingolipid backbone may determine different membrane organizations; how both membrane composition and lateral organization can modulate its interaction with small molecules; and finally the development of a lipid bilayer interface using gold as substrate so that optical and electrochemical techniques could be employed for the study of membrane-related phenomena. In order to achieve a comprehensive biophysical characterization of the diverse lipid systems investigated throughout this thesis, whether free standing bilayers or SLB formed on mica, silicon or gold, a wide set of techniques was required – AFM, ellipsometry, cyclic voltammetry, QCM, SPR, fluorescence spectroscopy, fluorescence microscopy and X-ray scattering. For example, AFM has been employed throughout this work and its use helped to characterize not only the lateral organization of SLB, but also real-time changes occurring at the bilayer structure due to the interaction with small molecules, and to clearly distinguish between SLB of distinct lipid composition. Moreover, it corroborated the formation of planar lipid bilayers undoubtedly different from unfused vesicles, lipid tubular structures, or other non-planar lipid arrays, also identified throughout this work for certain experimental conditions.

Another topic explored in the course of this thesis was the influence exerted by the solid substrate on the properties of the lipid bilayers prepared. Concerning the preparation of SLB composed by the DOPC/DPPC/Chol (2:2:1) ternary mixture it was determined that depending on the solid substrate used there is an influence not only on the phase behavior in terms of l_o and l_d area fraction but also the shape of the domains. Regarding the substrates used in this work for the preparation of SLB it was found that the l_o/l_d area fractions of the lipid bilayers formed on mica were in good agreement with the ones predicted by its phase diagram. Though, lipid bilayers prepared on silicon and gold exhibited a considerable deviation from the expected value. Moreover, Au (111) also has a strong impact in the shape of the domains, which appear as triangular and with

angular shapes for SLB formed directly on gold, following the topography of Au(111). In opposition, SLB formed on mica and silicon exhibit round-shaped domains, as observed for free-standing bilayers. Other authors have also reported how substrate topology may influence the shape, size and fraction of lipid domains.[5] The authors hypothesized that due to substrate topology cholesterol may be transferred from the SLB to the vesicles present in the medium during the steps of vesicle fusion and cooling. This process would lead to a decreased content in cholesterol of the SLB in comparison to the vesicles used for their preparation and, thus, to a lower fraction of ordered domains.

SLB on mica were also used to study the POPC/PhyCer binary mixture and, ultimately, to help determine the phase diagram for this system. This ceramide is present as the backbone in major sphingolipids from organisms belonging to the Plantae and Fungi kingdoms. By the combined use of fluorescence spectroscopy, both steady-state and time-resolved AFM, confocal fluorescence microscopy and X-ray scattering it was possible to establish the type of phase diagram for that binary system which was crucial to then define the several phase coexistence boundaries, and their important biological implications. Indeed, the results point to the formation of complexes between POPC and PhyCer at two distinct molar proportions: POPC 3 : 1 PhyCer and POPC 1 : 2 PhyCer. These complexes can be described as individual molecular entities with unique properties differing from those of pure POPC or PhyCer phases. PhyCer differs from ceramide by the presence of a hydroxyl group at position C-4 of the sphingoid base instead of a *trans* double bond. The phase diagrams already published for ceramide mixed with POPC do no predict the formation of complexes[6-7], which show how a small structural difference can strongly influence lipid phase behavior. In addition, up to date mostly complexes involving cholesterol have been reported for lipid systems[8-9] and, moreover, in those studies only one complex was found to be formed for the whole range of lipid compositions. Interestingly, data presented in this dissertation reveals that the biophysical properties of these POPC/PhyCer complexes are quite similar to those of gel domains recently found in yeast under physiological conditions[1], hence mixtures containing PhyCer or PhyCer-derived sphingolipids are a good starting point for the *in vitro* study of the interaction with antifungal drugs of domains that mimic the gel domains identified in *Saccharomyces cerevisiae*. In fact, recent works also report the formation of rigid and time-stable structures in the membranes of different organisms[3]. Such results might, indeed, shed some light about the controversial thematic related to the actual role of lipid phase separation *in vivo* under physiological conditions,

in the formation of micro/nanodomains, and as biologically relevant diffusion barriers. Undeniably, much remains to be enlightened regarding the organization of lipids in both model systems and biomembranes.

Another chief purpose of this thesis was to create a lipid-based platform that could be used in the future development of biosensing interfaces or employed in the detection of membrane-interacting electroactive molecules, as well as to increase our understanding on the structure and function of lipid nanodomains, through the use of electrochemistry in parallel with AFM (and other surface characterization techniques, such as ellipsometry; total internal reflectance fluorescence is also envisaged in a near future). To that end gold surfaces were used. Since the formation of a SLB on gold was not as straightforward as in mica due to its hydrophobicity, the formation of a planar and continuous ternary lipid bilayer (exhibiting l_o and l_d phase coexistence) was firstly essayed on bare gold due to its biological relevance. In addition, the presence of such bilayer would be more easily ascribed than a single component bilayer due to the presence of lipid domains with ~1 nm height difference from the surrounding bilayer. The formation of a planar and continuous lipid bilayer was only achieved under specific buffer conditions. In fact, the presence of chloride ions in the deposition buffer led to the formation of tubular structures which are a consequence of an incomplete fusion of vesicles. A recent report has also explored how the deposition of vesicles on oxidized gold is related to their size and buffer conditions[10]. The authors have found that independently of vesicles size and buffer conditions, vesicles adsorb without rupture, although they deform. Whether only water or PBS is used, the deformation of the vesicles does not proceed in the same manner. In the case of water various levels of deformation were observed, whereas if PBS is used vesicles deform more homogeneously becoming almost flat. Although it is not discussed by the authors, the roughness of the substrate also plays a preponderant role for the complete rupture of vesicles, and this is the reason why Au (111) has been used in the present work. Despite AFM images revealed that the lipid bilayers prepared on bare gold seemed to be continuous, cyclic voltammetric experiments of the blocking effect exert by the SLB to the $K_3Fe(CN)_6$ redox process showed that they should present small pores or defects. In order to overcome this limitation previous gold modification was employed.

MUA and Cys were the two SAM studied in this work. While it had already been shown that MUA is a suitable surface modification regarding the formation of a SLB on gold, a monolayer of Cys was, for the first time, employed for such purpose. Nonetheless, the properties of MUA

monolayer did not fit one of the purposes of developing a lipid-based interface on gold, which is to take advantage of the conductive nature of gold. Due to its very compact nature MUA hinders the electronic transfer between electroactive species in solution and the gold electrode. The SLB formed on top of Cys-modified gold were planar, continuous, compact and stable as confirmed by AFM and cyclic voltammetry. This arrangement proved to be an efficient interface for conducting fundamental studies as in the evaluation and quantification of the interaction of biologically relevant small electroactive species with membranes of various compositions. Moreover, this lipid-based interface might have the potential to be applied in the development of biosensing platforms, for example in the detection of enzymatically generated analytes by proteins immobilized in the membrane. The field of biosensing is continuously growing with new methodologies and strategies being reported constantly. Recently, a biosenssor based on a biomembrane-like film composed of didodecyldimethylammoniumbromide has been reported, which was built on an alkanethiol and diazonium salt modified glassy carbon electrode[11]. This interface incorporates gold nanoparticles modified with myoglobin with the purpose of hydrogen peroxide detection. This interface has proved its electrochemical biosensing ability for the detection of hydrogen peroxide. Gold, enables not only electrochemical transduction but also optical a methodology also employed for biosensing purposes, especially in the case of immunosensing[12-15]. In this way, gold is one the most polyvalent surfaces since it allows the application of a wide variety of characterization techniques.

The evaluation of the interaction of small molecules with lipid membranes was another chief topic of this thesis. How the interaction of small molecules with lipid membranes processes and which type of lipid phases are mainly involved in that mechanism is another relevant thematic in the field of biomembranes. The interaction of ethanol with lipid membranes, in this case lipid bilayers supported on mica, was followed in real time by AFM, which is, perhaps, the most suitable technique to visualize the effects induced by ethanol due to its exceptional lateral and axial resolutions. Prior to this work it was already known that the interaction of ethanol with lipid bilayers leads to the interdigitation of the lipids' acyl chains[16]. The present work helped to unravel the effects of ethanol on lipid systems exhibiting phase separation – gel/fluid and l_d/l_o. It is shown that ethanol effects appear to be more dependent on the type of lipid phases present than on lipid composition since independent lipid bilayers both displaying l_o/l_d coexistence, though differing in their higher transition temperature lipid (DPPC in one case, PSM in the other), underwent the same morphological alterations upon exposure to ethanol, with the ordered and disordered phases

becoming thinner at the same time, whereas the expansion was only observed for the disordered phase. Moreover, for the fluid/gel system a thinning of the bilayer is firstly observed for the fluid phase with the thickness reduction in gel occurring only at higher ethanol concentrations. These results clearly show that the lateral organization can modulate the interaction of small molecules with the membrane, which points to the relevance of using the proper lipid systems when conducting this kind of experiments. Additionally, other authors, using lipid mixtures that model the membranes of yeast cells, thus employing ergosterol instead of cholesterol, have reported that the increase in sterol[17-18] or unsaturated phospholipid content makes the membrane more resilient to ethanol effects. Therefore, a gel membrane would be more susceptible to ethanol actions than a l_o/gel and this one less resistant than a l_o/l_d.

Noteworthy is the fact that the approach employed – from the simplest single-phase and single-component systems to the more complex phase-separating and multicomponent ones[19-20] – for the study of the effects of ethanol was essential for the understanding of the effects observed in the systems of higher complexity. As often expressed during this thesis, one of the main advantages of biomimetic model systems is their simplicity, at least when compared with biological membranes, especially in living cells or organisms. Hence, only a limited number of components should comprise these systems and the complexity should be increased solely if necessary. Usually, the best approach is to use models as simple as possible sharing a property of interest with the biological counterpart, rather than prepare a very complex mixture that, still, does not match the biological system and makes results interpretation more challenging. Nevertheless, regarding the heterogeneous and compartmentalized nature of biomembranes[21], the use of lipid mixtures is often required in order to recreate this heterogeneity.

The interaction of lipid membranes with electroactive molecules, namely quercetin and epinephrine, was also assessed. At first, since the interaction of quercetin with lipid membranes was already characterized in literature, this antioxidant was used in order to evaluate the performance of the lipid interface developed. Because the results obtained were promising regarding the performance of the lipid interface, this platform was used to studied the interaction of epinephrine with membranes, which up to date was undisclosed. Liposomes were used in fluorescence spectroscopy studies as a first approach to evaluate the interaction, suggesting this to be rather weak. Despite the small changes in epinephrine intrinsic fluorescence, membrane-bound epinephrine was clearly detected by cyclic voltammetry using the lipid interface developed in the

course of this thesis. The possibility of detecting only the adsorbed molecules and to quantitatively determine epinephrine surface concentration in the membrane in each lipid system employed, allowed estimating a membrane/water partition coefficients for epinephrine, a method that had never been employed in membrane-small molecule interaction studies, to the best of our knowledge. One of the main achievements of this work was to show the potential of using, when possible, both fluorescence spectroscopy and cyclic voltammetry. In fact, the collection of techniques used in the characterization of SLB formed on gold throughout this thesis is unusual and to the best of my knowledge no reports in the literature mention the use of the same combination of techniques. By combining both fluorescence and electrochemical data it was possible to conclude that epinephrine anisotropy becomes negative when bound to the membrane, most likely, due to a reorientation of its absorption or emission dipole, and estimate its relative degree of immobilization in different lipid systems. Likewise, the detection of the low amounts of membrane-bound epinephrine highlights the high sensitivity of this platform and motivates exploiting its use as a biosensing interface in the near future.

The results presented in this dissertation have helped to clarify or understand some mechanisms associated with membrane lipid organization and function. Notwithstanding, they also raise new questions and challenges that should be addressed in the future. For instance, it will be important to investigate and determine the phase diagram for the ternary system containing POPC, PhyCer and ergosterol, the major sterol found in fungi plasma membrane. This will bring a deeper understanding of the plasma membrane of fungi as well as the differences from its mammalian counterpart. These in turn can be used for the development of more effective antifungal agents. As mentioned above, other authors studied the effects of ethanol on model membranes containing ergosterol. In those studies binary and ternary systems containing phospholipids and ergosterol have been used. It would be interesting to compare ethanol or other molecules interaction with model membranes that more closely resemble fungi (containing both ergosterol and a phytosphingosine-based sphingolipid) plasma membrane, and confront them with the results described in this thesis in mammalian model systems (ternary mixtures containing cholesterol and SM). This is a pertinent question, especially because fungal infections resistant to treatment are an emerging public health issue[22].

This thesis also opens new prospects especially in what concerns the use of electrochemical or even optical approaches in the study of membrane-related phenomena. It would certainly be

exciting to employ FRAP in the study of lipid rafts prepared on top of gold surfaces with different modifications in order to understand if the lateral diffusion coefficients are similar to those determine in free-standing lipid bilayers. The use of TIRF would also be a valuable complement since it would allow to determine the biophysical properties of these domains and compare to the ones found for liposomes. The lipid-based platform developed presents a high sensitivity and could be employed to carry out the studies referred in the above paragraph regarding antifungal agents or other molecules whose interaction with the membrane is crucial for their mechanism of action. As already mentioned, an interesting outcome of the lipid-based interface developed or a similar one, would be its application for biosensing purposes. The market of biosensors is experiencing a great expansion and is expected to value 22.68 billion dollars by 2020, which is two times more than worthed at 2013[23]. One of the advantages of using a lipid-based interface is that the lipids' head group will inhibited the non-specific adsorption of proteins, which makes this platform suitable to use in the optical detection of the antibody-antigen biorecognition event[24,25]. Besides this type of signal transduction this platform can also be employed in the electrochemical detection of products generated by enzymatic reactions, as in the case of glucose[26] or dopamine detection[27].

References

1. Aresta-Branco, F.; Cordeiro, A. M.; Marinho, H. S.; Cyrne, L.; Antunes, F.; de Almeida, R. F. Gel domains in the plasma membrane of Saccharomyces cerevisiae: highly ordered, ergosterol-free, and sphingolipid-enriched lipid rafts. *J.Biol.Chem.* **2011,** *286*, 5043-5054.
2. Bagatolli, L. A.; Mouritsen, O. G. Is the fluid mosaic (and the accompanying raft hypothesis) a suitable model to describe fundamental features of biological membranes? What may be missing? *Front. Plant Sci.* **2013,** *4*.
3. de Almeida, R. F. M.; Joly, E. Crystallization around solid-like nanosized docks can explain the specificity, diversity, and stability of membrane microdomains. *Front. Plant Sci.* **2014,** *5*, 14.
4. Nicolson, G. L. The Fluid-Mosaic Model of Membrane Structure: Still relevant to understanding the structure, function and dynamics of biological membranes after more than 40 years. *Biochimica Et Biophysica Acta-Biomembranes* **2014,** *1838*, 1451-1466.
5. Goksu, E. I.; Longo, M. L. Ternary Lipid Bilayers Containing Cholesterol in a High Curvature Silica Xerogel Environment. *Langmuir* **2010,** *26*, 8614-8624.
6. Pinto, S. N.; Silva, L. C.; de Almeida, R. F. M.; Prieto, M. Membrane domain formation, interdigitation, and morphological alterations induced by the very long chain asymmetric C24 : 1 ceramide. *Biophysical Journal* **2008,** *95*, 2867-2879.
7. Silva, L.; de Almeida, R. F.; Fedorov, A.; Matos, A. P.; Prieto, M. Ceramide-platform formation and -induced biophysical changes in a fluid phospholipid membrane. *Mol.Membr.Biol.* **2006,** *23*, 137-148.
8. Radhakrishnan, A.; Anderson, T. G.; McConnell, H. M. Condensed complexes, rafts, and the chemical activity of cholesterol in membranes. *Proceedings of the National Academy of Sciences of the United States of America* **2000,** *97*, 12422-12427.

9. Radhakrishnan, A.; Li, X. M.; Brown, R. E.; McConnell, H. M. Stoichiometry of cholesterol-sphingomyelin condensed complexes in monolayers. *Biochimica Et Biophysica Acta-Biomembranes* **2001,** *1511*, 1-6.
10. Towns, E. N.; Parikh, A. N.; Land, D. P. Influence of Vesicle Size and Aqueous Solvent on Intact Phospholipid Vesicle Adsorption on Oxidized Gold Monitored Using Attenuated Total Reflectance Fourier Transform Infrared Spectroscopy. *The Journal of Physical Chemistry C* **2015,** *119*, 2412-2418.
11. Anjum, S.; Qi, W.; Gao, W.; Zhao, J.; Hanif, S.; Aziz ur, R.; Xu, G. Fabrication of biomembrane-like films on carbon electrodes using alkanethiol and diazonium salt and their application for direct electrochemistry of myoglobin. *Biosensors and Bioelectronics* **2015,** *65*, 159-165.
12. Burenin, A. G.; Urusov, A. E.; Betin, A. V.; Orlov, A. V.; Nikitin, M. P.; Ksenevich, T. I.; Gorshkov, B. G.; Zherdev, A. V.; Dzantiev, B. B.; Nikitin, P. I. Direct immunosensing by spectral correlation interferometry: assay characteristics versus antibody immobilization chemistry. *Anal. Bioanal. Chem.* **2015,** *407*, 3955-3964.
13. Choi, H. W.; Sakata, Y.; Ooya, T.; Takeuchi, T. Reflectometric interference spectroscopy-based immunosensing using immobilized antibody via His-tagged recombinant protein A. *J. Biosci. Bioeng.* **2015,** *119*, 195-199.
14. Seydack, M. Nanoparticle labels in immunosensing using optical detection methods. *Biosens. Bioelectron.* **2005,** *20*, 2454-2469.
15. Mitchell, J. Small Molecule Immunosensing Using Surface Plasmon Resonance. *Sensors* **2010,** *10*, 7323-7346.
16. Vierl, U.; Lobbecke, L.; Nagel, N.; Cevc, G. Solute Effects on the Colloidal and Phase-Behavior of Lipid Bilayer-Membranes - Ethanol-Dipalmitoylphosphatidylcholine Mixtures. *Biophysical Journal* **1994,** *67*, 1067-1079.
17. Vanegas, J. M.; Faller, R.; Longo, M. L. Influence of Ethanol on Lipid/Sterol Membranes: Phase Diagram Construction from AFM Imaging. *Langmuir* **2010,** *26*, 10415-10418.
18. Vanegas, J. M.; Contreras, M. F.; Faller, R.; Longo, M. L. Role of Unsaturated Lipid and Ergosterol in Ethanol Tolerance of Model Yeast Biomembranes. *Biophys. J.* **2012,** *102*, 507-516.
19. de Almeida, R. F. M.; Fedorov, A.; Prieto, M. Sphingomyelin/phosphatidylcholine/cholesterol phase diagram: Boundaries and composition of lipid rafts. *Biophysical Journal* **2003,** *85*, 2406-2416.
20. de Almeida, R. F.; Borst, J.; Fedorov, A.; Prieto, M.; Visser, A. J. Complexity of lipid domains and rafts in giant unilamellar vesicles revealed by combining imaging and microscopic and macroscopic time-resolved fluorescence. *Biophys.J.* **2007,** *93*, 539-553.
21. Malinsky, J.; Opekarova, M.; Grossmann, G.; Tanner, W. Membrane microdomains, rafts, and detergent-resistant membranes in plants and fungi. *Annual review of plant biology* **2013,** *64*, 501-29.
22. http://www.cdc.gov/fungal/antifungal-resistance.html, accessed July 27th 2015
23. http://www.marketsandmarkets.com/PressReleases/biosensors.asp, accessed July 27th 2015
24. Liley, M.; Bouvier, J.; Vogel, H. Incorporation and antibody recognition of a lipid-anchored membrane protein in supported lipid layers. *Journal of Colloid and Interface Science* **1997,** *194*, 53-58.
25. Kurihara, Y.; Sawazumi, T.; Takeuchi, T. Exploration of interactions between membrane proteins embedded in supported lipid bilayers and their antibodies by reflectometric interference spectroscopy-based sensing. *Analyst* **2014,** *139*, 6016-6021.
26. Trojanowicz, M.; Miernik, A. Bilayer lipid membrane glucose biosensors with improved stability and sensitivity. *Electrochimica Acta* **2001,** *46*, 1053-1061.
27. Fritzen-Garcia, M. B.; Zoldan, V. C.; Oliveira, I. R. W. Z.; Soldi, V.; Pasa, A. A.; Creczynski-Pasa, T. B. Peroxidase immobilized on phospholipid bilayers supported on au (111) by DTT self-assembled monolayers: Application to dopamine determination. *Biotechnology and Bioengineering* **2013,** *110*, 374-382